NATIONAL SCIENCE FOUNDATION

Print ISSN 1391-4588
E - ISSN 2362-0161
Volume 53 No. 4
December 2025

Journal of the National Science Foundation of Sri Lanka

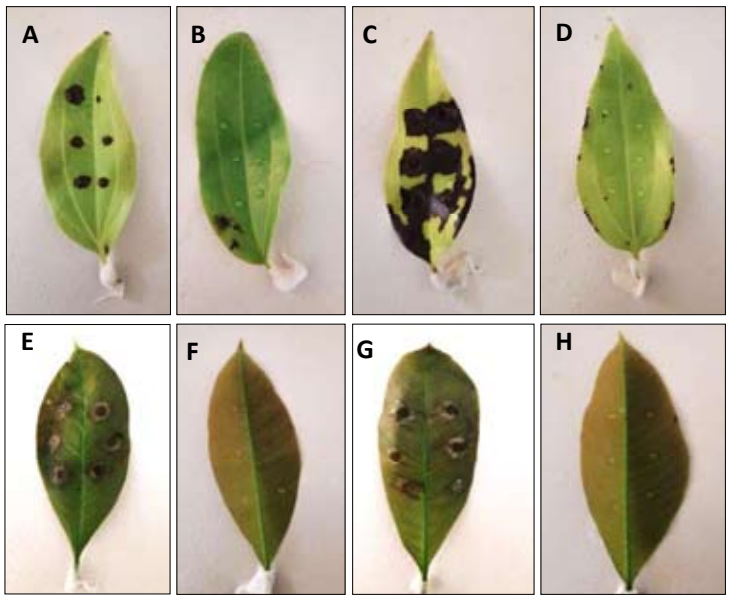

www.nsf.gov.lk

NATIONAL SCIENCE FOUNDATION

JOURNAL OF THE NATIONAL SCIENCE FOUNDATION OF SRI LANKA

Editorial Board

Ajit Abeysekera (Editor in Chief)
Pradeepa Bandaranayake
Nelum Deshappriya
J.K.D.S. Jayanetti
L.P. Jayatissa
P. Prasad M. Jayaweera
Jagath Manatunge
Jennifer Perera
S.S.N. Perera
Roshan G. Ragel
Rohini de A. Seneviratne
S.A.H.A. Suraweera
Pushpa Wijekoon
M.J.S. Wijeyaratne
Hiran Yapa

Language Editor

R.D. Guneratne

Editorial Office

Nadeeja Wickramarachchi (Principal Scientific Officer)
Upuli Ratnayake (Scientific Officer)
Bhagya Dasanayaka (Scientific Officer)

Graphic Designing & Typesetting
Kanchana Sewwandi

Contact details
Editorial Office, National Science Foundation,
47/5, Maitland Place, Colombo 07, Sri Lanka.

E-mail : jnsf@nsf.gov.lk
Phone : +94-11- 2696771
JNSF online submission portal :
https://jnsfsl.sljol.info/about/submissions
JNSF home page :
http://www.nsf.gov.lk/ index.php/nsfscience magazine

Publication : Published quarterly (March, June, September and December) by the National Science Foundation of Sri Lanka.

Manuscripts: Research Articles, Research Communications, Reviews and Correspondences in all fields of Science and Technology can be submitted for consideration for publication. A guide to the preparation of manuscripts is provided in each issue. The guidelines may also be obtained by visiting the NSF website or JNSF online submission portal.

Disclaimer: No responsibility is assumed by the National Science Foundation of Sri Lanka for statements and opinions expressed by contributors to this Journal.

Publication : free A publication fee of US$ 250 will be levied for each manuscript in two stages except, when the corresponding author is affiliated with a Sri Lankan institution.

- A processing fee of US$ 20 will belevied for each manuscript at peer-review stage.
- Remaining US$ 230 will be charged for accepted articles at the time of publication.

Copyright : © National Science Foundation of Sri Lanka

Articles in the Journal of the National Science Foundation of Sri Lanka are Open Access articles published under the Creative Commons CC-BY-ND License (http:// creative commons. org/licenses/by/4.0/). This license permits the use, distribution and reproduction, commercial and non-commercial, provided that the original work is properly cited and has not been changed anyway.

Indexing : **The JNSF is indexed in Science Citation Index Expanded, Journal Citation Reports/Science Edition, BIOSIS Previews, Zoological Record, Biological Abstracts, Chemical Abstracts, Scopus, DOAJ, TEEAL, Ulrich's, AGRICOLA and EBSCOhost, CAB Abstracts, SafetyLit, Journal TOCs, EBSCO Applied Science & Technology Source Ultimate**

JOURNAL OF THE
NATIONAL SCIENCE FOUNDATION
OF SRI LANKA

Volume 53 Number 4 December 2025

CONTENTS

EDITORIAL

307 **Symbiosis between science and technology**
Ajit Abeysekera

CORRESPONDANCE

309 **Public support for science might worsen policy**
BVE Hyde

RESEARCH ARTICLES

311 **A technique for extracting gravity anomalies originating from sediments deposited on folded oceanic crust**
DA Tantrigoda, MMPM Fernando and *SA Samaranayake*

317 **An upper bound for star chromatic index of simple connected sub-cubic graphs and applications**
CLR Fernando and *AMCUM Athapattu*

333 **Use of near infrared spectroscopy for rapid and non-destructive identification of morphologically similar seeds of different paddy varieties [*Oryza sativa* L.]**
KW Yasintha and *BM Jinendra*

345 **Seasonal variation in crop yield and reduction of phytic acid content through soaking and germination of kodo millet (*Paspalum scrobiculatum L.*) germplasm**
C Suneetha and *M Sukumar*

363 **Magnetic properties of body-centred cubic ferromagnetic thin films described by the fourth order perturbed Heisenberg Hamiltonian**
MSM Farhan and *P Samarasekara*

375 **Use of carbonised wood particles as filler replacement in hot mix asphalt**
TM Rengarasu, N Jegatheesan and *Wasala MKRTW Bandara*

391 **Ecological characterization of the 40-year-old regenerated rainforest patch in Olaboduwa-Kodigahakanda adds value in promoting forest-based nature tourism**
WAPU Ruwanmalie, IASR Ileperuma and *SMW Ranwala*

403 **Changes in crop productivity and the harvested area of rice grown in Sri Lanka over the last four decades (1979-2021) as affected by the season, district, and water management system**
SS Wijesooriya, HMKC Nawarathna, SS Kumari, A Sooriyarachchi, JMAK Jayaweera, C Perera and *LDB Suriyagoda*

421 **Faecal indicator bacteria and microbial source tracking as tools for testing water quality and sources of contamination of Rawan-Oya tributary of the Mahaweli River, in Sri Lanka**
GK Kapukotuwa, CL Abayasekara, KC Weerakoon and *RS Rajakaruna*

437 **Chest anteroposterior diameter measurement: Comparison of ultrasonic and manual methods across different BMI categories**
C Muralidharan and *MC Jobin Christ*

447 **A multidimensional study on Spotted Sardinella: Biometric, ecological, and heavy metal perspectives from Negombo, Sri Lanka**
WMNS Wijesooriya, HACC Perera, AMPM Abeysinghe and *KABP Perera*

RESEARCH COMMUNICATION

459 **First report of rubber circular leaf spot disease pathogen *Colletotrichum siamense* Prihastuti, L. Cai & K.D. Hyde in *Cinnamomum zeylanicum* blume in Sri Lanka**
AHMNR Aberathne, THPS Fernando and *EADD Siriwardena*

Guidelines for Contributors

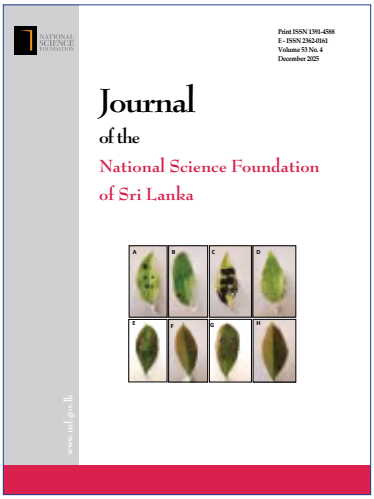

Cover: Inoculation of cinnamon and rubber leaves with *Colletotrichum siamense* cultures.
Top: Cinnamon leaves; A) non-wounded inoculated, B) non-wounded control, C) wounded inoculated, D) wounded control
Bottom: Rubber leaves; E) non-wounded inoculated, F) non-wounded control, G) wounded inoculated, H) wounded control
See J.Natn.Sci.Foundation Sri Lanka 2025 53(4): 459 - 464

J.Natn.Sci.Foundation Sri Lanka 2025 53 (4): 307
DOI: http://dx.doi.org/10.4038/jnsfsr.v53i4.12938

EDITORIAL

Symbiosis between science and technology

Mankind was familiar with technology long before science. However, following the periods of the scientific revolution and the industrial revolution, there has developed an increasingly symbiotic relationship between science and technology. New scientific discoveries provide the impetus for their creative use in technology and new technology provides new areas for investigation and new tools to do so. For example, the concept of the wave-particle duality of electrons was an essential element in the development of the electron microscope, which in its turn vastly opened up the microscopic world beyond the capability of the optical microscope. Thus, the 'need to know' how and why nature operates the way it does (science) and the 'need to do' and manipulate nature (technology), feed on one another. Today, new knowledge and related new technology are being created at a dizzying speed which makes it difficult to be even aware of important new developments other than in a narrow area of interest.

In this symbiotic relationship, technology is the component of major interest and concern to both government and industry due to its more obvious interaction with society. However, the line differentiating science from technology in many areas involving the application of science, such as gene technology, medicinal chemistry and semiconductors, is hazy. Often, the difference lies not in the methods, tools or theoretical background utilized, but in whether the focus is on a more distant potential outcome or on a more clearly defined immediate outcome. The rapid development of vaccines for COVID-19 was a clear example of how the symbiosis between science and technology benefitted mankind.

Ajit Abeysekera

J.Natn.Sci.Foundation Sri Lanka 2025 53 (4): 309 - 310
DOI: http://dx.doi.org/10.4038/jnsfsr.v53i4.12921

CORRESPONDANCE

Public support for science might worsen policy

BVE Hyde[1,2*]
[1] *Department of Population Health Sciences, Bristol Medical School, Canynge Hall, 39 Whatley Road, Bristol, United Kingdom, BS8 2PS.*
[2] *School of History, Law and Social Sciences, Bangor University, Main Arts Building, Bangor, Gwynedd, Wales, United Kingdom, LL57 2DG.*

Abstract: Evidence-based policy has become the gold standard for trustworthy governance, yet the relationship between trust and trustworthiness in science-policy interactions is more complex than commonly assumed. This letter argues that increased public trust in science may undermine policy quality because of policy-based evidence-making – the selective use of scientific evidence to justify predetermined political decisions. Drawing on political science literature and Britain's experience with evidence-based policy, it is argued that high trust allows policymakers to obscure necessary value judgements behind scientific authority. Efforts to increase trust in science, such as the National Academy of Sciences Sri Lanka's recent initiative to restore trust in science, must therefore consider these perverse incentives to avoid inadvertently compromising evidence-informed policymaking.

Keywords: evidence-based policy; policy-based evidence-making; public trust in science; cherry-picking; values in public policy.

The last thirty years have witnessed an explosive rise in evidence-based policy, driven particularly in the United Kingdom by the Blair Government (1997-2007). It's now widely recognized that good policy must be rooted in scientific evidence, whether that means grounding social policy in social science or anchoring public health policy in epidemiology. This is what makes policy trustworthy, which is why the editor of this journal has, quite rightly, reiterated the importance of applying scientific knowledge to public policymaking.

However, trust and trustworthiness are not synonymous, and their relationship is far more complex than typically assumed. There's growing evidence of perverse incentives and unintended consequences at the intersection of these concepts. Increases in trustworthiness can sometimes decrease trust. For instance, honesty and transparency – qualities that all theorists agree enhance the *trustworthiness* of science – have in some cases been found to diminish public *trust* in science.

Perhaps more troublingly, increases in trust can decrease the trustworthiness of policy. The use of evidence in policymaking is inherently political, and political scientists have long recognized that scientific evidence is often deployed merely to justify decisions already made rather than to inform deliberation. The mechanism behind this is cherry-picking, and the result is policy-based evidence-making.When the public expresses high levels of trust in and support for science, this doesn't necessarily encourage policymakers to engage more genuinely with evidence-*informed* policy. All it means is that they need to ensure that their policies are seen to be supported by science. Realistically, this means that policymakers will selectively invoke scientific authority to legitimize their predetermined policy positions.

The United Kingdom, from where I write, maintains a world-leading institutional commitment to evidence-based policy. What this "British experiment" has demonstrated is that policymakers have become adept at adhering to the *letter* of the law of evidence-based policy while systematically violating its *spirit*. One Chief Scientific Adviser recently wrote about his experiences in government, documenting how science is transformed in the "politics factory". His account of the challenges involved in navigating the politics of evidence has been echoed by scientific advisers worldwide, suggesting this is a systemic rather than an isolated problem.

* Corresponding author (b.hyde@bangor.ac.uk; https://orcid.org/0000-0002-1574-143X)

This article is published under the Creative Commons CC-BY-ND License (http://creativecommons.org/licenses/by-nd/4.0/). This license permits use, distribution and reproduction, commercial and non-commercial, provided that the original work is properly cited and is not changed in anyway.

High trust in science might therefore only reinforce existing patterns of selective evidence use. One way of looking at this is that the system won't be improved by increased public trust, but it won't be worse off either. However, there are distinct dangers introduced by increased public trust that might worsen public policymaking. Namely, not all policy decisions can be reduced to empirical questions; many involve irreducible value judgements. High public trust in science can have deleterious effects on policymaking insofar as it enables policymakers to evade necessary value-laden discussions by hiding behind "the science" they've strategically selected.

Consider as an illustrative example the medical fact that smoking shortens your life and, by any health measure, is a bad thing. It's very easy for policymakers to claim that "the evidence" unambiguously supports banning smoking because it harms health, but this framing ignores crucial non-health values that must be taken into account by the policymaker. A reduction in smoking increases longevity and older populations are significantly more expensive to look after due to the incidence of age-related illnesses. For nations with state health services like Britain and Sri Lanka, cost is an important consideration. Bioethicists have also argued that smoking has some social and moral benefits and can be personally valuable to individuals. To criminalize smoking requires an assessment of these economic and social values as well as the obvious health disbenefit that's established by the scientific literature. When trust in science is high, such value trade-offs become easier to obscure behind the veneer of scientific authority.

This has implications for the programme to increase trust in science launched by the National Academy of Sciences Sri Lanka and the Sri Lanka Association for the Advancement of Science. This initiative is timely, emerging in a context where many believe we're facing a global "crisis of trust" in institutions that's been worsening for at least forty years. However, their inquiry must avoid the simplistic assumption that both policymakers and the public are fully rational actors making considered judgements about scientific evidence. A substantial body of political science literature suggests otherwise. It should consider the potential perverse effects that increased trust in science may have on the trustworthiness of science, and vice versa. Without such consideration, well-intentioned efforts to rebuild trust may inadvertently undermine the very goals of evidence-informed policymaking they seek to advance.

REFERENCES

Abeysekera, A. (2025). Public trust in science and scientists. *Journal of the National Science Foundation of Sri Lanka*, *53*(3), 205.

Baron, J. (2018). A brief history of evidence-based policy. *Annals of the American Academy of Political and Social Science*; *678*(1), 40-50.

Bonneux, L., Barendregt, J. J., Nusselder, W. J., & Van der Maas, P. J. (1998). Preventing fatal diseases increases healthcare costs: cause elimination life table approach. *British Medical Journal*, *316*, 26.

Boyd, I. (2024). *Science and politics*. Cambridge: Polity.

Cairney, P. (2015). *The politics of evidence-based policy making.* Palgrave Macmillan.

Godfray, H. C. J. (2025). Notes from the "politics factory". *Science*, *387*, 723.

Hughes, C. E. (2007). Evidence-based policy or policy-based evidence? The role of evidence in the development and implementation of the Illicit Drug Diversion Initiative. *Drug and Alcohol Review*, *26*(4), 363-368.

Hyde, B. V. E. (2025). Lying increases trust in science. *Theory & Society, 54*(6)*,* 947-958. https://doi.org/10.1007/s11186-025-09635-1

John, S. (2017). Epistemic trust and the ethics of science communication: against transparency, openness, sincerity and honesty. *Social Epistemology*, *32*(2), 75-87.

Lubitz, J., Beebe, J., & Baker, C. (1995). Longevity and Medicare expenditures. *New England Journal of Medicine, 332*, 999-1003.

Marmot, M. G. (2004). Evidence based policy or policy based evidence? *British Medical Journal*, *328*(7445), 906-907.

Parkhurst, J. O. (2016). *The politics of evidence: from evidence-based policy to the good governance of evidence*. London: Routledge.

Strassheim, H., & Kettunen, P. (2014). When does evidence-based policy turn into policy-based evidence? Configurations, contexts and mechanisms. *Evidence & Policy*, *10*(2), 259-77.

Tyler, C. (2024). Why we need a body to oversee how science is used by governments. *Nature*, *635*, 545-546.

Valgarðsson, V., Jennings, W., Stoker, G., Bunting, H., Devine, D., McKay, L., & Klassen, A. (2025). A crisis of political trust? global trends in institutional trust from 1958 to 2019. *British Journal of Political Science*, *55*, e15.

van der Meer T. G. L. A., & Hameleers, M. (2026). Science and the crisis of trust. *Current Opinion in Psychology, 67*, 102202.

Weiss, C. H. (1977). *Using social research in public policy making*. Lexington, MA: Lexington Books.

Wilkinson, T. M. (2025). *The ethics of public health paternalism*. Oxford: Oxford University Press.

Wolff, J. (2019). *Ethics and public policy: a philosophical inquiry* (2nd ed.). London: Routledge.

J.Natn.Sci.Foundation Sri Lanka 2025 53 (4): 311 - 315
DOI: http://dx.doi.org/10.4038/jnsfsr.v53i4.12668

RESEARCH ARTICLE

Gravity modeling

A technique for extracting gravity anomalies originating from sediments deposited on folded oceanic crust

DA Tantrigoda[1*], MMPM Fernando[1] and SA Samaranayake[2]
[1] *Department of Physics, Faculty of Applied Sciences, University of Sri Jayewardenepura, Nugegoda.*
[2] *Department of Physical Sciences, Faculty of Applied Sciences, Rajarata University of Sri Lanka, Mihinthale.*

Submitted: 05 May 2025; Revised: 05 November 2025; Accepted: 27 November 2025

Abstract: Negative gravity anomalies observed over sediments accumulated on folded oceanic crust are usually caused by two negative density contrasts. The first is the contrast between low-density sediments lying on folded high-density oceanic crust and the second is the contrast between low-density oceanic crust immersed into the high-density upper mantle. Because the anomaly is caused by two regions with different densities, modeling it is not straightforward. Most standard methods only allow for modeling bodies with a single density contrast. This paper describes a Fourier technique to separate the anomaly caused by the sediment distribution facilitating its modeling using a standard method. It is assumed that the oceanic crust over the region under consideration has a constant thickness and that the densities of sediments, oceanic crust, and upper mantle are constant. The technique was tested with artificially generated negative gravity anomalies for a hypothetical case and found to work satisfactorily. Even though the two-dimensional version of the technique is described here for the sake of convenience, it can readily be extended to the three-dimensional case.

Keywords: Fourier transforms, gravity anomaly, inverse method, oceanic crust, sediments, upper mantle.

INTRODUCTION

Folding is one of the phenomena responsible for the Earth's present outward appearance with large-scale folding being a key mechanism of lithospheric deformation (McAdoo and Sandwell, 1985, Cloetingh et al., 2002, Munoz-Martin et al., 2010, Xie et al., 2024). Such folds can be seen in both continental and oceanic regions generally filled with sediments that create negative gravity anomalies. In continental regions, the negative anomaly is due to the density contrast between low density sediments and relatively high-density continental crust. However, in oceanic regions the anomaly is caused by two independent density contrasts (Altınoğlu et al., 2023). The first is the density contrast between sediments and folded oceanic crust, while the second is the density contrast between low-density oceanic crust folded into the upper mantle replacing the upper mantle material (Liu et al., 1982). This second component is also negative, but usually smaller than the first. When modeling this anomaly, it is necessary to consider that both source regions and the model will have two density contrasts. Most standard inversion techniques can only model gravity anomalies caused by a single density contrast (Talwani et al., 1959, Parker, 1973, Nagendra et al., 1996, Chakravarthi et al., 2002). Therefore, these methods cannot directly model gravity anomalies due to folded oceanic crust filled with sediments. This paper describes a method to separate the anomaly caused by the sediments from the total observed anomaly, making it easier to interpret using standard inversion techniques.

* Corresponding author (dhammika@tantrigoda.net; https://orcid.org/0000-0002-9046-1999)

This article is published under the Creative Commons CC-BY-ND License (http://creativecommons.org/licenses/by-nd/4.0/). This license permits use, distribution and reproduction, commercial and non-commercial, provided that the original work is properly cited and is not changed in anyway.

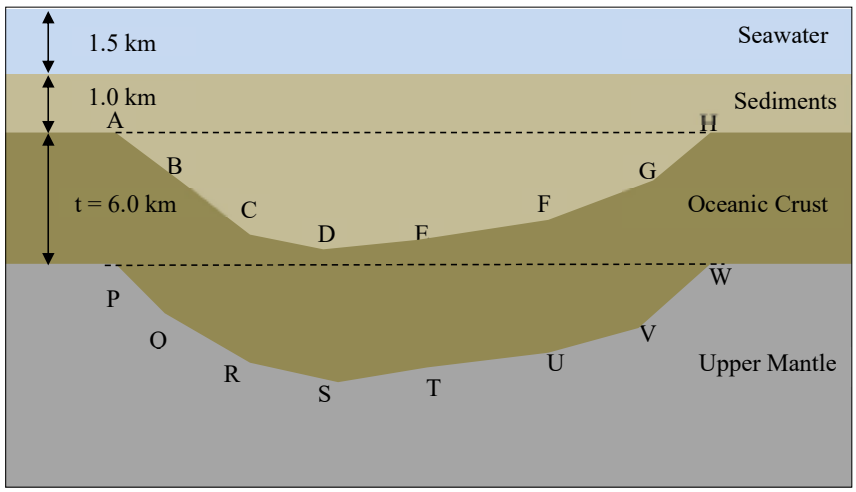

Figure 1: Sediments lying on folded oceanic crust.

METERIALS AND METHODS

Figure 1 shows a folded region of oceanic crust of thickness *t* filled with low density sediments. We assume that sediments lying above those trapped in the fold form a horizontal infinite slab. This slab and the water column above it, which also usually takes the form of an infinite slab, create a constant anomaly over and around the basin without contributing to the observed anomaly. Therefore, it is not necessary to consider these factors in the modelling process.

Let us consider a two-dimensional Cartesian coordinate system with the X-axis along the sea level and the Z-axis pointing vertically downward. Let $\Delta g_1(x,0)$ and $\Delta g_2(x,0)$ be the anomalies caused by the closed regions ABCDEFGHA and PQRSTUVWP (Figure 1), respectively, at sea level. The anomaly $\Delta g_1(x,0)$ is caused due to the density contrast between sediments and the oceanic crust while anomaly $\Delta g_2(x,0)$ is caused due to the density contrast between oceanic crust and the upper mantle material. If $\Delta g(x,0)$ is the total anomaly observed at sea level, then,

$$\Delta g(x,0) = \Delta g_1(x,0) + \Delta g_2(x,0) \quad ...(1)$$

Since we assume that the oceanic crust has a constant thickness, both ABCDEFGHA and PQRSTUVWP have the same geometry. If both regions have the same density contrast, then the gravity anomaly produced by ABCDEFGHA at a height *t* above the sea level is equal to the gravity anomaly produced by PQRSTUVWP at sea level. This means that the anomaly $\Delta g_2(x,0)$ would be equal to the anomaly $\Delta g_1(x,0)$ upward continued by a height *t* $(\Delta g_1(x,t))$ provided both bodies have the same density contrast. However, the body ABCDEFGHA has a density contrast of $(\rho_c - \rho_s)$ while the body PQRSTUVWP has a density contrast of $(\rho_m - \rho_c)$, where ρ_s, ρ_c and ρ_m are densities of sediments, oceanic crust, and upper mantle, respectively. Therefore, the anomaly $\Delta g_2(x,0)$ can be written as,

$$\Delta g_2(x,0) = \left(\frac{\rho_m - \rho_c}{\rho_c - \rho_s}\right) \Delta g_1(x,t) \quad ...(2)$$

Since Δg, Δg_1 and Δg_2 satisfy the Laplace's equation in Cartesian coordinates,

$$\Delta g(x,0) = \sum_k F(k)\, Exp(-ikx) \quad ...(3)$$

$$\Delta g_1(x,0) = \sum_k F_1(k)\, Exp(-ikx) \quad ...(4)$$

$$\Delta g_1(x,t) = \sum_k F_1(k)\, Exp(-ikx) Exp(-kt) \quad ...(5)$$

where, $F(k)$ and $F_1(k)$ are complex Fourier coefficients, k denotes the wave number and $\Delta g_1(x,t)$ is the anomaly $\Delta g_1(x,0)$ upward continued by a height *t*.

Substituting for $\Delta g_1(x,t)$ from (5) in (2),

$$\Delta g_2(x,0) = \left(\frac{\rho_m - \rho_c}{\rho_c - \rho_s}\right) \sum_k F_1(k) Exp(-ikx) Exp(-kt) \quad ...(6)$$

Substituting for Δg, Δg_1 and Δg_2 from (3), (4) and (6) in (1) and rearranging terms,

$$F_1(k) = \frac{F(k)}{1+\left(\frac{\rho_m-\rho_c}{\rho_c-\rho_s}\right)Exp(-kt)} \quad ...(7)$$

Using the above relationship, $F_1(k)$ can be calculated for all k values as $F(k)$ is the Fourier coefficients of the observed anomaly, which is a known quantity. The inverse Fourier transform of $F_1(k)$ will give the component of the gravity anomaly due to the sediments filled in the folded oceanic crust.

Testing of the method

Gravity anomaly due to the two-dimensional structure shown in Figure 1 was calculated using the method described by Talwani et al., (1959). This was performed by calculating the anomaly caused by the density contrast between sediments and oceanic crust and that due to the density contrast between the oceanic crust and upper mantle separately, and then adding them together. Density values used were 2300 kgm^{-3}, 2900 kgm^{-3} and 3300 kgm^{-3} for sediments, oceanic crust and the upper mantle, respectively (Bott, 1971; Woollard, 1959).

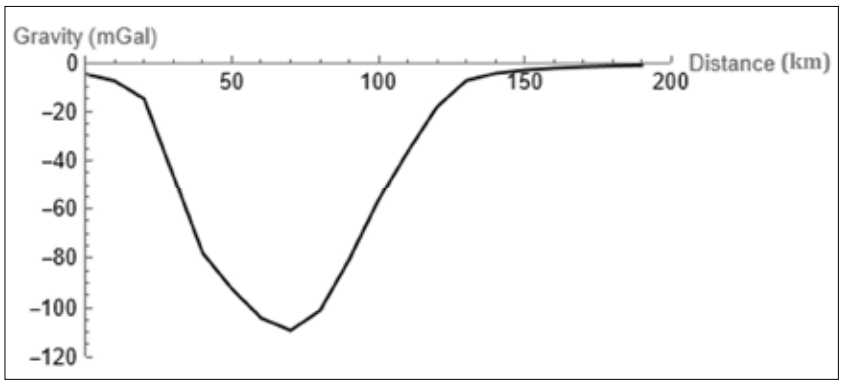

Figure 2: Directly calculated gravity anomaly due to the two source regions

The total anomaly directly calculated from the two source regions is shown in Figure 2. The anomaly attributed to the sediments in the folded oceanic crust was determined by extracting it from the total anomaly using the method described here (Figure 3). This anomaly was then compared with the directly calculated anomaly attributed to the same body with the results given in Figure 4. It is evident that these two anomalies are remarkably close to each other and the root mean square difference between two anomalies is 0.99 mGal**.**

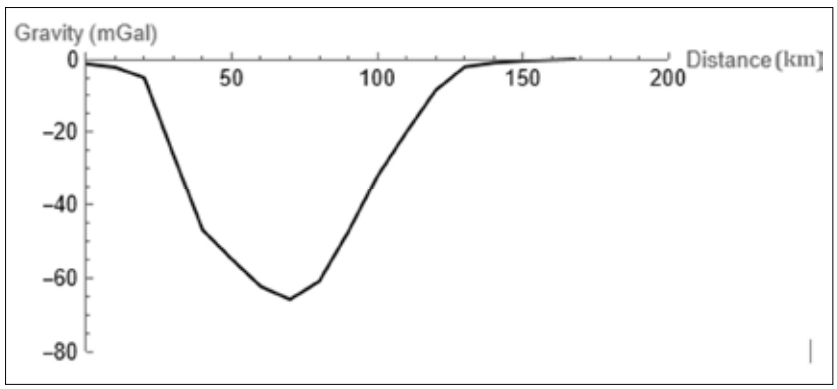

Figure 3: The anomaly due to the sediments in the folded oceanic crust, extracted from the method described in this paper

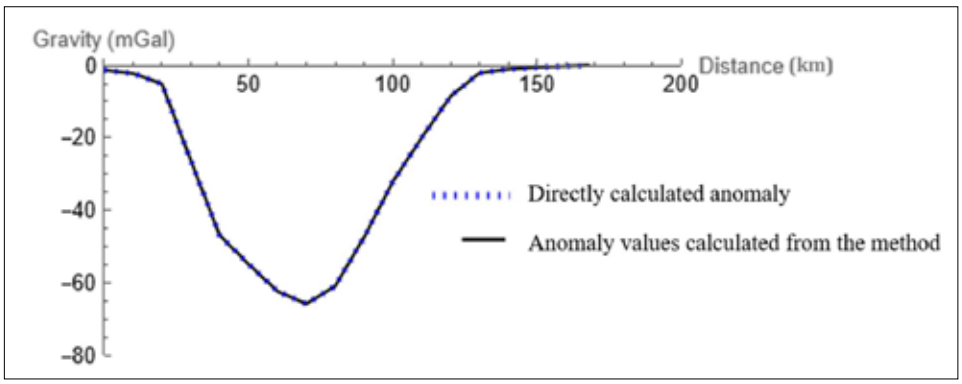

Figure 4: Comparison of gravity anomalies due to sediments obtained using the new technique with directly calculated anomaly due to the same body

Extension to the three-dimensional case

The above method can easily be extended to anomalies caused by three-dimensional sedimentary basins formed as a result of the accumulation of sediments in folded oceanic crust partly immersed in the upper mantle. Let $\Delta g(x,y,0)$ be the gravity anomaly measured over a rectangular region over the basin at sea level and $\Delta g_1(x,y,0)$ be the anomaly due to the sediments trapped in the basin over the same region. Let $F(k_x,k_y)$ and $F_1(k_x,k_y)$ be their Fourier transforms and symbols k_x and k_y denote wave numbers corresponding to x and y directions. Following a series of steps similar to those followed in the two-dimensional case, it can be shown that,

$$F_1(k_x,k_y) = \frac{F(k_x,k_y)}{1 + \left(\frac{\rho_m - \rho_c}{\rho_c - \rho_s}\right) Exp\left\{-\left({k_x}^2 + {k_y}^2\right)^{1/2} t\right\}} \quad ...[8]$$

It is possible to extract the Fourier transform of the gravity anomaly $\Delta g_1(x,y,0)$ starting from the Fourier transform of the observed anomaly using the above equation and hence the anomaly due to the sediments.

RESULTS AND DISCUSSION

A method for extracting the component of the gravity anomaly caused by sediments lying on folded oceanic crust is presented. This method utilises the fact that two regions contributing to the anomaly (Figure 1) have the same geometry, which is a direct result of assuming the oceanic crust has a constant thickness. A test conducted with a gravity anomaly due to a known structure demonstrates that the method works satisfactorily.

An important assumption made in the method's formulation is that the thickness of oceanic crust is constant. Normally, a thickness of 6 km is assumed as the average value in calculations related to oceanic regions. To determine the impact of varying crust thickness from this value, a test was conducted in the frequency domain. Let $F_t(k)$ be the Fourier transform of the gravity anomaly due to the sediments extracted using equation (7) when the thickness of oceanic crust is 't' while $F_6(k)$ is the Fourier transform of the gravity anomaly due to the same sediments extracted using the same equation assuming the thickness of the oceanic crust is 6 km. The fractional error caused due to this assumption can be written using (7) as,

$$\frac{F_t(k) - F_6(k)}{F_t(k)} = 1 - \frac{1 + \left(\frac{\rho_m - \rho_c}{\rho_c - \rho_s}\right) Exp(-kt)}{1 + \left(\frac{\rho_m - \rho_c}{\rho_c - \rho_s}\right) Exp(-k6)} \quad ...[9]$$

The above fractional error and hence the percentage error were calculated for the Fourier coefficients for an anomaly that extends over a range of 200 km sampled at 10 km intervals with the thickness values of t equal to 1, 2, 3…….10 km. These calculations show that the Fourier coefficients can be calculated satisfactorily when the actual thickness t is in the range of 4 to 9 km. It was also noted that the highest error, amounting to 11%, occurs when the thickness t is 4 km for the k value corresponding to 20 km. For all the other coefficients, the error is less when t lies in the above range. Additionally, it was observed that the error is significantly lower for small k values corresponding to long wavelengths. Therefore, the assumption that the thickness of oceanic crust is 6 km had a noticeable effect only on the low wavelength features rather than the long wavelength features. The overall

shape determined by long and intermediate level features is not affected much by this assumption. This illustrates that using 6 km as the thickness of the oceanic crust does not lead to a serious error, and the proposed method generally provides satisfactory results.

In this method, it was also assumed that the thickness of sediments lying above the sediments trapped in the folded oceanic crust is of constant thickness and does not contribute to the observed anomaly. However, it is possible for these sediments to take the shape of a small-angled wedge, which can generate a gravity anomaly. In such a situation, the anomaly due to the wedged shaped sediments could be removed and the method can be still used.

CONCLUSION

Based on the results of several tests conducted, it can be generally concluded that the method described in this paper works satisfactorily. This method may also have useful applications in the interpretation of gravity anomalies caused by folded layered structures with approximately parallel sides in continental areas.

REFERENCES

Altınoğlu, F.F., Sarı, C. & Şalk, M. 2023. 'Mapping of the structural lineaments and sedimentary basin depth in the Denizli Graben (Western Anatolia) from Bouguer gravity data', *Minerals*, *13*(10), p.1276. doi:10.3390/min13101276.

Bott, M.H.P. 1971. Interior of the Earth. McGraw Hill, Edward Arnold, London.

Chakravathi, V., Raghuram, H. & Singh, S. 2002. 3-D forward gravity modeling of basement interfaces above which the density contrast varies continuously with depth. *Computers & Geosciences, 28*, 53-57.

Cloetingh, S.A.P.L., Burov, E., Beekman, F., Andeweg, B., Andriessen, P.A.M., Garcia-Castellanos, D., De Vicente, G. and Vegas, R., 2002. Lithospheric folding in Iberia. *Tectonics*, *21*(5), pp.5-1.

Liu, C. S., Sandwell, D. T. & Curray, J. R. 1982. The negative gravity field over the 85 E Ridge. *Journal of Geophysical Research: Solid Earth, 87*, 7673-7686.

McAdoo, D.C., Sandwell, D.T., 1985. Folding of oceanic lithosphere. J. Geophys. Res. 90 (B10), 8563–8569.

Muñoz-Martín, A., De Vicente, G., Fernández-Lozano, J., Cloetingh, S.A.P.L., Willingshofer, E., Sokoutis, D. and Beekman, F., 2010. Spectral analysis of the gravity and elevation along the western Africa–Eurasia plate tectonic limit: Continental versus oceanic lithospheric folding signals. *Tectonophysics*, *495*(3-4), pp.298-314.

Nagendra, R., Prasad, P. & Bhimasankaram, V. 1996. Forward and inverse computer modeling of a gravity field resulting from a density interface using Parker-Oldenberg method. *Computers & Geosciences, 22*, 227-237.

Parker, R. 1973. The rapid calculation of potential anomalies. *Geophysical Journal International,* 31, 447-455.

Talwani, M., Worzel, J. L. & Landisman, M. 1959. Rapid gravity computations for two-dimensional bodies with application to the Mendocino submarine fracture zone. *Journal of geophysical research, 64*, 49-59.

Woollard, G. P., 1959. Crustal structure from gravity and seismic measurements, Journal of Geophysical Research, Vol. 64, No. 10, 1521-1545.

Xie, R., Chen, F., Li, S. & Zhao, Q. 2024. 'Various lithospheric deformation patterns derived from continental collision: Insights from rheology and structure', *Solid Earth*, *15*, pp. 789–804. doi:10.5194/se-15-789-2024.

J.Natn.Sci.Foundation Sri Lanka 2025 53 (4): 317 - 331
DOI: http://dx.doi.org/10.4038/jnsfsr.v53i4.12645

RESEARCH ARTICLE

Graph Theory

An upper bound for star chromatic index of simple connected sub-cubic graphs and applications

CLR Fernando* **and AMCUM Athapattu**
Department of Mathematics, Faculty of Science, University of Peradeniya, Peradeniya.

Submitted: 24 April 2025; Revised: 22 July 2025; Accepted: 29 July 2025

Abstract: This paper explores the star edge coloring of simple connected sub-cubic graphs, which is a more restricted way of edge coloring. The idea of star edge coloring was introduced by two mathematicians Liu and Deng in 2008, motivated by its vertex version. Since then, star edge coloring has been studied extensively by many researchers. Computing the star chromatic index $\chi'_{st}(G)$ for a graph G is a challenging problem, and finding an algorithm for it is an active area of research in graph theory. So, numerous studies have been conducted introducing upper bounds for the star chromatic index. One of the primary objectives of this research is to establish a better upper bound for the star chromatic index of simple connected sub-cubic graphs, partially answering the conjecture in Lužar et al., 2017, posed by Dvorak, et al. in 2013: "If G is a sub-cubic graph, then $\chi'_{st}(G) \leq 6$". The method of star edge coloring for 2-connected graphs, used in this paper mainly based on the decomposition of the graph into a matching and a 2-factor. That can also be expanded into real-world situations, like branching companies, and planning cities.

Keywords: 2-connected graphs, simple graphs, star chromatic index, star edge coloring, sub-cubic graphs.

INTRODUCTION

Graph theory provides the very foundation for modern mathematics, which furnishes a simple and appropriate framework through which problems containing relationships and connections between individuals or things could be modeled and resolved. Since its inception with the great Swiss mathematician Leonhard Euler's solution to the famous Koningsberg bridge problem in 1736, graph theory has developed into a cornerstone of modern mathematics, fostering both pure and applied mathematics.

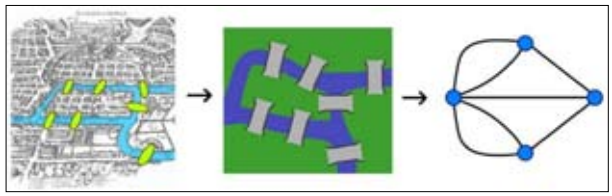

Figure 1: Graph Theory approach for the Koningsberg bridge problem

Definition 1. A simple graph G is a pair $(V(G), E(G))$ where $V(G)$ is a non-empty finite set of distinct vertices and $E(G)$ is a set of edges with no multi-edges or loops.

Definition 2. A cycle is a closed path in which the only vertex that repeats is the starting vertex.

Definition 3. A graph is called connected if it cannot be expressed as a union of disjoint graphs.

* Corresponding author (lakshithaf@sci.pdn.ac.lk; https://orcid.org/0009-0004-5716-8231)

This article is published under the Creative Commons CC-BY-ND License (http://creativecommons.org/licenses/by-nd/4.0/). This license permits use, distribution and reproduction, commercial and non-commercial, provided that the original work is properly cited and is not changed in anyway.

A graph is called 2-connected if the graph obtained by deleting a vertex with its incident edges is also connected.

Definition 4. A simple graph in which every vertex has the same degree is called regular.

Definition 5. A 3-regular graph is called cubic, and a graph with maximum degree 3 is called sub-cubic (Lužar et al., 2017).

Among the many topics that fall under the wide scope of graph theory, one of the most popular and significant is graph coloring, which is an assignment of "colors" to elements of a graph according to some given constraints. The interesting problems of graph coloring originated in a question concerning the coloring of regions on a map which led to the four-color problem. It was solved in 1976 and introduced the well-known four-color theorem by Appel, Haken, and Koch.

Theorem 1. (Four-Color Theorem) (Bona, 2016) Every simple planar graph is 4-colorable

Definition 6. An edge coloring of a graph is a function assigning colors to the edges of the graph in such a way that any two adjacent edges receive different colors (Verma & James, 2019).

The chromatic index of a graph G, $\chi(G)$ is the minimum k such that G is edge k-colorable.

A graph G is considered to be properly vertex (or edge) colored if two adjoining vertices (or edges) are colored uniquely. Star coloring introduced by Grunbaum (1973) is a path-based coloring in which no path of length 3 is bi-colored. The name "star coloring" was derived from the fact that in a star coloring, the induced sub-graphs formed by the vertices of any two colors have connected components that are star graphs.

Definition 7. A star coloring is a proper vertex coloring in which there are no bi-colored paths or cycles on more than 3 vertices. Star chromatic number, $\chi_{st}(G)$ is the minimum k such that G admits a k-star-coloring (Horacek, 2019).

Following this, Fertin et al. (2004) observed that in a star vertex coloring any bi-chromatic subgraph is in the form of a galaxy. Where a galaxy is a forest composing only of stars according to Gallian (2022). This coloring was introduced along with the acyclic coloring of graphs and several results of star coloring in comparison with the acyclic coloring of graphs can be noted in Albertson et al. (2004) and Brause et al. (2022). A similar concept to star coloring, but applied to the edges, was introduced by Liu and Deng (2007).

Definition 8. Let $f: E(G) \rightarrow [k]$ be a proper edge coloring of a graph G. If f is a star (vertex) coloring of $L(G)$, then f is a star edge coloring of G. (Horacek, 2019).

Equivalently, a proper edge coloring of a graph G is called a star edge coloring if there are neither bi-chromatic paths nor bi-chromatic cycles of length four. (Bezegova et al., 2013; Lužar et al., 2017)

The minimum number of colors for which G admits a star edge coloring is called the star chromatic index and it is denoted by $\chi'_{st}(G)$.

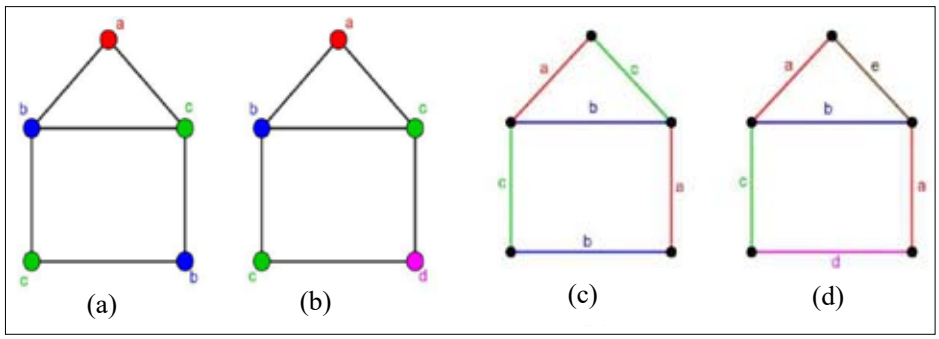

Figure 2: (a)Vertex coloring, (b)Star vertex coloring, (c)Edge coloring and (d)Star edge coloring of the House graph

In (a), the rectangle forms a cycle of 4 vertices which is bi-colored. Hence it is not a star vertex coloring. To obtain a star vertex coloring, the color of the bottom right vertex is changed as shown in (b). Hence, $\chi_{st}(G) = 4$.

In (c), there are two paths of length 4 which are bi-colored (the red-blue path and green-blue path). Hence it is not a star edge coloring. To obtain a star edge coloring, the colors of two edges are changed (one from each bi-colored path) as shown in (d). Hence $\chi'_{st}(G) = 5$.

Through the years, several results and theorems have emerged in said topic which can be seen in Bezegova et al. (2016), Lei and Shi (2020), Casselgren et al. (2021), and Evangeline Lydia and Vijaya Xavier Parthipan (2022), etc.

In 2007 and 2008, the pioneers of star edge coloring Liu & Deng worked on finding upper bounds for some types of graphs. Also, they gave an upper bound for any graph of the maximum degree Δ.

Theorem 2. For the path graph P_n $(n \geq 2)$ and the cycle graph C_n $(n \geq 3)$ (Lužar et al., 2017),

$$\chi'_{st}(P_n) = \begin{cases} 1, & n = 2 \\ 2, & n = 3,4 \\ 3, & n \geq 5 \end{cases} \quad \text{and} \quad \chi'_{st}(C_n) = \begin{cases} 3, & n \neq 5 \\ 4, & n = 5 \end{cases}$$

For any integer $n \geq 4$, the wheel graph W_n (resp. the fan graph F_n) is the n-vertex graph obtained by joining a vertex to each of the $n-1$ vertices of the cycle graph C_{n-1} (resp. the path graph P_{n-1}). (Lei & Shi, 2020)

Theorem 3. For W_n $(n \geq 4)$ and F_n $(n \geq 4)$ (Lužar et al., 2017),

$$\chi'_{st}(W_n) = \begin{cases} n+2, & n = 5 \\ n+1, & n = 4,6,7 \\ n-1, & n \geq 8 \end{cases} \quad \text{and}$$

$$\chi'_{st}(F_n) = \begin{cases} n+1, & n = 5 \\ n, & n = 3,4,6,7 \\ n-1, & n \geq 8 \end{cases}$$

Theorem 4. Let G be a graph with maximum degree $\Delta \geq 7$. Then, $\chi'_{st}(G) \leq \lceil 16(\Delta-1)^{3/2} \rceil$ (Liu & Deng, 2008).

Theorem 5. Every graph G with $\Delta = 4$ satisfies $\chi'_{st}(G) \leq 14$ (Wang et al., 2019).

In 2013, Dvorak et al. worked on finding an upper bound for star chromatic index of complete graphs and later by Melinder (2020) and Casselgren et al. (2021) developed that upper bound.

Theorem 6. The star chromatic index of the complete graph K_n satisfies (Dvořák et al., 2013).

$$2n(1+O(1)) \leq \chi'_{st}(K_n) \leq n\frac{2^{2\sqrt{2}(1+O(1))\sqrt{\log n}}}{(\log n)^{1/4}}$$

Theorem 7. If G is a bipartite graph, then $\chi'_{st}(G) \leq \Delta^2 - \Delta + 1$ (Melinder, 2020).

Theorem 8. For any bipartite graph $K_{r,d}$ with $r, d \geq 1$, $\chi'_{st}(K_{r,d}) \leq 15\lceil d/8 \rceil \lfloor r/8 \rfloor$ (Casselgren et al., 2021).

The girth of a graph with a cycle is the length of its shortest cycle. A graph with no cycle has infinite girth (Lei & Shi, 2020).

Theorem 9. Let G be a sub-cubic planar graph with girth at least 7. If G has a perfect matching, then $\chi'_{st}(G) \leq 6$ (Casselgren et al., 2021).

In 2016, Bezegova et al. worked on star edge coloring of trees, and outerplanar graphs. A **tree** is a connected undirected graph with no cycles.

Theorem 10. Let T be a tree with maximum degree Δ. Then $\chi'_{st}(G) \leq \left\lfloor \frac{3}{2}\Delta \right\rfloor$ (Bezegova et al., 2013).

Theorem 11. Let T be a sub-cubic tree. Then $\chi'_{st}(G) \leq 4$ (Bezegova et al., 2013).

A graph G is outerplanar if and only if it contains no subgraph homeomorphic to K_4 or $K_{2,3}$ except $K_4 - x$, where x denotes an edge of K_4 (Syszo, n.d.).

Theorem 12. Let G be an outer-planar sub-cubic graph. Then $\chi'_{st}(G) \leq 5$ (Bezegova et al., 2013).

A cactus is a connected graph H such that any two cycles in H have at most one vertex in common, and hence, in the case of sub-cubic graphs, any two cycles in H are vertex-disjoint.

A cactus is a (multi)graph in which every block is a cycle or an edge (Das, n.d.).

Theorem 13. If G is a cactus with maximum degree Δ, then $\chi'_{st}(T) \leq \left\lfloor \frac{3}{2}\Delta \right\rfloor + 1$ (Omoomi et al., 2019).

In 2013, Dvorak et al. introduced the best known upper bound for star chromatic index of sub-cubic graphs, and referring to that in 2019, Luzar et al. obtained the best known upper bound for list star chromatic index of sub-cubic graphs. Those two theorems and their proofs are the main references used to find the new best upper bound for star chromatic index in this work.

Theorem 14. If G is a sub-cubic graph, then $\chi'_{st}(G) \leq 7$ (Dvořák et al., 2013).

Dvorak et al. (2013) observed that all sub-cubic graphs they have encountered could be colored using only 6 colors. So, they posed the following conjecture and problems.

Conjecture 1. If G is a sub-cubic graph, then $\chi'_{st}(G) \leq 6$.

Question 1. Is it true that $ch'_{st}(G) \leq 7$ for every sub-cubic graph G? (Perhaps even ≤ 6?)

Question 2. Is it true that $ch'_{st}(G) = \chi'_{st}(G)$ for every graph G?

The Question 1 is explicitly proved in (Lužar et al., 2017). The concepts they used and the observations we made are discussed below.

Theorem 15. If G is a sub-cubic graph, then $ch'_{st}(G) \leq 7$ (Lužar et al., 2017).

Theorem 16. Let G be a sub-cubic graph without bridges and with at most one vertex of degree at most 2. Then, there is a matching M that covers all vertices of degree 3 (Lužar et al., 2017).

Note that a set of edges that do not have common vertices is called a matching and a 2-factor graph is a subgraph of a given graph which contains disjoint cycles. A connector (aka bridge) is a single edge that connects two cycles.

The supergraph $\hat{G}$ of a 2-connected sub-cubic graph G is the graph obtained by introducing edges between pairs of vertices of degree 2 in G until it contains at most one vertex of degree 2 (multiple edges are valid but not loops) (Lužar et al., 2017).

Since there is always an even number of odd vertices in a graph, an eventual vertex v of degree 2 from the Theorem 16 is never covered by M' and hence, as an immediate corollary of the above we have that $\hat{G}$ contains a 2-factor F where, clearly, v is a part of a cycle. Connecting the cycles of F with the minimum number of edges of M such that the resulting graph is connected, we obtain a spanning cactus ψ of $\hat{G}$.

Theorem 17. A supergraph $\hat{G}$ of any 2-connected sub-cubic graph G can be decomposed into a spanning cactus ψ and a matching M' such that every vertex of $\hat{G}$ is contained in some cycle of ψ (Lužar et al., 2017).

Observation 1. Referring to the proof of Theorem 17, for any connected sub-cubic graph G, obtain the supergraph $\hat{G}$, decompose it into a spanning cactus ψ and a matching M'. Color the edges in M' so that edges at distance at most 2 receive distinct colors. Since there are at most 4 edges of M'at distance 2 from any $e \in E(M')$, at most 4 colors are needed to color M'. Hence, it is possible to color the cactus if there are 3 remaining colors after the matching is colored, as any cycle (except C_5) can be star edge colored with 3 colors. So, the method in (Lužar et al., 2017) is possible if there are 7 colors. But for 6 colors, this would not work as any cycle cannot be star edge colored with only 2 colors.

Algorithm for star edge coloring of a simple connected sub-cubic graph

Let $\mathcal{Q}_3$ be the collection of simple connected sub-cubic graphs. For $G \in \mathcal{Q}_3$,

- Step I: Obtain a collection of disjoint cycles $\mathcal{C}(G)$ (or a collection of disjoint cycles and paths) such that each vertex of G is contained in exactly one cycle (or path) $C \in \mathcal{C}(G)$. Let $\mathcal{M}(G)$ be the collection of remaining edges of G (which contains paths of length at most 2) such that $E(\mathcal{C}(G)) \cup E(\mathcal{M}(G)) = G$ and $E(\mathcal{C}(G)) \cap E(\mathcal{M}(G)) = \emptyset$.
- Step II: Color $e_{mi}, e_{mj} \in E(\mathcal{M}(G))$ such that if $d(e_{mi}, e_{mj}) \leq 2$, both edges get distinct colors, say α_k for $k \leq 6$.
- Step III:
  - Use the same α_k color of $e_{mi} \in E(\mathcal{M}(G))$ for $e_{ci} \in E(\mathcal{C}(G))$ where $d(e_{mi}, e_{ci}) \geq 3$.
  - Color the possible edges of $\mathcal{C}(G)$ using α_k colors such that $\nexists\, e_i, e_j \in E(G)$ with $d(e_i, e_j) \leq 2$ having the same color.
  - Color the remaining edges considering star edge coloring conditions using $\{\alpha_1, \alpha_2, \alpha_3, \alpha_4, \alpha_5, \alpha_6\}$ colors. This is always possible according to the Theorem 2.

Algorithm for the coloring of $\mathcal{M}(G)$:

Define $f: E\big(\mathcal{M}(G)\big) \to \{\alpha_k\}$ where $1 \leq k \leq 6$.

- Let $f(e_{m1}) = \alpha_1$.
- If $d(e_{m1}, e_{m2}) \geq 3$, $f(e_{m2}) = \alpha_1$.
  - If $d(e_{m1}, e_{m3}) \geq 3$, $d(e_{m2}, e_{m3}) \geq 3$, $f(e_{m3}) = \alpha_1$.
    - If $d(e_{m1}, e_{m4}) \geq 3$, $d(e_{m2}, e_{m4}) \geq 3$, $d(e_{m3}, e_{m4}) \geq 3$, $f(e_{m4}) = \alpha_1$.
    - If $d(e_{m1}, e_{m4}) \leq 2$, $d(e_{m2}, e_{m4}) \geq 3$, $d(e_{m3}, e_{m4}) \geq 3$, $f(e_{m4}) = \alpha_2$.
    - If $d(e_{m1}, e_{m4}) \geq 3$, $d(e_{m2}, e_{m4}) \leq 2$, $d(e_{m3}, e_{m4}) \geq 3$, $f(e_{m4}) = \alpha_2$.
    - If $d(e_{m1}, e_{m4}) \geq 3$, $d(e_{m2}, e_{m4}) \geq 3$, $d(e_{m3}, e_{m4}) \leq 2$, $f(e_{m4}) = \alpha_2$.
    - If $d(e_{m1}, e_{m4}) \leq 2$, $d(e_{m2}, e_{m4}) \leq 2$, $d(e_{m3}, e_{m4}) \geq 3$, $f(e_{m4}) = \alpha_2$.
    - If $d(e_{m1}, e_{m4}) \leq 2$, $d(e_{m2}, e_{m4}) \geq 3$, $d(e_{m3}, e_{m4}) \leq 2$, $f(e_{m4}) = \alpha_2$.
    - If $d(e_{m1}, e_{m4}) \geq 3$, $d(e_{m2}, e_{m4}) \leq 2$, $d(e_{m3}, e_{m4}) \leq 2$, $f(e_{m4}) = \alpha_2$.
    - If $d(e_{m1}, e_{m4}) \leq 2$, $d(e_{m2}, e_{m4}) \leq 2$, $d(e_{m3}, e_{m4}) \leq 2$, $f(e_{m4}) = \alpha_2$.
  - If $d(e_{m1}, e_{m3}) \leq 2$, $d(e_{m2}, e_{m3}) \geq 3$, $f(e_{m3}) = \alpha_2$.
  - If $d(e_{m1}, e_{m3}) \geq 3$, $d(e_{m2}, e_{m3}) \leq 2$, $f(e_{m3}) = \alpha_2$.
  - If $d(e_{m1}, e_{m3}) \leq 2$, $d(e_{m2}, e_{m3}) \leq 2$, $f(e_{m3}) = \alpha_2$.
- If $d(e_{m1}, e_{m2}) \leq 2$, $f(e_{m2}) = \alpha_2$.
  - If $d(e_{m1}, e_{m3}) \geq 3$, $d(e_{m2}, e_{m3}) \geq 3$, $f(e_{m3}) = \alpha_1 \; or \; \alpha_2$.
  - If $d(e_{m1}, e_{m3}) \leq 2$, $d(e_{m2}, e_{m3}) \geq 3$, $f(e_{m3}) = \alpha_2$.
  - If $d(e_{m1}, e_{m3}) \geq 3$, $d(e_{m2}, e_{m3}) \leq 2$, $f(e_{m3}) = \alpha_1$.
  - If $d(e_{m1}, e_{m3}) \leq 2$, $d(e_{m2}, e_{m3}) \leq 2$, $f(e_{m3}) = \alpha_3$.

An upper bound for star chromatic index of simple connected sub-cubic graphs

Here, we present the theorem regarding the new upper bound for the star chromatic index of simple connected sub-cubic graphs ($G \in Q_3$) and develop an extended proof using the concepts in (Lužar et al., 2017).

Theorem 18. If G is a simple connected sub-cubic graph, then $\chi'_{st}(G) \leq 6$.

Definition 9. Define the distance between two edges $e_1, e_2 \in E(G)$ by $d(e_1, e_2) = N + 1$ where N is the number of edges between e_1 and e_2 in the shortest path.

Lemma 1. Let G_0 be the 3-regular graph of 10 vertices such that $v_i v_j \in E(G_0)$ for $v_i \in V(G_0)$ for $i = 0, 1, \ldots, 9$ whenever $j = \begin{cases} i+1, i+7, i+9 : i - even \\ i+1, i+3, i+9 : i - odd \end{cases}$ under $modulo\ 10$. Then $\chi'_{st}(G) \leq 6$.

Proof: Let G_0 be the 3-regular graph with 10 vertices satisfying the condition; $v_i v_j \in E(G_0)\ for\ v_i \in V(G_0)$ for $i = 0, 1, \ldots, 9$ whenever $j = \begin{cases} i+1, i+7, i+9 : i - even \\ i+1, i+3, i+9 : i - odd \end{cases}$ under $modulo\ 10$.

Since $\deg(v) = 3$ for all $v \in V(G_0)$, G_0 is a supergraph. According to Theorem 17, G_0 can be decomposed into a cactus and a matching. Consider the decomposition of G_0 into the cycle $C(G_0)$ that contains each vertex, and the matching $M(G_0)$ consisting of five disjoint edges as shown in Figure 3. Observe that $d(e_i, e_j) = 2$ for all e_i, e_j in either $M(G_0)$ or $C(G_0)$ whenever $d(e_i, e_j) \neq 1$. For $M(G_0)$, follow the Step II in the previous algorithm. Since $d(e_i, e_j) = 2$ for all $e_i, e_j \in \mathrm{E}(\mathrm{M}(\mathrm{G}_0))$, assign five distinct colors $\{a, b, c, d, e\}$. Color the possible edges in $C(G_0)$ according to the Step III in the algorithm. While coloring, it is necessary to maintain the condition that $e_i, e_j \in \mathrm{E}(\mathrm{C}(\mathrm{G}_0))$ get distinct colors whenever $d(e_m, e_c) = 3$. Then, for the remaining five non-adjacent edges of $C(G_0)$ use a different color. This will give a star edge coloring for G_0 as shown in Figure 4.

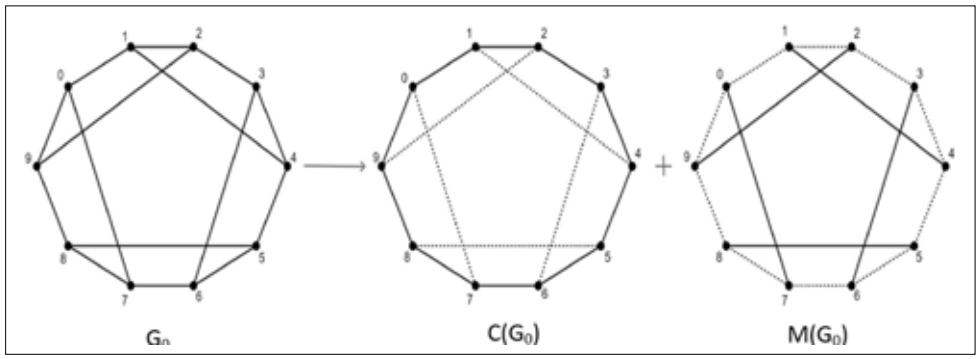

Figure 3: Decomposition of G_0 into the cycle $C(G_0)$ and the matching $M(G_0)$

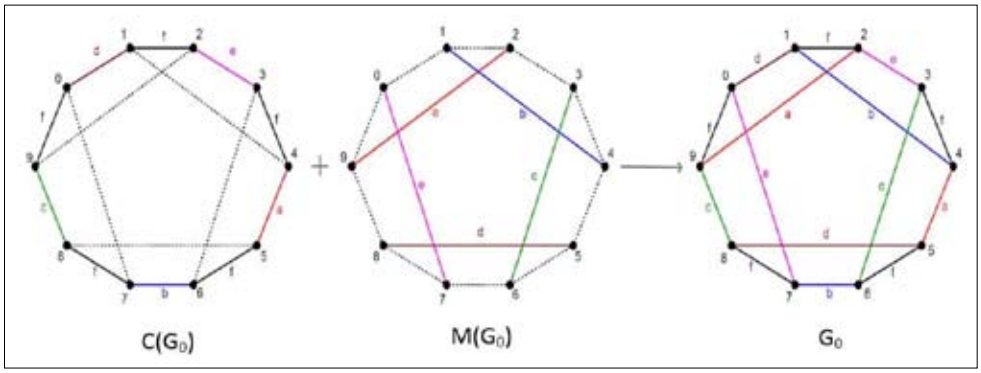

Figure 4: Star edge coloring of the cycle $C(G_0)$ and the matching $M(G_0)$

Corollary 1. The graph $G_0 - e$ where $e \in E(G_0)$ has $\chi'_{st}(G_0 - e) \leq 6$.

Proof: This can be considered as two cases as shown in the Figure 5.

Let $G_0 - e = \begin{cases} G_1 : e \in E(\mathrm{M}(G_0)) \\ G_2 : e \in E(\mathrm{C}(G_0)) \end{cases}$. Then the result is obvious by the Lemma 1.

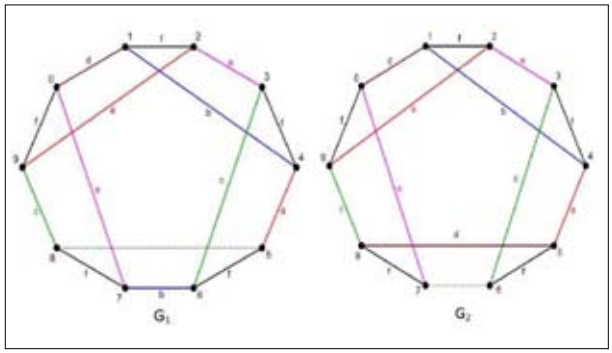

Figure 5: Star edge coloring of G_1 and G_2

Lemma 2. Let G_{1i} be the simple 2-connected sub-cubic graph obtained by adding *i* vertices to G_1 for *i* = 1,2,...,*n*. Then $\chi'_{st}(G_{1i}) \leq 6$ for all *i*.

Proof: Consider as cases by adding finite number of vertices with their adjacent edges to the graph G_1 so that the resulting graph $G_{1i} \in Q_3$ where it has at most two vertices $v_1, v_2 \in V(G_{1i})$ with $deg(v_1), deg(v_2) \leq 2$. i.e. obtain a supergraph or a graph with as many edges as possible under the required conditions.

Let G_{11} be the graph obtained by adding a vertex u to the graph G_1. In order to obtain a simple 2-connected sub-cubic graph, there should be two edges that connect u to G_1 as shown in Figure 6. Color the newly added two edges using the colors of the edges of G_1 at distance 3.

Note 1. If $d(e_1, e_2) = 3$ for e_1, $e_2 \in E(G_0)$, then they are colored with the same color from the list $\{a, b, c, d, e\}$. So, for an edge $e_E \in E(G_{1(i+1)})$ where $e_E \notin E(G_{1i})$, there is always an edge $e \in E(G_{1i})$ which is colored either from the list above or the color f and that guarantees a color for e_E.

For the succeeding cases, after G_{1i} is obtained, break it at the degree 2 vertex to get $G_{1(i+1)}$. So, G_{12} is obtained by breaking G_{11} at u and adding an edge $u - v$. There is only one new edge ($u - v$) to color and by the Note 1, there is always a color either from an edge at distance 3 or from a non-adjacent edge which does not violate the star edge coloring conditions. See the Figure 6. For the consequent two cases; G_{13} and G_{14}, the coloring is shown in Figure 7.

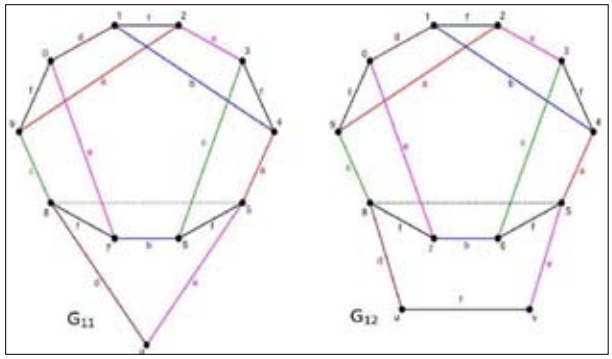

Figure 6: Star edge coloring of G_{11} and G_{12}

When coloring G_{11}, newly added edges should be colored with the colors of the edges at distance 3. If the edge−5*u* is colored first, there are two possibilities: *d* or *e*. If *d* is chosen for the edge−5*u*, there will be no color for the edge−8*u* from an edge at distance 3. So, the only possible color for the edge−5*u* is *e*, and the edge−8*u* should be colored with *d*.

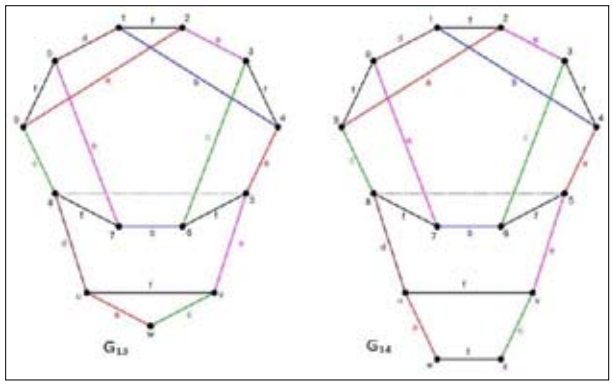

Figure 7: Star edge coloring of G_{13} and G_{14}

Note that, *i* vertices were added to G_1 in such a way that the resulting graph $G_{1i} \in Q_3$ has at most two vertices v_1, $v_2 \in V(G_{1i})$ such that $\deg(v_1), \deg(v_2) \leq 2$. There, $G_{1(i+1)}$ is obtained by modifying G_{1i}. But there can be few possibilities for G_{1i} according to the way the newly added *i* vertices are connected. For example, consider G_{16}.

See the Figure 8 which depicts some possible ways to connect newly added 6 vertices to G_1 to obtain simple 2-connected sub-cubic graphs where it has at most two vertices $v_1, v_2 \in V(G_{16})$ such that $\deg(v_1), \deg(v_2) \leq 2$. In a similar way explained above, such cases can also be handled.

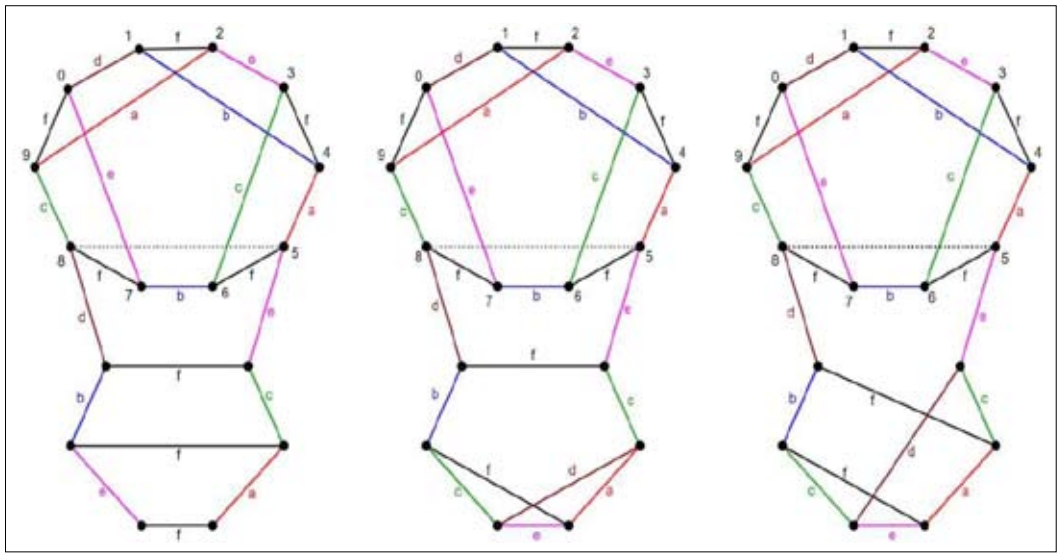

Figure 8: Star edge coloring of some possibilities of G_{16}

Suppose the graph $G_{1i} \in \mathcal{Q}_3$ obtained by adding i vertices to G_1 is having more than two vertices $v_m \in V(G_{1i})$ with $\deg(v_m) \leq 2$. Clearly such graphs are subgraphs of the above considered G_{1i}'s. So, those are obviously star edge colorable using 6 colors.

Hence, this expansion can be done for finitely many vertices as far as the resulting graph $G_{1i} \in \mathcal{Q}_3$. So, $\chi'_{st}(G_{1i}) \leq 6$ holds for all i = 1,2,...,n.

Lemma 3. Let G_{2i} be the graph obtained by adding i vertices to G_2 such that $G_{2i} \in \mathcal{Q}_3$ for all i = 1,2,...,n. Then $\chi'_{st}(G_{2i}) \leq 6$ for all i.

Proof: This can be proved in a similar manner to Lemma 2.

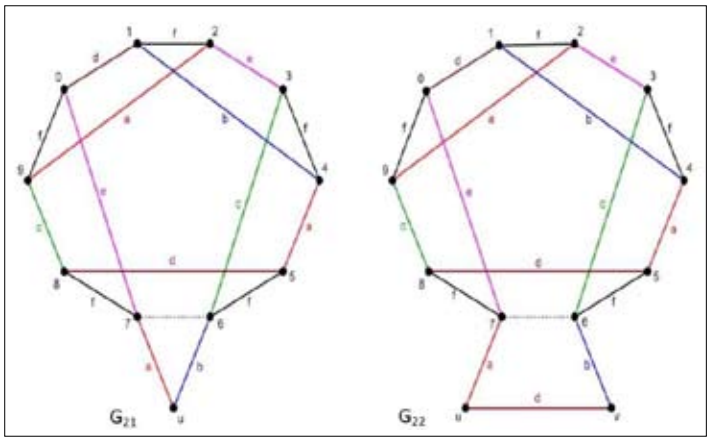

Figure 9: Star edge coloring of G_{20} and G_{22}

When coloring G_{21}, newly added edges should be colored with the colors of the edges at distance 3. Since the edge−6u can only be colored with the color b, the edge−7u should be colored with the color a.

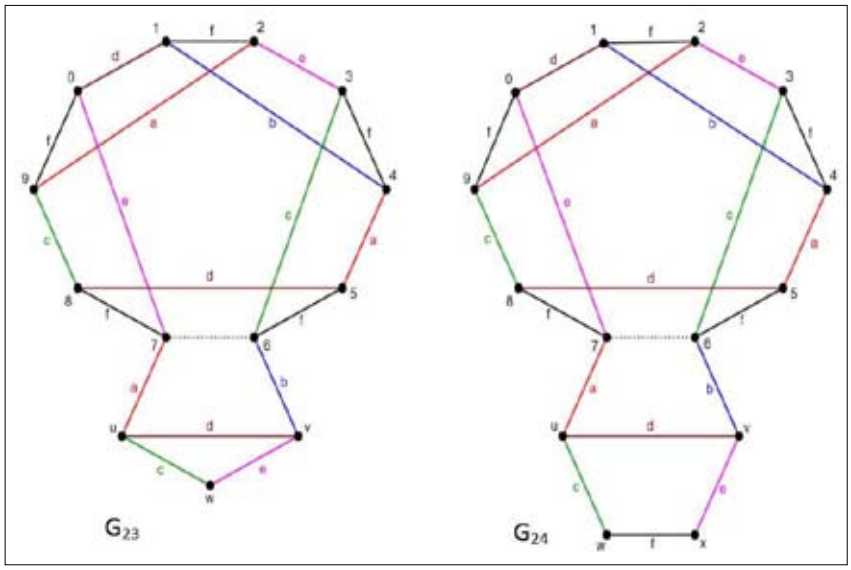

Figure 10: Star edge coloring of G_{23} and G_{24}

Now we present the proof of the main theorem; Theorem 18.

Proof : Consider cases as shown in the following diagram:

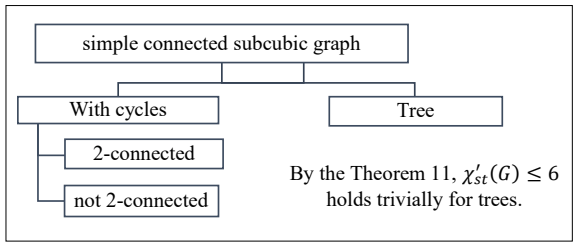

Figure 11: Flow of the proof of the theorem 18

First, suppose that $G \in Q_3$ is 2-connected. Referring to Theorems 15 and 16, if G is a supergraph then it can be decomposed into a matching $\mathcal{M}(G)$ and a collection of disjoint cycles (2-factor) $\mathcal{C}(G)$ such that each vertex of G is contained in exactly one $C \in \mathcal{C}(G)$. If G is not a supergraph, then there is more than one vertex of degree 2 and there are no vertices of degree 1. So, G can be decomposed into a collection of paths of length at most 2; $\mathcal{M}(G)$ and a collection of disjoint cycles and paths; $\mathcal{C}(G)$ such that every vertex of G is contained exactly in one cycle or path of $\mathcal{C}(G)$. That is, if $G \in Q_3$, then it can be decomposed into a collection of paths of length at most 2; $\mathcal{M}(G)$ and a collection of disjoint cycles and paths; $\mathcal{C}(G)$ such that $G = \mathcal{C}(G) \cup \mathcal{M}(G)$ and $E(\mathcal{C}(G)) \cap E(\mathcal{M}(G)) = \emptyset$.

Let $\{\alpha_1, \alpha_2, \alpha_3, \alpha_4, \alpha_5, \alpha_6\}$ be the set of distinct six colors that are available. In this method, first, a star edge coloring for $\mathcal{M}(G)$ should be given, and then referring to that, a star edge coloring for $\mathcal{C}(G)$ can be obtained. Any $G \in Q_3$ can be categorized considering its' $\mathcal{M}(G)$ as follows;

- Case I: $d(e_i, e_j) \geq 3$ for all $e_i, e_j \in E(\mathcal{M}(G))$
  Use the color α_1 for all $e_i \in E(\mathcal{M}(G))$.Since five colors available for the edges in $\mathcal{C}(G)$, referring to Theorem 2, it is always possible to star edge color. Therefore, $\chi'_{st}(G) \leq 6$.
- Case II: $d(e_i, e_j) = 2$ for i,j = 1,2 and $d(e_i, e_j) \geq 3$ for all $i, j \neq 1,2$ where $e_i, e_j \in E(\mathcal{M}(G))$
  Use α_1 and α_2 for the edges e_1 and e_2. Then all the other edges in $\mathcal{M}(G)$ can be colored by either α_1 or α_2. By the Theorem 2, the cycles and paths in $\mathcal{C}(G)$ can be colored by the remaining 4 colors. Therefore, $\chi'_{st}(G) \leq 6$.

- Case III: $d(e_i, e_j) = 2$ for $i,j = 1,2,3$ and $d(e_i, e_j) \geq 3$ for all $i, j \neq 1,2,3$ where $e_i, e_j \in E(\mathcal{M}(G))$
  Use three distinct colors α_1, α_2 and α_3 for e_1, e_2 and e_3. Use any of those colors to color the remaining edges in $\mathcal{M}(G)$. Three more colors are remaining to color $\mathcal{C}(G)$. Referring to Theorem 2, if $C_5 \notin \mathcal{C}(G)$, then $\mathcal{C}(G)$ can be star edge colored. If $C_5 \in \mathcal{C}(G)$, then consider the three possibilities shown in Figure 12.

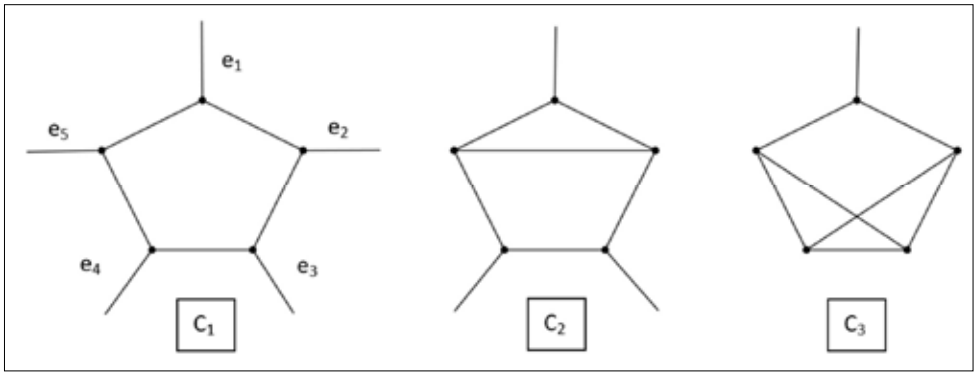

Figure 12: Possible arrangements of edges in $M(G)$ with regard to the C_5

In C_1, $d(e_i, e_{i+1}) = 2$ and $d(e_i, e_{i+2}) = 3$ where $e_i \in E(\mathcal{M}(G))$ for $i,j = 1,2,3$. Hence, the pairs of edges e_1, e_4 and e_3, e_5 can be colored using two colors and another color should be used for e_2. So only three colors are needed to color the edges in $\mathcal{M}(G)$. Note that, the only edge in $\mathcal{M}(G)$ that is colored with a unique color, say α, is e_2. Also note that, for each $e \in E(\mathcal{M}(G))$,there is an edge $z \in C_5$ such that $d(e, z) = 3$. The edge $z \in C_5$ such that $d(e_2, z) = 3$ receives the same color α. Since already there were three remaining colors for the cycle C_5, now with the color α, there are four colors available for the cycle. Hence it is star edge colorable by the Theorem 2, and consequently, C_1 is star edge colorable with six colors. Note that in C_2 and C_3, there are less edges in $\mathcal{M}(G)$, hence similarly, it can be shown that, the cycle C_5 in both C_2 and C_3 has four available colors. So, even if $C_5 \in \mathcal{C}(G)$, the graph G is still star edge colorable with six colors. Therefore, whether or not $C_5 \in \mathcal{C}(G)$, $\chi'_{st}(G) \leq 6$.

- Case IV: $d(e_i, e_j) = 2$ for $i,j = 1,2,3,4$ and $d(e_i, e_j) \geq 3$ for all $i, j \neq 1,2,3,4$ where $e_i, e_j \in E(\mathcal{M}(G))$

There are four edges of $\mathcal{M}(G)$ such that all four are at distance 2 from each other. So, use four distinct colors; α_1, α_2, α_3 and α_4 for them. And all the other edges in $\mathcal{M}(G)$ can be colored using any of those four colors. Note that previously, in the Corollary 1 and Lemmas 2, 3 all the possibilities for G having four edges in $\mathcal{M}(G)$ at distance 2 from each other are covered. So, by referring to those, $\chi'_{st}(G) \leq 6$ can be shown.

- Case V: $d(e_i, e_j) = 2$ for $i,j = 1,2,3,4,5$ where $e_i, e_j \in E(\mathcal{M}(G))$

Note that if there are five edges at distance 2 from each other, since only sub-cubic graphs are considered, the only graph that can be obtained is the 3-regular graph of 10 vertices. One way of illustrating it is given in the Lemma 1, where $d(e_i, e_j) = 2$ for all non-adjacent $e_i, e_j \in E(G)$ and any other 3-regular graph of 10 vertices may have less constraints. So, referring to Lemma 1, any such graph is having $\chi'_{st}(G) \leq 6$.

Throughout all the five cases, all the simple 2-connected sub-cubic graphs were covered, and shown that for any such graph, the result holds.

Finally, consider the simple connected sub-cubic graph having cycles but not 2-connected. i.e. the graph has at least a single bridge (aka connectors) which connects two blocks. So, in this case separate the blocks by deleting the bridge. Then as shown in above, treat the blocks as separate simple 2-connected sub-cubic graphs. Once the blocks are colored, then use a color which is in a non-adjacent edge for the connector such that the star edge conditions are not violated. So, concluding all the cases, it is proved that for any simple connected sub-cubic graph G, $\chi'_{st}(G) \leq 6$, as required.

DISCUSSION

The method of star edge coloring introduced earlier can be verified using the Sagemath software. A random simple connected sub-cubic graph can be obtained by Sagemath software using the code provided in the Appendix section.

After the graph is colored using the algorithm, it can be observed that the previously introduced upper bound for the star chromatic index holds for any simple connected sub-cubic graphs. Also, by giving the adjacency matrix to the software, one can obtain a suitable graph as shown in the following two examples:

Example 1.

```
M = Matrix([[0,0,1,1,1,0,0,0,0,0,0,0,0,0,0,0], [0,0,0,0,1,0,1,0,1,0,0,0,0,0,0,0],
[1,0,0,0,0,1,0,0,0,0,0,1,0,0,0,0], [1,0,0,0,1,0,0,0,1,0,0,0,0,0,0,0], [1,1,0,1,0,0,0,0,0,0,0,0,0,0,0,0],
[0,0,1,0,0,0,1,0,1,0,0,0,0,0,0,0], [0,1,0,0,0,1,0,1,0,0,0,0,0,0,0,0], [0,0,0,0,0,0,1,0,0,0,0,0,0,0,0,0],
[0,1,0,1,0,1,0,0,0,0,0,0,0,0,0,0], [0,0,0,0,0,0,0,0,0,1,1,0,0,0,0,0], [0,0,0,0,0,0,0,0,0,1,0,1,0,1,0,0],
[0,0,1,0,0,0,0,0,0,1,1,0,0,0,0,0], [0,0,0,0,0,0,0,0,0,0,0,0,1,1,1,1], [0,0,0,0,0,0,0,0,0,0,1,0,1,0,0,1],
[0,0,0,0,0,0,0,0,0,0,0,0,1,0,0,1], [0,0,0,0,0,0,0,0,0,0,0,0,1,1,1,0]])

G2= Graph(M)
show(G2)
```

Code 1 : Sagemath code and output

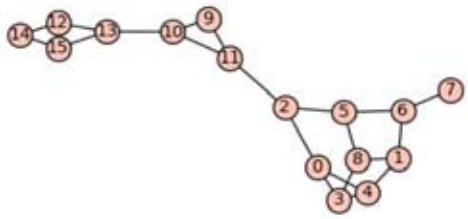

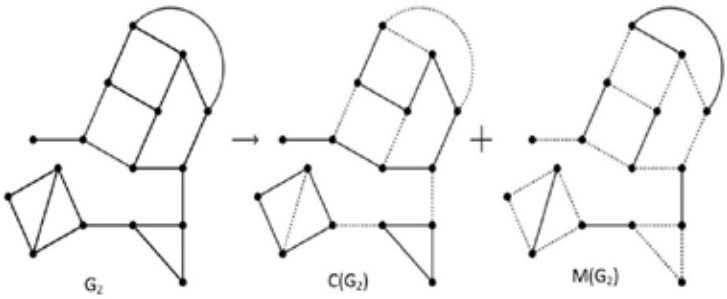

Figure 13: Decomposition of the graph G_2

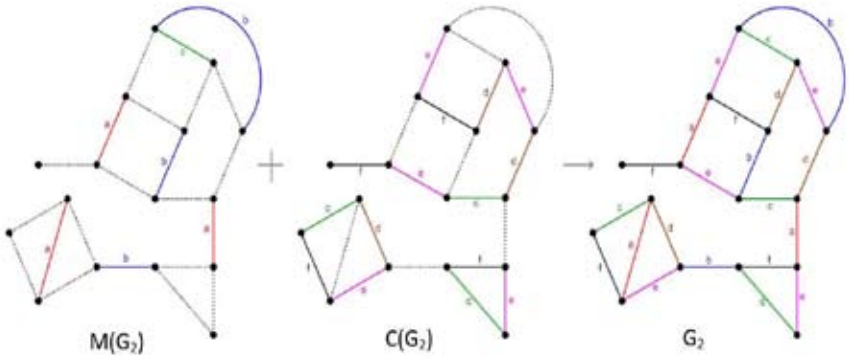

Figure 14: Coloring of the graph G_2

Example 2. Without using an adjacency matrix, a random graph that satisfies the simple, connected, sub-cubic conditions can be obtained by giving the coordinates as shown below.

```
G3 = { 0:[1,6,13], 1:[0,2,3], 2:[1,12,15], 3:[1,14,15], 4:[13,14,15], 5:[6,7,11], 6:[0,5,7], 7:[5,6,8],
8:[7,12,16], 9:[17,18,19], 10:[17,18,19], 11:[16,17,5], 12:[2,8,18], 13:[0,4,14], 14:[3,4,13],
15:[2,3,4], 16:[8,11,19], 17:[9,10,11], 18:[9,10,12], 19:[9,10,16]}
Graph(G3).show()
```

Code 2 : Sagemath code and output

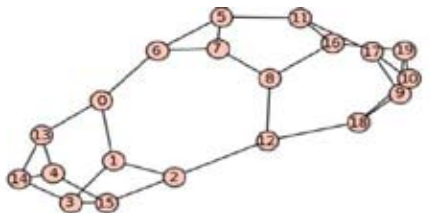

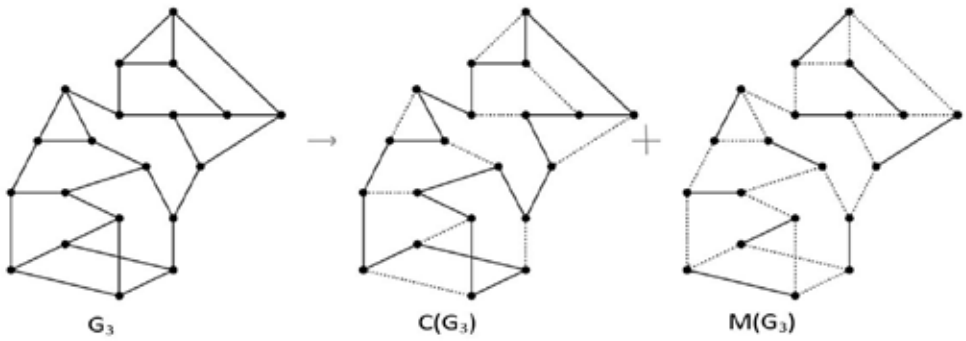

Figure 15: Decomposition of the graph G_3

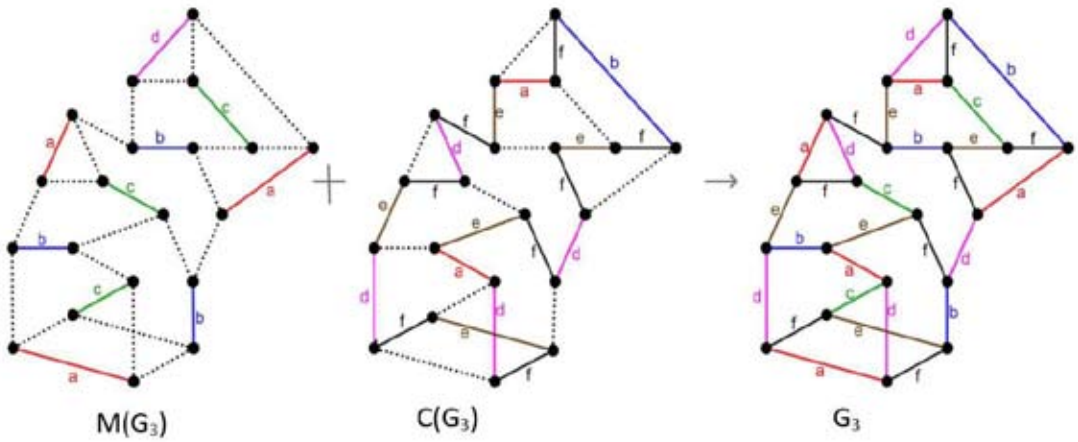

Figure 16: Coloring of the graph G_3

Applications

In real time applications, coloring is used in scheduling, network designing, clustering, etc. For example, in an art gallery for placing the security cameras so that the full gallery is covered coloring is used.

Suppose a clothing brand wants to find the best places to initiate their new branches in a region so that anyone in that neighborhood can visit their outlets. Due to the high capital cost, they can't open a branch in each city. What they want to do is to find places to open new outlets so that anyone from neighboring cities can reach. The area can be illustrated by a graph, where each vertex represents a city and each edge represents a road that connects two cities. Depending on the population and available locations to initiate a new branch in each road, roads can be weighted and then, it can be star edge colored using the introduced algorithm. We can say that the company can open a new outlet in each road with that same color.

To obtain a sub-cubic graph, either the Kruskal's algorithm or the Prim's algorithm can be used with the condition $\deg(v) \leq 2$ for all $v \in V(G)$ where G is the spanning graph with the highest weight. In this application, Kruskal's algorithm is used as it selects the highest weighted edges randomly.

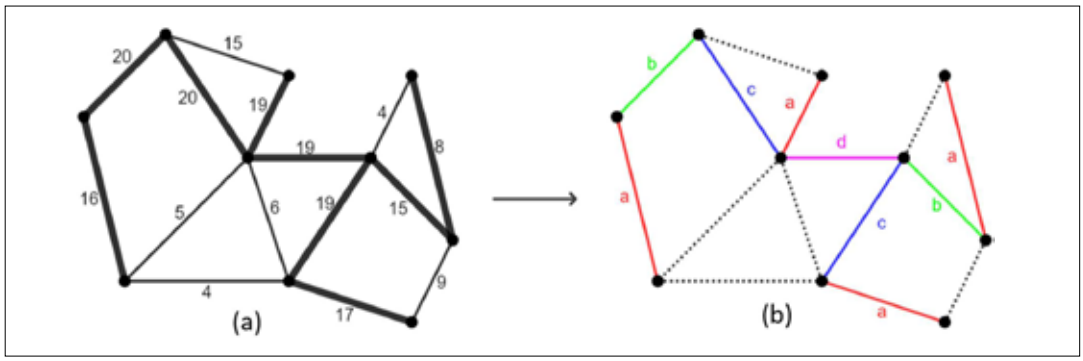

Figure 17: Star edge coloring applied to branching of a clothing brand

(a) The graph represents the area considered. Each vertex denotes a city and an edge denotes a road. The roads are weighted depending on the population and available locations for the shop in each road. The Kruskal's algorithm is used, with the sub-cubic condition is not violated.

(b) The selected graph is star edge colored using the introduced algorithm. The company can initiate new branches on the pink(d) colored edge(road) so that anyone from any city in the region can reach this outlet crossing at most 2 cities, hence this is the most cost effective choice of location to open a new branch.

CONCLUSION

In conclusion, this research has partially answered the conjecture: "If G is a sub-cubic graph, then $\chi'_{st}(G) \leq 6$ " which was posed by Dvorak et al. in 2013. It was successfully proved that above conjecture is true for any simple connected sub-cubic graph. Also, we have introduced a method to obtain a star edge coloring for any simple connected sub-cubic graph.

Our findings not only contribute to the theoretical understanding of graph coloring but also have potential implications for practical applications in areas such as network design and scheduling.

This method of coloring fails when there are loops or multi-edges in the graph. But as observed, we couldn't find any sub-cubic graph that cannot be star edge colored with 6 colors. Hence, it remains as a future direction for this research to prove that $\chi'_{st}(G) \leq 6$ for sub-cubic graphs with loops or multi-edges.

REFERENCES

Bezegová, L., Lužar, B., Mockovčiaková, M., Soták, R., & Škrekovski, R. (2013a). Star edge coloring of some classes of graphs. *Journal of Graph Theory*, 81(1), 73-82. https://doi.org/10.1002/jgt.21862

Bona, M. (2016). *Walk Through Combinatorics: An Introduction To Enumeration And Graph Theory* (4th ed.). *World*

Scientific Publishing Company.

Casselgren, C. J., Granholm, J. B., & Raspaud, A. (2021a). On star edge colorings of bipartite and subcubic graphs. *Discrete Applied Mathematics*, 298, 21–33. https://doi.org/10.1016/j.dam.2021.03.007

Dvořák, Z., Mohar, B., & Šámal, R. (2013). Star chromatic index. *Journal of Graph Theory*, 72(3), 313–326. https://doi.org/10.1002/jgt.21644

Horacek, K. M. (2019). Edge colorings of graphs on surfaces and star edge colorings of Edge colorings of graphs on surfaces and star edge colorings of sparse graphs sparse graphs. *Graduate Thesis, Dessertations, and Problem Reports.* https://doi.org/10.33915/etd.3910

Das, K. (n.d.). Cactus Graphs and Some Algorithms. https://doi.org/10.48550/arXiv.1408.4005

Liu, Xinsheng & Deng, Kai. (2008). An upper bound on the star chromatic index of graphs with $\Delta >= 7$. *Journal of Lanzhou University. Natural Sciences.* 44. https://www.researchgate.net/publication/265945355_An_upper_bound_on_the_star_chromatic_index_of_graphs_with_7

Lužar, B., Mockovčiaková, M., & Soták, R. (2017a). Note on list star edge-coloring of subcubic graphs. *Journal of Graph Theory*, 90(3), 304–310. https://doi.org/10.1002/jgt.22402

Melinder, V. (2020). Upper bounds on the star chromatic index for bipartite graphs. *Linköping University, Department of Mathematics, Mathematics and Applied Mathematics.*. https://urn.kb.se/resolve?urn=urn:nbn:se:liu:diva-164938

Omoomi, B., Dastjerdi, M. V., & Yektaeian, Y. (2019). Star edge coloring of Cactus graphs. http://arxiv.org/abs/1911.02343

Verma, S., & James, M. (2019). Chromatic Index, Total Coloring and Diameter of Pan and Tadpole Graphs. *Journal of Computer and Mathematical Sciences*, *10*(6), 1294–1301. https://www.researchgate.net/publication/334820747_Chromatic_Index_Total_Coloring_and_Diameter_of_Pan_and_Tadpole_Graphs

Wang, Y., Wang, Y., & Wang, W. (2019). Star edge-coloring of graphs with maximum degree four. *Applied Mathematics and Computation*, *340*, 268–275. https://doi.org/10.1016/j.amc.2018.08.035

Appendix : The Sagemath code formulated to generate a random simple connected sub-cubic graph is included below.

```
from sage.graphs.graph_generators import graphs
def get_subcubic_connected_graph(vertices, seed=None):
    ""Generate a simple connected graph with maximum degree 3.
    Parameters:
        vertices (int): The number of vertices in the graph.
        seed (int, optional): Random seed for reproducibility.
    Returns:
        Graph: A simple connected graph with maximum degree 3.""
import random
random.seed(seed) # Set seed for reproducibility if provided
while True:
    # Generate a random graph with edges added randomly
    G = graphs.RandomGNP(vertices, 0.3, seed=random.randint(0, 10**6))
    for v in G.vertices():
        while G.degree(v) > 3:
            G.delete_edge(G.random_edge())
  # Check for connectivity
   if G.is_connected() and max(G.degree()) <= 3:
        return G
  # Generate a simple connected subcubicgraph
 vertices = 10
  subcubic_graph = get_subcubic_connected_graph(vertices)
   subcubic_graph.show()
```

J.Natn.Sci.Foundation Sri Lanka 2025 53 (4): 333 - 343
DOI: http://dx.doi.org/10.4038/jnsfsr.v53i4.12124

RESEARCH ARTICLE

Postharvest Technology

Use of near infrared spectroscopy for rapid and non-destructive identification of morphologically similar seeds of different paddy varieties [*Oryza sativa* L.]

KW Yasintha[1*] and BM Jinendra[2]
[1] *Department of Applied and Natural Sciences, University College of Matara, University of Vocational Techonlogy Sri Lanka.*
[2] *Department of Agricultural Engineering, Faculty of Agriculture, University of Ruhuna, Mapalana, Kamburupitiya, Sri Lanka.*

Submitted: 21 May 2024; Revised: 28 September 2025; Accepted: 29 September 2025

Abstract: Rice production systems and breeding programmes often require handling large numbers of paddy samples, where maintaining sample identity is critical. Conventional identification methods, such as morphological and molecular analyses, are reliable but laborious and time-consuming. To address this, the present study evaluated the use of near-infrared (NIR) spectroscopy (588–1091 nm) combined with soft independent modeling of class analogy (SIMCA) for rapid discrimination of paddy seed varieties. A total of 750 seed samples representing five varieties (Bg300, Bg352, Bg357, Bg359, and Bw363) were scanned, and SIMCA prediction models were developed using Pirouette 3.11 software. Model parameters were optimized to enhance classification performance. The influence of moisture content (MC) at four levels (10%, 12%, 15%, and 23%) during seed handling was also investigated. The SIMCA models achieved variety-specific classification accuracies of 89% (Bg300), 83% (Bg352), 88% (Bg357), 87% (Bg359), and 84% (Bw363). When averaged across all varieties, correct identification rates were 82% at 10% MC, 83% at 12% MC, 88% at 15% MC, and 92% at 23% MC. The results confirm an increasing trend in predictive accuracy with elevated MC, attributable to stronger variety-specific water-related absorbance features in the NIR region. Overall, the study demonstrates that NIR spectroscopy combined with SIMCA provides a rapid, non-destructive, and feasible approach for varietal identification of paddy seeds, particularly effective under equalized moisture levels. This method holds strong potential for field-level application, offering faster and more reliable variety authentication compared to conventional practices.

Keywords: NIR spectroscopy, morphologically similar paddy varieties, *Oryza sativa* L., principal component analysis, soft independent modeling of class analogy.

INTRODUCTION

In everyday rice breeding trials, within rice breeding stations and in processing systems such as large scale warehouses worldwide, there are hundreds of paddy samples from different varieties to be handled. Exact identification of the correct variety to be used in breeding is essential since an error may cause a significant impact on results and ultimately ends up with wrong decisions, wasting time and money. The task of identifying paddy variety is more difficult and complicated when one is identifying the level of purity of paddy varieties (Liu *et al.*, 2005). In some cases, good quality paddy seed cultivars can be falsified by poor quality cultivars or other fallacious cultivars, affecting the quality, yield and value of rice (Wenwen *et al.*, 2013). Also before releasing a variety, it should be tested for its identity and unity. On the other hand, as a seasonal crop, the harvest of the paddy is being handled in large scale storage warehouses as bulk, together with their representative samples. In case of proper handling of a large number of samples in various events, there is a need for a quick and reliable method for identifying the exact variety or

* Corresponding author (wikyasintha@gmail.com; https://orcid.org/0000-0001-8888-5410)

This article is published under the Creative Commons CC-BY-ND License (http://creativecommons.org/licenses/by-nd/4.0/). This license permits use, distribution and reproduction, commercial and non-commercial, provided that the original work is properly cited and is not changed in anyway.

the cultivar of the varieties, as commercial value, genetic characteristics, and quality of rice mainly depends on the type and grade of the rice variety. Different paddy varieties vary in size, shape, and constitution, and variety is considered as an imperative factor which influences the cooking and processing quality of rice (Namaporn *et al.*, 2011). It is clear that quality parameters of a rice variety have significant impact on consumer demand.

Traditional methods of paddy variety identification which require field planting, such as seedling methods (Sasaki, 2004), morphological characteristics (Hussain *et al.*, 2010) and field planting (Song *et al.*, 2010) need long periods of time. Currently, the variety identification of paddy seed is mainly done by chemical methods such as electrophoresis (Bertrand *et al.*, 2006), HPLC (high performance liquid chromatography), (Huebner *et al.*, 1991) or GC-MS (gas chromatography-mass spectrometry) (Wu *et al.*, 2012). Varietal characteristics are determined through these tests based on proteins, fats, moisture, and amino acids of single seed, and serious overlaps of these components exist among seeds. Further, DNA tests should be performed to determine the structure and composition of genetic materials of seeds (Jing *et al.*, 2019). Although these methods can give relatively more exact results, they have many limitations. Implementations of the chemical methods are time consuming and have shortcomings when the available amount of sample is limited. It is also highly expensive for inspection as well as instrument maintenance. Variety identification through electrophoresis is not applicable to routine control (Bertrand *et al.*, 2006). The measurements require experimental equipment that is complicated, expensive, and highly specialized. Further, non-destructive identification of paddy varieties on a large scale cannot be accomplished by chemical methods or by the paddy field method (Liu *et al.*, 2005).

All the above mentioned methods cannot be used effectively to detect paddy varieties in large scale handling. Instead, it is important to develop a simple, rapid and reliable identification method. (Jing *et al.*, 2019). Therefore, this effort was taken to develop a non-destructive, rapid, and reliable method to identify paddy seed varieties. There are reports on using NIR imaging based paddy seed identification with expensive Indium Gallium Arsenide laboratory setups (Wenwen *et al.*, 2013). The system consists of a laboratory where the sample is kept in a dark room and samples are illuminated using two tungsten halogen lamps (150 W X2). The used wavelength range, 1100-2500 nm, is not usable for simplified field level instrument application. Using lab instruments outfitted with InGaAs (Indium Gallium Arsenide) detectors that span the extended short-wave NIR band (1100–2500 nm), prior research has documented NIR imaging–based rice identification. Although InGaAs instruments are more accurate and sensitive, their high capital cost and the need of specific high power consumed lighting such as tungsten-halogen lamps and dark-room settings, make them inconvenient for field-level robust use. Despite the availability of specific novel portable devices with InGaAs detectors, they are still too expensive for frequent large-scale robust seed handling when it is compared to low-cost, simplified short wave NIR field spectrometers. Moreover, when the 1100–2500 nm range is to be applied, it either requires a stable AC mains power connection or a large battery system to operate the high-energy light sources to stimulate the InGaAs detectors. This not only increases the cost but also demands stable laboratory conditions to avoid strong water absorption interferences. These practical limitations, *i.e.*, cost, energy requirements, and sensitivity to background water absorption have made this wavelength region altogether unsuitable for routine field-level identification of rice seeds. By contrast, the visible–shortwave NIR range (588–1091 nm) is compatible with more affordable silicon-based detectors, enabling the development of lightweight handheld devices.

short wave-near infrared (NIR) spectroscopy has been used for a few decades to investigate physicochemical properties of paddy, such as moisture content (Kawamura *et al.*, 2006), protein content (Barton *et al.*, 1998), amylase content (Delwiche *et al.*, 1995; Barton *et al.*, 1998; Delwiche *et al*., 1996), whiteness (Barton *et al.*, 1998; Delwiche *et al.*, 1995), milling degree (Delwiche *et al.*, 1996), hardness (Awanthi *et al.*, 2019) and cooking quality (Windham *et al.*, 1997). Beyond research purposes, rapid identification of rice varieties has important practical applications, such as preventing admixture of seed lots in warehouses, maintaining pure parental lines for multiplication trials in seed paddy production for specific agro-climatic zones, supporting seed certification and quality assurance, enabling fair trade, and protection of farmers against mislabeling.

However, there are no reports on using short wave-NIR spectroscopy for the identification of paddy seed varieties as a quick, non-destructive, and chemical free method. Therefore, this study was conducted to assess the possibility of use of SW-NIR spectroscopic methodology to identify paddy seed samples, as it will be a rapid, non-destructive, chemical free, and affordable field level application, and to build up and optimize a spectroscopic SIMCA discrimination model to predict seed samples from five different paddy varieties, as well as to investigate the effect of moisture content in seed samples for NIR prediction results.

MATERIALS AND METHODS

Sample Preparation

A number of 750 seed samples from each of five improved paddy varieties which are recommended for general planting by the Department of Agriculture were obtained from Rice Research Institute (RRI) of Batalagoda, Sri Lanka. The selected varieties, Bg300, Bg352, Bg357, Bg359, and Bw363, are widely planted and improved paddy cultivars which had been produced in the same year to avoid any effect of seed age. Paddy samples were prepared with different moisture contents in order to develop a NIR model which can be used to detect paddy varieties in different stages of post-handling activities such as harvesting, milling and storage. Within the post-harvest process of paddy handling, proper moisture content of the seeds should be available. When harvesting, rice seed moisture content should be within the range20-25%, as higher moisture content results in more losses due to many green and unfilled grains, while lower moisture content results in more losses from shattering. The desired moisture range for paddy threshing is 20-25% in order to minimize incomplete threshing and grain damage. The ideal moisture range for paddy milling is 14-15%. The moisture content of paddy grain should be less than 14%, and the ideal is 12% for long time storage (IRRI, 2021). Therefore, paddy samples, with moisture contents of 23%, 15% and 12% were prepared to acquire spectral data. In this study, systematic laboratory control was applied to maintain paddy seed moisture content at 23%, 15%, and 12%. The final MC% was assessed using the time-consuming gravimetric method. However, in practical applications, this procedure can be simplified. For instance, according to the literature, the same NIR spectrometer can be employed to detect paddy seed moisture content almost instantly and with high accuracy by applying a PLS model (partial least squares) developed for this purpose. In the way forward, quick moisture standardization could also be achieved by creating specific RH environments, rather than soaking with various methods, through the use of saturated solutions of a salt such as lithium chloride, in a closed container.

Preparation of raw paddy samples

Paddy samples were winnowed to remove paddy straw and other impurities. Then all the samples which were in storage condition were weighed, and the moisture content of samples was determined through the oven drying method (IRRI, 2021). A spectrum was taken from each of the 150 seeds of each variety.

Preparation of paddy samples under different moisture contents

To analyze model performances based on the various moisture contents, seeds were soaked in cold water for 24 hrs. Then the paddy seed samples were dehydrated until the moisture content reaches 23% and the samples were packed using polysack bags. Then they were kept under room temperature (27 °C) in order to allow reaching equilibrium moisture among all paddy seeds. All rice samples were treated in the same manner—soaking, draining, drying, and packing into polysack bags. Each sample reached a moisture content of 23% as confirmed by the gravimetric method (IRRI, 2021). Then spectra were taken from each sample. The same procedure was repeated to prepare paddy samples with 15% and 12% moisture content.

Data collection

All individual 750 paddy samples were used to obtain the NIR spectra to be analyzed and to use for the model building process.

Instrument and spectra acquisition

A handheld type NIR Spectrometer FQA-NIR Gun (588-1091 Shizuoka Shibuya Seiki, Hamamatsu, Japan), was used to acquire the reflectance spectra from 588 nm up to 1091 nm at 2 nm steps of five paddy seed varieties. In order to improve the accuracy of spectral data, background noises had to be avoided. The rigid steel probe in the original instrument [1(a)] was not suitable for paddy seed spectra measurement. A newly modified, specially designed best fitted probe [Figure 1(b)], which was reported previously and tested for biological samples, was used to avoid environmental interferences (Balasuriya *et al.*, 2010). A custom-built probe extension was fabricated using a foamed rubber block measuring 50 × 40 × 50 mm (length, width, and height). The original NIR instrument probe (10 × 15 × 15 mm) was inserted into the top surface of the block by removing a cube of matching size. Two cylindrical holes, each 10 mm in diameter, were drilled along the 50 mm height of the rubber block to provide a path for the light source to reach the sample and for the light of the reflectance spectra to return to the instrument detector. After doing several trials, a white polypropylene container of 5 cm diameter was selected to hold paddy seeds at the time of taking spectra, as it avoids the light interference further. The cylindrical sample cups measured 5 cm in diameter and 10 mm in height. Each cup was filled to its full 10 mm height, and a quartz screen was positioned on top

during measurements. The bottom surface of the probe extension was gently pressed against the quartz screen while spectra were recorded, ensuring that no gap existed between the probe extension and the quartz surface above the sample cup.

This approach is intended for the qualitative discrimination of paddy samples rather than for the detection of material quantities based on their absolute chemical constituents. For example, in quantitative mode prediction using a PLS model, or when identifying the spectroscopic signature of paddy sample spectra, the influence of the custom probe extension or the sample holder material would be a critical consideration.

The method presented here is based on supervised classification, utilizing known paddy seed samples as the reference class to ensure accurate identification. As the applied methodology has successfully differentiated the samples with satisfactory results, consistent with the reference samples, the effect of the sample holder material on the spectra becomes negligible. Nevertheless, we acknowledge that the sample holder and probe extension material may potentially influence the information captured by the spectra. However, since these factors are common to all spectra collected in this study, any such influence is effectively cancelled out, rendering their impact on model accuracy insignificant.

Seed samples were filled into 5 cm diameter container and the seed surface was closed by the quartz screen when the spectra were taken [Figure 1(c)]. The sample cup was always filled with seeds to its top edge, ensuring that an equal amount of paddy was exposed in every spectral observation. This arrangement in the sample presentation setup eliminated any possible interference from ambient light. Furthermore, no measurable temperature increase was detected during the measurements, as the spectral integration time was as short as 100 milliseconds. One hundred and fifty seed samples per variety were illuminated by the NIR spectrometer and the reflectance spectra were recorded. Accordingly, there were 750 spectra in the data set.

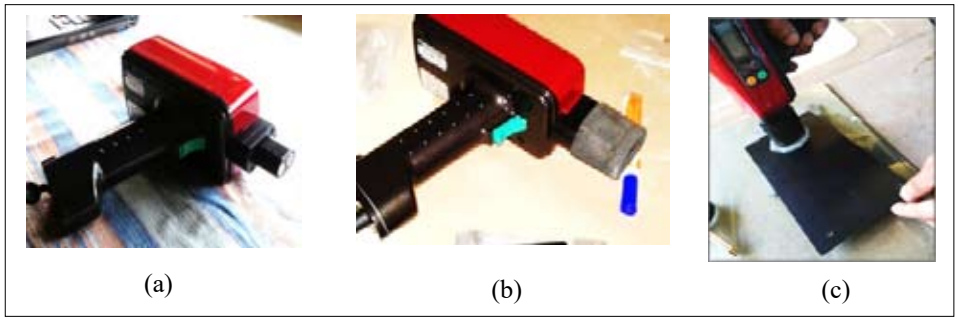

Figure 1: NIR spectra acquisition (a - The NIR instrument with original rigid steel probe. b - The instrument with the newly modified best fitted probe. c - Aequiring the NIR spectra using the modified probe)

Spectral data analysis

Prior to data analysis, the head and tail of spectral data that contained noise and baseline shift were removed. Although the instrument covered 588 – 1091 nm, noisy edge regions below 630 nm and above 1080 nm were clipped during preprocessing, leaving an effective working range of 630–1080 nm for analysis. Then principal component analysis (PCA) was done in order to remove outliers of the data set according to the Mahalanobis distance. From the total of 750 spectra, 20 spectra (≈ 2.6%) were excluded. These were likely due to physical breakdown of paddy (*e.g.*, cracked seed coats or broken seeds) or interference from outside light caused by insufficient pressure applied when pressing the probe against the quartz screen. To minimize outliers, precautions such as careful seed placement, applying gentle but consistent pressure of the probe against the quartz screen, and repeating doubtful scans were adopted.

Out of the 750 spectra, 500 spectra were used for the training set and 250 spectra were used to create a prediction set for the model evaluation process. Spectra were selected alternatively as 10 spectra for training set and 5 spectra for prediction set. Paddy seed variety prediction was achieved by soft independent modeling of class analogy (SIMCA). Spectra from each variety Bg300, Bg352, Bg357, Bg359, and Bw363 were assigned as discriminate class 1, 2, 3, 4, and 5 respectively in the SIMCA algorithm in Pirouette software (Informetrix, Woodinville, WA).

Moisture content (MC) has a prominent effect on near-infrared (NIR) spectra because water strongly absorbs wavelengths around 746 nm, 970 nm etc., which correspond to the third overtone of the water absorbance bands. Increasing MC therefore can alter the baseline, peak intensity, and scattering properties of the spectra, making different mathematical treatments effective for the samples having different moisture contents.

RESULTS AND DISCUSSION

Prediction performance of SIMCA

The NIR spectra obtained from paddy samples were used to prepare a SIMCA model based on different mathematical treatment options. The best prediction results obtained for the tested paddy varieties under different moisture contents were summarized as follows.

There were 150 sample spectra from one variety, of which 100 were used to prepare the model set and the remaining 50 were used as the prediction set. Out of the 50 samples, the number of spectra correctly classified was expressed as a percentage in Table 1. For instance, 43/50 corresponded to 86%. In some cases, a few outliers in the prediction set produced slightly different results, such as 46/49 = 94%. These findings highlight that while the model performed consistently well, occasional misclassifications can influence the overall prediction accuracy.

As shown in the table, there is an increasing trend in the results with the elevated moisture in the samples. from the table, it is clear that in the prediction models, the maximum number of erroneously classified spectra was recorded as 10 out of the 50 spectra (prediction under 10% and 12% moisture).

Table 1: Summary of results under different moisture contents

	10% MC.	12% MC.	15% MC	23% MC	% prediction
Bg 300	84	84	94	95.91	89.5
Bg 352	84	82	80	86	83
Bg 357	80	80	90	100	87.5
Bg 359	80	86	92	92	87.5
Bg 363	82	81	83	87	83.25
% prediction	82	82.6	87.8	92.182	

SIMCA Prediction results of 10% moisture content

The highest number of correct classifications were obtained based on the mathematical treatments given below, for moisture content of 10%. Fifty spectra were evaluated for each variety, and the highest number of misclassifications (10 spectra) were recorded for the Bg357 and Bg359 varieties.

Mathematical treatment

- » Baseline correction (linear fit)
- » Mean centre (Optimal factors – 10)
- » 1st derivative 9
- » Smooth

According to the above model configuration, 80% or higher correct classifications were obtained for five paddy seed varieties with 10% moisture content. It was observed that the maximum accuracy rate of prediction was possible only up to 84%.

Table 2: Summary of results for 10% moisture content

Variety	% prediction
Bg 300	84
Bg 352	84
Bg 357	80
Bg 359	80
Bg 363	82

SIMCA Prediction results of 12% moisture content

At 12% moisture content, more than 80% correct classifications were recorded for all the varieties based on the mathematical treatments given below. Only one sample of no match was recorded for the variety Bg352.

- » Mean centre10
- » 1st derivative 7
- » Smooth
- » Baseline correction (linear fit)

Table 3: Summary of results for 12% moisture content

Variety	% prediction
Bg 300	84
Bg 352	82
Bg 357	80
Bg 359	86
Bg 363	81

SIMCA Prediction results of 15% moisture content

According to the SIMCA performance of 15% moisture content, 80% correct classifications for the variety Bg352 and 83.33% for the variety Bg363 were recorded, and more than 90% correct classifications were obtained for varieties Bg300, Bg357, and Bg359.

Mathematical treatment

- » Mean center10
- » 1st derivative5

Table 4: Summary of results under 15% moisture content

Variety	% prediction
Bg 300	94
Bg 352	80
Bg 357	90
Bg 359	92
Bg 363	83

SIMCA Prediction results of 23% moisture content

Based on pereto 5 and 2nd derivative 15 mathematical treatment, the highest correct classification results of 100%, was recorded for the variety of Bg357 and more than 85% correct classifications were recorded for the rest of the varieties as well.

Table 5: Summary of results under 23% moisture content

Variety	% prediction
Bg 300	95.91
Bg 352	86
Bg 357	100
Bg 359	92
Bg 363	87

According to the prediction results, different varieties have shown different correct classifications rates in the SIMCA models constructed for different moisture contents. However, more than 80% correct classifications were obtained for all selected varieties under tested moisture content. The sample arrangement in the SIMCA model configurations shows that the separation of different varieties in three-dimensional principal component space was arranged according to the specific characteristics of each variety. According to the previously reported research (Li *et al.*, 2008) on "Non-destructive prediction of storage time of paddy seeds by Vis/NIR spectroscopy", the best model was achieved with a high discrimination accuracy rate of 97.5%. Thus, NIR technology has proved consistency in its successes for various applications in the paddy industry.

Spectra of misclassified samples showed weaker absorption in the 970 nm and 1030 nm regions, corresponding to O–H stretching overtones of water and C–H vibrations of starch. Since the same varieties may differ slightly in starch (80–84%) and protein (7–9%) content (Xinkang *et al.*, 2023), these compositional differences are likely to modulate the observed bands. The results suggest that both starch structure and protein secondary vibrations contribute to varietal discrimination, with subtle variations being sufficient to influence classification outcomes.

Higher model performances, more than 86% of correct classifications, were obtained at 23% moisture out of the tested moisture contents of 10%, 12%, 15% and 23%. The amount of moisture should be less than 14%, and preferably less than 12% for extended storage times (Gummert, 2010). A moisture amount of 10% is the best moisture level for the storage of rice

seeds. Hence, the SIMCA model developed for the 10% moisture level can be used to identify tested rice varieties in storage condition.

The highest correct classifications are recorded at a moisture content of 23%. In view of the SIMCA performances for 10%, 12%, 15%, and 23% moisture contents, it is noted that, when increasing the moisture content of paddy seeds, the number of correct classifications is also increasing. Some paddy samples are recorded as "no matches". The "no matches" could potentially be reduced by increasing the number of spectra in the model-building set (Balasuriya *et al.*, 2010).

The tested five varieties of paddy are very similar in physical characteristics such as their colour, shape and kernel characters. So the spectral features of all varieties are almost similar. One of the research projects, similar to our work, on "transmission NIR spectroscopy for discrimination of geographical origins of rice" by Jaejin *et al.*, (2010) has indicated that the overall spectral features between Korean and Chinese rice samples which were used for their research were almost identical. Rice is composed of approximately 80~84% starch and 7~9% protein. Fats, minerals, and vitamins are the other minor constituents. Therefore, the resulting NIR features are obviously dominated by those of starch. As starch is a huge polymer of glucose, with a molecular weight ranging from 50,000 to 200,000 Daltons, it would be hard to find spectral differences from starch for discrimination. Conversely, although the protein content is relatively much lower, this could provide valuable spectral clues for discrimination, because of the higher variability in the chemical structure (Xia *et al.*, 2013). Therefore, the latent variable working behind the classifications would be these differences in the varieties. Other than that, the micro level structural variations and colour variations that are invisible to the human eye in the seed coat may play an important role. The limited financial resources available for this project did not permit detailed constituent analysis to be included in this study. Nevertheless, a research proposal is currently being formulated to enable more comprehensive investigations into the biochemical and structural bases of correct varietal identification. Such an extension would provide stronger evidence for the mechanistic role of starch and protein features in spectral classification.

Average spectra observation of paddy seed varieties

According to the average spectra, samples of paddy seed varieties showed relatively higher NIR radiation reflectance at 10% moisture content and lowest reflectance at 23% moisture content. That means higher light absorbance in higher moisture content and lower light absorbance in lower moisture content. Similar to our findings, Sineenart & Sontisuk (2012) have indicated in their research on "Detection for moisture content of sweet tamarind flesh by transmittance short wavelength near-infrared spectroscopy", that averaged absorbance of low moisture content was reported less than that of middle and high moisture content. However, the pattern of light absorbance has altered with 12% and 15% moisture contents.

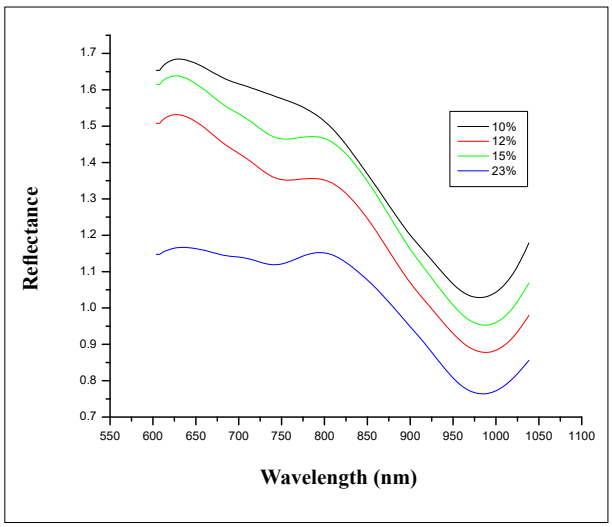

Figure 2: Average spectra of Bg 300

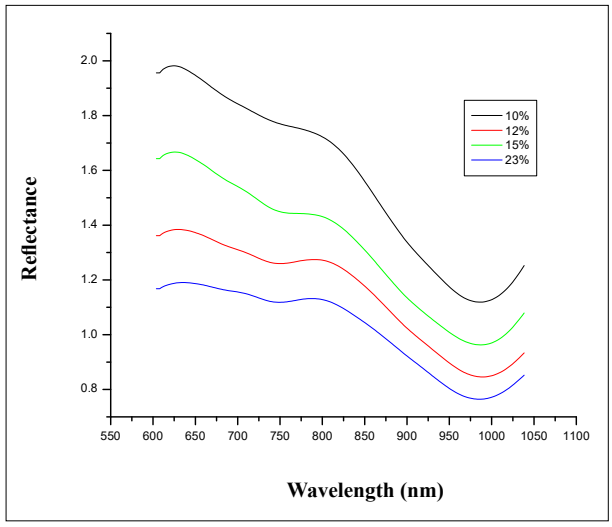

Figure 3: Average spectra of Bg 352

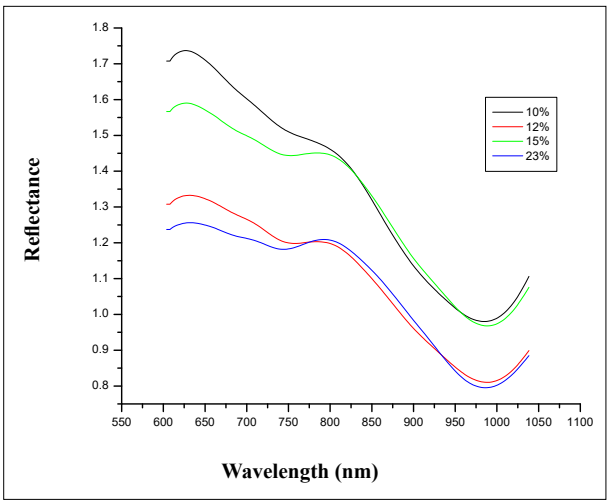

Figure 4: Average spectra of Bg 357

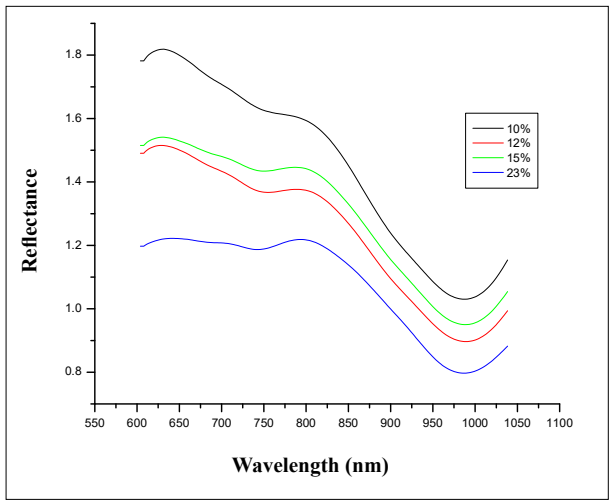

Figure 5: Average spectra of Bg 359

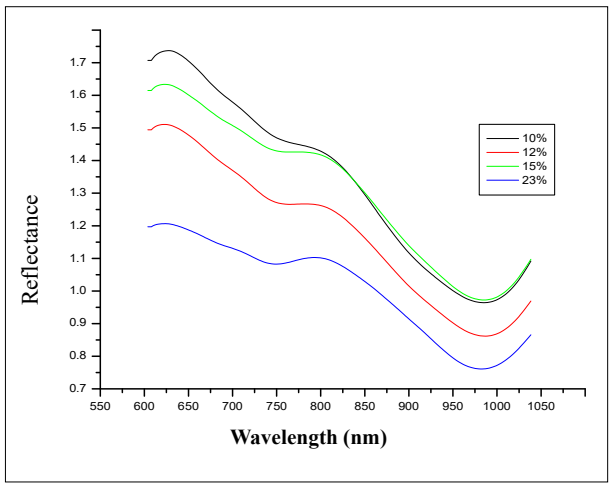

Figure 6: Average spectra of Bw 363

A considerable effort was made to illustrate and present the spectral differences between samples under different scenarios. However, due to the very low amplitude on a single y-axis scale, it was not possible to present these differences graphically. This limitation underscores the sensitivity of NIR methods, where subtle but meaningful differences may not always be visually discernible yet can still be captured effectively through chemometric modeling.

Different rice varieties at the same moisture content have identical relative moisture on a dry matter basis, according to the gravimetric definition. However, the absolute amount of water present in each sample cup may vary across varieties because of differences in bulk density arising from kernel size and shape. This observation highlights the importance of considering physical grain characteristics in addition to chemical composition when interpreting NIR-based varietal discrimination. When looking at the average spectra of all paddy varieties it is clear that the pattern of absorbance at different amounts of moistures is almost similar from 630 to 800 nm. That means, macro level individual characteristics of all the samples are more or less similar at the visible region. When considering average spectra, their pattern of absorbance was slightly differing when the moisture

contents in the samples were differing at the NIR range 800 nm to 1100 nm, compared to the visible region. According to the distance between baselines of different moisture levels, it is clear that when the prevailing moisture content of the samples is changed, the amount of radiation absorbance of the varieties also change.

There is a strong relationship between water and biological samples and their functionality. Aquaphotomics is the new discipline that is used to define the application of spectrophotometry in the visible/near infrared region to the understanding of the effect of water on the structure and functioning of biological systems (Tsenkova, 2007). This result are consistent with the previous report that all of these sample types are dominated by water and water strongly absorbs NIR light energy. This research has demonstrated the consistency of the concept Aquaphotomics that higher moisture in the sample results in higher radiation absorbance and better accuracy in results.

Discriminating power

The discriminating power graphs in the SIMCA sub plot of results indicate the most effective wavelength for the classification. According to the graph wavelengths close to 740 nm have higher discriminating power. Therefore, we may further investigate possible simplified instrumentation for paddy seed variety detection by using these wavelengths.

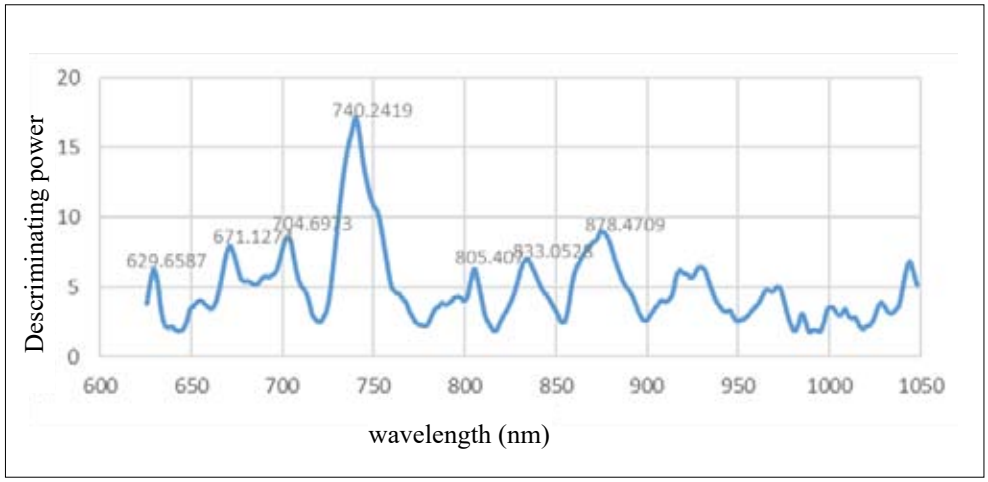

Figure 7: SIMCA discriminating power

CONCLUSION

An increasing trend in correct classification accuracy was observed with elevated sample moisture levels, reaching the highest average accuracy (92%) at 23% MC. This can be attributed to the fact that water molecules exhibit strong and distinct absorbance bands in the NIR region for the biological sample (Jinendra *et al.*, 2010), particularly around 740 nm and 878 nm. At higher MC levels, these water-associated signals enhance overall spectral contrast, making varietal differences more pronounced and easier for the SIMCA model to capture.

The mis-classification of up to 20% of spectra had little impact on the overall identification of paddy seed varieties. For instance, when spectra of 50 samples were used to represent a single variety in the prediction set, then a 20% error means that only 10 spectra were misclassified while the remaining 40 were correctly assigned into their correct group. Since the majority of spectra clustered within the correct varietal group, the intended variety is reliably revealed. This demonstrates that even with moderate error rates, replicate sampling provides robustness and ensures accurate varietal classification.

The developed SIMCA models for the identification of investigated studied rice varieties, namely Bg300,

Bg352, Bg357, Bg359, and Bw363, were successfully accomplished at a rate of 80% or better accuracy. The developed methodology provides higher identification accuracy when multiple spectra from a single sample are analyzed. By collecting several spectra and assigning the sample to the class indicated by the majority of correctly classified spectra, the overall reliability of the sample identification is enhanced. Elevated moisture content in the paddy sample indicated higher NIR absorbance and also higher accuracy. The research successfully demonstrated the potential of using NIR spectroscopic SIMCA approach for the identification of five tested paddy seed varieties under 10% to 23% moisture range.

Acknowledgement

We gratefully acknowledge Shibuya Seiki Co Ltd., Japan, for providing the NIR spectrometer to carry out this research and Dr.(Mr.) Lionel Nugaliyadde for helping to reach the Rice Research and Development Institute (RRDI), Bathalagoda, Sri Lanka, to get the seed samples from studied rice varieties.

REFERENCES

Xinkang, L., Chunmin, G., Lin, W., Liting, J., Xiangjin, F., Qinlu, L., *et al.* (2023). Rice Storage Proteins: Focus on Composition, Distribution, Genetic Improvement and Effects on Rice Quality. *Rice Science*, 207-221. doi.org/10.1016/j.rsci.2023.03.005

Awanthi, M., Jinendra, B., Nawaratne, S., & Nawaratne, C. (2019). Adaptation of visible and short wave Near Infrared (VIS-SW-NIR) COMMON PLS model for quantifying paddy hardness. *Journal of Cereal Science, 89*, 102795. doi:org/10.1016/j.jcs.2019.102795

Balasuriya, J., Katsutomo, T., Shinichiro, K., Maria, V., Shinya, Y., & Roimiana, T. (2010). Near infrared spectroscopy and aquaphotomics: Novel approach for rapid *in vivo* diagnosis of virus infected soybean. *Biochemical and Biophysical Research Communications, 397*, 685-690.

Barton, F., Windham, W., Champagene, E., & Lyon, B. (1998). Optimal Geo-metries for the Development of Rice Quality Spectroscopic Chemometric Models. *Cereal Chemistry, 75*(3), 315-319.

Bertrand, D., Robert, P., & Loisel, W. (2006). Identification of some wheat varieties by near infrared reflectance spectroscopy. *Journal of the science of food and Agriculture spectroscopy, 36*(11), 1120–1124.

Cheng, F., & Ying, Y. (2004). Machine vision inspection of rice seed based on Hough transform. *Journal of Zhejiang University Science, 5*, 663- 667.

Delwiche, S., Bean, M., Miller, R., Webb, B. D., & Williams, P. (1995). Apparent Amylose Content of Milled Rice by Near-infrared Reflectance Spectrophotometry. *Cereal Chemistry, 72*(2), 182-187.

Delwiche, S., McKenzie, K., & Webb, B. (1996). Quality Characteristics in Rice by Near-infrared Reflectance Analysis of Whole-grain Milled Samples. *Cereal Chemistry, 73*(2), 257-263.

DOA. (2015). *Rice.* Retrieved 10 21, 2015, from Department of Agriculture: http://agridept.gov.lk/index.php/en/journals

Gummert, M. (2010). *Seed quality.* Retrieved 05 22, 2015, from knowledgebank: http://www.knowledgebank.irri.org/step-by-step-production/pre-planting/seed-quality

Guzman, J., & Peralta, E. (2008). Classification of Philippine rice grains using machine vision and artificial neural networks. *World conference on agricultural information and IT* (pp. 41-48.). Tokyo, Japan : IAALD AFITA WCCA.

Huebner, F., Hussain, A., Lookhart, G., Bietz, J., Bushuk, W., & Juliano, B. (1991). Discrimination of sister-line IR rice varieties by polyacrylamide-gel electrophoresis and reversed-phase high-performance liquid-chromatography. *Cereal Chemistry, 68*, 583-588.

Hussain, Z. P., Azmi, M., & Ahmad, S. O. (2010). Morphological Study of the Relationships between Weedy Rice Accessions (*Oryza sativa* Complex) and Commercial Rice Varieties in Pulau Pinang Rice Granary Area. *Tropical Lifesciences Research, 21*(2), 27-40.

IRRI. (2021). *Measuring Moisture Content*. Retrieved 08 12, 2021, from http://www.knowledgebank.irri.org/step-by-step-production/postharvest/milling/milling-and-quality/measuring-moisture-content-in-milling#in-drying

Jaejin, K., Jihye, Y., Si Jun, P., & Hoeil, C. (2010, 10 15-18). Transmission NIR Spectroscopy for Discrimination of Geographical Origins of Rice. *The 2nd Asian Symposium on Near Infrared Spectroscopy*, p. 121.

Jing, Z., Mingliang, L., Tao, P., Lijun, Y., & Jiemei, C. (2019). Purity analysis of multi-grain rice seeds with non-destructive visible and near infrared spectroscopy. *Computers and Electronics in Agriculture, 104882*, 164.

Kawamura, S., Natsuga, M., & Itoh, K. (2006). Visual and Near-infrared Reflectance Spectroscopy for Determining Physicochemical Properties of Rice. *American Society of Association Executives Annual International Meeting* (pp. 1069- 1076). Orlando: American Society of Agricultural and Biological

Engineers.

Li, X., He, Y., & Wu, C., (2008). Non-destructive discrimination of paddy seeds of different storage age based on Vis/NIR spectroscopy. *Journal of Stored Products Research, 44*(3), 264–268.

Liu, Z., Cheng, F., Ying, Y., & Rao, X. (2005). Identification of rice seed varieties using neural network. *Journal of Zhejiang University Science , 6*(11), 1095- 1100.

Namaporn, A., Sumaporn, K., & Athapol, N. (2011). Rapid Variety Identification of Pure Rough Rice. *Cereal Chemistry, 88*(5), 490-496. doi:10.1094/CCHEM-03-11-0025

Sasaki, R. (2004). Characteristics and Seedling Establishment of Rice Nursing Seedlings. *Japan Agricultural Research Quarterly, 38*(1), 7-13. doi:10.6090/jarq.38.7

Song, C., Weihui, Z., Fengrong, Z., & Guoping, Z. (2010). Effect of Planting Method on Grain Quality and Nutrient Utilization for No-Tillage Rice. *Communications in Soil Science and Plant Analysis, 42*(11), 1324-1335. doi:.org/10.1080/00103624.2011.571737

Tsenkova, R. (2007). AquaPhotomics: water absorbance pattern as a biological marker for diesease diagnosis and diesease undestanding. *Aquaphotomics, 18*, 15-17.

Wenwen, K., Chu, Z., Fei, L., Pengcheng, N., & Yong, H. (2013). Rice Seed Cultivar Identification Using Near-Infrared Hyper spectral Imaging and Multivariate Data Analysis. *Journal of sensors, 13*(7), 8916-8927.

Windham, W., Lyon, B., Champagne, A., Barton, E., Webb, B., McClung, F., *et al*. (1997). Prediction of Cooked Rice Texture Quality Using Near-infrared Reflectance Analysis of Whole-grain Milled Samples. *Cereal Chemistry, 74*(5), 626- 632.

Wu, J., Yu, H., Dai, H., Mei, W., Huang, X., Zhu, S., & Peng, M. (2012). Metabolite profiles of rice cultivars containing bacterial blight-resistant genes are distinctive from susceptible rice. *44*, 650- 659.

Xia, L., Shen, S., Liu, Z., & Sun, H. (2013). Identification of geographical origins of rice with pattern recognition technique by near infrared spectroscopy. *Spectroscopy and Spectral Analysis, 33*, 102- 105.

J.Natn.Sci.Foundation Sri Lanka 2025 53 (4): 345 - 362
DOI: http://dx.doi.org/10.4038/jnsfsr.v53i4.12570

RESEARCH ARTICLE

Crop Science

Seasonal variation in crop yield and reduction of phytic acid content through soaking and germination of kodo millet (*Paspalum scrobiculatum L.*) germplasm

C Suneetha and M Sukumar*
Centre for Food Technology, A.C. Tech, Anna University, Chennai 600025, Tamil Nadu, India.

Submitted: 02 February 2025; Revised: 12 August 2025; Accepted: 07 November 2025

Abstract: Kodo millet (*Paspalum scrobiculatum* L.) is a nutrient-rich, gluten-free grain with significant potential for enhancing food security. However, its high phytic acid content limits mineral bioavailability, necessitating strategies for reduction. This study evaluated 75 kodo millet germplasms sourced from ICRISAT and cultivated under surface drip irrigation during the 2022-2023 Rabi (dry/winter season) and 2023-2024 Kharif (wet/monsoon season) at the University of Hyderabad. Two-way ANOVA was used to identify IPs 69 as the highest-yielding variety across both seasons, while IPs 240 (Kharif) and IPs 236 (Rabi) were the lowest yielding. Seasonal variations influenced overall productivity, with Rabi conditions favouring grain production. Phytic acid levels were analysed in husked and dehusked grains, showing significant genetic variation but minimal seasonal influence on post-harvest dehusking. To enhance mineral bioavailability, response surface methodology (RSM) was used to optimize soaking (20.63 h, 38.49 °C, pH 4.08) and germination (36.29 h, 27.29 °C, 65.18% moisture) conditions. Soaking alone resulted in a substantial reduction of phytic acid by 48.11%, while soaking followed by germination led to a total reduction of 53.97%, indicating that germination contributed only a marginal additional decrease beyond soaking. These findings demonstrate that soaking is the primary contributor to phytic acid degradation, with germination playing a supplementary role. This study highlights the importance of selecting high-yielding, nutritionally superior kodo millet varieties while optimizing post-harvest treatments to improve their dietary value. The findings underscore the role of genetic diversity, environmental conditions, and processing interventions in determining the grain's nutritional and agronomic potential. Future research should focus on integrating advanced breeding strategies and optimized processing methods to enhance the bioavailability of essential micronutrients, ensuring kodo millet's broader adoption in sustainable food systems.

Keywords: Kodo millet flour, micro nutrient bioavailability, millet germplasms, *Paspalum scrobiculatum* L., phytic acid

INTRODUCTION

India has been cultivating kodo millets for over 3,000 years. Kodo millet (*Paspalum scrobiculatum* L.) belongs to the family Poaceae, subfamily Panicoideae, and tribe Paniceae. It is a tetraploid species (2n = 4x = 40) believed to have originated in the Indian subcontinent. The germplasm used in this study consisted of 75 genetically diverse accessions sourced from different agro-ecological regions of India, maintained at the ICRISAT. These accessions reflect a broad spectrum of genetic variability in terms of agronomic traits, phenology, and adaptability. Previous molecular and morphological characterizations of *P. scrobiculatum* have shown significant intra-specific variation, which provides a strong foundation for crop improvement and stress resilience breeding efforts (Kandlakunta & Golla, 2017). Before the 1980s, millets were a staple food for the poor, but they were gradually replaced by wheat and rice (Ghosh et al., 2024). Millets are nutritionally superior to major cereals, containing

* Corresponding author (sukumarcbt@gmail.com; https://orcid.org/0000-0003-0614-5473)

This article is published under the Creative Commons CC-BY-ND License (http://creativecommons.org/licenses/by-nd/4.0/). This license permits use, distribution and reproduction, commercial and non-commercial, provided that the original work is properly cited and is not changed in anyway.

higher levels of dietary fibre, resistant starches, vitamins, essential amino acids, storage proteins, and other bioactive compounds, which classify them as nutraceuticals (Saleem et al., 2023a). People today are increasingly aware of the health benefits of millets, which have long been considered a nutritional powerhouse, particularly in Indian communities. Millets are valued for their versatility in various dishes and their climate resilience, making them a sustainable crop option. Their renewed popularity stems from their rich nutritional profile and potential to improve overall health. They have become a modern superfood, gaining popularity in health diets (Kumar et al., 2022).

Furthermore, due to their high dietary fibre content, millets help prevent constipation, support regular bowel movements, and lower the risk of gastrointestinal issues (Nithiyanantham et al., 2019) The thermal effect of the antioxidants of kodo is also very effective (Yadav et al., 2009; Yadav et al., 2022). Individuals with gluten intolerance or celiac disease may benefit from kodo millet, since it is gluten-free (Saleem et al., 2023b). Additionally, its low glycaemic index makes it beneficial for managing blood sugar levels, making it a preferred choice for individuals with diabetes or metabolic disorders (Gupta, 2023; Kanimozhi & Sukumar, 2023)

Despite their nutritional advantages, millets contain anti-nutrients such as tannins, polyphenols, and phytic acid (Geisen et al., 2021), which reduce mineral bioavailability. The most common anti-nutrients in millets are tannins, polyphenols, and particularly phytic acid or phytate which is myoinositol 1,2,3,4,5,6-hexakis dihydrogen phosphate. It is the main storage form of phosphorus, making up 1-5% of the weight in cereals, legumes, nuts, oilseeds, and similar foods (Salim et al., 2023). Phytic acid, stored as phosphorus in seeds, can negatively affect the diet by hindering the absorption of minerals like zinc, magnesium, copper, calcium, and iron (Schlemmer et al., 2009). The recommended dietary allowances (RDAs) by the National Institute of Nutrition (NIN, 2020), for phosphorus in the human diet are as follows: ages 9–13 years: 1,250 mg/day. ; ages 14–18 years: 1,250 mg/day. ; ages 19 and older: 700 mg/day. Phytic acid has a chelating property that binds to minerals, making them unavailable. The removal of phytic acid enhances the bioavailability of various cations, thereby improving the nutritional value of the meal. Several methods have been developed to eliminate phytic acid from grains (Nout MJR, 1993; Sareen et al., 2024).

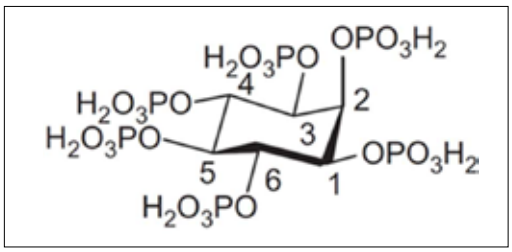

Figure 1: Structure of phytic acid in equatorial conformation. (Marolt & Kolar, 2021)

Anti-nutrients can be minimized using different processing techniques, such as soaking, germination or sprouting, cooking, malting, and fermenting the grains. Reducing phytic acid enhances mineral bioavailability (Sarkhel & Roy, 2022), thus improving the nutritional quality of millet-based diets. Studies have also associated high phytic acid levels with an increased risk of certain cancers. Several processing methods, including soaking, germination, fermentation, and cooking, help reduce phytic acid content (Sachdev et al., 2023). Among these, soaking and germination are widely preferred due to their ability to activate enzymes that degrade phytates (Ranjan et al., 2023). Optimizing these processes enhances the bioavailability of key nutrients, making kodo millet a more viable dietary option (Nobis et al., 2023).

This study optimized soaking and germination conditions to reduce phytic acid in kodo millet using response surface methodology (Dey et al., 2023a). Seventy-five germplasm varieties were cultivated and analysed for phytic acid content in grains with and without husk. The effects of soaking (time, temperature, and pH) and germination (time, temperature, and moisture) on phytic acid degradation were evaluated. Statistical analysis using ANOVA identified significant influencing factors, and RSM determined the optimal conditions for maximum phytic acid reduction, improving the nutritional potential of kodo millet (Gupta et al., 2015a; Mohana Priya et al., 2025).

MATERIALS AND METHODS

Source of raw material

A total of 75 different varieties of kodo millet (*Paspalum scrobiculatum* L.) germplasm core collection has been selected by the ICRISAT gene bank from various states of India such as IPs68, IPs69, IPs91, IPs105 from Bihar; IPs919 from Jharkhand; IPs593 from Gujarat; IPs699, IPs706, IPs709, IPs730, IPs741, IPs744, IPs764, IPs777, IPs782, IPs785, IPs793, IPs795, IPs803, IPs814, IPs828,

IPs862, IPs870, IPs872, IPs883, IPs891, IPs908 from Maharashtra; IPs155, IPs159, IPs172, IPs176, IPs181, IPs207, IPs208, IPs236, IPs240, IPs245, IPs254, IPs429, IPs597, IPs599, IPs606, IPs614, IPs622, IPs627, IPs628, IPs630, IPs645, IPs648, IPs653, IPs654, IPs670 from Madhya Pradesh; IPs274, IPs275, IPs, IPs279, IPs280, IPs287, IPs292, IPs293, IPs669, IPs694, IPs695, IPs928 from Tamil Nadu; IPs318, IPs319, IPs329 from Orissa, IPs585 from unknown location; IPs344, IPs358, IPs368, IPs388, IPs415 from Uttar Pradesh; and IPs4, IPs5, IPs13 from West Bengal. The grains of these 75 kodo millet core germplasms, sourced from the ICRISAT gene bank, were meticulously cultivated in the fields of the University of Hyderabad. All of them represent traditional cultivars or landraces.

Chemicals required

The Megazyme Assay Kit was procured from Megazyme Ltd, Ireland. Ascorbic acid, Sulphuric acid, Ammonium molybdate, Trichloroacetic acid, Hydrochloric acid, Sodium hydroxide were purchased from HiMedia Private Limited, India.

Crop cultivation and harvesting of kodo millet

The study was conducted at the University of Hyderabad, Hyderabad, during the Rabi season (November 2022) and the Kharif season (July 2023). The University of Hyderabad is located in Gachibowli, Hyderabad, Telangana, at a latitude of 17°27′00″ North and a longitude of 78°20′45″ East, with an elevation of approximately 576 meters above mean sea level. All 75 genetically diverse genotypes of Kodo millet germplasms (Upadhyaya et al., 2014) were grown in a randomized block design (Ram et al., 2024) during two seasons from 14th November 2022 to April 25th 2023 in the Rabi season, and from 29th July 2023 to December 20th 2023 in the Kharif season. Millets can thrive in regions with as little as 350 mm of rainfall, making them resilient crops well-suited to withstand harsh climate conditions. The selected geographical land has a pH of 6.0 – 7.5, and receives direct sunlight for 6 – 8 h. Kodo millet is primarily cultivated in India's warm and arid regions. The minimum water requirement for maize is 400 mm, while sorghum requires 500 to 600 mm (Sukanya, 2022.) Kodo millet is typically planted at the start of the monsoon or early in the rainy season.

Seeds were sorted according to their accession numbers and sown in three replications of direct sowing, a common method for kodo millet cultivation. Each accession was planted in single rows measuring 3 meters in length, with a spacing of 30 cm by 10 cm. Observations were taken from five randomly chosen plants within each accession for qualitative and quantitative traits. Proper levelling of the land was done to avoid water stagnation and to ensure that there were no uneven areas. The crop was drip-irrigated to supply water at specific time intervals providing water directly to the roots. Seeds were sown in a randomized pattern that differed in each replication.

Pesticides were used to reduce shoot flies, which affect the yield of the crop. Germination, 50% flowering, days to anthesis, panicle emergence, time from seed set to maturity, senescence, and plant lodging were recorded. Fertilizers were used to enhance growth at 50% germination and 50% flowering stage (Gamulin et al., 2024) . The field was arranged with the accession number of each variety labelled with tags attached to iron rods, for each of the three replications in the field layout. Physiological properties of harvested seeds were estimated to evaluate the yield per plant along with seed weight, colour, and shape.

Estimation of phytic acid

The phytic acid content was estimated for the husked and dehusked grains of all millet varieties. Phytic acid content was measured using the K-PHYT Phytic Acid 05/19 (Phytate)/Total Phosphorus kit (Megazyme, Wicklow, Ireland) according to the manufacturer's instructions with minor modifications. In brief, 100 mg of seed flour was added to 2 mL of 0.66 M HCl and mixed by shaking at room temperature overnight. The resulting extract (1.5 mL) was centrifuged for 10 minutes at 16,000 g, and 0.5 mL of the supernatant was neutralized with 0.5 mL of 0.75 M NaOH. A 12.5 µL portion of the neutralized sample was used for the enzymatic dephosphorylation reaction and subsequent total phosphorus (Ptot) quantification. Simultaneously, another 12.5 µL of the neutralized sample was used to quantify inorganic phosphate (Pi). After enzymatic treatment, both total phosphorus and free phosphate were analysed in a spectrophotometer set at 655 nm. Standards were plotted following the manufacturer's instructions. For every batch of samples used in the colorimetric analysis of phosphorus, a corresponding phosphorus calibration curve was created simultaneously with the same batch of colour reagent. The assay specifically measures phosphorus released as "available phosphorus" from phytic acid, myo-inositol (phosphate)n, and monophosphate esters via phytase and alkaline phosphatase (Boncompagni et al., 2018). The experiments were conducted in triplicate for both seasons of each sample with husk and without husk (dehusked) for 75 varieties of the kodo millet germplasm.

Statistical analysis

The grain yield of 75 Kodo millet germplasms was evaluated across Rabi 2022–2023 and Kharif 2023 seasons using a two-way ANOVA performed using Microsoft Excel (Data Analysis ToolPak) to assess seasonal and varietal influences. The yield data were recorded for both husked and dehusked grains to determine differences in grain productivity and post-harvest characteristics. Based on the two-way ANOVA results, three germplasm varieties with the highest yield obtained during post-harvest (Mahajan et al., 2024), and phytic acid content were selected for further experiments (Singamsetti et al., 2022).

Processing of optimized grains

Kodo millet grains underwent soaking and germination treatments to evaluate phytic acid reduction. Soaking was performed at different times (6–24 h), temperature (25–45 °C), and pH levels (4–7), followed by germination under varying durations (12–48 h), temperature (20–40 °C), and moisture levels (35–75%). Phytic acid content was quantified using the K-PHYT Phytic Acid Kit (Megazyme, Ireland) after enzymatic dephosphorylation (Godrich et al., 2023). The experiment was conducted in triplicates, and data were statistically analysed to determine the impact of treatments on phytic acid degradation (Bhuvaneshwari et al., 2020) .

Response surface methodology (RSM)

The study employed a box–behnken design (BBD) under response surface methodology (RSM) to optimize phytic acid reduction in kodo millet through soaking and germination, using Design-Expert software version 13**.** Independent variables for soaking included time (h), temperature (°C), and pH, while for germination, they included time (h), temperature (°C), and moisture (%). The BBD experimental design generated multiple combinations of these factors with triplicate central points (Buenaño et al., 2024). Phytic acid content was quantified using the K-PHYT Phytic Acid Kit (Megazyme, Ireland) after enzymatic dephosphorylation. ANOVA was performed to determine the significance of variables, and the optimal conditions for maximum phytic acid degradation (%) were obtained through the desirability function method, which identifies the combination of factors that produces the most favorable overall response (Dey et al., 2023b).

RESULTS AND DISCUSSION

Effect of season on crop yield of various germplasm kodo millet grains

Grain yield is a multifaceted trait affected by numerous other component traits. This study on grain yield analysis

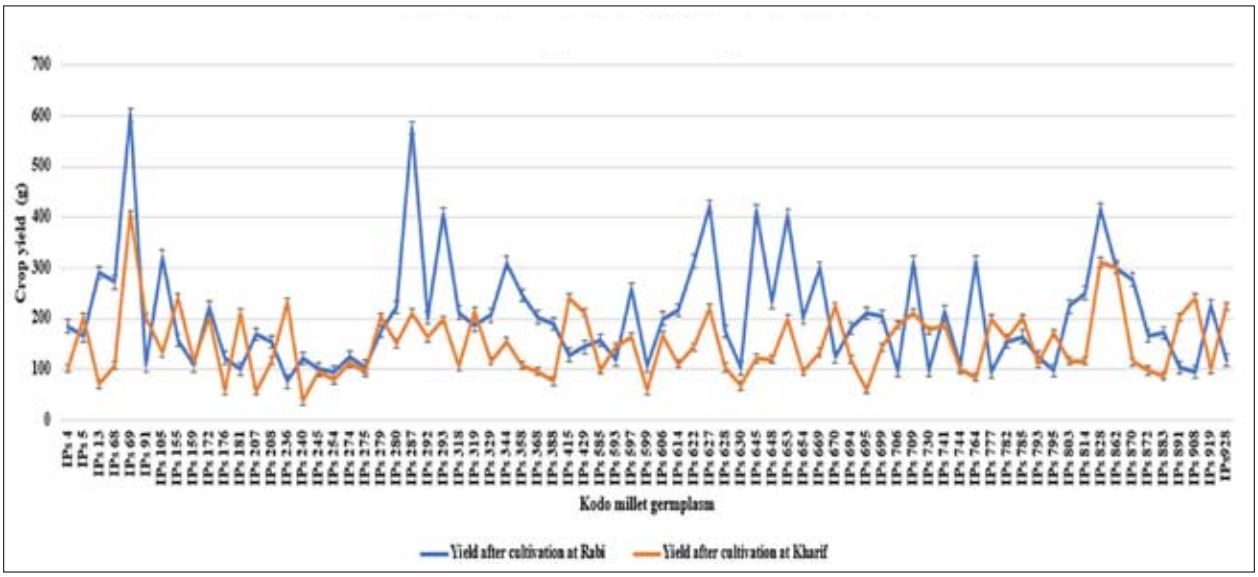

Figure 2: Comparison of the effect of different seasons on the yield of various kodo millet germplasm.

showed that the two different seasons significantly influence yield for each plant variety (Supplementary table 1). Yield per plant was calculated as the average value of three samples obtained from three replications (Figure 2). In this study the seasons and environment played a crucial role in crop yield. Previous studies have shown similar effects on hybrid maize varieties (Mohammed et al., 2016). Recent studies in other millets further substantiate our study. Comparable findings have been reported in pearl millet, where genotype-by-environment interactions had a strong influence not only on the yield but also on associated traits such as starch and mineral content. A recent G×E analysis highlighted the necessity of evaluating pearl millet across multiple seasons to identify stable and high-performing genotypes (Rouamba et al., 2024).

The above results provide insights into the relationships between yield in different seasons, which enhances the effectiveness for the development of elite traits. To ensure statistical reliability additional validation across larger datasets and environments is required (Silva et al., 2024; Preethi & Revadekar, 2013).

The yield distribution of 75 kodo millet germplasm during the Rabi and Kharif seasons is depicted in the box plots (Figure 3). Kharif yields were comparatively lower, with a median of approximately 151 g and an interquartile range of about 101–201 g. The minimum yield was 38.1 g (IPs240), while the maximum yield reached 405.2 g (IPs69). In contrast, the Rabi season yields were significantly higher, with a median of around 185 g and an interquartile range of 122–250 g. Outliers exceeding 575 g were observed in Rabi (e.g., IPs287, IPs69), highlighting the presence of elite high-yielding accessions. Other studies on kodo millet by (SR *et al.,* 2024) under the Kharif season found that treatments employing different organic amendments resulted in significant differences in yield among accessions, further supporting the presence of elite accessions with markedly higher yields under improved management and environmental conditions.

The higher medians, broader yield range, and superior outliers in Rabi indicate that this season provides more favourable conditions for millet cultivation compared to Kharif. These differences are likely attributed to optimal temperature, rainfall, and soil moisture availability during Rabi, which enhance crop growth and grain filling. Similar seasonal trends in yield advantage during Rabi have been reported in studies on small millet productivity, supporting the potential of Rabi cultivation for identifying germplasm with stable and superior yield performance.

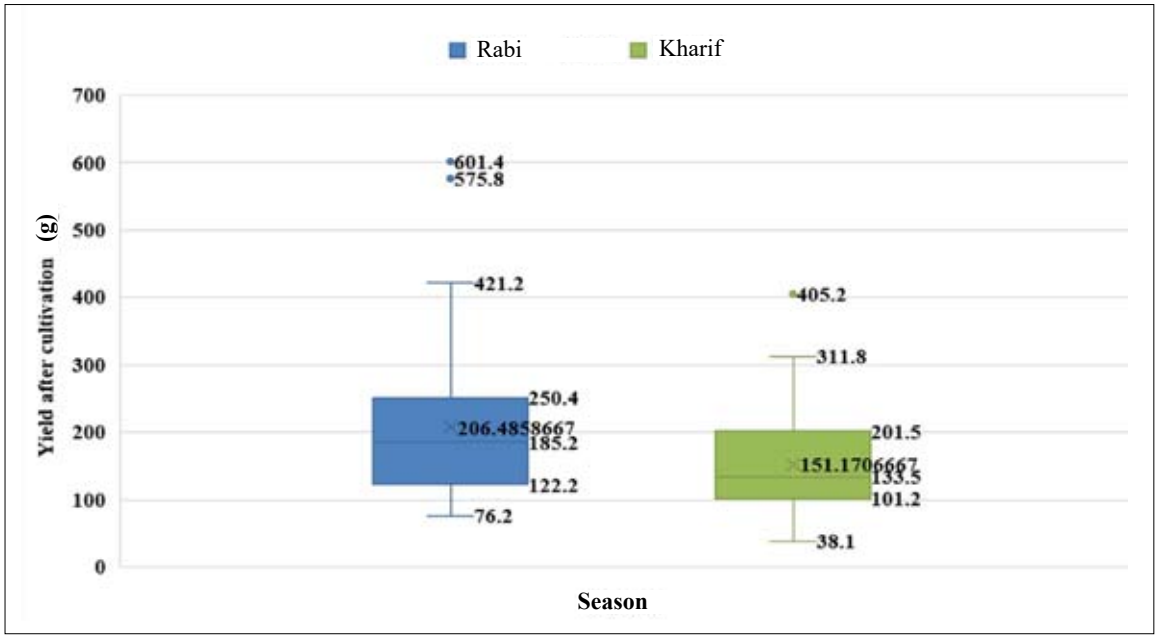

Figure 3: Box plot showing the yield distribution of kodo millet germplasm during Rabi and Kharif seasons.

Estimation and comparison of phytic acid analysis in husked and dehusked grains

Supplementary Table 2 shows the presence of phytic acid (PA) content in kodo millet grains grown during Rabi (R) – with husk (WH) & dehusked (DH) grains, and Kharif (K) – with husk (WH) & dehusked (DH) grains. The top five varieties with the highest PA content under Rabi-WH conditions were IPs 597 (1.0639 g), IPs 585 (0.9821 g), IPs 429 (0.9778 g), IPs 69 (0.9742 g), and IPs 208 (0.9726 g). Under Rabi-DH conditions, the highest PA content was recorded in IPs 597 (0.9913 g), followed by IPs 155 (0.8896 g), IPs 176 (0.8865 g), IPs 606 (0.8766 g), and IPs 319 (0.871 g). These current findings are consistent with previously reported results on dehusked grains of kodo millet (Singh et al., 2024a). The five highest phytic acid content varieties of Kharif-WH were IPs670s - 1.2695 g; IPs883 - 1.1949 g; IPs593 - 1.1834 g; IPs870 - 1.146 g; and IPs155 - 1.1256 g. The highest PA content germplasm varieties of Kharif-DH were IPs706 - 1.1174 g; IPs645 - 1.1057 g; IPs741 - 0.9907 g; IPs694 - 0.9127 g; and IPs329 - 0.8911 g. The highest PA content was shown in the germplasm variety IPs670-1.2695/100 g grown in Kharif-WH. The results indicated that the lowest values were recorded in Rabi-WH and were selected for further analysis. The ANOVA revealed significant differences in phytic acid content among kodo millet germplasms with husk across Rabi and Kharif seasons (Figure 4a). A strong genetic influence was observed ($F = 5.96$, $P < 0.001$), along with a significant seasonal effect ($F = 8.17$, $P = 0.0055$), indicating environmental conditions impact phytic acid accumulation. These findings highlight the potential for selecting low-phytic acid accessions and optimizing cultivation practices to enhance nutritional quality.

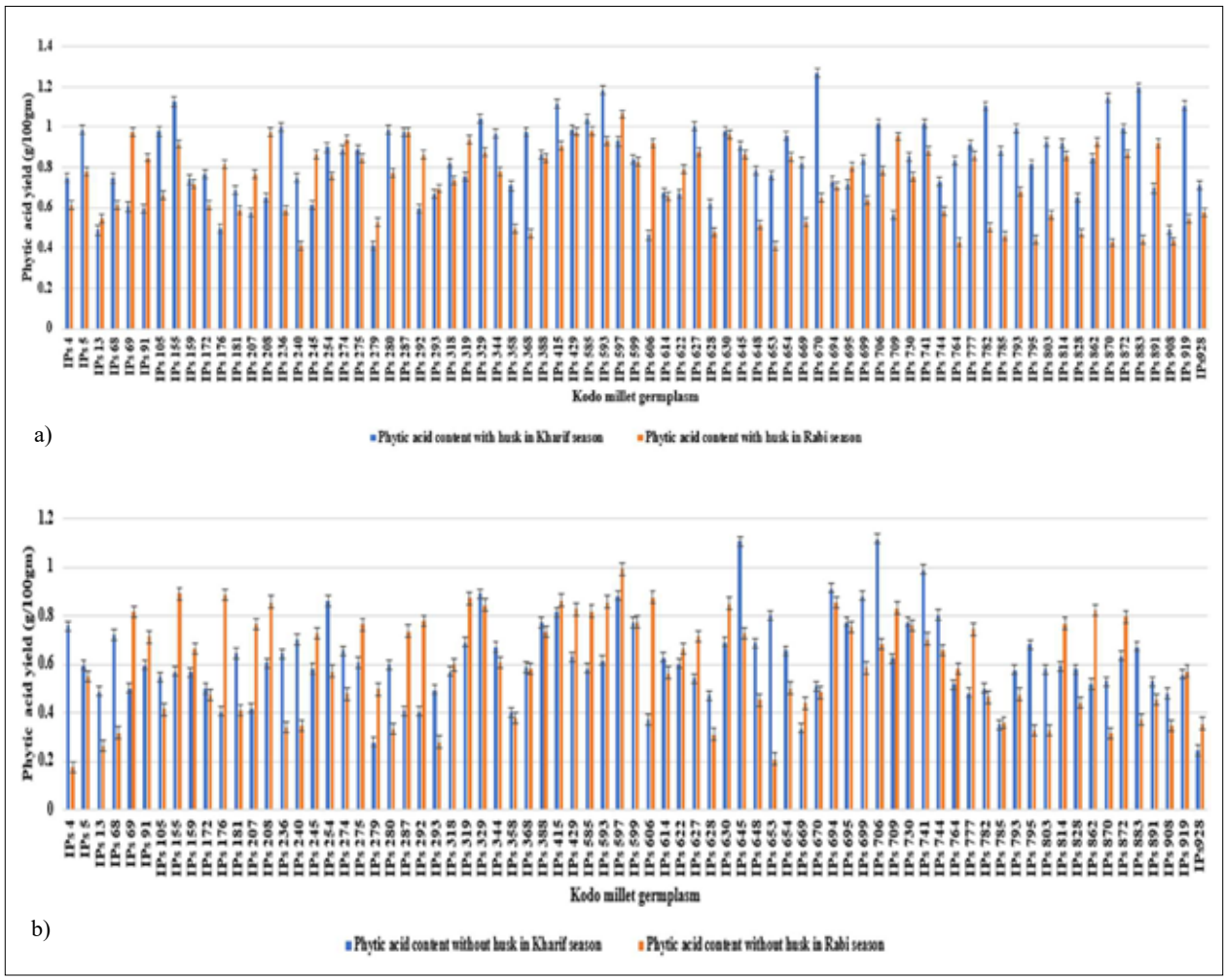

Figure 4: Comparison of phytic acid content of kodo millet grains in Kharif & Rabi season; a) with husk; b) dehusked

Significant differences were found for phytic acid assay analysis between the two seasons for the with-husk trait, as shown in Figure 4a. The five highest PA content varieties of R-WH husk and K-WH were considered to estimate the average PA content. From the results, the Kharif season has the PA content with an average mean value of 1.18 g/100 g, which is higher than the Rabi season with husk, with an average mean value of 0.99 g/100 g.

A two-way ANOVA on dehusked grains (Figure 4.b**)** confirmed genetic factors as the primary determinant of phytic acid content ($F = 1312.53$, $P < 0.001$), while seasonal variation had no significant impact ($F = 1.266$, $P = 0.264$). Consequently, seasonal variation no longer affects phytic acid content after husk removal (Tullu et al., 2001).

Table 1(a): Analysis of variance of phytic acid (g/100 g) in kodo millet grains with husk cultivated in different seasons

Source of variation	Sum of squares (SS)	Degrees of freedom (df)	Mean square (MS)	F- statistic	P-value	F critical value
Rows (Accession)	17.453	74	0.235	5.955	2.64E-13	1.469
Columns (season)	0.323	1	0.323	8.169	0.005	3.970

Table 1(b): Analysis of variance of phytic acid (g/100gm) in dehusked kodo millet grains cultivated in different seasons.

Source of variation	Sum of squares (SS)	Degrees of freedom (df)	Mean square (MS)	F- statistic	P-value	F crit
Rows (Accession)	4002.858	75	53.37144	1312.531	0	1.465625
Columns (season)	0.051491	1	0.051491	1.266276	0.264055	3.968471

Although the two seasons exhibited distinct differences, the PA content in each accession was relatively similar, with minimal variation. The phytic acid content among the accessions in R-DH were: IPs 597 (1.0639 g/100 g) > IPs 585 (0.9821 g/100 g) > IPs 429 (0.9778 g/100 g) > IPs 69 (0.9742 g/100 g) > IPs 208 (0.9726 g/100 g). In the K-DH samples, the phytic acid content were: IPs 670s (1.2695 g/100 g), IPs 883 (1.1949 g/100 g), IPs 593 (1.1834 g/100 g), IPs 870 (1.146 g/100 g), and IPs 155 (1.1256 g/100 g). The results demonstrated that the lowest values, illustrated in Figures 4a. and 4b, were observed in Rabi-WH and selected for further analysis. Similar to our findings, Singh *et al.,* (2024b), reported that dehusked kodo millet grains contained significantly lower levels of phytic acid compared to whole grains, while processing consistently reduces its content and improves mineral bioavailability (Shobana *et al.,* 2013). These studies corroborate our results that Rabi with husked grains had lower PA levels than Kharif, but the seasonal effect diminished after husk removal. Our results showing seasonal variation in phytic acid content of kodo millet align with recent findings that phytate levels in cereals are significantly influenced by cropping system and harvest year (Korge *et al.,* 2025)

Effect of soaking intervals and germination time on phytic acid content reduction using RSM:

The response surface methodology (RSM) analysis, performed using Design-Expert software version 13, demonstrated that both soaking and germination significantly influenced phytic acid degradation in kodo millet (Sharma *et al.,* 2016).

Effect of soaking in kodo millet

The model F-value of 362.26 confirms statistical significance, with only a 0.01% probability of occurring due to noise. P-values < 0.0500 indicate significant model terms. The predicted R^2 (0.9804) aligns well with the adjusted R^2 (0.9960), with a difference < 0.2, confirming model reliability.

The adeq precision ratio of 59.716 indicates a strong signal-to-noise ratio (Table 4b) (Zhang & Bai, 2014). Analysis by RSM and the 3D response surface plot (Figure 5) show that soaking time, temperature, and pH significantly impact phytic acid degradation. The optimized conditions of 20.63 h soaking, 38.49 °C, and pH 4.08 resulted in 48.11% degradation, aligning with high-degradation regions in the 3D plot. Extended soaking (18–24 h) and elevated temperatures (~40–45 °C) enhance enzymatic activity and phytic acid diffusion. Additionally, acidic conditions (pH ~4) promote phytase activity, accelerating phytic acid breakdown *(Lu* et al., 2024).

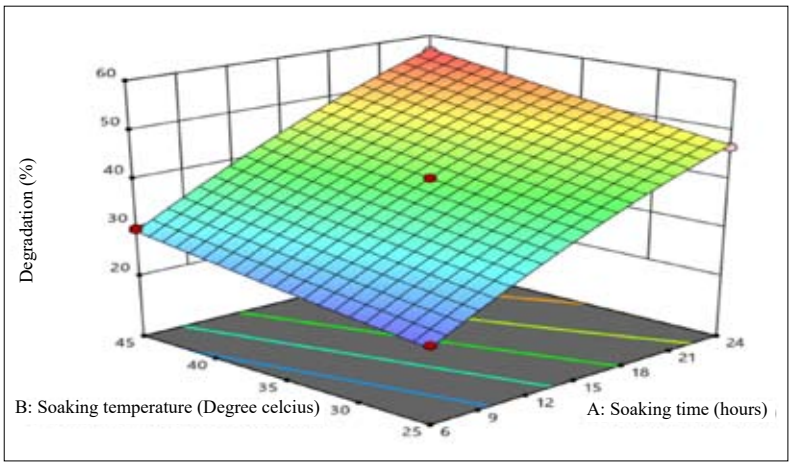

Figure 5: 3D surface plot of soaking conditions on phytic acid reduction.

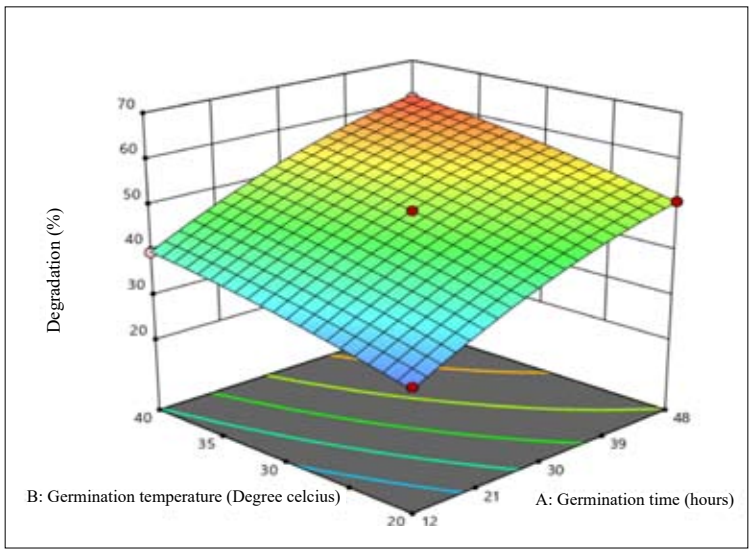

Figure 6): 3D surface plot of germination conditions on phytic acid reduction.

Effect of germination on kodo millet

The model F-value of 493.01 confirms statistical significance, with only a 0.01% probability of occurring due to noise. The P-value of < 0.0500 indicates significant model terms. The predicted R^2 (0.9856) closely aligns with the adjusted R^2 (0.9971), confirming model reliability. The adeq precision ratio of 69.522 indicates a strong signal (Gupta et al., 2015b).

An RSM analysis and the 3D response surface plot (Figure 6) show that germination time, temperature, and moisture significantly influence phytic acid degradation. The optimized conditions of 36.29 h for germination, at 27.29 °C, and 65.18% moisture achieved a 53.97% reduction in phytic acid, as determined by the box-behnken design (BBD). Extended germination (30–48 hours) and moderate temperatures (~27–40 °C) enhance phytase activity, improving mineral bioavailability. However, excessive moisture or prolonged germination may not yield further benefits (Maldonado-Alvarado et al., 2023).

These findings confirm that controlled germination effectively reduces phytic acid levels, enhancing the nutritional quality of plant-based foods.

Unlike other cereals and grains, millets can be germinated easily and have significantly more nutrients, boosting the bioavailability of micro nutrients (Harshitha et al., 2024). This, further increases the intake of vitamins, and other supplementary foods (Senthilnathan & Muthusamy, 2022).

As a result, the body can absorb minerals such as iron and zinc more efficiently, promoting improved digestion. According to a review, sprouted grains have a lower glycaemic index (Lestari et al., 2017), making them an excellent choice for individuals who need to manage their blood sugar levels regularly (Ikram et al., 2021). Parallel studies on germinated legumes contained more essential amino acids, which are the building blocks of protein that help repair muscles and strengthen your immune system (Semba et al., 2021). Sprouted grains are high in fibre, which helps maintain a healthy gut and encourages regular bowel movements. They can also reduce the risk of digestive problems, such as irritable bowel syndrome (IBS). The current study revealed that soaking and germination of kodo millets can decrease antinutrient phytic acid and increase micronutrient absorption.

CONCLUSION

This study highlights the potential of optimizing soaking and germination conditions to reduce the phytic acid content in kodo millet, thereby improving mineral bioavailability. The findings confirm that genetic factors dominate phytic acid levels, while seasonal variation has minimal influence after dehusking. Optimized soaking conditions (20.63 h, 38.49 °C, pH 4.08) alone accounted for a major reduction in phytic acid (48.11%), whereas soaking followed by germination (36.29 h, 27.29 °C, 65.18% moisture) resulted in a total reduction of 53.97%. This indicates that germination by itself contributes only a relatively small additional reduction beyond the effect achieved through soaking. These results provide valuable insights into improving the nutritional profile of kodo millet, making it a more accessible and functional food ingredient. Additionally, integrating these optimized techniques with modern food processing methods, such as puffing and popping, can enhance the commercial viability of kodo millet as a ready-to-eat product. The findings of this study can also aid in the pre-selection and release of elite cultivars with improved yield and nutritional properties, contributing to sustainable millet production and helping the way forward for future research on new genetic variations and a promising crop for food security.

REFERENCES

Barcelos, Q. de L., Ishikawa, F. H., Costa, L. C., Pádua, P. F. de, Abreu, Â. de F. B., Ramalho, M. A. P., Santos, J. B. dos, & Souza, E. de. (2024). Investigating the resistance of common bean germplasm to *Colletotrichum lindemuthianum* and its implications for breeding. *Crop Breeding and Applied Biotechnology*, *24*(4). https://doi.org/10.1590/1984-70332024v24n4a49

Bhuvaneshwari, G., Nirmalakumari, A., & Kalaiselvi, S. (2020). Impact of soaking, sprouting on antioxidant and anti-nutritional factors in millet grains. *Journal of Phytology*, 62–66. https://doi.org/10.25081/jp.2020.v12.6384

Boncompagni, E., Orozco-Arroyo, G., Cominelli, E., Gangashetty, P. I., Grando, S., Tenutse Kwaku Zu, T., Daminati, M. G., Nielsen, E., & Sparvoli, F. (2018). Antinutritional factors in pearl millet grains: Phytate and goitrogens content variability and molecular characterization of genes involved in their pathways. *PLoS ONE*, *13*(6). https://doi.org/10.1371/journal.pone.0198394

Buenaño, L., Ali, E., Jafer, A., Zaki, S. H., Hammady, F. J., Khayoun Alsaadi, S. B., Karim, M. M., Ramadan, M. F., Omran, A. A., Alawadi, A., Alsalamy, A., & Kazemi,

A. (2024). Optimization by Box–Behnken design for environmental contaminants removal using magnetic nanocomposite. *Scientific Reports*, *14*(1), 6950. https://doi.org/10.1038/s41598-024-57616-8

Dey, S., Saxena, A., Kumar, Y., Maity, T., & Tarafdar, A. (2023a). Optimizing the effect of ultrasonication and germination on antinutrients and antioxidants of kodo (Paspalum scrobiculatum) and little (Panicum sumatrense) millets. *Journal of Food Science and Technology*, *60*(12), 2990–3001. https://doi.org/10.1007/s13197-023-05837-6

Dey, S., Saxena, A., Kumar, Y., Maity, T., & Tarafdar, A. (2023b). Optimizing the effect of ultrasonication and germination on antinutrients and antioxidants of kodo (Paspalum scrobiculatum) and little (Panicum sumatrense) millets. *Journal of Food Science and Technology*, *60*(12), 2990–3001. https://doi.org/10.1007/s13197-023-05837-6

Gamulin, N., Zorić, M., Karagić, Đ., & Terzić, S. (2024). Assessing green manure impact on wheat productivity through Bayesian analysis of yield monitor data. Frontiers in Plant Science, 15, Article 1323124. https://doi.org/10.3389/fpls.2024.1323124

Geisen, S., Krishnaswamy, K., & Myers, R. (2021). Physical and Structural Characterization of Underutilized Climate-Resilient Seed Grains: Millets, Sorghum, and Amaranth. *Frontiers in Sustainable Food Systems*, *5*. https://doi.org/10.3389/fsufs.2021.599656

Ghosh, K., Vinodkumar, T., Singh, R., Singh, A., & Ilavarasan, R. (2024). Promising potential of millets as the staple of our plate: an Indian perspective. In *Discover Food* (Vol. 4, Issue 1). Springer Nature. https://doi.org/10.1007/s44187-024-00176-7

Godrich, J., Rose, P., Muleya, M., & Gould, J. (2023). The effect of popping, soaking, boiling and roasting processes on antinutritional factors in chickpeas and red kidney beans. *International Journal of Food Science & Technology*, *58*(1), 279–289. https://doi.org/10.1111/ijfs.16190

Gupta, R. K., Sharma, P. K., & Pandey, A. (2023). Importance of millets w.s.r. to medicinal and nutritional value: A review. *International Journal of AYUSH*, *12*(2), 8–14. https://www.researchgate.net/publication/369476394

Gupta, R. K., Gangoliya, S. S., & Singh, N. K. (2015a). Reduction of phytic acid and enhancement of bioavailable micronutrients in food grains. *Journal of Food Science and Technology*, *52*(2), 676–684. https://doi.org/10.1007/s13197-013-0978-y

Gupta, R. K., Gangoliya, S. S., & Singh, N. K. (2015b). Reduction of phytic acid and enhancement of bioavailable micronutrients in food grains. *Journal of Food Science and Technology*, *52*(2), 676–684. https://doi.org/10.1007/s13197-013-0978-y

Harshitha, T., Ramesh, J., Gawali, P. P., Adusumilli, S., Dasalkar, A. H., & Yannam, S. K. (2024). Impact of ultraviolet radiation coupled with thermal treatment on the foxtail millet flour properties. *Journal of Food Measurement and Characterization*, *18*(8), 7145–7159. https://doi.org/10.1007/s11694-024-02726-0

Ikram, A., Saeed, F., Afzaal, M., Imran, A., Niaz, B., Tufail, T., Hussain, M., & Anjum, F. M. (2021). Nutritional and end-use perspectives of sprouted grains: A comprehensive review. In *Food Science and Nutrition* (Vol. 9, Issue 8, pp. 4617–4628). John Wiley and Sons Inc. https://doi.org/10.1002/fsn3.2408

Kandlakunta, B., & Golla, S. D. (2017). Nutritional and health benefits of millets. *Indian Institute of Millets Research (IIMR),* Hyderabad, India. 1–24. http://www.millets.res.in

Kanimozhi, N. V., & Sukumar, M. (2023). Stability and bio accessibility of heme iron from Glycine max and Vigna unguiculata for the enhancement strategies in yoghurt fortification. *Journal of Agriculture and Food Research*, *12*. https://doi.org/10.1016/j.jafr.2023.100596

Korge, M., Alaru, M., Keres, I., Möll, K., Talgre, L., Voor, I., Altosaar, I., & Loit-Harro, E. (2025). Phytate Content in Cereals Impacted by Cropping System and Harvest Year. *Foods*, *14*(3). https://doi.org/10.3390/foods14030446

Kumar, L., Naresh, R. K., Tiwari, H., Kataria, S. K., Saharan, S., Reddy, B. R., Singh, O., Qidwai, S., & Singh, R. P. (2022). Millets for Food and Nutritional Security in the Context of Climate Resilient Agriculture: A Review. *International Journal of Plant & Soil Science*, 939–953. https://doi.org/10.9734/ijpss/2022/v34i232504

Lestari, L. A., Huriyati, E., & Marsono, Y. (2017). The development of low glycemic index cookie bars from foxtail millet (Setaria italica), arrowroot (Maranta arundinacea) flour, and kidney beans (Phaseolus vulgaris). *Journal of Food Science and Technology*, *54*(6), 1406–1413. https://doi.org/10.1007/s13197-017-2552-5

Lu, J., Zamaratskaia, G., Langton, M., Röhnisch, H. E., & Karkehabadi, S. (2024). Minimizing anti-nutritional factors in wet protein extraction from Swedish faba beans through the application of response surface methodology. *Food Chemistry*, *460*, 140700. https://doi.org/10.1016/j.foodchem.2024.140700

Mahajan, M., Singla, P., & Sharma, S. (2024). Sustainable postharvest processing methods for millets: A review on its value-added products. *Journal of Food Process Engineering*, *47*(1). https://doi.org/10.1111/jfpe.14313

Maldonado-Alvarado, P., Pavón-Vargas, D. J., Abarca-Robles, J., Valencia-Chamorro, S., & Haros, C. M. (2023). Effect of Germination on the Nutritional Properties, Phytic Acid Content, and Phytase Activity of Quinoa (Chenopodium quinoa Willd). *Foods*, *12*(2), 389. https://doi.org/10.3390/foods12020389

Marolt, G., & Kolar, M. (2021). Analytical methods for determination of phytic acid and other inositol phosphates: A review. In *Molecules* (Vol. 26, Issue 1). MDPI AG. https://doi.org/10.3390/MOLECULES26010174

Mohammed, R., Are, A. K., Munghate, R. S., Bhavanasi, R., Polavarapu, K. K. B., & Sharma, H. C. (2016). Inheritance of resistance to sorghum shoot fly, atherigona soccata in Sorghum, Sorghum bicolor (L.) Moench. *Frontiers in Plant Science*, *7*(APR2016). https://doi.org/10.3389/fpls.2016.00543

Mohana Priya, M., Sangeetha, V., Jeevanantham, A., & Jeevabharathi, R. (2025). Optimization and formulation of nutrient-rich millet pasta using RSM. *Journal of Chemical Health Risks*, *15*(1), 1–12. https://www.jchr.org

Nithiyanantham, S., Kalaiselvi, P., Mahomoodally, M.

F., Zengin, G., Abirami, A., & Srinivasan, G. (2019). Nutritional and functional roles of millets—A review. *Journal of Food Biochemistry*, 43(7), e12859. https://doi.org/10.1111/jfbc.12859

Nobis, A., Berg, B., Gastl, M., & Becker, T. (2023). Changes in bioavailability of zinc during malting process and wort production. *European Food Research and Technology*, *249*(1), 157–165. https://doi.org/10.1007/s00217-022-04141-5

Nout MJR. (1993). Processed weaning foods for tropical climates. *International Journal of Food Science and Nutrition*, *43*, 213–221.

Preethi, B., & Revadekar, J. V. (2013). Kharif foodgrain yield and daily summer monsoon precipitation over India. *International Journal of Climatology*, *33*(8), 1978–1986. https://doi.org/10.1002/joc.3565

Ram, G., Choudhary, Dr. A., & Deshmukh, Y. (2024). Effect of different sowing windows and nutrient levels on yield attributes, yield and economics of barnyard millet during rabi season. *International Journal of Advanced Biochemistry Research*, *8*(11S), 241–244. https://doi.org/10.33545/26174693.2024.v8.i11sd.2882

Ranjan, R., Singh, S., Dhua, S., Mishra, P., Chauhan, A. K., & Gupta, A. K. (2023). Kodo Millet (Paspalum scrobiculatum): Bioactive Profile, Health Benefits and Techno- Functionality. In *Nutri-Cereals: Nutraceutical and Techno-Functional Potential* (pp. 193–211). CRC Press. https://doi.org/10.1201/9781003251279-8

Rezzouk, F. Z., de Lima, V. J., Diez-Fraile, M. C., Aparicio, N., Serret, M. D., & Araus, J. L. (2023). Assessing performance of European elite bread wheat cultivars under Mediterranean conditions: Breeding implications. *Field Crops Research*, *302*, 109089. https://doi.org/10.1016/j.fcr.2023.109089

Rouamba, A., Shimelis, H., Drabo, I., Mrema, E., & Gangashetty, P. I. (2024). Screening pearl millet genotypes for resistance to Striga hermonthica and compatibility to Fusarium oxysporum f.sp. strigae. *Crop Protection*, *178*, 106573. https://doi.org/10.1016/j.cropro.2024.106573

Sachdev, N., Goomer, D. S., Singh, D. L. R., Pathak, D. V. M., Aggarwal, D. D., & Chowhan, D. R. K. (2023). Current status of millet seed proteins and its applications: A comprehensive review. In *Applied Food Research* (Vol. 3, Issue 1). Elsevier B.V. https://doi.org/10.1016/j.afres.2023.100288

Saleem, S., Mushtaq, N. U., Shah, W. H., Rasool, A., Hakeem, K. R., Seth, C. S., Tahir, I., & Rehman, R. U. (2023a). Millets as smart future food with essential phytonutrients for promoting health. In *Journal of Food Composition and Analysis* (Vol. 124). Academic Press Inc. https://doi.org/10.1016/j.jfca.2023.105669

Saleem, S., Mushtaq, N. U., Shah, W. H., Rasool, A., Hakeem, K. R., Seth, C. S., Tahir, I., & Rehman, R. U. (2023b). Millets as smart future food with essential phytonutrients for promoting health. *Journal of Food Composition and Analysis*, *124*, 105669. https://doi.org/10.1016/j.jfca.2023.105669

Salim, R., Nehvi, I. B., Mir, R. A., Tyagi, A., Ali, S., & Bhat, O. M. (2023). A review on anti-nutritional factors: unraveling the natural gateways to human health. *Frontiers in Nutrition*, *10*. https://doi.org/10.3389/fnut.2023.1215873

Sareen, B., Pudake, R. N., Sevanthi, A. M., & Solanke, A. U. (2024). Biotechnological approaches to reduce the phytic acid content in millets to improve nutritional quality. In *Planta* (Vol. 260, Issue 4, p. 99). https://doi.org/10.1007/s00425-024-04525-9

Sarkhel, S., & Roy, A. (2022). Phytic acid and its reduction in pulse matrix: Structure–function relationship owing to bioavailability enhancement of micronutrients. *Journal of Food Process Engineering*, *45*(5). https://doi.org/10.1111/jfpe.14030

Schlemmer, U., Frølich, W., Prieto, R. M., & Grases, F. (2009). Phytate in foods and significance for humans: Food sources, intake, processing, bioavailability, protective role and analysis. In *Molecular Nutrition and Food Research* (Vol. 53, Issue SUPPL. 2, pp. S330–S375). Wiley-VCH Verlag. https://doi.org/10.1002/mnfr.200900099

Semba, R. D., Ramsing, R., Rahman, N., Kraemer, K., & Bloem, M. W. (2021). Legumes as a sustainable source of protein in human diets. *Global Food Security*, *28*. https://doi.org/10.1016/j.gfs.2021.100520

Senthilnathan, K., & Muthusamy, S. (2022). Optimal process condition (UV-C): Quantitative findings on the mineral profile, bio-active profile, and changes in the quality attributes of fresh microgreen juice. *Journal of Food Processing and Preservation*, *46*(8). https://doi.org/10.1111/jfpp.16780

Sharma, Seema & Saxena, Dharmesh & Riar, Charanjit. (2016). Analysing the effect of germination on phenolics, dietary fibres, minerals and γ-amino butyric acid contents of barnyard millet (Echinochloa frumentaceae). Food Bioscience. *13*. 60-68. 10.1016/j.fbio.2015.12.007.

Shobana, S., Krishnaswamy, K., Sudha, V., Malleshi, N. G., Anjana, R. M., Palaniappan, L., & Mohan, V. (2013). *Finger Millet (Ragi, Eleusine coracana L.)* (pp. 1–39). https://doi.org/10.1016/B978-0-12-410540-9.00001-6

Silva, R. M. da, Thurow, L. B., Nardino, M., Oliveira, V. F. de, Lopes, J. L., Maltzahn, L. E., Venske, E., Pegoraro, C., Maia, L. C. da, & Oliveira, A. C. (2024). Identification of RILs for agronomic and grain quality traits in rice through Intraspecific crosses. *Crop Breeding and Applied Biotechnology*, *24*(1). https://doi.org/10.1590/1984-70332024v24n1a05

Singamsetti, A., Shahi, J. P., Zaidi, P. H., & Seetharam, K. (2022). Study on applicability of Genotype × Yield × Trait (GYT) biplots over Genotype × Trait (GT) biplots in selection of maize hybrids across soil moisture regimes. *Indian Journal of Agricultural Research*, *56*(6), 683–690. https://doi.org/10.18805/IJARe.A-5850

Singh, S. M., Joshi T, J., Sivaranjani, S., & Rao, P. S. (2024a). Effect of hydrothermal pre-treatment on dehulling and nutritional characteristics of Kodo millet. *Journal of Food Measurement and Characterization*, *18*(9), 7700–7713. https://doi.org/10.1007/s11694-024-02758-6

Singh, S. M., Joshi T, J., Sivaranjani, S., & Rao, P. S. (2024b). Effect of hydrothermal pre-treatment on dehulling and nutritional characteristics of Kodo millet. *Journal of Food*

Measurement and Characterization, *18*(9), 7700–7713. https://doi.org/10.1007/s11694-024-02758-6

SR, K., CH, R., HK, P., K, C., & AJ, P. (2024). Effect of different organic sources on growth, yield and economics of kodo millet (Paspalum scrobiculatum L.). *International Journal of Research in Agronomy*, *7*(8), 102–105. https://doi.org/10.33545/2618060X.2024.v7.i8b.1194

Sukanya, T. S. (2022). Cropping system in millets. *Indian Institute of Millets Research (IIMR)*, Hyderabad, India, 1–32. https://www.researchgate.net/publication/359081395

T., D., S., K., Swapnil, G. K., D., P., S., K. K., P., D., M., & S., P. (2024). Evaluation of Genetic Variability in Different Genotypes of Finger Millet (Eleusine coracan L.) through Path and Multivariate Analysis. *Asian Journal of Soil Science and Plant Nutrition*, *10*(3), 82–106. https://doi.org/10.9734/ajsspn/2024/v10i3321

Tullu, A., Kusmenoglu, I., McPhee, K. E., & Muehlbauer, F. J. (2001). Characterization of core collection of lentil germplasm for phenology, morphology, seed and straw yields. *Genetic Resources and Crop Evolution*, *48*(2), 143–152. https://doi.org/10.1023/A:1011254629628

Upadhyaya, H. D., Dwivedi, S. L., Upadhyaya, H. D., Singh, S., Vetriventhan, M., & Sharma, S. (2014). Forming core collections in barnyard, kodo, and little millets using morphoagronomic descriptors. *Crop Science*, *54*(6), 2673–2682. https://doi.org/10.2135/cropsci2014.03.0221

Yadav, B. S., Sharma, A., & Yadav, R. B. (2009). Studies on effect of multiple heating/cooling cycles on the resistant starch formation in cereals, legumes and tubers. *International Journal of Food Sciences and Nutrition*, *60*(SUPPL.4), 258–272. https://doi.org/10.1080/09637480902970975

Yadav, G. P., Dalbhagat, C. G., & Mishra, H. N. (2022). Effects of extrusion process parameters on cooking characteristics and physicochemical, textural, thermal, pasting, microstructure, and nutritional properties of <scp>millet-based</scp> extruded products: A review. *Journal of Food Process Engineering*, *45*(9). https://doi.org/10.1111/jfpe.14106

Zhang, H. W., & Bai, X. L. (2014). Optimization of extraction conditions for phytic acid from rice bran using response surface methodology and its antioxidant effects. *Journal of Food Science and Technology*, *51*(2), 371–376. https://doi.org/10.1007/s13197-011-0521-y

Supplementary Table 01: Estimates of crop yield of 75 Kodo millet accessions cultivated during the Rabi and Kharif seasons

Accession Identifier (Core germplasm samples)	Yield (Rabi season, g)	Yield (Kharif season, g)
IPs 4	185.2±0.01	101.4±0.23
IPs 5	166.2±0.07	202±0.01
IPs 13	291.5±0.17	71.5±0.74
IPs 68	271.6±0.09	107.6±0.17
0.IPs 69	601.4±0.02	405.2±0.14
IPs 91	108.4±0.12	201.5±0.20
IPs 105	321.4±0.05	133.5±0.19
IPs 155	157.6±0.05	241.2±0.05
IPs 159	108.8±0.04	117.2±0.85
IPs 172	222.1±0.02	201.5±0.41
IPs 176	122.78±0.18	58.2±0.73
IPs 181	100.2±0.12	211.5±0.12
IPs 207	169.4±0.26	57.2±0.33
IPs 208	154.2±0.08	117.2±0.61
IPs 236	76.2±0.06	231.5±0.09
IPs 240	122.2±0.43	38.1±0.06
IPs 245	101.6±0.65	94.6±0.71
IPs 254	95.28±0.01	79.5±0.69
IPs 274	125.2±0.02	112.5±0.12
IPs 275	105±0.81	94.2±0.35
IPs 279	175.36±0.43	204.2±0.27
IPs 280	222.8±0.06	151.2±0.38
IPs 287	575.8±0.03	211.4±0.01
IPs 292	201.44±0.18	162.4±0.11
IPs 293	407.25±0.43	197.5±0.75
IPs 318	211.87±0.08	105.4±0.85
IPs 319	187.2±0.03	214.2±0.30
IPs 329	206.3±0.05	116.4±0.27
IPs 344	309.8±0.30	155.4±0.01
IPs 358	247.1±0.43	107.2±0.01
IPs 368	202.66±0.01	95.4±0.14
IPs 388	190.5±0.28	77.1±0.76
IPs 415	129±0.21	241.2±0.30
IPs 429	144.2±0.22	211.5±0.08
IPs 585	157.5±0.45	98.5±0.25
IPs 593	119.1±0.32	144.5±0.86
IPs 597	258.2±0.12	164.2±0.19
IPs 599	106.4±0.01	58.4±0.06
IPs 606	199.8±0.32	166.9±0.44
IPs 614	217±0.62	111.2±0.33

Accession Identifier (Core germplasm samples)	Yield (Rabi season, g)	Yield (Kharif season, g)
IPs 622	313±0.75	144.5±0.71
IPs 627	421.2±0.11	221±0.47
IPs 628	175.5±0.17	103.8±0.22
IPs 630	102.4±0.26	68.4±0.09
IPs 645	411.2±0.35	121.5±0.22
IPs 648	233.1±0.81	119.4±0.20
IPs 653	404.2±0.22	200.1±0.01
IPs 654	201.2±0.89	96.4±0.22
IPs 669	300±0.18	133.5±0.17
IPs 670	124.5±0.80	224.7±0.73
IPs 694	181.2±0.85	119.4±0.19
IPs 695	211.3±0.75	59.7±0.08
IPs 699	205.1±0.83	144.5±0.05
IPs 706	99.4±0.62	188.3±0.85
IPs 709	311.4±0.01	211.5±0.89
IPs 730	97.2±0.42	177.6±0.01
IPs 741	214.1±0.47	188.2±0.07
IPs 744	109.2±0.27	101.2±0.72
IPs 764	311.4±0.30	84.5±0.83
IPs 777	94.7±0.04	199.5±0.21
IPs 782	154.8±0.09	161.5±0.19
IPs 785	164.7±0.11	201.2±0.11
IPs 793	124.2±0.06	111.4±0.05
IPs 795	97.2±0.27	171.4±0.73
IPs 803	224.1±0.05	116.5±0.57
IPs 814	250.4±0.42	116.5±0.60
IPs 828	414.2±0.16	311.8±0.23
IPs 862	301.2±0.08	299.4±0.15
IPs 870	277.1±0.72	114.5±0.09
IPs 872	166.7±0.04	97.8±0.33
IPs 883	172.6±0.69	87.5±0.41
IPs 891	103.4±0.23	203.4±0.20
IPs 908	94.8±0.03	241.3±0.52
IPs 919	224.8±0.20	100±0.64
IPs928	119.4±0.09	224.6±0.02

Supplementary Table 02: Estimation of phytic acid (g/100 g) in kodo millet grains with husk cultivated in the two seasons

Accession Identifier (Core germplasm samples)	Rabi season - kodo millet grains with husk - Phytic acid (g/100 g) Grains with Husk	Kharif season - kodo millet grains with husk - Phytic acid (g/100 g) Grains with Husk
IPs04	0.6120±0.003	0.7499±0.002
IPs05	0.7810±0.014	0.9881±0.002
IPs13	0.5450±0.012	0.4879±0.037
IPs 68	0.6121±0.002	0.7450±0.009
IPs69	0.9742±0.006	0.6042±0.011
IPs91	0.849±0.010	0.5950±0.058
IPs105	0.6637±0.012	0.9784±0.043
IPs155	0.9166±0.055	1.1256±0.007
IPs159	0.7157±0.014	0.7389±0.024
IPs172	0.6124±0.003	0.7668±0.012
IPs176	0.8131±0.023	0.4945±0.082
IPs181	0.5896±0.006	0.6869±0.022
IPs207	0.7652±0.010	0.5782±0.038
IPs208	0.9726±0.014	0.6504±0.052
IPs236	0.5865±0.014	0.9986±0.027
IPs240	0.4108±0.007	0.7495±0.031
IPs245	0.8667±0.006	0.6135±0.022
IPs254	0.7573±0.041	0.8983±0.016
IPs274	0.9409±0.011	0.8887±0.039
IPs275	0.8455±0.009	0.8908±0.035
IPs279	0.5271±0.011	0.4092±0.041
IPs280	0.7708±0.071	0.9872±0.035
IPs287	0.9767±0.071	0.9725±0.007
IPs292	0.8640±0.002	0.5932±0.012
IPs293	0.6957±0.003	0.6703±0.028
IPs318	0.7340±0.062	0.8220±0.007
IPs319	0.9361±0.019	0.7564±0.070
IPs329	0.8772±0.024	1.0439±0.086
IPs344	0.7778±0.006	0.9699±0.023
IPs358	0.4981±0.005	0.7087±0.018
IPs368	0.4710±0.021	0.9725±0.013
IPs388	0.8449±0.047	0.8644±0.006
IPs415	0.9066±0.041	1.1165±0.032
IPs429	0.9778±0.074	0.9876±0.026
IPs585	0.9821±0.011	1.0407±0.039
IPs593	0.9344±0.014	1.1834±0.002
IPs597	1.0639±0.051	0.9295±0.028
IPs599	0.8276±0.041	0.8386±0.034
IPs606	0.9191±0.096	0.4634±0.034
IPs614	0.6575±0.013	0.6726±0.049

Accession Identifier (Core germplasm samples)	Rabi season - kodo millet grains with husk - Phytic acid (g/100 g) Grains with Husk	Kharif season - kodo millet grains with husk - Phytic acid (g/100 g) Grains with Husk
IPs622	0.7913±0.057	0.6668±0.023
IPs627	0.8746±0.050	1.0078±0.036
IPs628	0.4766±0.002	0.6177±0.007
IPs630	0.9650±0.018	0.9813±0.038
IPs645	0.8639±0.007	0.9085±0.024
IPs648	0.5134±0.008	0.7842±0.047
IPs653	0.4113±0.013	0.7593±0.014
IPs654	0.8513±0.051	0.9557±0.056
IPs669	0.5271±0.054	0.8240±0.018
IPs670	0.6526±0.021	1.2695±0.017
IPs694	0.7082±0.024	0.7320±0.005
IPs695	0.8019±0.041	0.7171±0.020
IPs699	0.6387±0.008	0.8376±0.007
IPs706	0.7839±0.07	1.0166±0.008
IPs709	0.9534±0.01	0.5659±0.031
IPs730	0.7523±0.091	0.8501±0.084
IPs741	0.8847±0.024	1.0170±0.007
IPs744	0.5839±0.054	0.7293±0.067
IPs764	0.4318±0.047	0.8322±0.024
IPs777	0.8590±0.061	0.9119±0.011
IPs782	0.5049±0.038	1.1048±0.028
IPs785	0.4586±0.024	0.8824±0.032
IPs793	0.6807±0.081	0.9917±0.013
IPs795	0.4439±0.007	0.8140±0.004
IPs803	0.5644±0.004	0.9273±0.008
IPs814	0.8590±0.051	0.9209±0.002
IPs828	0.4752±0.011	0.6508±0.025
IPs862	0.9263±0.027	0.8450±0.039
IPs870	0.4264±0.034	1.1460±0.023
IPs872	0.8677±0.033	0.9917±0.046
IPs883	0.4428±0.051	1.1949±0.026
IPs819	0.9219±0.041	0.6965±0.045
IPs908	0.4324±0.034	0.4900±0.084
IPs919	0.5458±0.017	1.1061±0.008
IPs928	0.5774±0.061	0.7126±0.031

Supplementary Table 03: Estimation of phytic acid (g/100 gm) in dehusked kodo millet grains cultivated in the two seasons

Accession Identifier (Core germplasm samples)	Rabi season - dehusked kodo millet grains- Phytic acid (g/100 g)	Kharif season - dehusked kodo millet grains - Phytic acid (g/100 g)
IPs04	0.1742±0.021	0.7578±0.042
IPs05	0.5491±0.011	0.5948±0.005
IPs13	0.2637±0.043	0.4878±0.018
IPs 68	0.3166±0.007	0.7207±0.023
IPs69	0.8157±0.017	0.5007±0.044
IPs91	0.7124±0.029	0.5950±0.058
IPs105	0.4131±0.022	0.5471±0.06
IPs155	0.8896±0.004	0.5711±0.059
IPs159	0.6652±0.027	0.5663±0.002
IPs172	0.4726±0.027	0.4981±0.023
IPs176	0.8865±0.061	0.4051±0.050
IPs181	0.4108±0.024	0.6449±0.084
IPs207	0.7667±0.051	0.4175±0.018
IPs208	0.8573±0.081	0.6051±0.002
IPs236	0.3409±0.061	0.6421±0.020
IPs240	0.3455±0.017	0.7019±0.009
IPs245	0.7271±0.084	0.5817±0.015
IPs254	0.5708±0.034	0.8611±0.016
IPs274	0.4767±0.024	0.6545±0.008
IPs275	0.7640±0.011	0.6063±0.022
IPs279	0.4957±0.061	0.2784±0.013
IPs280	0.3340±0.071	0.5988±0.026
IPs287	0.7361±0.005	0.4071±0.007
IPs292	0.7772±0.007	0.4046±0.009
IPs293	0.2778±0.009	0.4949±0.020
IPs318	0.5981±0.611	0.5710±0.027
IPs319	0.8710±0.034	0.6911±0.019
IPs329	0.8449±0.041	0.8911±0.021
IPs344	0.6066±0.052	0.6701±0.081
IPs358	0.3778±0.034	0.4014±0.081
IPs368	0.5821±0.072	0.5881±0.029
IPs388	0.7344±0.011	0.7715±0.031
IPs415	0.8639±0.034	0.8154±0.066
IPs429	0.8276±0.027	0.6301±0.041
IPs585	0.8191±0.067	0.5841±0.024
IPs593	0.8575±0.094	0.6141±0.517
IPs597	0.9913±0.037	0.8814±0.047
IPs599	0.7746±0.051	0.7715±0.051
IPs606	0.8766±0.017	0.3711±0.081
IPs614	0.5650±0.005	0.6271±0.099

Accession Identifier (Core germplasm samples)	Rabi season - dehusked kodo millet grains- Phytic acid (g/100 g)	Kharif season - dehusked kodo millet grains - Phytic acid (g/100 g)
IPs622	0.6639±0.064	0.6017±0.044
IPs627	0.7134±0.081	0.5418±0.841
IPs628	0.3113±0.014	0.4710±0.241
IPs630	0.8513±0.002	0.6914±0.841
IPs645	0.7271±0.081	1.1057±0.571
IPs648	0.4526±0.009	0.6881±0.441
IPs653	0.2082±0.051	0.8021±0.755
IPs654	0.5019±0.080	0.6551±0.141
IPs669	0.4387±0.043	0.3342±.0841
IPs670	0.4839±0.067	0.5084±0.084
IPs694	0.8534±0.019	0.9127±0.035
IPs695	0.7523±0.046	0.7751±0.051
IPs699	0.5847±0.039	0.8821±0.049
IPs706	0.6839±0.051	1.1174±0.057
IPs709	0.8318±0.067	0.6227±0.117
IPs730	0.7590±0.003	0.7751±0.077
IPs741	0.7049±0.191	0.9907±0.025
IPs744	0.6586±0.040	0.8041±0.051
IPs764	0.5807±0.028	0.5160±0.078
IPs777	0.7439±0.084	0.4814±0.060
IPs782	0.4644±0.064	0.5001±0.054
IPs785	0.3590±0.028	0.3511±0.081
IPs793	0.4752±0.024	0.5771±0.035
IPs795	0.3263±0.030	0.6804±0.041
IPs803	0.3264±0.051	0.5803±0.011
IPs814	0.7677±0.071	0.5914±0.011
IPs828	0.4428±0.039	0.5803±0.026
IPs862	0.8219±0.049	0.5175±0.028
IPs870	0.3134±0.061	0.5296±0.018
IPs872	0.7948±0.017	0.6335±0.007
IPs883	0.3714±0.077	0.6731±0.033
IPs819	0.4544±0.054	0.5285±0.011
IPs908	0.3461±0.011	0.4801±0.015
IPs919	0.5714±0.040	0.5568±0.013
IPs928	0.3548±0.066	0.2450±0.038

J.Natn.Sci.Foundation Sri Lanka 2025 53 (4): 363 - 373
DOI: http://dx.doi.org/10.4038/jnsfsr.v53i4.12405

RESEARCH ARTICLE

Magnetism

Magnetic properties of body-centred cubic ferromagnetic thin films described by the fourth order perturbed Heisenberg Hamiltonian

MSM Farhan[1*] and P Samarasekara[2]
Department of Physical Science, Facalty of Applied Science, Trincomalee Campus, Eastern University, Sri Lanka.
Department of Physics, Facalty of Science, University of Peradeniya, Peradeniya, Sri Lanka.

Submitted: 21 October 2024; Revised: 11 November 2025; Accepted: 27 November 2025

Abstract: This research investigates the magnetic properties of body-centred cubic (bcc) ferromagnetic thin films with three spin layers, using a detailed model known as the fourth-order perturbed Heisenberg Hamiltonian. Ferromagnetic thin films are essential for modern technologies, such as magnetic sensors and spintronic devices, because their magnetic behaviour can be precisely controlled. We investigated the influence of magnetic anisotropy and spin exchange interactions on the spatial distribution of magnetic energy across the layers. Using MATLAB simulations, we created 3-D and 2-D graphs to analyse energy in relation to the spin exchange interaction and azimuthal angle. Our results show that the total magnetic energy can vary significantly, reaching orders of 10^{17} when the fourth-order anisotropy constant in the bottom spin layer is minimized. In contrast, when the middle spin layer has lower anisotropy, the total magnetic energy decreases to the order of 10^{13}, indicating that it becomes easier for the magnetic moments to rotate. We also found that the angle between consecutive magnetic easy and hard directions is not always 90 degrees, and interchanging layers leads to slight changes in energy maxima and minima. Importantly, the total magnetic energy is significantly higher in configurations with two spin layers, ranging from 10^{42} to 10^{43}, compared to those with three layers. These results underscore the sensitivity of bcc ferromagnetic thin films to variations in magnetic anisotropy and provide important insights for future applications in magnetic storage, sensors, and spintronic technologies.

Keywords: Fourth order perturbed Heisenberg Hamiltonian, magnetic anisotropy constant, magnetic thin films, Spin exchange interaction, spin layers.

INTRODUCTION

Ferromagnetic thin films are important for many modern technologies, such as hard drives, magnetic sensors, and spintronics devices. These films are valuable because their magnetic properties can be controlled at very small scales. The behaviour of these films depends on various factors like interactions between spins, magnetic anisotropy (which defines the preferred direction of magnetization), dipole interactions, and external magnetic fields. Among these materials, thin films with a body-centred cubic (bcc) structure are particularly interesting due to their unique atomic arrangement. In films with three spin layers, the magnetic properties can be complex, as each layer behaves differently based on how the spins interact and align. A key factor that influences their behaviour is magnetic anisotropy, which determines the direction in which the material is easiest to magnetize. Other factors like stress and dipole interactions also play a big role in the magnetic properties of these films.

To understand these properties, researchers often use the Heisenberg Hamiltonian model, which takes into account interactions between spins and the effects of magnetic anisotropy. In previous studies, simpler versions of this model were used to describe thin film magnetism, but for a more detailed analysis, we apply the fourth-order perturbed Heisenberg Hamiltonian.

* Corresponding author (farhanmsm@esn.ac.lk; https://orcid.org/0009-0001-8708-9460)

This article is published under the Creative Commons CC-BY-ND License (http://creativecommons.org/licenses/by-nd/4.0/). This license permits use, distribution and reproduction, commercial and non-commercial, provided that the original work is properly cited and is not changed in anyway.

This version of the model includes higher-order effects like second and fourth-order anisotropy, which helps us better understand how magnetic energy changes across the different spin layers.

Ferromagnetic materials have a natural magnetization, meaning they maintain a magnetic moment even without an external magnetic field. This happens because the spins of electrons are arranged in a regular pattern within regions called magnetic domains. The spin exchange interaction between atoms causes the magnetic moments to align. If the spin exchange constant (J) is positive, the moments align parallel, but if J is negative, they align in opposite directions (antiparallel). Above a certain temperature, called the Curie temperature, the magnetization disappears, and the material becomes paramagnetic. At higher temperatures, the magnetic behaviour follows the Curie-Weiss law. Ferromagnetism comes from unpaired electron spins in the outer subshells of atoms. However, the measured magnetic moments of materials often differ from theoretical predictions due to subshell overlap. When a magnetic field is applied, magnetization increases as spins in different domains rotate and domain walls move. In thin magnetic films, stress can affect magnetization during the heating and cooling process (annealing) because of differences in thermal expansion between the film and its substrate. This stress-induced magnetic anisotropy is similar in strength to the material's natural magneto-crystalline anisotropy, and it influences the material's coercivity, which is a measure of its resistance to becoming demagnetized (Samarasekara & Cadieu, 2001a, 2001b).

Ferromagnetic films have been studied using various models. For example, Monte Carlo simulations have been used to explore the magnetic hysteresis (how magnetization changes with applied magnetic fields) in ferromagnetic thin films grown on special substrates (Zhao *et al.*, 2002). The Ising model has been applied to study the magnetic properties of films with alternating layers (Bentaleb *et al.*, 2002). Additionally, the structural and magnetic properties of two-dimensional FeCo alloys have been determined using first-principles band structure theory (Spisak & Hafner, 2005). The magnetic behaviour of nickel layers on copper has also been studied using the Korringa-Kohn-Rostoker Green's function method (Ernst *et al.*, 2000).

In this manuscript, the total magnetic energy of ferromagnetic thin films is described by solving the classical Heisenberg Hamiltonian. This approach considers all relevant energy terms, including magnetic energy, spin dipole interaction energy, spin exchange interaction energy, second and fourth-order magnetic anisotropy constants, stress-induced anisotropy, and the demagnetization factor. The fourth-order perturbed Heisenberg Hamiltonian, incorporating all seven magnetic energy parameters, is explained for the bcc structure with three spin layers. MATLAB software was used to plot 3-D and 2-D graphs of energy as a function of spin exchange interaction and the azimuthal angle of the spin. The main objective of this study is to investigate how variations in the anisotropy constants of different spin layers influence the magnetic energy minima and maxima in bcc structure ferromagnetic thin films. This helps clarify how layer-dependent anisotropy affects the overall magnetic stability and behaviour of these films.

MODEL

The Heisenberg Hamiltonian of ferromagnetic films can be formulated as follows (Samarasekara *et al.*, 2009, Samarasekara & De Silva, 2007, Samarasekara, 2008).

$$H = -\frac{J}{2}\sum_{m,n}\vec{S}_m.\vec{S}_n + \frac{\omega}{2}\sum_{m\neq n}\left(\frac{\vec{S}_m.\vec{S}_n}{r_{mn}^3} - \frac{3(\vec{S}_m.\vec{r}_{mn})(\vec{r}_{mn}.\vec{S}_n)}{r_{mn}^5}\right) - \sum_m D_{\lambda_m}^{(2)}(S_m^z)^2 - \sum_m D_{\lambda_m}^{(4)}(S_m^z)^4 - \sum_{m,n}[\vec{H} - (N_d\vec{S}_n/\mu_0)].\vec{S}_m - \sum_m K_s \sin 2\theta_m \quad ...(01)$$

Here $\vec{S}_m$ and $\vec{S}_n$ are two spins. The above equation can be simplified into the following form

$$E(\theta) = -\frac{1}{2}\sum_{m,n=1}^{N}\left[\left(JZ_{|m-n|} - \frac{\omega}{4}\Phi_{|m-n|}\right)\cos(\theta_m - \theta_n) - \frac{3\omega}{4}\Phi_{|m-n|}\cos(\theta_m + \theta_n)\right] - \sum_{m=1}^{N}(D_m^{(2)}cos^2\theta_m + D_m^{(4)}cos^4\theta_m + H_{in}sin\theta_m + H_{out}cos\theta_m) + \sum_{m,n=1}^{N}\frac{N_d}{\mu_0}cos(\theta_m - \theta_n) - K_s\sum_{m=1}^{N}sin2\theta_m \quad ...(02)$$

Here N, $m\,(or\,n)$, J, $Z_{|m-n|}$, ω, $\Phi_{|m-n|}$, $\theta_m(\theta_n)$, $D_m^{(2)}$, $D_m^{(4)}$, H_{in}, H_{out}, N_d and K_s are the total number of layers, layer index, spin exchange interaction, number of nearest spin neighbors, strength of long range dipole interaction, partial summations of dipole interaction, azimuthal angles of spins, second and fourth order anisotropy constants, in plane and out of plane applied magnetic fields, demagnetization factor, and stress induced anisotropy constants, respectively.

The spin structure is considered to be slightly disoriented. Therefore, the spins could be considered to have angles distributed about an average angle θ. By choosing azimuthal angles as

$$\theta_m = \theta + \varepsilon_m \text{ and } \theta_n = \theta + \varepsilon_n \quad ...(03)$$

Where the ε's are small positive or negative angular deviations,

Then, $\theta_m - \theta_n = \varepsilon_m - \varepsilon_n$ and $\theta_m + \theta_n = 2\theta + \varepsilon_m + \varepsilon_n$ ...(04)

Substituting equations (3) and (4) in the classical Heisenberg Hamiltonian (2), results in

$$E(\theta) = -\frac{1}{2}\sum_{m,n=1}^{N}\left[\left(JZ_{|m-n|} - \frac{\omega}{4}\Phi_{|m-n|}\right)\cos(\varepsilon_m - \varepsilon_n) - \frac{3\omega}{4}\Phi_{|m-n|}\cos(2\theta + \varepsilon_m + \varepsilon_n)\right] - \sum_{m=1}^{N}(D_m^{(2)}cos^2(\theta + \varepsilon_m)$$
$$+ D_m^{(4)}cos^4(\theta + \varepsilon_m) + H_{in}sin(\theta + \varepsilon_m) + H_{out}cos(\theta + \varepsilon_m)) + \sum_{m,n=1}^{N}\frac{N_d}{\mu_0}cos(\varepsilon_m - \varepsilon_n) - K_s\sum_{m=1}^{N}sin2(\theta + \varepsilon_m) \quad ...(05)$$

The cosine and sine terms can be expanded up to the fourth order of $\varepsilon_m\varepsilon_m$ and $\varepsilon_n\varepsilon_n$ as following.

$$E(\theta) = E_0 + E(\varepsilon) + E(\varepsilon^2) + E(\varepsilon^3) + E(\varepsilon^4) \quad ...(06)$$

Here,

$$E_0 = -\frac{1}{2}\sum_{m,n=1}^{N}\left(JZ_{|m-n|} - \frac{\omega}{4}\Phi_{|m-n|}\right) + \frac{3\omega}{8}cos2\theta\sum_{m,n=1}^{N}\Phi_{|m-n|} - cos^2\theta\sum_{m=1}^{N}D_m^{(2)} - cos^4\theta\sum_{m=1}^{N}D_m^{(4)} - N(H_{in}sin\theta$$
$$+ H_{out}cos\theta + K_s sin2\theta) + \frac{N_d N^2}{\mu_0} \quad ...(07)$$

$$E(\varepsilon) = -\frac{3\omega}{8}sin2\theta\sum_{m,n=1}^{N}\Phi_{|m-n|}(\varepsilon_m + \varepsilon_n) + sin2\theta\sum_{m=1}^{N}D_m^{(2)}\varepsilon_m + 2cos^2\theta sin2\theta\sum_{m=1}^{N}D_m^{(4)}\varepsilon_m - H_{in}cos\theta\sum_{m=1}^{N}\varepsilon_m$$
$$+ H_{out}sin\theta\sum_{m=1}^{N}\varepsilon_m - 2K_s cos2\theta\sum_{m=1}^{N}\varepsilon_m \quad ...(08)$$

$$E(\varepsilon^2) = \frac{1}{4}\sum_{m,n=1}^{N}\left(JZ_{|m-n|} - \frac{\omega}{4}\Phi_{|m-n|}\right)(\varepsilon_m - \varepsilon_n)^2 - \frac{3\omega}{16}cos2\theta\sum_{m,n=1}^{N}\Phi_{|m-n|}(\varepsilon_m + \varepsilon_n)^2 + cos2\theta\sum_{m=1}^{N}D_m^{(2)}\varepsilon_m^2$$
$$+ 2cos^2\theta(cos^2\theta - 3sin^2\theta)\sum_{m=1}^{N}D_m^{(4)}\varepsilon_m^2 + \frac{H_{in}}{2}sin\theta\sum_{m=1}^{N}\varepsilon_m^2 + \frac{H_{out}}{2}cos\theta\sum_{m=1}^{N}\varepsilon_m^2 - \frac{N_d}{2\mu_0}\sum_{m,n=1}^{N}(\varepsilon_m - \varepsilon_n)^2 + 2K_s sin2\theta\sum_{m=1}^{N}\varepsilon_m^2$$

...(09)

$$E(\varepsilon^3) = \frac{\omega}{16} sin2\theta \sum_{m,n=1}^{N} \Phi_{|m-n|} (\varepsilon_m + \varepsilon_n)^3 - \frac{4}{3} sin\theta cos\theta \sum_{m=1}^{N} D_m^{(2)} \varepsilon_m^3 \; -4 sin\theta cos\theta \left(\frac{5}{3} cos^2\theta - sin^2\theta\right) \sum_{m=1}^{N} D_m^{(4)} \varepsilon_m^3$$
$$+ \frac{H_{in}}{6} cos\theta \sum_{m=1}^{N} \varepsilon_m^3 - \frac{H_{out}}{6} sin\theta \sum_{m=1}^{N} \varepsilon_m^3 \; + \frac{4}{3} K_s cos2\theta \sum_{m=1}^{N} \varepsilon_m^3 \qquad ...(10)$$

$$E(\varepsilon^4) = -\frac{1}{48} \sum_{m,n=1}^{N} \left(JZ_{|m-n|} - \frac{\omega}{4} \Phi_{|m-n|}\right) (\varepsilon_m - \varepsilon_n)^4 + \frac{\omega}{64} cos2\theta \sum_{m,n=1}^{N} \Phi_{|m-n|} (\varepsilon_m + \varepsilon_n)^4 \; - \frac{1}{3} cos2\theta \sum_{m=1}^{N} D_m^{(2)} \varepsilon_m^4$$
$$- \left(\frac{5}{3} cos^4\theta - 8 cos^2\theta sin^2\theta + sin^4\theta\right) \sum_{m=1}^{N} D_m^{(4)} \varepsilon_m^4 \; - \frac{H_{in}}{24} sin\theta \sum_{m=1}^{N} \varepsilon_m^4 - \frac{H_{out}}{24} cos\theta \sum_{m=1}^{N} \varepsilon_m^4$$
$$+ \frac{N_d}{24\mu_0} \sum_{m,n=1}^{N} (\varepsilon_m - \varepsilon_n)^4 \; - \frac{2}{3} K_s sin2\theta \sum_{m=1}^{N} \varepsilon_m^4 \qquad ...(11)$$

For films with three spin layers, $N = 3$. Therefore, m and n change from 1 to 3.

$$E_0 = -\frac{3}{2}\left(JZ_0 - \frac{\omega}{4}\Phi_0\right) - 2\left(JZ_1 - \frac{\omega}{4}\Phi_1\right) + \frac{3\omega}{8} cos2\theta (3\Phi_0 + 4\Phi_1) - cos^2\theta (D_1^{(2)} + D_2^{(2)} + D_3^{(2)})$$
$$- cos^4\theta \left(D_1^{(4)} + D_2^{(4)} + D_3^{(4)}\right) - 3(H_{in} sin\theta + H_{out} cos\theta + K_s sin2\theta) + 9\frac{N_d}{\mu_0} \qquad ...(12)$$

$$E(\varepsilon) = -\frac{3\omega}{4} sin2\theta [\Phi_0(\varepsilon_1 + \varepsilon_2 + \varepsilon_3) + \Phi_1(\varepsilon_1 + 2\varepsilon_2 + \varepsilon_3)] + sin2\theta (D_1^{(2)} \varepsilon_1 + D_2^{(2)} \varepsilon_2 + D_3^{(2)} \varepsilon_3)$$
$$+ 2 cos^2\theta sin2\theta \left(D_1^{(4)} \varepsilon_1 + D_2^{(4)} \varepsilon_2 + D_3^{(4)} \varepsilon_3\right) - H_{in} cos\theta (\varepsilon_1 + \varepsilon_2 + \varepsilon_3) + H_{out} sin\theta (\varepsilon_1 + \varepsilon_2 + \varepsilon_3)$$
$$- 2K_s cos2\theta (\varepsilon_1 + \varepsilon_2 + \varepsilon_3) \qquad ...(13)$$

$$E(\varepsilon^2) = \frac{1}{2}\left(JZ_1 - \frac{\omega}{4}\Phi_1\right) ({\varepsilon_1}^2 + 2{\varepsilon_2}^2 + {\varepsilon_3}^2 - 2\varepsilon_1\varepsilon_2 - 2\varepsilon_2\varepsilon_3) - \frac{3\omega}{8} cos2\theta [2\Phi_0({\varepsilon_1}^2 + {\varepsilon_2}^2 + {\varepsilon_3}^2)$$
$$+ \Phi_1({\varepsilon_1}^2 + 2{\varepsilon_2}^2 + {\varepsilon_3}^2 + 2\varepsilon_1\varepsilon_2 + 2\varepsilon_2\varepsilon_3)] + cos2\theta (D_1^{(2)} {\varepsilon_1}^2 + D_2^{(2)} {\varepsilon_2}^2 \; + D_3^{(2)} {\varepsilon_3}^2)$$
$$+ 2 cos^2\theta (cos^2\theta - 3 sin^2\theta) \left(D_1^{(4)} {\varepsilon_1}^2 + D_2^{(4)} {\varepsilon_2}^2 + D_3^{(4)} {\varepsilon_3}^2\right) + \frac{H_{in}}{2} sin\theta ({\varepsilon_1}^2 + {\varepsilon_2}^2 + {\varepsilon_3}^2)$$
$$+ \frac{H_{out}}{2} cos\theta ({\varepsilon_1}^2 + {\varepsilon_2}^2 + {\varepsilon_3}^2) - 2\frac{N_d}{\mu_0} ({\varepsilon_1}^2 + {\varepsilon_2}^2 + {\varepsilon_3}^2 - \varepsilon_1\varepsilon_2 - \varepsilon_1\varepsilon_3 - \varepsilon_2\varepsilon_3)$$
$$+ 2K_s sin2\theta ({\varepsilon_1}^2 + {\varepsilon_2}^2 + {\varepsilon_3}^2) \qquad ...(14)$$

$$E(\varepsilon^3) = \frac{\omega}{8} sin2\theta[4\Phi_0({\varepsilon_1}^3 + {\varepsilon_2}^3 + {\varepsilon_3}^3) + \Phi_1({\varepsilon_1}^3 + 3{\varepsilon_1}^2\varepsilon_2 + 3\varepsilon_1{\varepsilon_2}^2 + 2{\varepsilon_2}^3 + 3{\varepsilon_2}^2\varepsilon_3 + 3\varepsilon_2{\varepsilon_3}^2 + {\varepsilon_3}^3)]$$

$$-\frac{4}{3} sin\theta cos\theta \left(D_1^{(2)}{\varepsilon_1}^3 + D_2^{(2)}{\varepsilon_2}^3 + D_3^{(2)}{\varepsilon_3}^3\right) - 4sin\theta cos\theta \left(\frac{5}{3}cos^2\theta - sin^2\theta\right)$$

$$\left(D_1^{(4)}{\varepsilon_1}^3 + D_2^{(4)}{\varepsilon_2}^3 + D_3^{(4)}{\varepsilon_3}^3\right) + \frac{H_{in}}{6} cos\theta({\varepsilon_1}^3 + {\varepsilon_2}^3 + {\varepsilon_3}^3) - \frac{H_{out}}{6} sin\theta({\varepsilon_1}^3 + {\varepsilon_2}^3 + {\varepsilon_3}^3)$$

$$+\frac{4}{3} K_s cos2\theta({\varepsilon_1}^3 + {\varepsilon_2}^3 + {\varepsilon_3}^3) \qquad ...(15)$$

$$E(\varepsilon^4) = -\frac{1}{24}\left(JZ_1 - \frac{\omega}{4}\Phi_1\right)({\varepsilon_1}^4 - 4{\varepsilon_1}^3\varepsilon_2 + 6{\varepsilon_1}^2{\varepsilon_2}^2 - 4\varepsilon_1{\varepsilon_2}^3 + 2{\varepsilon_2}^4 - 4{\varepsilon_2}^3\varepsilon_3 + 6{\varepsilon_2}^2{\varepsilon_3}^2$$

$$-4\varepsilon_2{\varepsilon_3}^3 + {\varepsilon_3}^4) + \frac{\omega}{32} cos2\theta[8\Phi_0({\varepsilon_1}^4 + {\varepsilon_2}^4 + {\varepsilon_3}^4) + \Phi_1({\varepsilon_1}^4 + 4{\varepsilon_1}^3\varepsilon_2 + 6{\varepsilon_1}^2{\varepsilon_2}^2$$

$$+4\varepsilon_1{\varepsilon_2}^3 + 2{\varepsilon_2}^4 + 4{\varepsilon_2}^3\varepsilon_3 + 6{\varepsilon_2}^2{\varepsilon_3}^2 + 4\varepsilon_2{\varepsilon_3}^3 + {\varepsilon_3}^4)] - \frac{1}{3} cos2\theta(D_1^{(2)}{\varepsilon_1}^4 + D_2^{(2)}{\varepsilon_2}^4$$

$$+D_3^{(2)}{\varepsilon_3}^4) - \left(\frac{5}{3}cos^4\theta - 8cos^2\theta sin^2\theta + sin^4\theta\right)\left(D_1^{(4)}{\varepsilon_1}^4 + D_2^{(4)}{\varepsilon_2}^4 + D_3^{(4)}{\varepsilon_3}^4\right)$$

$$-\frac{H_{in}}{24} sin\theta({\varepsilon_1}^4 + {\varepsilon_2}^4 + {\varepsilon_3}^4) - \frac{H_{out}}{24} cos\theta({\varepsilon_1}^4 + {\varepsilon_2}^4 + {\varepsilon_3}^4) + \frac{N_d}{6\mu_0}({\varepsilon_1}^4 - 2{\varepsilon_1}^3\varepsilon_2 + 3{\varepsilon_1}^2{\varepsilon_2}^2$$

$$-2\varepsilon_1{\varepsilon_2}^3 + {\varepsilon_2}^4 - 2{\varepsilon_1}^3\varepsilon_3 + 3{\varepsilon_1}^2{\varepsilon_3}^2 - 2\varepsilon_1{\varepsilon_3}^3 + {\varepsilon_3}^4 - 2{\varepsilon_2}^3\varepsilon_3 + 3{\varepsilon_2}^2{\varepsilon_3}^2$$

$$-2\varepsilon_2{\varepsilon_3}^3) - \frac{2}{3} K_s sin2\theta({\varepsilon_1}^4 + {\varepsilon_2}^4 + {\varepsilon_3}^4) \qquad ...(16)$$

The first order perturbation term can be expressed in terms of a row and column matrix with all seven terms in each, as follows.

$$E(\varepsilon) = \vec{\alpha}.\vec{\varepsilon} \qquad ...(17)$$

Here the terms of α are given by α_1, α_2 and α_3.

$$\alpha_1 = -\frac{3\omega}{4} sin2\theta(\Phi_0 + \Phi_1) + sin2\theta D_1^{(2)} + 2cos^2\theta sin2\theta D_1^{(4)} - H_{in}cos\theta + H_{out}sin\theta - 2K_s cos2\theta \qquad ...(18)$$

$$\alpha_2 = -\frac{3\omega}{4} sin2\theta(\Phi_0 + 2\Phi_1) + sin2\theta D_2^{(2)} + 2cos^2\theta sin2\theta D_2^{(4)} - H_{in}cos\theta + H_{out}sin\theta - 2K_s cos2\theta \qquad ...(19)$$

$$\alpha_3 = -\frac{3\omega}{4} sin2\theta(\Phi_0 + \Phi_1) + sin2\theta D_3^{(2)} + 2cos^2\theta sin2\theta D_3^{(4)} - H_{in}cos\theta + H_{out}sin\theta - 2K_s cos2\theta \qquad ...(20)$$

The second order perturbation term can be expressed in terms of a 2 × 2 × 2 matrix, a row matrix and a column matrix, as follows.

$$E(\varepsilon^2) = \frac{1}{2}\vec{\varepsilon}.C.\vec{\varepsilon} \quad ...(21)$$

Elements of the 3 × 3 matrix (C) are delineated by

$$C_{11} = JZ_1 - \frac{\omega}{4}\Phi_1 - \frac{3\omega}{4}cos2\theta(2\Phi_0 + \Phi_1) + 2cos2\theta D_1^{(2)} + 4cos^2\theta(cos^2\theta - 3sin^2\theta)D_1^{(4)} + H_{in}sin\theta + H_{out}cos\theta - \frac{4N_d}{\mu_0} + 4K_s sin2\theta \quad ...(22)$$

$$C_{12} = C_{21} = C_{23} = C_{32} = -JZ_1 + \frac{\omega}{4}\Phi_1 - \frac{3\omega}{4}cos2\theta\Phi_1 + \frac{2N_d}{\mu_0} \quad ...(23)$$

$$C_{13} = C_{31} = \frac{2N_d}{\mu_0} \quad ...(24)$$

$$C_{22} = 2\left(JZ_1 - \frac{\omega}{4}\Phi_1\right) - \frac{3\omega}{2}cos2\theta(\Phi_0 + \Phi_1) + 2cos2\theta D_2^{(2)} + 4cos^2\theta(cos^2\theta - 3sin^2\theta)D_2^{(4)} + H_{in}sin\theta + H_{out}cos\theta - \frac{4N_d}{\mu_0} + 4K_s sin2\theta \quad ...(25)$$

$$C_{33} = JZ_1 - \frac{\omega}{4}\Phi_1 - \frac{3\omega}{4}cos2\theta(2\Phi_0 + \Phi_1) + 2cos2\theta D_3^{(2)} + 4cos^2\theta(cos^2\theta - 3sin^2\theta)D_3^{(4)} + H_{in}sin\theta + H_{out}cos\theta - \frac{4N_d}{\mu_0} + 4K_s sin2\theta \quad ...(26)$$

The third order perturbation term can be expressed in terms of a 2 × 2 matrix, a row matrix and a column matrix, as follows.

$$E(\varepsilon^3) = \varepsilon^2.\beta.\vec{\varepsilon} \quad ...(27)$$

Elements of the 3 × 3 matrix (β) are specified by

$$\beta_{11} = \frac{\omega}{8}sin2\theta(4\Phi_0 + \Phi_1) - \frac{4}{3}sin\theta cos\theta D_1^{(2)} - 4sin\theta cos\theta\left(\frac{5}{3}cos^2\theta - sin^2\theta\right)D_1^{(4)} + \frac{H_{in}}{6}cos\theta - \frac{H_{out}}{6}sin\theta + \frac{4}{3}K_s cos2\theta \quad ...(28)$$

$$\beta_{12} = \beta_{21} = \beta_{23} = \beta_{32} = \frac{3\omega}{8}sin2\theta\Phi_1 \quad ...(29)$$

$$\beta_{13} = \beta_{31} = 0 \quad ...(30)$$

$$\beta_{22} = \frac{\omega}{4}sin2\theta(2\Phi_0 + \Phi_1) - \frac{4}{3}sin\theta cos\theta D_2^{(2)} - 4sin\theta cos\theta\left(\frac{5}{3}cos^2\theta - sin^2\theta\right)D_2^{(4)} + \frac{H_{in}}{6}cos\theta - \frac{H_{out}}{6}sin\theta + \frac{4}{3}K_s cos2\theta \quad ...(31)$$

$$\beta_{33} = \frac{\omega}{8}sin2\theta(4\Phi_0 + \Phi_1) - \frac{4}{3}sin\theta cos\theta D_3^{(2)} \cdot - 4sin\theta cos\theta\left(\frac{5}{3}cos^2\theta - sin^2\theta\right)D_3^{(4)} + \frac{H_{in}}{6}cos\theta - \frac{H_{out}}{6}sin\theta + \frac{4}{3}K_s cos2\theta \quad ...(32)$$

The fourth order perturbation term can be expressed in terms of a 2 × 2 matrix, a row matrix and a column matrix, as follows.

$$E(\varepsilon^4) = \varepsilon^3.F.\vec{\varepsilon} + \varepsilon^2.G.\varepsilon^2 \quad ...(33)$$

Elements of the 3 × 3 matrix (F and G) are delineated by

$$F_{11} = -\frac{1}{24}\left(JZ_1 - \frac{\omega}{4}\Phi_1\right) + \frac{\omega}{32}cos2\theta(8\Phi_0 + \Phi_1) - \frac{1}{3}cos2\theta D_1^{(2)} - \left(\frac{5}{3}cos^4\theta - 8cos^2\theta sin^2\theta + sin^4\theta\right)D_1^{(4)} - \frac{H_{in}}{24}sin\theta - \frac{H_{out}}{24}cos\theta + \frac{N_d}{6\mu_0} - \frac{2}{3}K_s sin2\theta \quad ...(34)$$

$$D_1^{(4)} - \frac{H_{in}}{24}sin\theta - \frac{H_{out}}{24}cos\theta + \frac{N_d}{6\mu_0} - \frac{2}{3}K_s sin2\theta \quad ...(34)$$

$$F_{21} = F_{23} = F_{32} = \frac{1}{6}\left(JZ_1 - \frac{\omega}{4}\Phi_1\right) + \frac{\omega}{8}cos2\theta\Phi_1 - \frac{N_d}{3\mu_0} \quad ...(35)$$

$$F_{13} = F_{31} = -\frac{N_d}{3\mu_0} \quad ...(36)$$

$$F_{22} = -\frac{1}{12}\left(JZ_1 - \frac{\omega}{4}\Phi_1\right) + \frac{\omega}{16}cos2\theta(4\Phi_0 + \Phi_1)$$

$$-\frac{1}{3}cos2\theta D_2^{(2)} - \left(\frac{5}{3}cos^4\theta - 8cos^2\theta sin^2\theta + sin^4\theta\right)$$

$$D_2^{(4)} - \frac{H_{in}}{24}sin\theta - \frac{H_{out}}{24}cos\theta + \frac{N_d}{6\mu_0} - \frac{2}{3}K_s sin2\theta \quad ...(37)$$

$$F_{33} = -\frac{1}{24}\left(JZ_1 - \frac{\omega}{4}\Phi_1\right) + \frac{\omega}{32}cos2\theta(8\Phi_0 + \Phi_1)$$

$$-\frac{1}{3}cos2\theta D_3^{(2)} - \left(\frac{5}{3}cos^4\theta - 8cos^2\theta sin^2\theta + sin^4\theta\right)$$

$$D_3^{(4)} - \frac{H_{in}}{24}sin\theta - \frac{H_{out}}{24}cos\theta + \frac{N_d}{6\mu_0} - \frac{2}{3}K_s sin2\theta \quad ...(38)$$

$$G_{11} = G_{22} = G_{33} = 0 \quad ...(39)$$

$$G_{12} = G_{21} = -\frac{1}{8}\left(JZ_1 - \frac{\omega}{4}\Phi_1\right) + \frac{3\omega}{32}cos2\theta\Phi_1 + \frac{N_d}{4\mu_0} \quad ...(40)$$

$$G_{23} = G_{32} = -\frac{1}{8}\left(JZ_1 - \frac{\omega}{4}\Phi_1\right) + \frac{3\omega}{32}cos2\theta\Phi_1 + \frac{N_d}{2\mu_0} \quad ... (41)$$

$$G_{13} = G_{31} = \frac{N_d}{4\mu_0} \quad ...(42)$$

Therefore, the total magnetic energy given in equation (6) can be deduced to

$$E(\theta) = E_0 + \vec{\alpha}.\vec{\varepsilon} + \frac{1}{2}\vec{\varepsilon}.C.\vec{\varepsilon} + \varepsilon^2.\beta.\vec{\varepsilon} + \varepsilon^3.F.\vec{\varepsilon} + \varepsilon^2.G.\varepsilon^2 \quad ...(43)$$

For the minimum energy of the second order perturbed term

$$\vec{\varepsilon} = -C^+.\alpha \quad ...(45)$$

Here C^+ is the pseudo inverse of matrix C. C^+ can be found using

$$C.C^+ = 1 - \frac{E}{N} \quad ...(45)$$

Here E is the matrix with all elements given *by* $E_{mn} = 1$. I is the identity matrix.
Therefore, from the matrix equation (44)

$$\varepsilon_1 = -(C_{11}^+\alpha_1 + C_{12}^+\alpha_2 + C_{13}^+\alpha_3) \quad ...(46)$$

$$\varepsilon_2 = -(C_{21}^+\alpha_1 + C_{22}^+\alpha_2 + C_{23}^+\alpha_3) \quad ...(47)$$

$$\varepsilon_3 = -(C_{31}^+\alpha_1 + C_{32}^+\alpha_2 + C_{33}^+\alpha_3) \quad ...(48)$$

After substituting ε in equation (43), the total magnetic energy can be determined.

RESULTS AND DISCUSSION

All the graphs presented in this manuscript were generated for ferromagnetic thin films featuring a bcc lattice structure with three distinct spin layers. Specifically, for films with a bcc (001) orientation, the parameters used are as follows: $Z_0 = 4$, $Z_1 = 1$, $Z_2 = 0$ and $\Phi_0 = 9.0336$, $\Phi_1 = -0.3275$ as referenced in previous studies (Hucht & Usadel, 1997, Hucht & Usadel, 1999, Usadel & Hucht, 2002). These values correspond to key structural and magnetic characteristics of the bcc (001) films, influencing the overall magnetic behaviour and energy configurations analyzed in the simulations.

A 3-D plot of energy versus angle and spin exchange interaction is given in Figure 1 for $\frac{D_1^{(4)}}{\omega} = 5$, $\frac{D_2^{(4)}}{\omega} = 10$ and $\frac{D_3^{(4)}}{\omega} = 10$. Here other parameters are fixed at $\frac{H_{in}}{\omega} = \frac{H_{out}}{\omega} = \frac{N_d}{\mu_0\omega} = \frac{D_1^{(2)}}{\omega} = \frac{D_2^{(2)}}{\omega} = \frac{D_3^{(2)}}{\omega} = \frac{K_s}{\omega} = 10$ for this simulation. The peaks along the direction of the angle are closely packed compared to the second and third order perturbed cases (Samarasekara, 2006, Samarasekara *et al.*, 2009, Samarasekara, 2010, Samarasekara & Mendoza, 2010, Samarasekara, 2011). The energy maxima can be observed at $\frac{J}{\omega} =$ 2, 25, 50, 73. The major maximum is observed at about $\frac{J}{\omega} =$ 73. Energy in these graphs is in the order of 10^{17}. For bcc

structured ferromagnetic thin films with two spin layers, the total magnetic energy reached 10^{35} (Farhan & Samarasekara, 2024). The total magnetic energy was significantly higher in the two spin layers for the same structure.

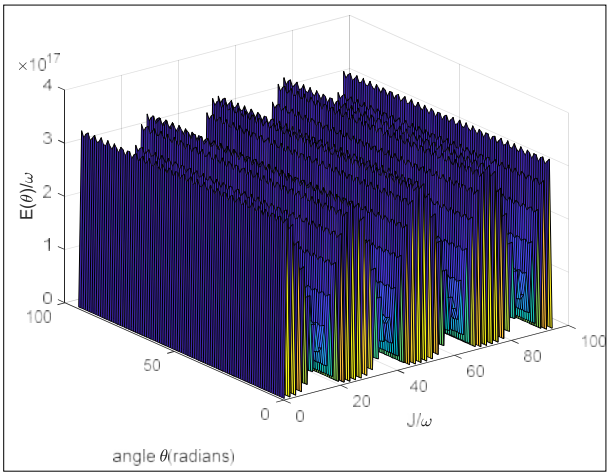

Figure 1: 3-D plot of energy versus angle and spin exchange interaction for $\frac{D_1^{(4)}}{\omega} = 5$, $\frac{D_2^{(4)}}{\omega} = 10$ and $\frac{D_3^{(4)}}{\omega} = 10$.

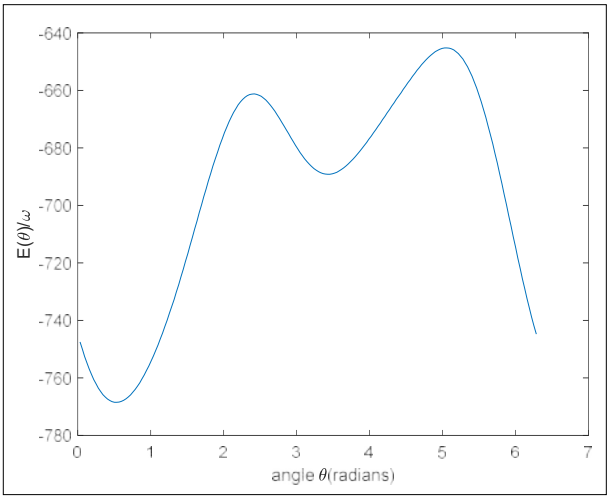

Figure 2: 2-D graph of energy versus angle

Figure 2 shows the graph of energy versus angle for $\frac{J}{\omega} =$ 73. In this graph, energy maxima are observed at 2.419 and 5.058 radians, with the major maximum occurring at around 5.058 radians. Energy minima are found at 0.5341 and 3.456 radians, with the major minimum at approximately 0.5341 radians. The angle between consecutive magnetic easy and hard directions is not 90 degrees. The shape of the graph differs from that observed in simple cubic structured ferromagnetic thin films with two spin layers (Farhan & Samarasekara, 2023).

Figures 3 represents the 3-D plot of energy versus angle and spin exchange interaction for $\frac{D_1^{(4)}}{\omega} = 10$, $\frac{D_2^{(4)}}{\omega} = 10$ and $\frac{D_3^{(4)}}{\omega} = 5$. Here other parameters are fixed at $\frac{H_{in}}{\omega} = \frac{H_{out}}{\omega} = \frac{N_d}{\mu_0\omega} = \frac{D_1^{(2)}}{\omega} = \frac{D_2^{(2)}}{\omega} = \frac{D_3^{(2)}}{\omega} = \frac{K_S}{\omega} = 10$ for this simulation. Energy maxima are observed at $\frac{J}{\omega} =$ 2, 19, 44, 67, 90, with the major maximum occurring at about $\frac{J}{\omega} = 67$. The energy values are in the order of 10^{14}. The total magnetic energy decreases when the bottom and top spin layers are interchanged, while the middle spin layer remains at a constant.

Figure 4 shows the graph of energy versus angle for $\frac{J}{\omega} = 67$. In this graph, energy maxima are observed at 2.356 and 5.058 radians, with the major maximum occurring around 5.058 radians. Energy minima are found at 0.5341 and 3.424 radians, with the major minimum at approximately 0.5341 radians. The angle between consecutive magnetic easy and hard directions is not 90 degrees. When compared to Figure 2, the maximum and minimum values change slightly when the bottom and top spin layers are interchanged, while the middle spin layer remains constant.

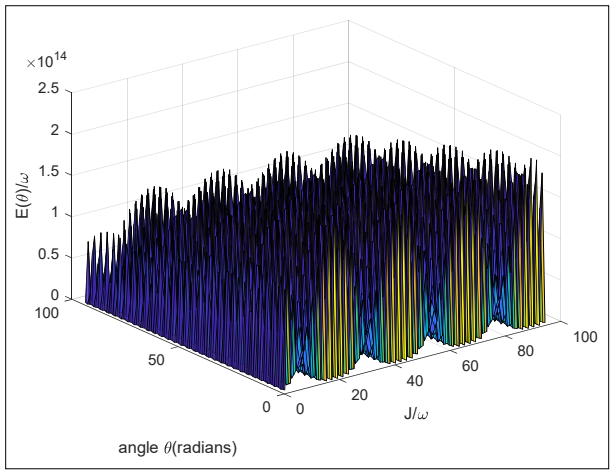

Figure 3: 3-D plot of energy versus angle and spin exchange interaction for $\frac{D_1^{(4)}}{\omega} = 10$, $\frac{D_2^{(4)}}{\omega} = 10$ and $\frac{D_3^{(4)}}{\omega} = 5$.

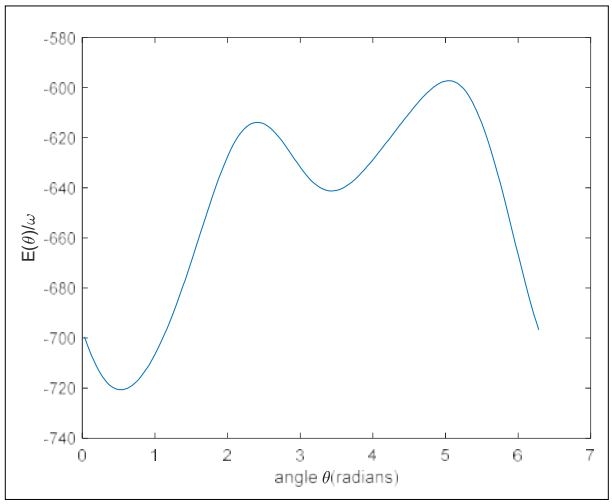

Figure 4: 2-D graph of energy versus angle

Figures 5 represents the 3-D plot of energy versus angle and spin exchange interaction for $\frac{D_1^{(4)}}{\omega} = 10$, $\frac{D_2^{(4)}}{\omega} = 5$ and $\frac{D_3^{(4)}}{\omega} = 10$. Here other parameters are fixed at $\frac{H_{in}}{\omega} = \frac{H_{out}}{\omega} = \frac{N_d}{\mu_0 \omega} = \frac{D_1^{(2)}}{\omega} = \frac{D_2^{(2)}}{\omega} = \frac{D_3^{(2)}}{\omega} = \frac{K_s}{\omega} = 10$ for this simulation. Energy maxima are observed at $\frac{J}{\omega} =$ 2, 23, 48, 71, with the major maximum occurring at about $\frac{J}{\omega} = 71$. Energy in these graphs is in the order of 10^{13}. The total magnetic energy decreases when the middle spin layer is smaller than the bottom and top spin layers. Comparing the 3-D plots in Figures 1, 3, and 5, the total energy ranges from 10^{13} to 10^{17}. Additionally, the energy maxima shift slightly when the values of the spin layers change. In the same structure with two spin layers, the total magnetic energy range is observed to be from 10^{42} to 10^{43}. It is clear that the total magnetic energy significantly changes as the number of spin layers increases for the same structure. The total magnetic energy in the 3-D graph of energy versus angle and stress induced anisotropy constant is to be observed from 10^{11} to 10^{21} with the same spin layer and structure (Farhan & Samarasekara, 2024). A lower energy gap is observed between the highest and lowest magnetic energy when changing the parameters for the same spin layer and structure.

Figure 6 shows the graph of energy versus angle for $\frac{J}{\omega} = 71$. In this graph, energy maxima are observed at 2.419 and 5.058 radians, with the major maximum occurring at approximately 5.341 radians. Energy minima are found at 0.5341 and 3.456 radians, with the major minimum at around 0.5341 radians. The angle between consecutive magnetic easy and hard directions is not 90 degrees. According to Figures 2 and 6, the maximum and minimum values remain unchanged when the bottom and middle spin layers are interchanged, while the top spin layer remains constant.

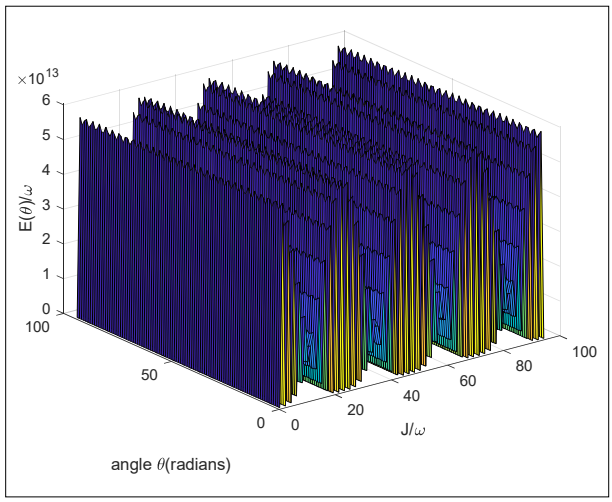

Figure 5: 3-D plot of energy versus angle and spin exchange interaction for $\frac{D_1^{(4)}}{\omega} = 10$, $\frac{D_2^{(4)}}{\omega} = 5$ and $\frac{D_3^{(4)}}{\omega} = 10$.

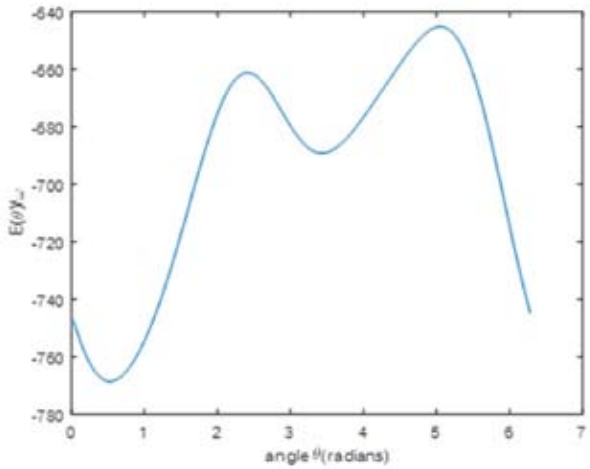

Figure 6: 2-D graph of energy versus angle

CONCLUSION

In conclusion, our study of bcc-structured ferromagnetic thin films with three spin layers, using the fourth-order perturbed Heisenberg Hamiltonian, has provided valuable insights into the magnetic energy distribution under varying parameter conditions. The findings reveal that when the fourth-order magnetic anisotropy constant in the bottom spin layer is smaller than those in the middle and top spin layers, the total magnetic energy reaches the order of 10^{17}. In contrast, when the middle spin layer has a lower fourth-order anisotropy constant, the total magnetic energy decreases to the order of 10^{13}. This indicates that a reduced fourth-order anisotropy in the middle spin layer leads to lower energy barriers for rotating magnetic moments away from the easy axis. Additionally, the energy maxima shift slightly with changes in the values of the spin layers. For comparison, in the same structure with two spin layers, the total magnetic energy was observed to range between 10^{42} and 10^{43}, showing that the total magnetic energy significantly decreases as the number of spin layers increases. A lower energy gap is also observed between the highest and lowest magnetic energies when altering the parameters for the same spin layer and structure. Furthermore, in the 2D plots, the angle between consecutive magnetic easy and hard directions is consistently not 90 degrees, and the maximum and minimum energy values remain unchanged when the bottom and middle spin layers are interchanged, while the top spin layer stays constant. This study highlights the sensitivity of the magnetic behaviour of bcc-structured ferromagnetic thin films to variations in the magnetic anisotropy constants and spin exchange interactions across different spin layers. Furthermore, we note that extending these simulations to systems with a larger number of spin layers (higher N) could provide deeper insights into the energy behaviour of ferromagnetic thin films. Since manual calculations become increasingly complex as N increases, future studies will employ MATLAB and other computational tools to explore these extended systems. These findings deepen our understanding of magnetic energy configurations in thin films and offer insights that could be beneficial for future applications in magnetic storage devices, sensors, and spintronic technologies.

REFERENCES

Bentaleb, M., Aouad El, N., & Saber, M. (2002). Exact solution of the one-dimensional Ising model in a random oscillating magnetic field. *Chinese Journal of Physics,* 40(3), 307.

Ernst, A., Lueders, M., Temmerman, W.M., *et al.* (2000). Theoretical study of magnetic layers of nickel on copper: dead or alive? *Journal of Physics: Condensed Matter,* 12(26), 5599–5606. https://doi.org/10.1088/0953-8984/12/26/306

Farhan, M.S.M., & Samarasekara, P. (2023). Simple cubic structured ferromagnetic thin films with two spin layers explained by fourth order perturbed Heisenberg Hamiltonian. *In Proceedings of the 4th International Conference on Applied & Pure Sciences (ICAPS)* (p. 65). University of Kelaniya, Sri Lanka.

Farhan, M.S.M., & Samarasekara, P. (2024). Determination of bcc structured ferromagnetic thin films with two spin layers using the fourth order perturbed Heisenberg Hamiltonian. *In Proceedings of the 2nd International Conference on Multidisciplinary Research (ICMR)* (p. 18). Eastern University, Sri Lanka. https://doi.org/10.4038/cjs.v52i2.8155

Farhan, M.S.M., & Samarasekara, P. (2024). Exploring magnetic anisotropy in bcc-structured ferromagnetic thin films with three spin layers using the fourth order perturbed Heisenberg Hamiltonian. *Georgian Electronic Scientific Journals: Physics,* 1(30), 6–19.

Hucht, A., & Usadel, K.D. (1997). Reorientation transition of ultrathin ferromagnetic films. *Physical Review B 55:* 12309. https://doi.org/10.1103/PhysRevB.55.12309

Hucht, A., & Usadel, K.D. (1999). Theory of the spin reorientation transition of ultra-thin ferromagnetic films. *Journal of Magnetism and Magnetic Materials 203(1):* 88-90. DOI: 10.1016/S0304-8853(99)00197-3. https://doi.org/10.1016/S0304-8853(99)00197-3

Samarasekara, P. & Mendoza, W.A. (2011). Third order perturbed Heisenberg Hamiltonian of spinel ferrite ultra-thin films. *Georgian Electronic Scientific Journals: Physics,* 1(5), 15–24.

Samarasekara, P. (2006). Second order perturbation of Heisenberg Hamiltonian for non-oriented ultra-thin ferromagnetic films. *Electronic Journal of Theoretical Physics,* 3(11), 71–83.

Samarasekara, P. (2008). Influence of third order perturbation on Heisenberg Hamiltonian of thick ferromagnetic films. *Electronic Journal of Theoretical Physics,* 5(17), 227–236.

Samarasekara, P. (2010). Determination of energy of thick spinel ferrite films using Heisenberg Hamiltonian with second order perturbation. *Georgian Electronic Scientific Journals: Physics, 1(3), 46–52.*

Samarasekara, P., & Cadieu, F.J. (2001). Magnetic and structural properties of RF sputtered polycrystalline lithium mixed ferrimagnetic films. *Chinese Journal of Physics,* 39(6), 635–640.

Samarasekara, P., & Cadieu, F.J. (2001). Polycrystalline Ni ferrite films deposited by RF sputtering techniques. *Japanese Journal of Applied Physics,* 40(5R), 3176. https://doi.org/10.1143/JJAP.40.3176

Samarasekara, P., & De Silva, S.N.P. (2007). Heisenberg Hamiltonian solution of thick ferromagnetic films with

second order perturbation. *Chinese Journal of Physics,* 45(2-I), 142–150.

Samarasekara, P., & Mendoza, W.A. (2010). Effect of third order perturbation on Heisenberg Hamiltonian for non-oriented ultra-thin ferromagnetic films. *Electronic Journal of Theoretical Physics,* 7(24), 197–210.

Samarasekara, P., Abeyratne, M.K., & Dehipawalage, S. (2009). Heisenberg Hamiltonian with second order perturbation for spinel ferrite thin films. *Electronic Journal of Theoretical Physics,* 6(20), 345–356.

Spisak, D., & Hafner, J. (2005). Theoretical study of FeCo/W(110) surface alloys. *Journal of Magnetism and Magnetic Materials,* 286, 386–389. https://doi.org/10.1016/j.jmmm.2004.09.096

Usadel, K.D., & Hucht, A. (2002). Anisotropy of ultrathin ferromagnetic films and the spin reorientation transition. *Physical Review B 66:* 024419. https://doi.org/10.1103/PhysRevB.66.024419

Zhao, D., Liu, F., Huber, D.L., *et al.* (2002). Step-induced magnetic-hysteresis anisotropy in ferromagnetic thin films. *Journal of Applied Physics,* 91(5), 3150–3153. https://doi.org/10.1063/1.1433179

J.Natn.Sci.Foundation Sri Lanka 2025 53 (4): 375 - 389
DOI: http://dx.doi.org/10.4038/jnsfsr.v53i4.12200

RESEARCH ARTICLE

Highway Engineering

Use of carbonised wood particles as filler replacement in hot mix asphalt

TM Rengarasu*, N Jegatheesan and Wasala MKRTW Bandara
Department of Civil & Environmental Engineering, University of Ruhuna, Galle, Sri Lanka.

Submitted: 31 May 2024; Revised: 14 October 2025; Accepted: 09 November 2025

Abstract: This study investigated the feasibility of using carbonised wood particles (CWP) as a sustainable filler replacement in hot mix asphalt (HMA), addressing both environmental concerns and construction material performance. Despite considerable research, the moisture susceptibility of HMA modified with CWP, possessing a wider particle size distribution, remains unestablished. Twenty five HMA mixes with varying CWP content (0 to 40 g, equivalent to 0 – 24% filler replacement by mass) and asphalt content (4 – 6%) were evaluated against ASTM standards for their Marshall stability and indirect tensile strength, moisture susceptibility, and water absorption. The results indicate a clear trade-off: incorporating CWP improved physical properties like void structure but significantly reduced the mechanical strength and moisture resistance. Marshall stability and indirect tensile strength decreased by up to 79% and 75%, respectively, with higher CWP contents. The study conclusively identified 12% CWP replacement (20 g) as the optimal dosage. This proportion maintains acceptable performance for medium-traffic highways while delivering significant sustainability benefits by reducing reliance on quarried mineral filler and repurposing industrial waste. This optimal balance offers a viable pathway for more eco-friendly pavement construction without compromising critical performance criteria for specific applications.

Keywords: Carbonised wood particles, hot mix asphalt, mineral filler, indirect tensile strength, Marshall properties.

INTRODUCTION

Hot mix asphalt (HMA) is the primary material used in the construction of flexible pavements. Typically, HMA consists of variously sized aggregates bonded together by asphalt. Aggregates constitute roughly 95% of HMA by weight (Ahmedzade & Sengoz, 2009; Sargın et al., 2013; Sapkota et al., 2023). The need for greater quantities of aggregates in HMA production has led to increased demand for quarrying (Akbulut & Gürer, 2007; Huang et al., 2007). However, the depletion of natural resources has raised serious concerns regarding the sustainability of pavement construction (Jegatheesan et al., 2020; Rengarasu et al., 2020). Escalating prices resulting from diminishing availability of natural resources have become a pressing issue in the global highway construction industry, particularly in countries where construction costs are a significant concern. Consequently, the pursuit of low-cost alternative materials to natural aggregates in HMA holds substantial priority in numerous countries.

The use of waste or industrial by-products, after some preprocessing, as an alternative to natural aggregates in highway construction (Jegatheesan et al., 2017; Jegatheesan et al., 2020; Rahman et al., 2020; Jegatheesan et al., 2021; Hoy et al., 2024), has gained global traction. Sawdust emerges as a potential alternative material, although it has received less attention in previous studies compared to other industrial byproducts, similar to fly ash or slag. In Sri Lanka, and indeed globally, significant quantities of sawdust are generated as waste from timber processing, with much of it being disposed of through landfilling or open burning, raising environmental concerns (Perera et al., 2005; Shyamalee et al.,

* Corresponding author (rengarasu@cee.ruh.ac.lk; https://orcid.org/0000-0002-6856-3032)

This article is published under the Creative Commons CC-BY-ND License (http://creativecommons.org/licenses/by-nd/4.0/). This license permits use, distribution and reproduction, commercial and non-commercial, provided that the original work is properly cited and is not changed in anyway.

2015). With nearly 4,000 sawmills and 680 furniture manufacturers producing 112,000 MT of sawdust annually as waste in Sri Lanka alone (Shyamalee et al., 2015), the viability of using wood sawdust as a substitute for HMA material has been the subject of numerous previous investigations (Xue et al., 2014; Jegatheesan et al., 2017; Osuya & Mohammed, 2017; Yasanthi et al., 2017; Guesmi et al., 2024; Karati & Kumar Roy, 2024).

Mineral filler, which consists of the portion of aggregate passing through the ASTM No.200 sieve, plays a crucial role in packing the mix to regulate air voids in HMA samples (Huang et al., 2007; Osuya & Mohammed, 2017). The body of research exploring sawdust in HMA primarily focuses on its use in two forms: as processed ash or as carbonised particles. Early work by Marteano et al., (2002) investigated partial replacement with raw sawdust, finding that a 50% replacement blend approached the characteristics of control samples (Marteano et al., 2002). However, the study lacked a comprehensive analysis of potential negative effects, such as binder drainage or long-term durability.

Subsequent research has largely focused on sawdust ash (SDA), obtained by combusting sawdust. Studies have shown that SDA, rich in Calcium Oxide (CaO), can improve the viscosity and rutting resistance of the asphalt binder (Adlinge et al., 2013; Xue et al., 2014; Hämäläinenet et al., 2025). Osuya & Mohammed (2017) reported enhanced bulk and strength properties with a 15% SDA replacement, while Yasanthi et al. (2017) observed a decrease in Marshall stability, indicating a potential compromise in medium-temperature stability. More recent investigations have explored optimal blend ratios; Boura & Hesami (2020) determined that a combination of limestone with 25% SDA could yield higher tensile strength than control mixes. However, a critical limitation of these SDA studies is the assumption that only the fraction passing through the 0.075 mm sieve (traditional filler size) is valuable, potentially overlooking the utility of larger particulate fractions.

An alternative approach involves using CWP, Jegatheesan et al. (2020) demonstrated that when processed sawdust was utilised as filler with polymer-modified bitumen, the strength properties of the HMA were enhanced. This suggests that the carbon structure of CWP may interact differently with the asphalt binder compared to the ash form. Furthermore, controlled carbonisation yields a residue with a wide particle size distribution, offering the potential to replace a broader range of aggregate particles, not just the fine filler fraction. This presents a significant opportunity to increase the volume of waste material utilised per ton of HMA produced.

Despite these advancements, two critical research gaps remain unaddressed. First, the moisture susceptibility of HMA modified with CWP has not been thoroughly established or mechanistically explained in prior literature. The highly porous nature of CWP raises valid concerns about water absorption and its impact on adhesive failure, which are critical for long-term pavement performance. Second, a small number of characteristics have been the subject of numerous earlier studies. A comprehensive evaluation encompassing volumetric properties, strength, moisture sensitivity and water absorption is necessary to fully understand the viability of CWP.

This study, therefore, aims to fill these gaps by conducting a systematic investigation into the feasibility of replacing the filler portion of HMA with CWP. The feasibility is comprehensively assessed based on a holistic suite of tests, including physical properties, Marshall strength properties, Indirect tensile strength, and critically, moisture susceptibility through tensile strength ratio, retained Marshall stability, and water absorption kinetics. The study explicitly determines the optimal replacement level that balances performance with sustainability goals.

MATERIALS AND METHODS

Broken stones and stone dust were used as the conventional materials in this study. For detailed descriptions of the conventional materials used in this study, please refer to Jegatheesan et al., 2020 and Jegatheesan et al., 2021. Carbonised wood particles were used as an alternative material to the filler of HMA. Wood sawdust undergoes a process of losing free and hygroscopic water as the temperature increases, with carbonisation commencing when the temperature exceeds 270 °C (Fung et al., 2006; Dias et al., 2016). To prevent the entire sawdust sample from turning into ash, the sample was heated only to its minimum ignition temperature of 400 °C (Fung et al., 2006). The wood sawdust sample, sourced from Albizia (*Albizia julibrissin*), was carbonised in the laboratory under air-tight conditions. The resulting CWP, characterised by an apparent specific gravity of 0.61 and absorption of 5.8%, were then dry sieved through a 1.18 mm sieve (No.16, ASTM C136), and the portion passing through was utilised. The gradation of CWP is depicted in Figure 1.

The mix proportions of combined aggregates and CWP were determined according to the ASTM D3515-01 design specifications, specifically adhering to the gradation requirements of the dense mix designation of 'D-4'. These gradation limits are outlined in Table 1.

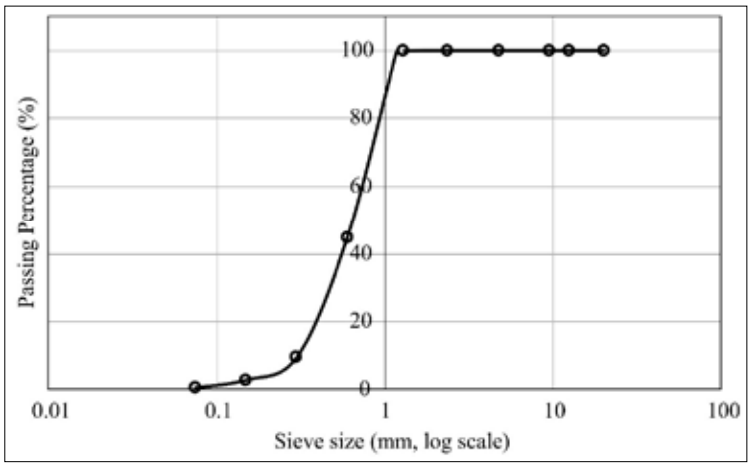

Figure 1: Particle size distribution of CWP (carbonised wood particles)

Table 1: The gradation limit for dense mix designation of 'D-4' given in ASTM

Sieve size (mm)	20	9.5	4.75	2.36	0.3	0.075
Lower limit (%)	90	56.0	35.0	23.0	5.0	2.0
Passing (%)	100	65.9	44.7	32.5	11.3	2.4
Upper limit (%)	100	80	65	49	19	8

The determination of particle size distribution of aggregates of different sizes is crucial in establishing the mix proportions of the aggregates in HMA (Kandhal & Mallick, 2001).

In this study, Marshall specimens with and without CWP were prepared according to ASTM D6926 specifications. Twenty five different HMA mixes were investigated, with CWP contents ranging from 0 to 40 g at 10 g intervals and asphalt contents ranging from 4% to 6% at 0.5% intervals. Here, 0 g CWP denotes the control sample. The CWP replacement levels were selected on a weight basis as 0 g, 10 g, 20 g, 30 g, and 40 g. This corresponds to a replacement of 0%, 6%, 12%, 18%, and 24% of the mass of the conventional mineral filler, respectively. This range was chosen for the following four reasons:

1. Incremental progression: The 10 g increments (approximately 6% mass replacement intervals) provide a systematic and sufficiently wide range to clearly observe trends and potential threshold effects. A finer increment would significantly increase the number of samples and laboratory workload without necessarily providing proportionally greater insight, while a coarser increment might miss critical performance changes.
2. Capturing a performance spectrum: The range from 0% to 24% replacement was designed to capture the full spectrum of behaviour, from performance nearly equivalent to the control to a significant degradation of properties. This allows for the clear identification of an "optimal" range where benefits are maximised, and drawbacks are minimised, as well as a "failure" point where the mixture becomes unacceptable.
3. Bridging past research: The selected range encompasses and extends beyond the replacement levels found in previous literature. For instance, studies on sawdust ash often focused on replacements up to 15-25% (Osuya & Mohammed, 2017; Boura & Hesami, 2020). By testing up to 24%, this study investigates the upper practical limit of CWP incorporation.

4. Practicality and statistical significance: Testing five distinct CWP levels, each at five asphalt contents and with three replicates, resulted in a total of 75 specimens. This provided a robust data set for statistical analysis while remaining a logistically feasible number of samples to produce and test under controlled conditions.

A volume-by-volume replacement approach was employed in this study. Because, replacing the filler on a weight basis would result in an increase in specimen volume (Mahmoud et al., 2013; Kuity et al., 2014), given a significant disparity between the specific gravity of CWP (0.61) and the conventional filler of HMA (2.71).

To elaborate, 10 g, 20 g, 30 g, and 40 g of CWP were utilised to substitute 6%, 12%, 18%, and 24% of the mass of filler in HMA, respectively. During the batching process, CWP and aggregates were preheated to a mixing temperature of 165 °C before being mixed with the asphalt binder. Compaction was promptly carried out using a Marshall hammer following ASTM D6926 at 135 °C immediately after the completion of mixing.

Initially, the physical properties of HMA were assessed, including bulk specific gravity (ASTM D2726), voids filled with binder, voids in mineral aggregate, and voids in the mix. Subsequently, specimens underwent the Marshall test to determine stability and flow values (ASTM D6927).

For each CWP modification, the optimal rates of conventional aggregates, CWP, and asphalt content were determined, considering the properties and standards utilised in the Marshall mix design.

The durability of HMA specimens, fabricated with optimal asphalt content for each CWP content, was further examined. Moisture within the HMA can cause adhesive or cohesive failure between asphalt and aggregate (Do et al., 2019), a longstanding concern recognised as a primary cause of pavement distress.

Consequently, the moisture sensitivity of optimum CWP-modified HMAs was assessed, taking into account the tensile strength ratio (ASTM D4867), retained Marshall strength, and water absorption. Two groups of optimum CWP-modified specimens, one moisture-conditioned and the other unconditioned, were analysed to evaluate the tensile strength ratio.

The first group of specimens was immersed in water at 60 ± 1 °C for 24 hours, while the second group was left to stabilise at room temperature. Indirect tensile strength values were calculated using Equation (1), and the tensile strength ratio was determined utilising the indirect tensile strength values obtained from the moisture-conditioned and unconditioned specimens, using Equation (2).

$$ITS = \frac{2P_{Max}}{\pi td} \quad ...(01)$$

Where, *ITS* is indirect tensile strength (MPa), P_{max} is peak load (N), *t* is the height of the specimen (mm), and *d* is the diameter of the specimen (mm).

$$TSR = \frac{T_1}{T_2} \times 100 \quad ...(02)$$

Where, T_1 is the average indirect tensile strength of moisture-conditioned HMA (MPa), and T_2 is the average indirect tensile strength of unconditioned HMA.

In addition to the tensile strength ratio, another moisture sensitivity test examined in this study was the retained Marshall stability. The Marshall stability ratio of moisture-conditioned and unconditioned specimens was utilised to calculate retained Marshall stability.

Specimens were moisture-conditioned by submerging them in water at 60 ± 1 °C. Subsequently, Marshall stability values for unconditioned and moisture-conditioned specimens were assessed in accordance with ASTM D6926. The retained Marshall stability was then determined using Equation (3).

$$RMS = \left(\frac{MS_1}{MS_2}\right) \times 100 \quad ...(03)$$

Where, retained Marshall stability the index of retained Marshall stability (%), MS_1 is the average Marshall stability of moisture-conditioned specimens (kN), and MS_2, is the average Marshall stability of unconditioned specimens (kN).

For the final test, specimens were immersed water in room temperature water. The variation in moisture content of the specimens over time was monitored according to ASTM D2726. Subsequently, the statistical significance of laboratory results was assessed using the R software environment (R Core Team, 2023). To evaluate the significant effect of each factor at a 95% confidence level ($\alpha = 0.05$), a two-factor analysis of variance (ANOVA) was employed.

The two-factor ANOVA was specifically chosen to test the null hypothesis that the means of the measured properties (e.g., Marshall stability, bulk specific gravity)

are equal across different levels of the two independent factors, asphalt content and CWP content. The factors were considered fixed effects. The model determined whether the variation in the data caused by these factors was significantly greater than the variation within the groups (error variance).

A significance level of 0.05 was selected for all tests, meaning there was a less than 5% probability that the observed results occurred by chance alone. For each dependent variable, the ANOVA produced an F-statistic and a corresponding p-value. An F-value greater than the critical F-value ($F_{critical}$) and a p-value less than 0.05 led to the rejection of the null hypothesis, confirming that the factor (either asphalt content or CWP) had a statistically significant effect on the property.

Following a significant result in the ANOVA, post-hoc analyses (e.g., Tukey's honest significant difference test) would typically be conducted to identify which specific levels of the factors (e.g., 20 g vs. 30 g CWP) differed from each other. The highly significant p-values ($p = 0.000$) and large F-values reported in Table 2 overwhelmingly confirm that both asphalt content and CWP content are major drivers of change in all measured HMA properties.

Additionally, a paired t-test was used to compare the means of moisture-conditioned and unconditioned samples for the tensile strength ratio and retained Marshall stability analyses. The paired t-test was the appropriate choice for these comparisons because the moisture-conditioned and unconditioned specimens were not independent; each conditioned specimen was intrinsically linked to an unconditioned specimen from the same optimum mix design. The test assessed the null hypothesis that the mean difference between the paired observations was zero. A p-value less than 0.05 (as reported for the decrease in stability, P-value=0.00) indicated a statistically significant effect of moisture conditioning on the strength of the HMA specimens.

RESULTS AND DISCUSSION

Physical properties

Bulk specific gravity

Variation of the bulk specific gravity with the dosage of asphalt content and CWP is shown in Figure 2. As shown in Table 2, the bulk specific gravity of modified HMA decreased significantly with increasing asphalt content and CWP. Because CWP have a lower specific gravity than conventional fillers in HMA, the bulk specific gravity of CWP-modified HMA is lower than the control. It was observed that the BSG of modified HMA decreased as the asphalt content increased, and this variation was like that of the control HMA. A similar reduction of bulk specific gravity with asphalt content was presented in past studies too (Hassan, 2005; Gashi et al., 2017). A maximum reduction of 4.6%, 6.6%, 8.8%, and 10.9% in bulk specific gravity for control HMA was observed at 10 g, 20 g, 30 g, and 40 g of CWP, respectively.

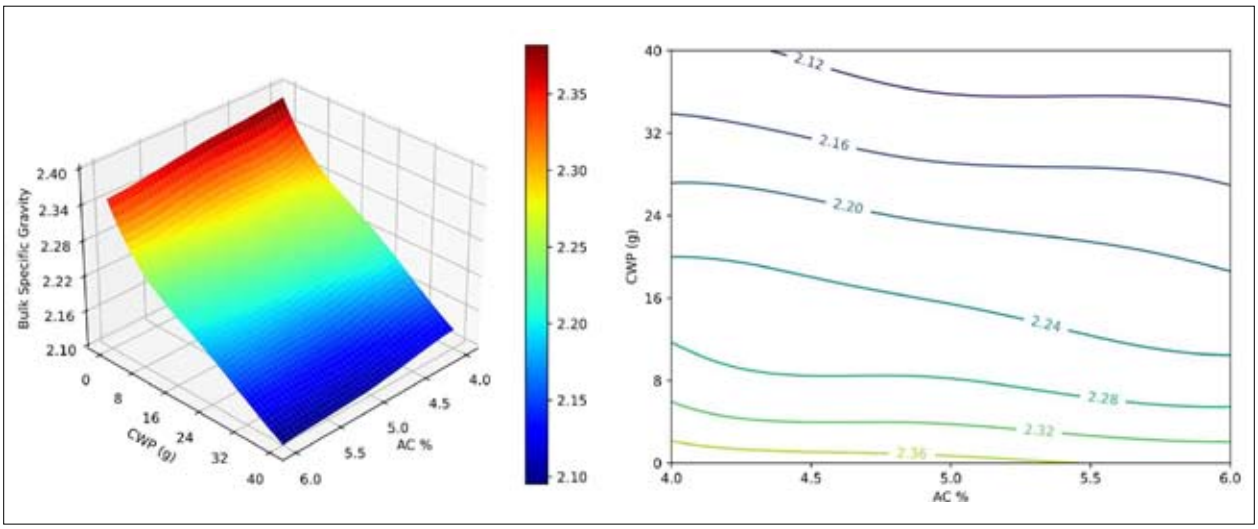

Figure 2: Bulk specific gravity of HMA (Hot mix asphalt) mixtures as a function of AC (asphalt content) and CWP (carbonised wood particles)

The significant reduction in bulk specific gravity observed is a direct consequence of the fundamental property difference between CWP and conventional mineral fillers. The apparent specific gravity of CWP (0.61) is substantially lower than that of the stone dust (2.71) it replaces. This introduces a larger volume of lighter material into the mix for the same weight replacement, effectively reducing the overall density of the compacted specimen. The trend is systematic: the greater the proportion of low-density CWP, the greater the reduction in bulk specific gravity. This correlation is strongly supported by the exceptionally high F-value (3639.3) for the CWP factor in the ANOVA (Table 2), indicating that CWP content is the dominant variable controlling bulk specific gravity. This reduction, while expected, is critical as it directly influences other volumetric properties and the structural mass of the pavement layer.

Table 2: ANOVA test results for physical and Marshall properties

Dependent variable	Independent variable	F-value	F_{cri}	α value
Marshall stability	asphalt content	21.1	3	0
	CWP	213.5	3	0
Marshall flow	asphalt content	33.2	3	0
	CWP	106.4	3	0
Bulk specific gravity	asphalt content	90.8	3	0
	CWP	3639.3	3	0
Voids in the mix	asphalt content	11.4	3	0
	CWP	9.2	3	0
Voids in mineral aggregates	asphalt content	460.4	3	0
	CWP	82.9	3	0
Voids filled by binder	asphalt content	229.2	3	0
	CWP	19.7	3	0

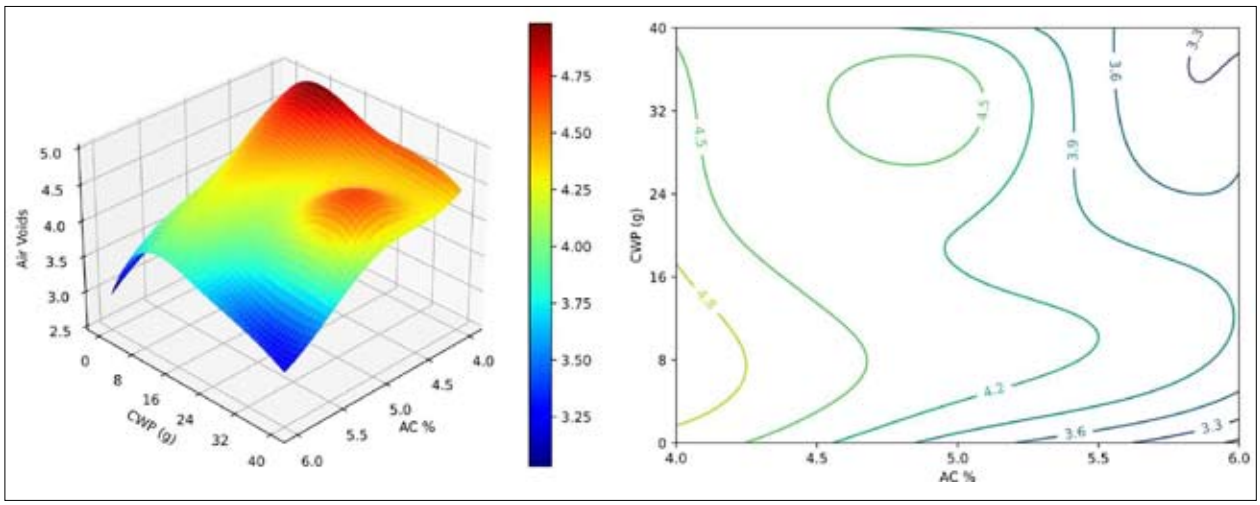

Figure 3: Voids in the mix response to asphalt content (AC) and CWP (carbonised wood particles) replacement

Voids in the mix

Variation in the voids in the mix of HMA with asphalt content and CWP content is shown in Figure 3. Initially, voids in the modified HMA mix increased, reached a maximum value, and further increased. The presence of CWP decreased voids in the mix. These observations could be attributed to the fact that air voids were increasingly filled by the fine component of CWP as it increased in the mix, which led to a decrease in the voids in the mix beyond 20 g of CWP replacement in the Marshall specimens. The increasing trend in voids in mix of HMA was due to inadequacy in the amount of fine content at low CWP content (from 0 g to 20 g) to pack the air voids in the HMA.

Table 3: Properties of optimum Hot mix asphalt

	Asphalt content				
Property	0 g	10 g	20 g	30 g	40 g
Bulk specific gravity	2.4	2.3	2.2	2.2	2.1
Voids in mix (%)	3.8	4.3	4.7	4.6	4.1
Voids in mineral aggregates (%)	16.4	16.4	16.0	16.0	15.3
Voids filled with binder (%)	77.1	73.5	73.8	71.5	73.1
Marshall stability (kN)	13.2	11.9	10.8	6.4	2.8
Marshall flow (0.25 mm)	13.5	13.6	15.5	16.8	18.2
Retained Marshall stability (%)	95.5	90.4	87.4	83.7	72.2
Indirect tensile strength (kPa)	843.8	682.8	557.0	308.3	200.9
Tensile strength ratio (%)	91.3	86.4	82.5	76.9	68.8
Water absorption (%)	0.86	1.38	1.90	3.53	6.70
Suitable traffic highway	High	High	Medium	Low	Failed

The voids in mix value decreased significantly with increasing asphalt content (see Table 3). Modified HMA had higher voids in mix values compared to the control at varying asphalt content levels, ranging from 4% to 6%. This indicated that the absorption of asphalt binder in modified HMA by the highly porous CWP at higher temperatures was significant, which tended to increase the voids in mix compared to control HMA. In all modifications tested in this study, the voids in mix values complied with the specifications for medium-traffic highways (Asphalt-Institute, 2014).

The non-linear response of voids in mix to CWP addition reveals a complex interaction between particle packing and binder absorption. The initial increase in voids in mix (from 0 g to 20 g CWP) is likely due to the introduction of rigid, porous CWP particles that disrupt the optimal packing achieved by the well-graded mineral aggregates, creating new, unfilled voids. However, beyond the 20 g threshold, the finer portion of the CWP begins to act as a filler, effectively occupying the voids between larger aggregate particles, leading to a decrease in voids in the mix. Concurrently, the pronounced decrease in voids in mix with increasing asphalt content is attributed to the dual role of the asphalt binder coating aggregates to reduce inter-particle voids, and being absorbed into the porous CWP, causing them to swell and further occupy space within the mix matrix.

Voids in mineral aggregates and voids filled with binder

A significant monotonic reduction in voids in mineral aggregates of modified HMA was observed as CWP content increased from 0 g to 40 g. This could be due to the fine portion of CWP, which tended to decrease the voids in mineral aggregates (Osuya & Mohammed, 2017). The Asphalt content voids in mineral aggregates of modified HMA increased significantly, and this increase in variation was similar to that of the control HMA. This could be attributed to the highly porous nature of CWP absorbing higher portions of asphalt in modified HMA at high mixing temperatures (Lesueur et al., 2012; Osuya & Mohammed, 2017; Bennert et al., 2018), which tended to increase in voids in mineral aggregates as the asphalt content increased. All voids in mineral aggregates values

of modified HMA satisfied specifications for medium traffic highways (Asphalt-Institute, 2014). Variation in the voids in mineral aggregates of HMA with asphalt content and CWP content is shown in Figure 4.

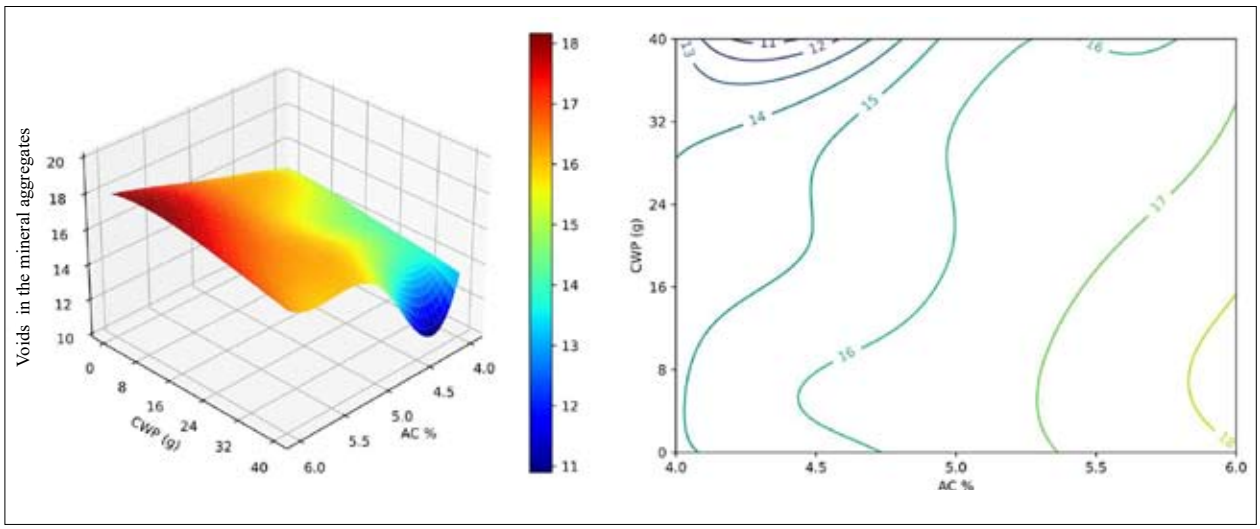

Figure 4: Variation of voids in mineral aggregates with asphalt content (AC) and CWP (carbonised wood particles) content

The voids filled with binder values of modified HMA ranged from 66% to 81%, with the highest voids filled with binder values observed at high asphalt content in each modification. Voids filled with binder in modified HMA initially decreased, reached a minimum, and then increased with increasing CWP content. However, as the asphalt content increased, the voids filled with binder of modified HMA (see Table 3) increased significantly. All voids filled with binder values for CWP-modified HMA met the medium-traffic highway specification (Asphalt-Institute, 2014). The variation in the voids filled with binder of modified HMA with CWP content and asphalt content is shown in Figure 5.

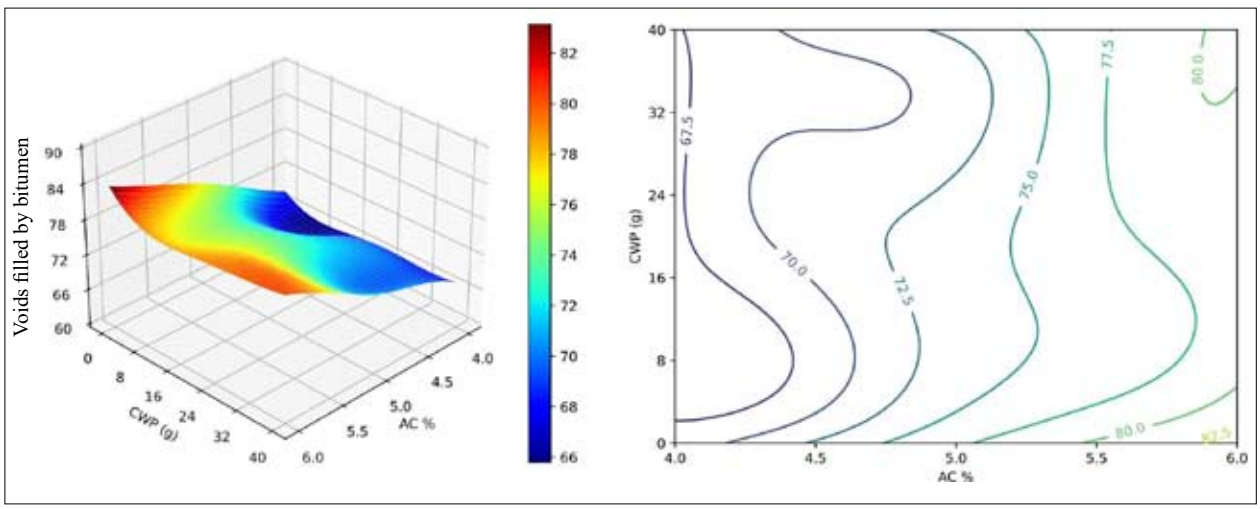

Figure 5: Variation of voids filled by binder with asphalt content (AC) and carbonised wood particles (CWP) content.

Marshall properties

Marshall stability

Marshall stability decreased monotonically as the CWP dosage increased. The presence of tiny particles in CWP reduced the contact between the aggregates (Osuya & Mohammed, 2017), leading to a reduction in the stiffness and Marshall stability of modified HMA. At lower CWP content, modified HMA showed desirable performance. When the asphalt content was set to 4.96% (which is the optimum asphalt content of the control sample), the percentages decreased in Marshall stability of modified HMA specimens compared to control HMA for 10 g, 20 g, 30 g, and 40 g of CWP contents were 10%, 16% 55%, and 79%, respectively.

Marshall stability of control HMA and modified HMA increased initially, reaching peak values of 11.9 kN, 10.8 kN, 6.4 kN, and 2.8 kN for CWP contents of 10 g, 20 g, 30 g, and 40 g, respectively. Marshall stability values at 10 g and 20 g of CWP satisfied specifications for heavy-traffic highways. However, the modified HMA made with 30 g CWP satisfied the specification for medium-traffic highways for asphalt content from 4.8% to 5.2%. Modified HMA with 40 g CWP content did not meet the Marshall stability specifications of medium-traffic highways (Asphalt-Institute, 2014). The Marshall stability variation with CWP content and asphalt content is shown in Figure 6.

The drastic reduction in Marshall stability (up to 79%) and increase in flow are the most critical mechanical findings. This behaviour can be mechanistically explained by two primary factors: (1) The introduction of fine, often plate-like CWP particles acts to lubricate the aggregate skeleton, reducing the internal friction and interlock between the coarse aggregates, which are the primary contributors to the mix's shear strength and stability. The increased Marshall flow values provide direct evidence of this reduced internal friction, indicating a more ductile but less resilient mixture. (2) The highly porous CWP absorbs a significant portion of the asphalt binder, meaning that for a given asphalt content, the amount of effective binder available to coat aggregates and provide cohesion is reduced. This creates a weaker matrix, making the mix more prone to deformation under load. The stability loss is therefore not just a function of the CWP itself but also of a consequential reduction in effective binder content.

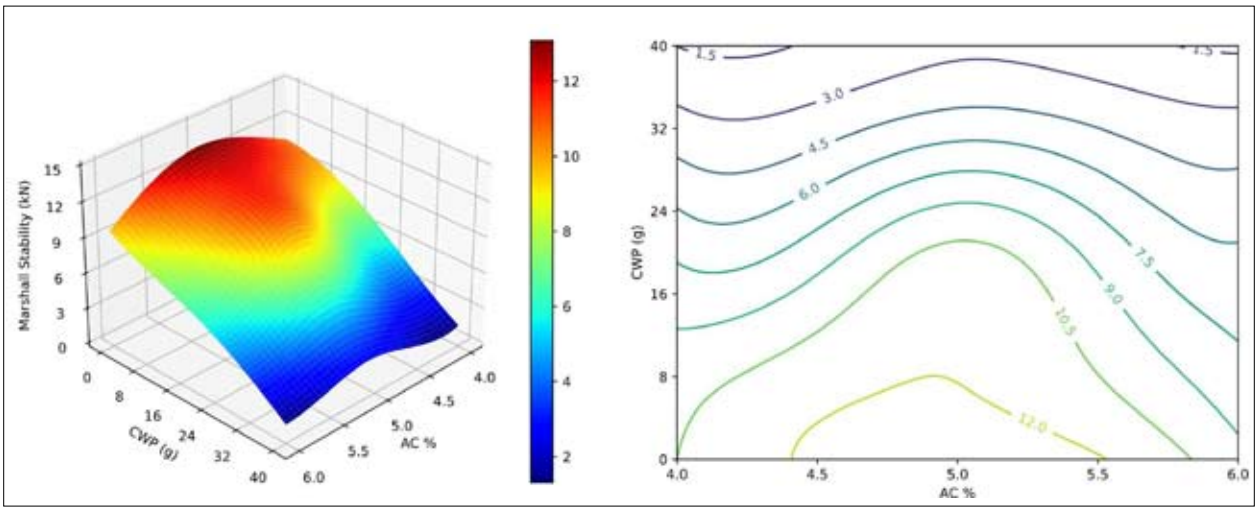

Figure 6: Variation of Marshall stability with asphalt content (AC) and carbonised wood particles (CWP) content.

The results indicate that at low doses (10 g to 20 g), the filler effect and potential slight stiffening of the binder (from absorbed light oils) can partially compensate for these negatives. However, beyond 20 g, the lubrication and absorption effects become dominant, leading to a precipitous drop in performance.

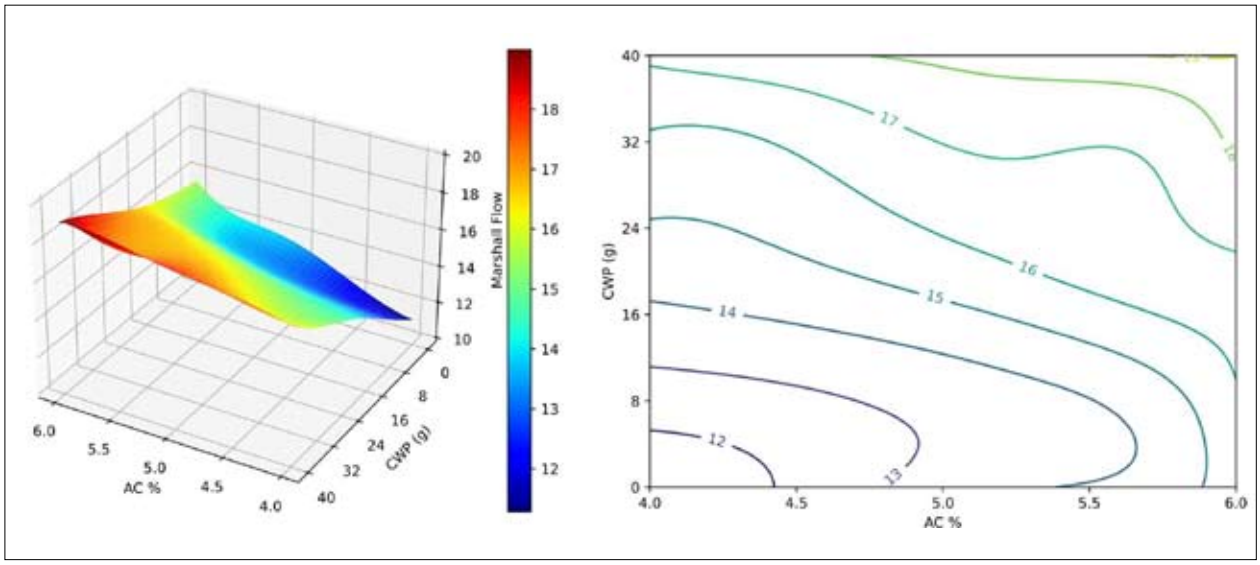

Figure 7: Variation of Marshall flow with asphalt content (AC) and carbonised wood particles (CWP) content.

Marshall flow

Marshall flow significantly increased as the dosage of CWP increased (Table 3). This indicates that the friction between the aggregates decreased with increasing CWP content in the HMA. The addition of 10 g, 20 g, 30 g, and 40 g of CWP resulted in 1%, 15%, 25%, and 35% increases in Marshall flow, respectively, compared to the control HMA made with 4.96%.

Similarly, in each modification tested in this study, an increase in asphalt content raised the Marshall flow in the modified HMA. A similar trend in Marshall flow was observed in the control HMA samples. Marshall flow was not within the specified range of the Asphalt Institute MS-2 specification for medium traffic highways at 40 g CWP content. However, the modified HMA mixes with 10 g and 20 g of CWP content satisfied specifications for medium-traffic highways. The Marshall flow specifications for light-traffic highways were met by HMA with 30 g of CWP. The variation in Marshall flow of modified HMA with Asphalt content and CWP content is shown in Figure 7.

Statistical analysis of physical and marshall properties

Statistical significances of physical and Marshall properties were examined at an alpha value of 0.05. Properties of modified and control HMAs were statistically differentiated using a two-factor ANOVA. Table 2 presents variance analyses for physical and Marshall properties. The obtained F-values were greater than the F-critical values, and the P-values were smaller than α of 5%, indicating that the effect of CWP and asphalt content on the characteristic values of modified HMA was significant for each property tested.

Indirect tensile test

The indirect tensile strength is commonly used to evaluate the relative field quality of asphalt mixes and the potential for rutting or cracking (Bennert et al., 2018; Jegatheesan et al., 2020). Increasing CWP content in HMA resulted in a significant decrease in the indirect tensile strength value (Figure 8). This is because the CWP tends to absorb the asphalt binder. Therefore, increasing CWP in HMA decreases ITS. The HMA samples modified with CWP of 10 g, 20 g, 30 g, and 40 g caused a 20%, 32%, 60%, and 75% decrease in indirect tensile strength compared to the control HMA, respectively. This suggests that increasing CWP content in the HMA mix can accelerate crack propagation.

Tensile strength ratio

The moisture sensitivity of CWP-modified HMA was investigated using tensile strength ratio. The variation in

the indirect tensile strength of optimum HMA with CWP content is shown in Figure 8. The indirect tensile strength of modified HMA significantly (P = 0.00) decreased as CWP content increased for both moisture-conditioned and unconditioned cases. Compared with the control sample, the indirect tensile strength of moisture-conditioned modified HMA decreased by 23%, 40%, 69%, and 82% at 10 g, 20 g, 30 g, and 40 g of CWP content, respectively. The availability of flat, larger surface particles stimulates the absorption of water by CWP, which could lead to decreased binding between the binder and aggregates. Modified HMA specimens containing 20 g or less CWP content complied with the ASTM specifications limit of 80%. Modified HMA specimens made with 30 g and 40 g had more sensitivity to moisture and would experience ravelling.

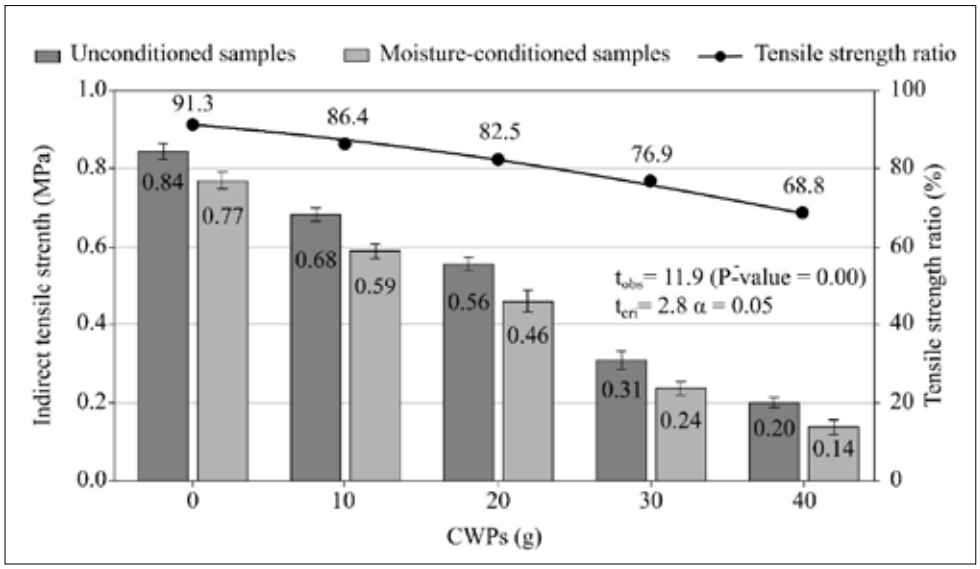

Figure 8: Variation of indirect tensile strength and tensile strength ratio of optimum modified HMA (Hot mix asphalt)

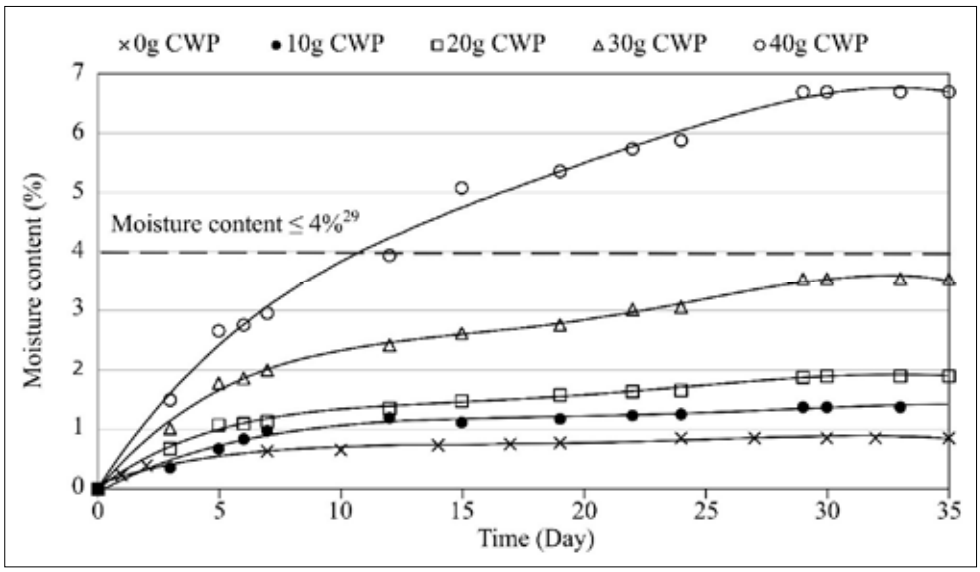

Figure 9: Variations in the water absorption of the optimum modified HMA (Hot mix asphalt)

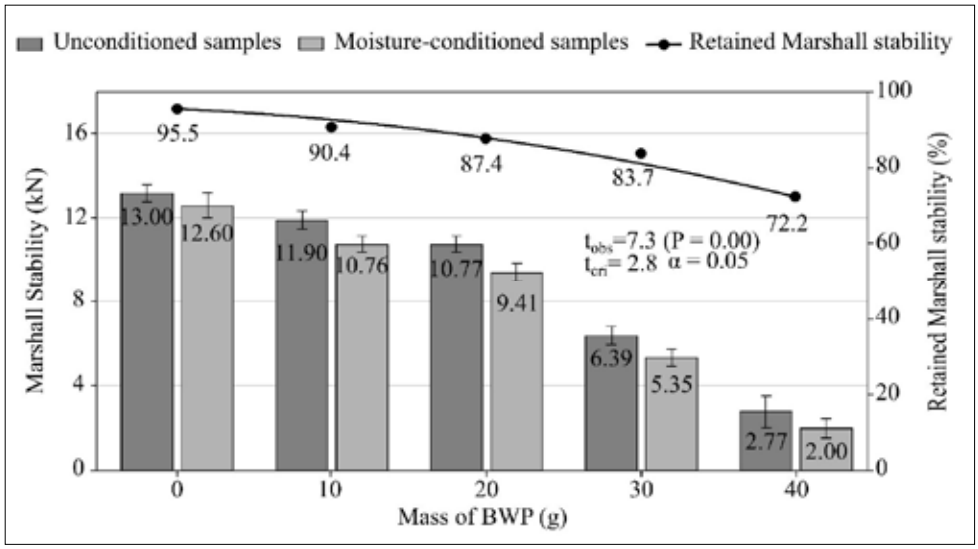

Figure 10: Marshall stability and retained Marshall stability of the optimum modified HMA (Hot mix asphalt)

The moisture susceptibility results (tensile strength ratio and RMS) and water absorption data are intrinsically linked and form a central part of the study's contribution. The porous and hydrophilic nature of CWP creates pathways for water to infiltrate the asphalt mixture. As shown in Figure 9, mixes with high CWP content (30 g, 40 g) act almost like a sponge, absorbing water rapidly. This water intrusion directly attacks the adhesive bond between the aggregate and the asphalt binder (stripping) and can also soften the asphalt binder itself.

Retained Marshall stability

Retained Marshall stability of modified HMA was also tested to determine its moisture susceptibility. Marshall stability of moisture-conditioned HMA was lower than that of unconditioned samples. With increasing CWP content, the decrease in Marshall stability of modified HMA compared to control HMA increased significantly (P-value=0.00). This increase could be attributed to the presence of more absorbed water between the binder and aggregate in comparison to the control HMA, which reduced the adhesion of the HMA mix (Ahmedzade & Sengoz, 2009).

The observed retained Marshall stability values were 95.5%, 90.4%, 87.4%, 83.7%, and 72.2% for the samples with 0 g, 10 g, 20 g, 30 g and 40 g CWP content, respectively. The observed retained Marshall stability values of HMA samples with 0 g, 10 g, 20 g, and 30 g CWP contents satisfied the retained Marshall stability limit of 80% set by the ASTM specifications. Moisture-conditioned and unconditioned Marshall stability of the optimum HMAs is shown in Figure 10.

The difference in water absorption of control HMA and modified HMA determined every 24 hours is shown in Figure 10. Water absorption at 10 g and 20 g of CWP shares a nearly similar trend with that of the control. The absorption rate of HMA made with 30 g and 40 g of CWP in the first few days was high compared to the mix made with 10 g and 20 g of CWP. From this, it can be concluded that increasing CWP in HMA decreases the water sensitivity resistance. Further, HMA specimens made with CWP less than 30 g complied with the specification requirement for water absorption (APRG, 1998).

Recommendations for practitioners and policymakers

Based on the findings of this study, practitioners are advised to strictly limit the replacement of CWP to 12% by mass of the filler in asphalt mixes for medium-traffic applications. To ensure performance, mix designs must account for higher binder demand and prioritise tensile strength ratio (TSR) testing (>80%) to guard against moisture damage. Initial use should target lower-stress applications like local roads or parking lots.

Policymakers can accelerate adoption by revising material specifications to include bio-fillers like CWP and implementing green procurement incentives, such as tax credits or preferential bidding for sustainable practices. Funding pilot projects and supporting wood waste recycling programs will validate long-term performance and formally integrate this technology into sustainable infrastructure strategies.

Limitations and future directions

While this study demonstrates the feasibility of using CWP in HMA for specific applications, several limitations must be acknowledged to contextualise the findings and guide future research.

The research was conducted under controlled laboratory conditions. The performance of CWP-modified HMA under real-world traffic loading, environmental weathering (UV radiation, etc.,), and long-term ageing has not been validated. The findings are based on CWP derived from a single wood species (*Albizia julibrissin*) carbonised at a specific temperature (400 °C). The properties of CWP can vary significantly with different wood types and pyrolysis conditions. The study utilised a conventional asphalt binder. The interaction of CWP with polymer-modified or other advanced binders could yield different results and remain unexplored. While cost savings are implied, a detailed economic analysis including carbonisation costs and a full lifecycle assessment (LCA) to quantify the environmental benefits was beyond the scope of this study.

The logical next step is the construction and long-term monitoring of pilot test sections on low-to-medium traffic roads to validate laboratory findings against real-world performance. Future work should investigate the impact of key variables such as wood species, particle size distribution of CWP, and carbonisation temperature on HMA performance to optimise the material properties. Research should explore combining CWP with polymer-modified binders or anti-stripping agents to mitigate the loss of moisture resistance and strength observed at higher replacement levels. Comprehensive studies on the long-term ageing characteristics (using methods like rolling thin film oven and pressure ageing vessel) and resistance to fatigue cracking of CWP-modified HMA are essential. Addressing these limitations in future work will be vital for transitioning this promising technology from laboratory validation to practical, widespread implementation in sustainable pavement construction.

CONCLUSION

This study comprehensively evaluated the feasibility of using CWP as a sustainable filler replacement in HMA.

(1) The findings demonstrate a clear trade-off: while CWP improve certain physical properties related to void structure, they significantly reduce mechanical strength and moisture resistance. The optimal replacement level was identified as 12% by mass of the filler (equivalent to 20 g in this study's mix design).
(2) At this optimum dosage, the modified HMA maintains satisfactory performance, meeting key specifications for medium-traffic highways. Specifically, mixes with 12% CWP replacement exhibited acceptable Marshall stability, flow, and most critically, moisture resistance, as validated by tensile strength ratio and retained Marshall stability values.
(3) The practical application of this finding is significant. It provides a validated formula for highway engineers to utilise a substantial volume of industrial waste (sawdust), reducing reliance on quarried mineral filler by 12%. This translates to direct cost savings on raw materials and contributes to more sustainable construction practices by diverting waste from landfills and reducing the environmental footprint of quarrying. However, replacements exceeding 12% (i.e., 30 g and 40 g CWP) led to a severe deterioration in strength and moisture resistance, rendering the mixes unsuitable for paved highways. Therefore, for the successful implementation of CWP-modified HMA, strict adherence to the 12% replacement limit is essential to balance sustainability goals with the necessary mechanical performance for medium-traffic applications.

While the study shows promise for using wood-derived carbonised waste powder (CWP) in asphalt, its findings are limited to laboratory conditions, a single wood type, and a conventional binder, leaving real-world performance unverified. Future research requires field testing and investigation into different materials, binders, and long-term durability to enable practical application.

REFERENCES

Adlinge, S. S., & Gupta, A. K. (2013). Pavement deterioration and its causes. *International journal of innovative research and development*, *2*(4), 437-450. https://www.iosrjournals.org/iosr-jmce/papers/sicete(civil)-volume6/60.pdf

Ahmedzade, P., & Sengoz, B. (2009). Evaluation of steel slag coarse aggregate in hot mix asphalt concrete. *Journal of Hazardous Materials, 165*(1-3), 300-305. https://doi.org/10.1016/j.jhazmat.2008.09.105

Akbulut, H., & Gürer, C. (2007). Use of aggregates produced from marble quarry waste in asphalt pavements. *Building and Environment, 42*(5), 1921-1930. https://doi.org/10.1016/j.buildenv.2006.03.012

APRG. (1998). Selection and Design of Asphalt Mixes: Australian Provisional Guide (APRG Report No. 18). Austroads.

Asphalt-Institute. (2014). Asphalt mix design methods (7th ed., Manual Series No. 2). The Asphalt Institute.

Bennert, T., Haas, E., & Wass, E. (2018). Indirect tensile test (IDT) to determine asphalt mixture performance indicators during quality control testing in New Jersey. *Transportation Research Record, 2672*(28), 394-403. https://doi.org/10.1177/0361198118793276

Boura, A. S., & Hesami, S. (2020). Laboratory evaluation of the performance of asphalt mixtures containing biomass fillers. *Road Materials and Pavement Design, 21*(7), 2040-2053. https://doi.org/10.1080/14680629.2019.1572528

Dias, A. F., Pirola, L. P., Takeshita, S., Lana, A. Q., Brito, J. O., & Andrade, A. M. D. (2016). Hygroscopicity of charcoal produced in different temperatures. *Cerne, 22*(4), 423-430. https://doi.org/10.1590/01047760201622032175

Do, T. C., Tran, V. P., Lee, H. J., & Kim, W. J. (2019). Mechanical characteristics of the tensile strength ratio method compared to other parameters used for moisture susceptibility evaluation of asphalt mixtures. *Journal of Traffic and Transportation Engineering (English Edition), 6*(6), 621-630. https://doi.org/10.1016/j.jtte.2018.01.009

Fung, P. Y., De Vos, A. I., Muruganathan, V., & Ng, H. S. (2006). Process for carbonising wood residues and producing activated carbon. U.S. Patent No. 7,029,273.

Gashi, E., Sadiku, H., & Misini, M. (2017). A review of aggregate and asphalt mixture specific gravity measurements and their impacts on asphalt mix design properties and mix acceptance. *International Journal of Advanced Engineering Research and Science, 4*(5), 237182. https://doi.org/10.22161/ijaers.4.5.31

Guesmi, M. L., Nafa, Z., Bordjiba, A., & Bouras, F. (2023). Partial Substitution of Asphalt Concrete Filler with Eco-Friendly Burnt Sawdust. *The Journal of Engineering and Exact Sciences, 9*(7), 16296-01e. https://doi.org/10.18540/jcecvl9iss7pp16296-01e

Hämäläinen, A., Vaismaa, K., & Kolisoja, P. (2025). Managing and Predicting the Condition of Paved Road Network in Finland: Essential Technical Information. *The Baltic Journal of Road and Bridge Engineering*, *20*(2), 24-42. https://doi.org/10.7250/bjrbe.2025-20.658

Hassan, H. F. (2005). Recycling of municipal solid waste incinerator ash in hot-mix asphalt concrete. *Construction and Building Materials, 19*(2), 91-98. https://doi.org/10.1016/j.conbuildmat.2004.05.010

Hoy, M., Horpibulsuk, S., Chinkulkijniwat, A., Suddeepong, A., Buritatum, A., Yaowarat, T., ... & Kantatham, K. (2024). Innovations in recycled construction materials: paving the way towards sustainable road infrastructure. *Frontiers in Built Environment*, *10*, 1449970.doi: 10.3389/fbuil.2024.1449970

Huang, Y., Bird, R. N., & Heidrich, O. (2007). A review of the use of recycled solid waste materials in asphalt pavements. Resources, *Conservation and Recycling, 52*(1), 58-73. https://doi.org/10.1016/j.resconrec.2007.02.002

Jegatheesan, N., Rengarasu, T. M., & Bandara, W. M. K. R. T. W. (2017). Suitability of recycled pet fibre and carbonised wood ash in hot mix asphalt concrete. In J. Manatunge (Ed.), Transactions of 111th Annual Sessions of the Institution of Engineers (pp. 623-630). Institution of Engineers Sri Lanka, Colombo.

Jegatheesan, N., Rengarasu, T. M., & Bandara, W. M. K. R. T. W. (2020). Mechanical properties of modified hot mix asphalt containing polyethene terephthalate fibres as binder additive and carbonised wood particles as fine aggregate replacement. *Asian Transport Studies, 6*, 100029. https://doi.org/10.1016/j.eastsj.2020.100029

Jegatheesan, N., Rengarasu, T. M., & Bandara, W. M. K. R. T. W. (2021). Modelling the properties of modified hot mix asphalt containing polyethene terephthalate fibres and carbonised wood particles *Journal of the Eastern Asia Society for Transportation Studies 14,* 1692-1711. https://doi.org/10.11175/easts.14.1692

Kandhal, P. S., & Mallick, R. B. (2001). Effect of mix gradation on the rutting potential of dense-graded asphalt mixtures. *Transportation Research Record, 1767*(1), 146-151. https://doi.org/10.3141/1767-18

Karati, S., & Kumar Roy, T. (2024). Evaluation of the Performance of Sawdust Ash in Bituminous Concrete against Moisture Damage. *Journal of Materials in Civil Engineering, 36*(4), 0402-4012. https://doi.org/10.1061/JMCEE7.MTENG-16769

Kuity, A., Jayaprakasan, S., & Das, A. (2014). Laboratory investigation on volume proportioning scheme of mineral fillers in asphalt mixture. *Construction and Building Materials, 68*, 637-643. https://doi.org/10.1016/j.conbuildmat.2014.07.012

Lesueur, D., Petit, J., & Ritter, H. J. (2012). Increasing the durability of asphalt mixtures by hydrated lime addition: What evidence? *European Roads Review, (20)*, 48-55. https://doi.org/10.1080/14680629.2012.743669

Mahmoud, E., Ibrahim, A., El-Chabib, H., & Patibandla, V. C. (2013). Self-consolidating concrete incorporating high volume of fly ash, slag, and recycled asphalt pavement. *International Journal of Concrete Structures and Materials, 7*(2), 155-163. https://doi.org/10.1007/s40069-013-0044-1

Marteano, D., Soediro, R., & Purwanto, D. (2002). The performance evaluation of hot rolled asphalt mixed with sawdust ash as a filler. *Pilar, 11*(2), 80-87. https://core.ac.uk/download/pdf/11705324.pdf

Perera, K. K. C. K., Rathnasiri, P. G., Senarath, S. A. S., Sugathapala, A. G. T., Bhattacharya, S. C., & Salam, P. A. (2005). *Biomass and Bioenergy. Biomass and Bioenergy, 29*(3), 199-213. https://doi.org/10.1016/

j.biombioe.2005.03.008

Rahman, M. T., Mohajerani, A., & Giustozzi, F. (2020). Recycling of waste materials for asphalt concrete and bitumen: A review. *Materials, 13*(7), 1495. https://doi.org/10.3390/ma13071495

Rengarasu, T. M., Juzaafi, M., Bandara, W. M. K. R. T. W., & Jegatheesan, N. (2020). Suitability of coal bottom ash and carbonized rice husk in hot mix asphalt. *Asian Transport Studies, 6*, 100013. https://doi.org/10.1016/j.eastsj.2020.100013

Sapkota, K., Yaghoubi, E., Wasantha, P. L. P., Van Staden, R., & Fragomeni, S. (2023). Mechanical characteristics and durability of HMA made of recycled aggregates. *Sustainability*, *15*(6), 5594. https://doi.org/10.3390/su15065594

Sargın, Ş., Saltan, M., Morova, N., & Serin, S. T. (2013). Evaluation of rice husk ash as filler in hot mix asphalt concrete. *Construction and Building Materials, 48*, 390-397. https://doi.org/10.1016/j.conbuildmat.2013.06.029

Shyamalee, D., Amarasinghe, A. D. U. S., & Senanayaka, N. S. (2015). Evaluation of different binding materials in forming biomass briquettes with sawdust. *International Journal of Scientific and Research Publications, 5*(3), 1-8.

Xue, Y., Wu, S., Cai, J., Zhou, M., & Zha, J. (2014). Effects of two biomass ashes on asphalt binder: Dynamic shear rheological characteristic analysis. *Construction and Building Materials, 56*, 7-15. https://doi.org/10.1016/j.conbuildmat.2014.01.075

Yasanthi, R. G. N., Rengarasu, T. M., Jegatheesan, N., & Bandara, W. M. K. R. T. W. (2017). Effect of temperature variation on hot mix asphalt concrete with sawdust ash used as aggregates. In Proceedings of Fifth International Symposium on Advances in Civil and Environmental Engineering Practices for Sustainable Development (pp. 244-251). Faculty of Engineering, University of Ruhuna, Hapugala, Galle, Sri Lanka.

Osuya, D. O., & Mohammed, H. (2017). Evaluation of sawdust ash as a partial replacement for mineral filler in asphaltic concrete. *Ife Journal of Science, 19*(2), 431-440. https://doi.org/10.4314/ijs.v19i2.23

J.Natn.Sci.Foundation Sri Lanka 2025 53 (4): 391 - 402
DOI: http://dx.doi.org/10.4038/jnsfsr.v53i4.12614

RESEARCH ARTICLE

Environmental Science

Ecological characterization of the 40-year-old regenerated rainforest patch in Olaboduwa-Kodigahakanda adds value in promoting forest-based nature tourism

WAPU Ruwanmalie, IASR Ileperuma and SMW Ranwala*
Department of Plant Science, Faculty of Science, University of Colombo, Colombo, Sri Lanka.

Submitted: 24 March 2025; Revised: 18 November 2025; Accepted: 27 November 2025

Abstract: Ecosystem and floristic characteristics have been extensively studied to address environmental disturbances and mitigation measures. However, their importance as key landscape elements in evoking natural attractiveness is less explored. This paper focuses on the ecological evaluation of the scenic beauty, carbon storage and ecosystem health of a forest fragment, Olaboduwa-Kodigahakanda in the suburbs of Colombo, through a quantitative approach to demonstrate the non-consumptive social value marketed for forest-based nature tourism. The forest accommodated 171 species of plants, 202 fauna including 69 bird species and 15 fish species, and 40 macro fungal species. A total of 32 threatened species were reported. The diversity of vegetation varied across the canopy, understory and undergrowth, and exhibited three distinct communities denoted by *Dipterocarpus zeylanicus*, *Mimosops elengi* and a mix of species. Plant age structure analysis confirmed a mid-successional forest regeneration phase enriched with endemic species *Artocarpus nobilis*, and *D. zeylanicus* in the canopy and *Gaertnera vaginans* in the understory. The living trees stored 134.82 ± 50.51 Mg/ha carbon, and 494.8 tons of CO_2e/ha greenhouse gasses, and showed satisfactory health in terms of greenness. School children were the key visitors engaged in nature exploration and educational day walks while youth preferred rock climbing as an adventure sport. Removal of invasive plants, enrichment planting of native species with regular monitoring and related follow up actions are recommended for forest management to offset impacts of disturbances while stream restoration initiatives would stimulate aquatic life. Strengthening local community participation in surveillance, management and revenue generation is crucial for sustainable nature tourism. The forest stands as a model for promoting forest-based nature tourism of secondary forest fragments in wet lowlands.

Keywords: Sub-urban forests, secondary forests, nature, biodiversity, eco-tourism, ecological value

INTRODUCTION

In recent years, the importance of forests in regulating climate, maintaining soil health, supporting biodiversity, and enhancing human well-being has become increasingly prominent and mainstreamed into policy decisions (Mace, 2005; CBD 2022). This has led to a growing societal demand in recognizing the social values of forest activities such as for tourism, recreation, and environmental education. Although fewer visitors are attracted to forests outside protected areas, smaller lesser-known forests in peri or sub-urban settings have gained popularity as people seek out areas for therapeutic motives, nature exploration, and recreational activities such as photography, camping, walking, hiking, rock climbing, and bird or animal-watching (SLTDA, 2020; Grebner et al., 2022; Mann et al., 2024; Lehto et al., 2025; Lin et al., 2025). Thus, nature has now become a playground for adventure and recreational experiences for humans with social media playing a significant role in promoting these destinations to both local and foreign

* Corresponding author (ranwala@pts.cmb.ac.lk; https://orcid.org/0000-0002-0965-9552)

This article is published under the Creative Commons CC-BY-ND License (http://creativecommons.org/licenses/by-nd/4.0/). This license permits use, distribution and reproduction, commercial and non-commercial, provided that the original work is properly cited and is not changed in anyway.

tourists, and thereby transforming lesser-known places into tourist attractions (Arts et al., 2021; Hung & Liou, 2023).

Ecosystem components and processes lay the foundation for the natural environment. Floristic features such as species composition and richness, density and distribution, and tree size and age create structural complexity for habitat niches of wildlife. Using ecological evidence, nature's social benefits, especially scenic and recreational offerings, greenhouse gas capturing potential etc. can be easily marketed to promote nature tourism and value addition to ecosystems dispelling the misconception of them being considered "useless". Such judgements are particularly important in safeguarding lesser-known small forest patches scattered in human dominated landscapes (Rolston & Coufal, 1991; Ng et.al., 2021; Lehto et al., 2025). Further, ecological characteristics reflect the detrimental impacts of human visitation and indicate the necessity of remedial measures (Cole, 2004; Marion et al., 2016) and provide insights into decisive aspects of ecosystem management. The adoption of a community-based approach in nature tourism creates environmental consciousness and motivation to develop positive socio-economic perspectives and actions in protecting the environment (Wickramasinghe, 2013).

The Southwestern lowlands of Sri Lanka contain a large number of undescribed small secondary forest patches with unique ecological characteristics, and their sustainability is confronted with increasing societal demands (MOFE, 1998; Fernando et al., 2015; Sumanapala & Wolf, 2020). This paper derives quantitative ecological evidence for non-consumptive social values marketable in forest-based nature tourism at Olaboduwa-Kodigahakanda, a patch of secondary rainforest, and propose management aspects to enhance its services. Inventories were prepared for flora, fauna, and, for the first time, for macro-fungi. Ecological and floristic features, diversity, age structure and regeneration capacity, living biomass and carbon stock, and forest health in terms of a greenness-index were quantified. Recreation offerings were consolidated, and recommendations for improvement of forest cover and hydrological aspects were proposed to sustain Olaboduwa-Kodigahakanda as a biologically rich and ecologically stable forest-based nature tourism destination.

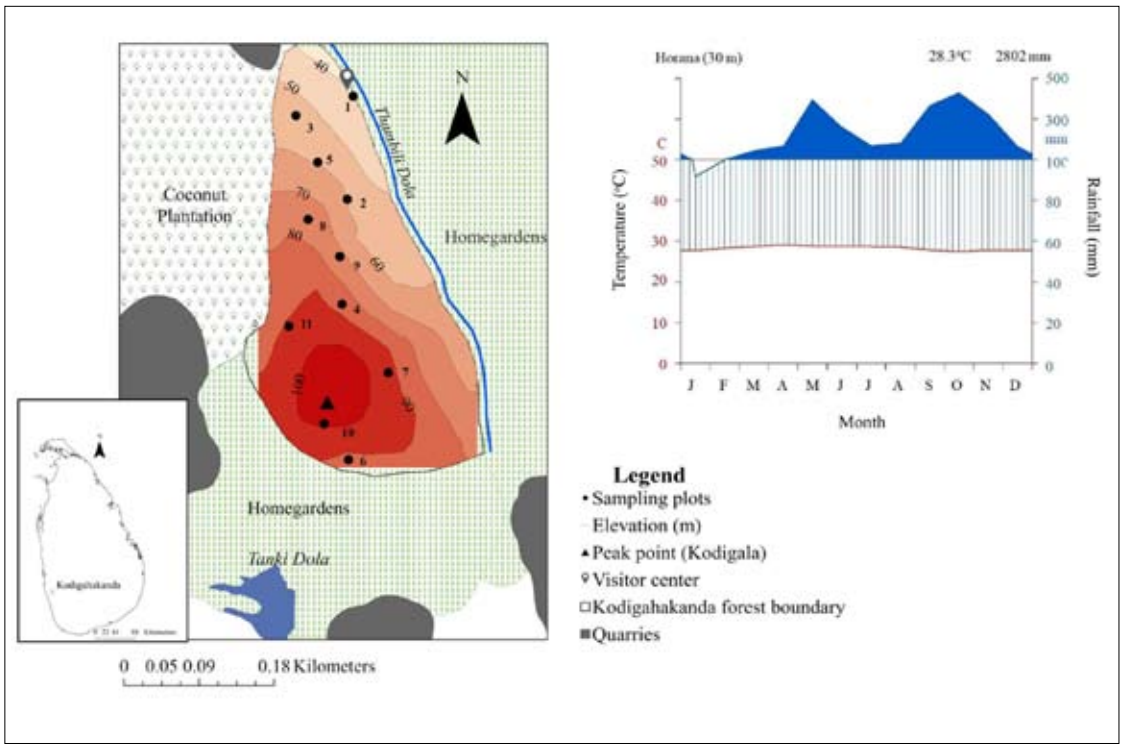

Figure 1: Location with sampling stands, and Climate map of Horana indicating the elevation, and the average annual temperature & rainfall

MATERIALS AND METHODS

Study site

The site Kodigahakanda (6°46'59"N-6°46'42"N, 80°0'50"E-80°0'56"E, 135-380msl,7.2ha) was named to locate Kodi-gala (115.2msl), the highest elevation in the suburbs of Colombo, which served as a trigonometrical station in the colonial period. In the 1860s the forest was cleared for planting coffee, and later for coconut. Since the early 1980s, after uprooting coconut trees, the ancestral owners of the land allowed it to regenerate naturally while safeguarding against destructive activities through community surveillance (Hettiarachchi, 2004). At present, the forest serves as the watershed for the stream Thembili dola. The forest lies on rocky terrain comprised of pre-Cambrian crystalline with red-yellow podzolic soil (Hettiarachchi, 2004), and experiences an average annual rainfall >2800 mm and a temperature of 28 °C (Figure 1).

Flora, macro-fungi, fauna and soil data collection

Vascular plants in accessible areas including eleven 10 m x10 m random sample stands were botanically identified using taxonomic literature and their conservation status was determined (MOE, 2020a). Fruiting bodies of macro fungi were collected monthly over a year with records of their habitat before they were photographed and identified (Kirk, 2024; GBIF, 2024). The canopy and understory of the stands were enumerated. Height, diameter at breast height (DBH) of canopy trees >5 m and ≥5 cm girth, and understory individuals 3-5 m tall and >1.3 cm girth were recorded. Four 2 m × 2 m sub-samples per stand were used for counting liana stems, undergrowth herbs, and seedlings <1 m in height. Forest canopy cover was estimated using hemispherical photography using a fish-eye lens 1.5 m above the ground. gap light analyzer (GLA) free software version 2.0 was used to analyze canopy images to calculate canopy openness (Frazer et al., 1999). Fauna was scientifically identified using taxonomic literature based on direct and indirect observations, acoustics, footprints, and faeces between 0600 h-1200 h, and 1500 h-1800 h for approximately 200 total hours. Their conservation status was determined (MOE, 2020b; 2021). Litter-less composite soil samples up to 15 cm in depth collected from stands were air dried, sieved and analyzed at 24 °C for pH (Thermo Scientific™) and electrical conductivity (Hanna™), moisture content followed by drying for 10-12 h at 105 °C (Sarkar & Haldar, 2010). The soil organic carbon was determined using the Walkley-Black colorimetric method, and total nitrogen (N), phosphorus (P), and potassium (K) of H_2SO_4 digested soil using Kjeldahl, Olsen and flame photometric methods, respectively (AOAC, 2005).

Analysis of floristic diversity, age structure, communities and heterogeneity

Canopy, understory, and undergrowth diversity of stands were quantified using Shannon Wiener (H′), Inverse Simpson's (1-D) and Margalef (D_{mg}) indices. The ecological dominance of species was determined by the important value index (IVI) (Crawley, 1989; Krebs, 2009) using PAST ecological software (version 4.03). The relevant formulae were $H' = \sum p_i . \ln (p_i)$; where p_i is the proportional abundance of species; $1\text{-}D = 1 - \sum [n_i (n_i -1) / N (N-1)]$, where, n_i is the number of individuals of species 'i', and N is the total number of individuals; $D_{mg} = (S-1)/ \ln (N)$, where, S is the total number of species and N is the total number of individuals of all species; IVI = relative density (RD) + relative basal cover (RC) + relative frequency (RF). Age structure analysis of all canopy individuals and the three most ecologically dominant tree species were depicted, and the regeneration status was determined (Crawley, 1989). Floristic communities were identified by subjecting species occurrences in stands to the Bray-Curtis dissimilarity index (Hao et al., 2019) followed by hierarchical clustering and the Vegan software of RStudio (R Core team, 2012). Synoptic significance values ($P<0.05$) were determined through the "synoptic indicator value index" (IndVal) for identifying key floristic communities. Species that scored >1.0 were considered as indicator species that are firmly associated with one community type. The "Indicspecies" package ($P<0.05$) was used to identify character species whose mean cover is high within a particular community (Kefalew et al., 2022). To quantify how strongly a species is associated with a specific plant community, synoptic indicator values obtained for each species in each floristic community were statistically analyzed ($P<0.05$) to name the community. The heterogeneity of vegetation was determined by the association of soil and floristic characteristics of stands (species occurrences, individuals, liana stem counts) projected using canonical correspondence analysis (CCA) using PAST ecological software version 4.03.

Biomass and carbon stock of living trees and green-house gas capturing potential

Carbon stock was estimated using DBH, allometric equations and wood density values available for trees and lianas (FAO, 2024). The formulae used were: Above ground biomass of trees (AGB_{Tree}) in kg $tree^{-1}$ = $0.0673 \times (\rho D^2 H)^{0.976}$, where, ρ is wood density (gcm^{-3}),

D is the DBH (cm), and H is the tree height in meters (m) (Chave et al., 2014); Belowground biomass of trees (BGB_{Tree}) = exp [-1.0587 + 0.8836 ln (AGB (Tree)] (Cairns et al., 1997); Above ground biomass of lianas (AGB_{Liana}) = exp [-1.484 + 2.657 ln (D)] where, D is the DBH of the liana stem; Below ground biomass of lianas (BGB_{Liana}) = AGB (Liana) x 0.26, and total carbon stock of trees (MgC ha^{-1}) = Above and below ground biomass (Mg ha^{-1}) x 0.47. The carbon stock of lianas was computed to be 50% of the above and below ground liana biomass. (Gerwing & Farias, 2000; IPCC, 2006; Babu & Parthasaran, 2019; Neth et al., 2022). A conversion factor of 0.50 was used to convert biomass (dry weight) to carbon equivalents (CO2e) to identify the green- house gas capturing potential (Petersson et al., 2012).

Forest health

The health of an ecosystem reflects productivity, ecological functioning and resilience, as well as the success of management practices. This is assessed by both, the normalized difference vegetation index (NDVI) and Greenness Index (GI) (Pandapotan et al. 2016; Ali et al., 2018; Rumat et al., 2018; Chandler et al., 2021). For image analysis, Sentinel-2 multispectral satellite imagery (2021) of the study area, and Sinharaja and Kanneliya forests as reference sites were obtained from the Copernicus program of the European Space Agency, cloud filtered and downloaded (https://browser.dataspace.copernicus.eu/, dated February 2024). Following pre-processing, and raster and band clipping, both GI and NDVI for the forests were calculated and mapped using the equations; GI = G / (R + G + B) and NDVI = (N - R) / (N + R); where, G = Band 3 (Green); R = Band 4 (Red); B = Band 2 (Blue) and N = Band 8 (Near-infrared). ArcGIS Pro software was used for NDVI and GI calculations and mapping (Weier & Herring, 2000; Meter group, 2024).

Visitation analysis

Information on visitors and recreation activities that took place at Olaboduwa-Kodigahakanda were extracted from visitor book records (2014-2023) and available entrance tickets issued for adventure sports (2020-2023).

RESULTS AND DISCUSSION

Flora, macro fungi and fauna

The forest accommodated a total of 171 plant species common to lowland rainforests. Among them 90% were native, 8.7% endemic, 9.9% exotic, and 6.4% were threatened. Among the 69 plant families, Fabaceae, Rubiaceae, Euphorbiaceae and Malvaceae were highly represented (SI Table1A). Some orchid species such as *Eulophia epidendraea* (J. Koenig ex Retz.) C.E.C. Fisch, *Sarcanthus peninsularis* Dalzell.*, Thrixspermum pulchellum* (Thw.) Schltr.*,* and *Dendrobium aphyllum* (Roxb.) C.E.C. Fisch, recorded in previous inventories (Kotagama, 1986; Hettiarachchi, 2004; Palihawardana, 2015) were not found possibly due to changes in the microclimate over the years. The threat to flora was also evident by the presence of two endangered plant species (*Rungia latior* Nees, and *Areca concinna* Thwaites), and nine plant species in the vulnerable category (*Trichopus zeylanicus* (Gaertn.) R.Br., *Erythrina variegate* L., *Grona heterocarpa* (L.) Verdc., *Cinnamomum verum* J. Presl, *Tolypanthus gardneri* (Wight & Arn.) Benth., *Horsfieldia iryaghedhi* (Gaertn.) Warb**.,** *Nepenthes distillatoria* L., *Guettarda speciosa* L., *Saraca asoca* (Roxb.) W.J.de Wilde]. Charismatic plant species of the forest were identified as *Begonia malabarica* Lam. (for having the largest flower of the genus), and *Memecylon* spp. (for representing many species including the threatened *M. rivulare* Thw. and *M. grande* Retz.), which added vibrant colours to enhance landscape aesthetics. A notable feature of the forest was the richness (9%) of liana species. Lianas account for 10% to 45% of woody stems and 35% of the diversity of woody species in tropical forests and perform an integral role in forest regeneration, the maintenance of species diversity and ecosystem processes (Marshell et al., 2020). In forest canopies with low disturbances, lianas help to protect plants from strong winds, weed invasion (via competition), and herbivory. However, increased light levels in canopy gaps may stimulate prolific growth of lianas impeding tree growth and survival (Toledo-Aceves and Swaine, 2007; Ingwell et al., 2010; Schnitzer and Bongers, 2011; Visser et al., 2018; Meunier et al., 2021). Hence, managing the liana population assists in the regeneration of degraded forests towards uninterrupted succession.

The occurrence of 40 macro-fungi species belonging to 6 orders and 17 families was reported with wide representation in the Agaricales and Polyporales orders. Many (31 species) were saprophytes, while 10 were mutualistic (mostly mycorrhizal) and 9 were parasitic taxa (SI Table1-B). The soil inhabiting fungi (11 species) represented the families Lyophyllaceae, Fomitopsidaceae, Gomphaceae, Sclerodermataceae, Hygrophoraceae and Clavariaceae. Others occupied mostly dead wood, twigs and dried leaves with live wood serving as the substratum only for *Oudemansiella australis* G. Stev. & G.M. Taylor.

The forest accommodated a total of 202 species of fauna (23 mammal, 69 bird, 29 reptile, 8 amphibian, 57 butterfly and 15 fish species) which included 12.3 % endemic species, and 9.4% threatened species (SI Table 1-C). Observing fauna provided recreational pleasure to people while the presence of the Atlas moth (*Attacus atlas* Linnaeus, 1758) added special conservation value and attraction for educational tours.

Floristic details and forest management aspects

The forest canopy of Olaboduwa-Kodigahakanda reached a height of 10 to 15 m, roofing a dense understory and sparse undergrowth. The diversity of the canopy, understory and undergrowth varied broadly across the forest (SI-Table 2). The Shannon-Weiner Index (H') reflecting species diversity exhibited the widest range for the understory (0.556- 2.432) compared to the forest undergrowth (0-1.528) and canopy (0.888-2.032). The inverse Simpsons Index (1-D), which reflects both species diversity and evenness, showed a broad range for the undergrowth (0-0.760) than understory (0.290-0.895) and canopy (0.542-0.840). Plant species richness as reflected by the Margalef's index (D_{mg}) also exhibited a broad range for the understory (0.692-3.301) than the canopy (0.805-3.119) and undergrowth (0-2.118) reflecting the diverse nature of the strata. The eastern slope of the forest leading to Thambili dola reported the highest canopy diversity while the lowest was reported in stands with high abundance of *D. zeylanicus*. Rocky areas reflected the least values for diversity and richness in undergrowth. The aggressive invader *Oclandra stridula* (Thw.) C.E.C. Fisch. was reported from the understory of this area. Regular removal by digging out could control their spread and may suppress its dominance while facilitating the growth of other native species (Madawala and Wijewickrama, 2021). The introduction of threatened and common medicinal species of lowland rainforests e.g., *Costus speciosus* (Thebu), *Strobilanthes* sp., *Sonerila* sp., *Impatiens* sp., to the forest understory would improve the naturalistic beauty of the forest interior.

Based on IVI values, *Artocarpus nobilis* Thw., *D. zeylanicus, Melicopelunu-ankenda* (Gaertn.) T.G. Hartley, *Aporosa cardiosperma* (Gaertn.) T.G. Hartley, *Alstonia macrophylla* Wall. ex G. Don*, Tabernaemontana dichotoma* (L.) Poir*., Mimusops elengi* L. were canopy dominant species (SI Table 3). Importantly, the endemic species *A. nobilis* and *D. zeylanicus* together accounted for 25% of canopy dominance, which is an uncommon feature of a regenerating forest. Hence, encouraging the diversification of canopy tree species may improve the resilience of the ecosystem. Nevertheless, *A. macrophylla* trees raised over the canopy indicated an ill-fated condition. Its prolific seed production, long-distance dispersal, and longer viability period in the soil bank undoubtedly promotes its establishment and aggressive spread all over the forest unless immediate control measures are taken. Being a timber species, its adverse effects on native vegetation are often overlooked. Hand pulling of seedlings and digging of saplings on a regular basis will reduce its population density while debarking and basal cutting are recommended for destroying large trees (Jayawardhane & Gunaratne, 2022). The dominance of endemic species in the understory, *Gaertnera vaginans* (DC.) Thwaites and *Phoenix pusilla* Gaertn. is another notable feature of this forest. However, the dominant species of the undergrowth *Nephrolepis biserrata*, and *Clidemia hirta* (L.) D. Don. are said to displace native vegetation at a rapid rate (Duenas- Lopez, 2022; Bhatta et al., 2023), hence requiring adoption of measures to control their populations followed by the re-establishment of undergrowth with native species.

The age structure of forest canopy tress was abundant in the 10 – 20 cm and 25 – 30 cm stem diameter classes (Figure 2) with an average DBH of 18.46 ± 10.04 cm. Canopy openness (24.13 ± 4.03%) and a forest stand structure deviating away from the typical reverse J shape (condition between positively skewed and normal) indicated a mid-succession stage of regeneration (Crawley, 1989). The age structure of dominant canopy species varied (Figure 3). Seedlings of *A. nobilis* and *A. cardiosperma* were scanty due to possible consumption of seeds by rodents, and this is a matter of concern for their future survival. In contrast, *D. zeylanicus* seedling population was exceptionally high in its dominant zone (Figure 3). Absence of *A. macrophylla* saplings suggest possible elimination because of competition with native species followed by stem exclusion during succession. However, monitoring growth of seedlings into saplings of both *D. zeylanicus* and *A. macrophylla* should not be overlooked in forest regeneration.

The forest vegetation was zoned into three major plant communities (*D. zeylanicus*, *M. elengi* community and mixed plant species) as indicated by the Bray and Curtis dissimilarity index at a dissimilarity range of 0.5 – 0.7 (Figure 4). This provided a solid scientific foundation to confirm the ambiguous zonation explained by tour guides during field visits. *D. zeylanicus* and *M. elengi* remained as indicator species in their respective communities (SI-Table 4). According to personal communication with owners, before clearing in the 1860s, Kodigahakanda was

predominantly dominated by *D. zeylanicus* and the small patch which had been left since then is the area where it dominates at present. *A. nobilis* and *Goniothalamus* sp. were the characteristic species of the mixed plant community.

The CCA biplots indicated that soil moisture is relatively influential in species distribution. However, many species clustered around N, P, K, and C gradients indicated their preference for fertile soil, except for one stand which represented the rocky area (Figure 5).

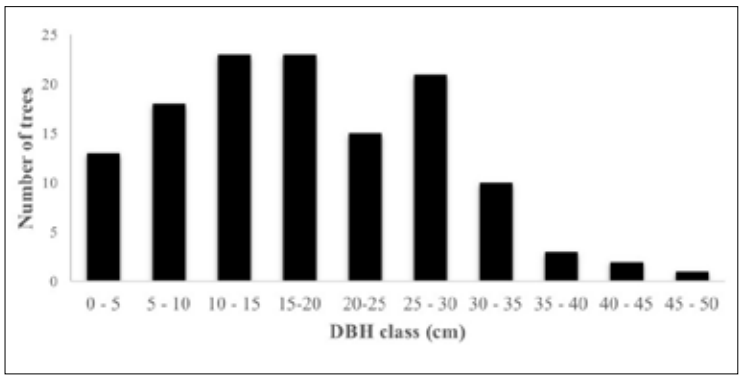

Figure 2: Diameter class categories of canopy trees

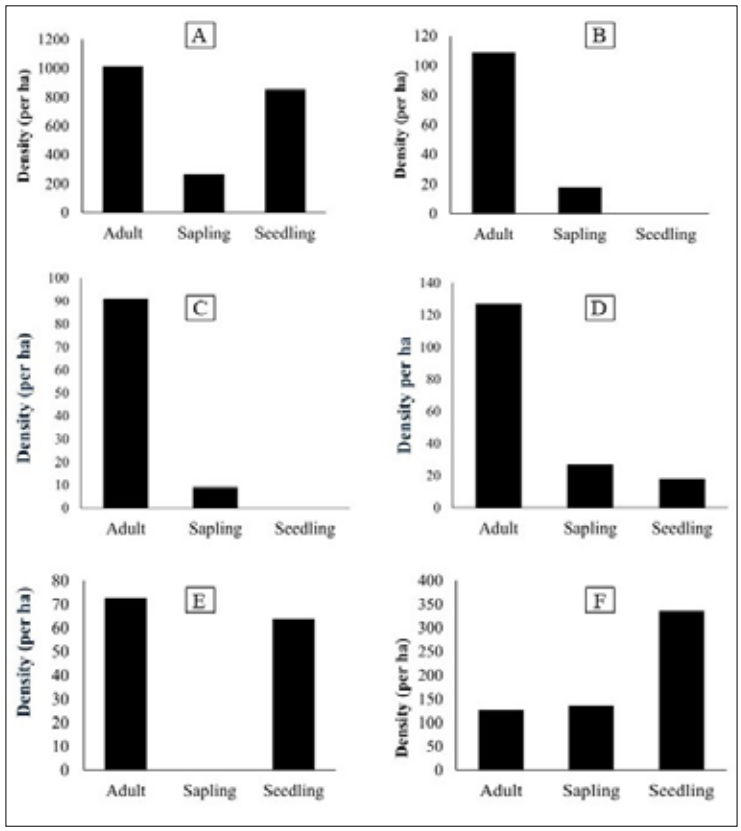

Figure 3: Age structure distribution of (A) all canopy trees, (B) *A. nobilis,* (C) *A. cardiosperma* (D) *M. lunu-ankenda*, , (E) *A. macrophylla,* (F) *D. zeylanicus*

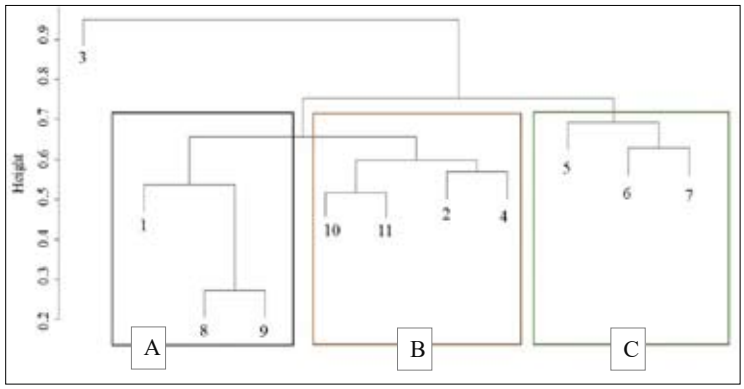

Figure 4: Bray-Curtis hierarchical clustering dendrogram of vegetation dissimilarity representing three communities; A): *D. zeylanicus* community, B): *M. elengi* community, and C): mixed plant community.

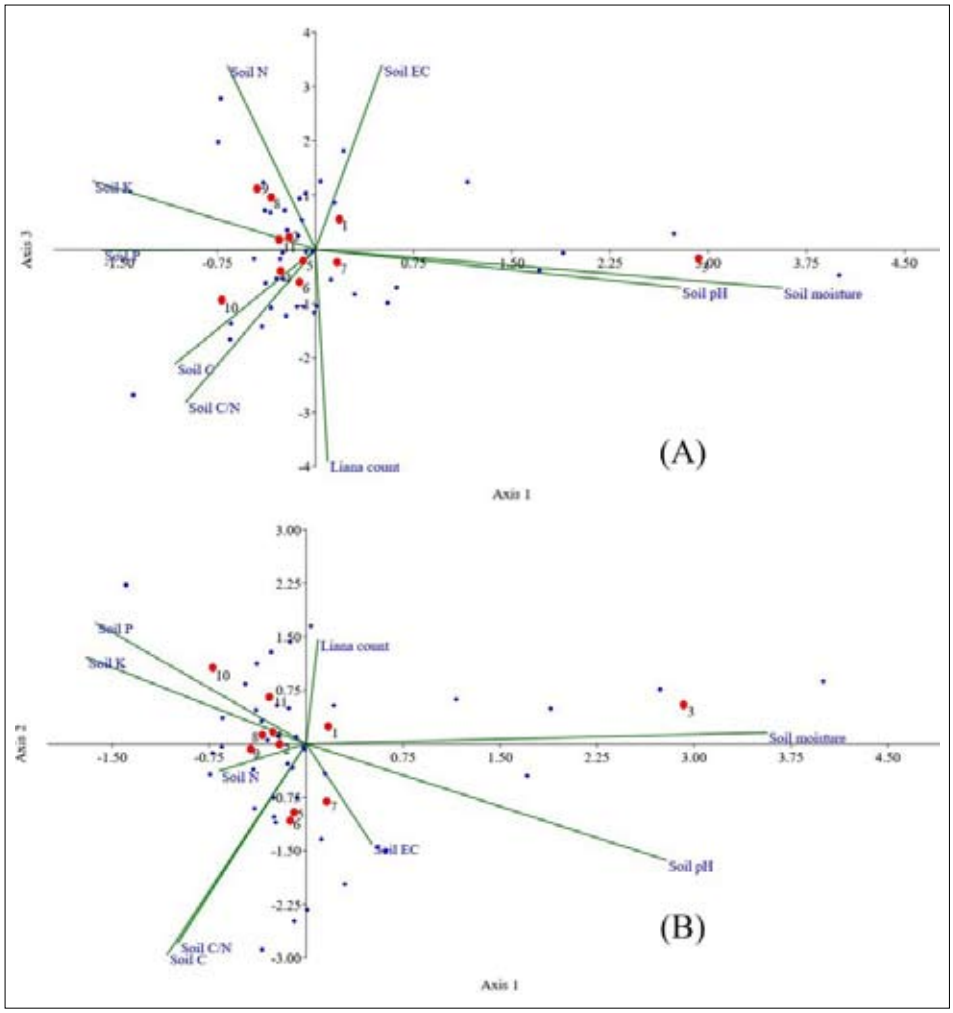

Figure 5: Canonical Correspondence Analysis (CCA) biplots of site heterogeneity analysis (A) between axis 1 & 3, (B) axis 1 & 2, for which high Eigen values were 0.669, 0.390, 0.351, respectively. Blue dots represent plant species, and red dots represent sampling plots.

Biomass and carbon stock of living trees

Trees and lianas contributed 80% and 20%, respectively, to the total woody biomass of the forest. In primary tropical lowland forests, liana biomass has been estimated to be 5 to 10% of the total woody biomass whereas in secondary forests it may approach 30% (Gerwing & Farias, 2000, Schnitzer & Bongers, 2011). The estimation of above and below ground carbon stock (CS) of Kodigahakanda forest was 134.82 ± 50.51 MgC ha^{-1} to which trees contributed 81.2% and lianas 18%. This low value is expected for a regenerating forest compared to optimum values estimated from closed forests such as Sinharaja, which accounted for 336.8 MgC ha^{-1} only for above ground carbon (Kumarathunge & Iqbal, 2009). The contribution of individual canopy tree species to the CS of the forest was driven by the relative stem cover of the three ecologically dominant tree species, particularly by large trees of *D. zeylanicus* (Figure 6A). The lowest CS was accounted for in sample stands with high liana stem count (Figure 6B) due to their thinner stems for sequestering CO_2 despite their efficient investment of energy compared to trees at the canopy level (Van der Heijden et al., 2013). Nevertheless, the forest exhibited a capacity to trap 494.8 tons of CO_2e/ha greenhouse gasses.

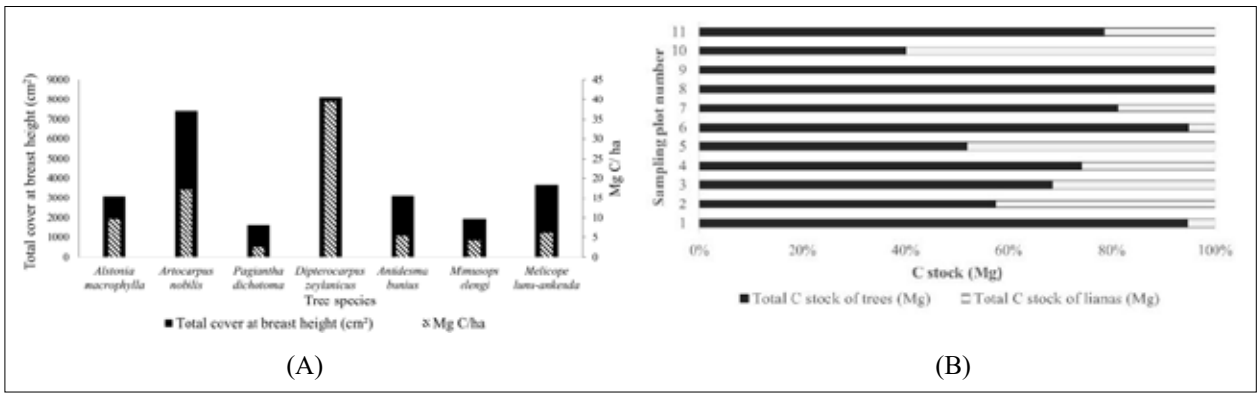

Figure 6: A) Carbon stock partitioning of canopy tree species, and B) trees and lianas in sample stands

Forest health, NDVI assessment, Index of greenness and suggestions for site improvements

An average NDVI value of 0.698 was obtained for Olaboduwa-Kodigahakanda indicating a dense green forest canopy despite its secondary origin. Generally, an NDVI value range of 0.6-0.8 indicates dense vegetation such as in tropical rainforests and a moderate range of 0.2-0.3 is typical for shrubs and grasslands (Weier & Herring, 2000; Meter group, 2024). A broad NDVI range of 0.44 – 0.77 across the forest indicates the heterogeneity of regenerating vegetation with lower values towards the eastern side and higher values in the core regions (Figure 7). The GI assessment ranged from 0.34-0.39 with an average of 0.36 and displayed similar ranges to Sinharaja (0.32-0.36 with an average of 0.34) and for Kanneliya (0.33-0.37 with an average of 0.35).

Being the watershed for the Thambili Dola stream, the Olaboduwa-Kodigahakanda forest requires to maintain a dense canopy; hence, enrichment planting of species that strengthen community structure, ecological succession and resilience is vital. Focusing on wild fruit trees would attract more birds and bats facilitating passive regeneration through ornithochory. Strengthening stream restoration would not only enhance aesthetics of the landscape but also to strengthen hydrological aspects and aquatic life functionally linking with the forest ecosystem. This is crucial since Tanki Dola remains a stagnant patch of water whereas in the past, four main streams ('Tanki Dola', 'Pili Dola', 'Nas Dola', and 'Dikgal Dola') descended from the forest (Hettiarachchi, 2004). Form-based restoration by physically altering components of a stream can restore its natural shape, enhance water flow and reduce erosion. Process-based restoration activities such as removing anthropogenic barriers to stream flow and pollution control are vital to maintain the health of the ecosystem (Wohl et al. 2015).

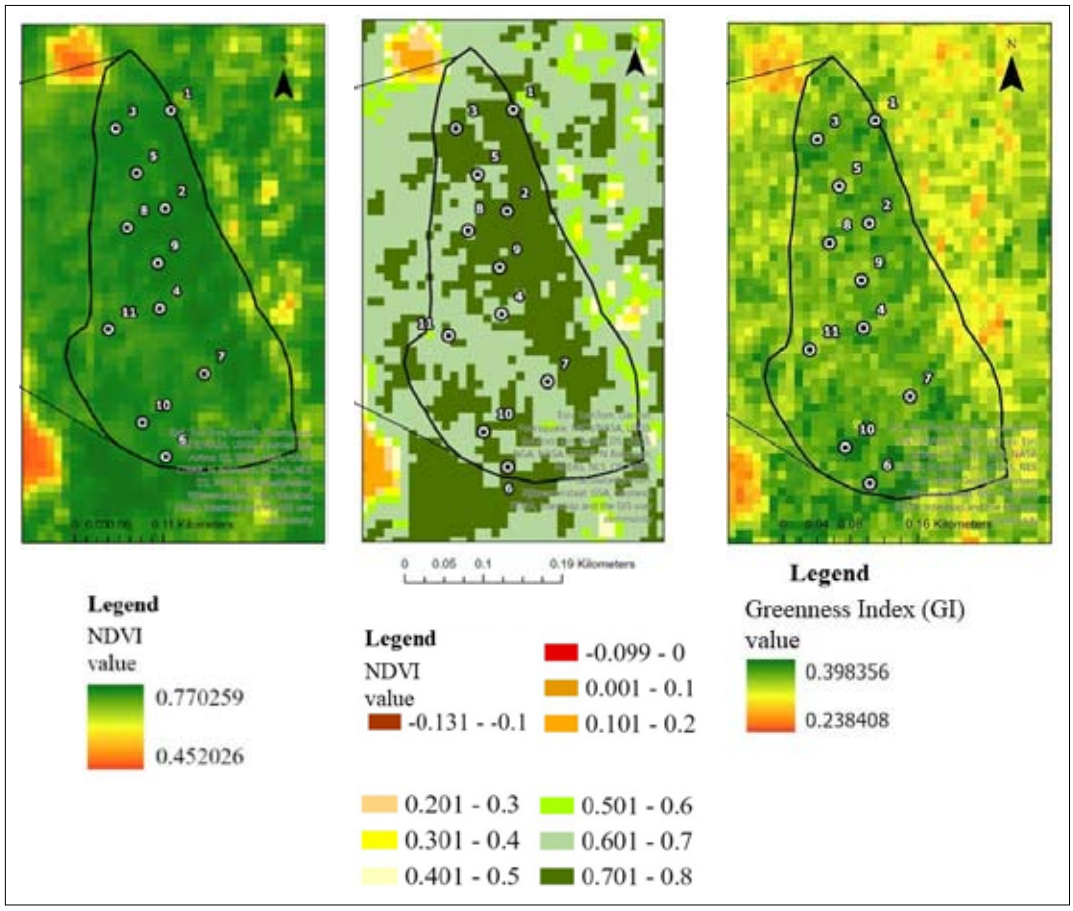

Figure 7: A) NDVI map (B) Classified NDVI ranks (C) Greenness Index (GI)

Recreation offerings and visitation

Olaboduwa-Kodigahakanda has been visited mainly by school children residing within a 10-25 km radius, mostly in groups of 20-50 individuals and occasionally 50-100. They are often involved in Scouting and Guiding activities (40%), environmental pioneer guides (28%), educational field visits (8%), and camping events (8%). Children from schools located beyond 25 km have visited only for day walks (16%). Educational visits often involve briefing students on identifying plants and animals, observing the heterogenous nature of vegetation, and learning the cultural importance of Kodigala. Adventure sports, notably rock climbing under guidance, are offered as outbound training offered for youth and adult groups.

It is apparent that marketing the aesthetics and other recreational offerings, carbon sequestration capacity and green status of the forest could widen opportunities for therapeutic relaxation, meditation, research, activity-based fun and learning-games that generate income while appreciating the natural environment. Especially at a time when economic needs drive people to take part in environmentally damaging practices, it is crucial to link local people with nature and improve attitudes and behaviors towards environmental consciousness and respect for the local natural wealth and culture. The civil organization associated with Olaboduwa-Kodigahakanda conducts tour guide training sessions for youth from the local community and connect them with visitor groups. However, only 12 school-aged individuals (including recent school leavers) work in this capacity on a paid basis. Besides this engagement, many opportunities exist for the local community, especially as food vendors and transportation providers.

Developing site-specific models of forest-based nature tourism with local community participation in a

socio- environmentally responsible and economically viable manner is essential to ensure sustainability of nature-tourism. Such models have shown success in Sri Lanka despite limited efforts and commitments to uplift the industry (Wickramasinghe, 2013; Sumanapala and Wolf, 2020). Over the recent years, private forest owners have shown increased commitment to enhancing forest benefits and aspiring to conserving small forest patches (Fahrig, 2020, Mayer, 2019), which is considered vital by the UN Decade of Environment Restoration 2030 proclaimed by the United Nations General Assembly (UNGA resolution A/RES/73/284). Although public-private partnerships in forest management through nature tourism have been encouraged in Sri Lanka, private forest owners engaged in conservation, environmental education, nature tourism and community development have not received sufficient attention.

Introducing a policy-level strategy to link the forest ecology of small forest patches with sustainable nature tourism could be a practical approach to motivate private ownership and the neighborhood community to improve the production capacity and multiple benefits delivered by forests of small spatial scales supporting the conservation approach of a 'small habitat matrix' in mitigating climate change and forest degradation (Panagopoulos, 2009; Fahrig, 2020, Ng et al, 2020).

CONCLUSION

The structural and compositional characteristics that have developed over an in-destructible 40 years of forest succession at Olaboduwa-Kodigahakanda have provided insights into aspects of value addition to small forest patches. Together with its geo-morphological features, the areas floristic characteristics and wildlife have not only created a scenic landscape for recreational activities, but also an opportunity for revenue generation shared among the members of the local community engaged in tourism. To ensure long term sustainability of social values, ecosystem restoration and monitoring initiatives are recommended. A site specific forest-based tourism model with good governance and community participation will attract nature loving and conservation- oriented tourists, improving the image and prospects for Olaboduwa-Kodigahakanda while serving as a model destination for uplifting sustainable forest-based tourism.

Acknowledgement

We sincerely thank Mr. Rohan de Soysa, Chairperson of the Kodigahakanda Trust Fund, for permitting research at Kodigahakanda, and to Mr. Karunadasa Munagama, president of the Mihithala Mithuro society, for his support in necessary arrangements for field work.

REFERENCES

Ali, A., Saleem, U., Shaiza, B., Ahmad, A., Khan, M.A. (2018). Quantifying forest carbon stocks by integrating satellite images and forest inventory data. *Austrian Journal of Forest Science, 135*, 93–117.

AOAC. (2005). *Official Methods of Analysis of Association of Official Analytical Chemists* (18th edition). Washington, DC.

Arts, I., Fischer, A., Duckett, D., Van der Wal, R. (2021). The Instagrammable outdoors – Investigating the sharing of nature experiences through visual social media. *People and Nature, 3*,1244–1256. https://doi.org/10.1002/pan3.10239

Babu, K.N. & Parthasarathy, N. (2019). Assessment of liana diversity and carbon stock in differently disturbed tropical dry evergreen forests of southern India. *Tropical Plant Research. 6*(1), 74-89. https://doi.org/10.22271/tpr.2019.v6.i1.012

Bhatta S., Shrestha B.B., Pyšek P. (2023). Invasive alien plants in South Asia: Impacts and management. *NeoBiota, 88*, 135–167. https://doi.org/10.3897/neobiota.88.104118

Cairns, M.A., Brown, S., Helmer, E.H., Baumgardner, G.A. (1997). Root biomass allocation in the world's upland forests. *Oecologia, 111*(1), 1-11. https://doi.org/10.1007/s004420050201

CBD. (2022). *Convention on Biological Diversity*. Kunming-Montreal Global Biodiversity Framework (UN Environment Programme) Convention on Biological Diversity. (2022). *Kunming–Montreal Global Biodiversity Framework*. https://www.cbd.int/gbf/

Chandler, C. J., Van der Heijden, G. M., Boyd, D.S., Foody, G.M. (2021). Detection of spatial and temporal patterns of liana infestation using satellite-derived imagery. *Remote Sensing, 13*(14), 2774. https://doi.org/10.3390/rs13142774

Chave, J., Réjou-Méchain, M., Burquez, A., Chidumayo, E., Colgon, M, Delitti, W., Duque, A., Eid, T., Fearnside, P., Goodman, R., Henry, M., Martinex-Yrizar, A., Mugasha, W., Muller-Landau, H., Mencuccini, M., Nelson, B., Ngomanda, A., Nogueira, E., Ortiz, E., Vieilledent, G. (2014). Improved pantropical allometric models to estimate the above ground biomass of tropical forests. *Global Change Biology, 20*, 3177–3190. https://doi.org/10.1111/gcb.12629

Cole, D. N. (2004). Impacts of hiking and camping on soil and vegetation: A review. *Environ. Impacts Ecotourism*, 41 - 60. https://doi.org/10.1079/9780851998107.0041

Crawley, M. J. (1989). Physical structure of plant communities. In M. J. Crawley (Ed.), *Plant ecology* (2nd ed., pp. 505–510). Blackwell Scientific Publications.

Duenas Lopez. (2022). *Nephrolepis biserrata* (Giant Sward fern). https://www.cabidigitallibrary.org/doi/10.1079/cabicompendium.36007

Fahrig, L. (2020). Why do several small patches hold more species than few large patches? *Global Ecology and Biogeography, 29*(4), 615-628. https://doi.org/10.1111/geb.13059

FAO. (2024). *Wood density values of trees and lianas - Appendix 1 - list of wood densities for tree species from tropical America, Africa, and Asia*. https://www.fao.org/3/w4095e/w4095e0c.htm,

Fernando, S., Senaratna, A., Pallewatta, N., Lokupitiya, E., Manawadu, L., Imbulana, U., De Silva, I., Ranwala, S. (2015) *Assessment of Key Policies and Measures Report on Drivers of Deforestation and Forest Degradation in Sri Lanka*. UN-REDD Programme, Sri Lanka. https://doi.org/10.13140/RG.2.2.15886.15688

Frazer, G.W., Canham, C.D., and Lertzman, K.P. (1999). *Gap light analyzer (GLA). User's Manual and program Documentation: Version 2.0,* Simon Fraser University, Burnaby, British Columbia, and the Institute of Ecosystem Studies, Millbrook, NY

GBIF. (2024). *Index Fungorum*. http://www.indexfungorum.org/,

Gerwing, J. J., & Farias, D. L. (2000). Integrating liana abundance and forest stature

into an estimate of total aboveground biomass for an eastern Amazonian Forest. *Journal of Tropical Ecology, 16*, 327–335. http://dx.doi.org/10.1017/S0266467400001437

Grebner, D. L., Bettinger, P., Siry, J. P., & Boston, K. (2022). Forest recreation. In D. L. Grebner, P. Bettinger, J. P. Siry, & K. Boston (Eds.), *Introduction to forestry and natural resources* (2nd ed., pp. 173–197). Academic Press. https://doi.org/10.1016/B978-0-12-819002-9.00007-9

Hao, M., Corral-Rivas, J. J., Socorro González-Elizondo, M., Narayanagowda, K., Nava-Miranda, M.G., Zhang, C., Zhao, X., Gadow, K.V. (2019). Assessing biological dissimilarities between five forest communities. *Forest Ecosystems, 6*(1). https://doi.org/10.1186/s40663-019-0188-9

Hettiarachchi, S. L. N. (2004). *Kodigahakanda*. Kodigahakanda Trust Fund.

Hung, W. & Liou, G. (2023). How is the effect of social media on intention to outdoor recreations? A study using personal social connections as a moderator. *Heliyon*,*9* (11), 22268. https://doi.org/10.1016/j.heliyon.2023.e22268

IPCC. (2006). *Guidelines for greenhouse gas inventories*. https://www.ipcc.ch/report/2006-ipcc-guidelines-for-national-greenhouse-gas-inventories/.

Jayawardhane J., & Gunaratne A.M.T.A. (2022). Influence of *Alstonia macrophylla* spread on the restoration success of pine conversion programs in Sri Lanka. *Journal of Tropical Forest Science, 34* (3), 285-295. https://doi.org/10.26525/jtfs2022.34.3.285

Kefalew, A., Soromessa, T., Demissew, S. (2022). Plant diversity and community analysis of Sele-Nono Forest, southwest Ethiopia: Implication for Conservation Planning. *Botanical Studies, 63*(1), 23. https://doi.org/10.1186/s40529-022-00353-w

Kirk, P. M. (2024). *Species Fungorum Plus*. In: *Catalogue of Life.* Amsterdam, Netherlands. DOI: https://doi.org/10.48580/dg9ld-4hj

Kotagama, S., Subasinghe, R., Zoysa, N., Jansen, M. (1986). *Kodigahakanda Biodiversity Report* (unpublished), Field Ornithology Group, University of Colombo.

Krebs, C. J. (2009). *Ecology: The experimental analysis of distribution and abundance* (6th ed.). Pearson Benjamin Cummings.

Kumarathunge, D., & Iqbal, M. (2009). Biomass estimation in some dry zone forests in Sri Lanka from forest inventory data. In *Proceedings of the International Forestry and Environment Symposium* (Vol. 14, pp. 173–190). https://doi.org/10.31357/fesympo.v14i0.367

Lehto, C., Sirén, A., Hedblom, M. Fredman, P. (2025). A conceptual framework of indicators for the suitability of forests for outdoor recreation. *Ambio, 54*, 184–197. https://doi.org/10.1007/s13280-024-02091-8

Lin, B., Zhang, Y. C., Lee, W. (2025). Tourists' perceptions of proximity tourism: Insights from sentiment analysis and fsQCA. *Journal of Outdoor Recreation and Tourism, 49*, 100848. https://doi.org/10.1016/j.jort.2024.100848

Mace, G. H., & Masundire, J. B. (2005). Ecosystems and human well-being, current state and trends. In R. Hassan, R. Scholes, & N. Ash (Eds.), *Millennium Ecosystem Assessment*. Island Press.

Mann, C., Hernández-Morcillo, M., Ikei, H., Miyazaki, Y. (2024). The socioeconomic dimension of forest therapy: A contribution to human well-being and sustainable forest management, *Trees, Forests and People, 18*, 100731. https://doi.org/10.1016/j.tfp.2024.100731

Marion, J.L., Leung, Y.F., Eagleston, H., Burroughs, K. (2016). A review and synthesis of recreation ecology research findings on visitor impacts to wildness and protected natural areas. *Journal of Forestry – Washington, 114*, 352–362. https://doi.org/10.5849/jof.15-498

Marshall, A. R., Platts, P. J., Chazdon, R.L., Seki, H., Campbell, M.J., Phillips, O.L., Gereau, R.E., Marchant, R., Liang, J., Herbohn, J., Malhi, Y., Pfeifer, M. (2020). Conceptualizing the global forest response to Liana proliferation. *Frontiers in Forests and Global Change, 3*, 35. https://doi.org/10.3389/ffgc.2020.00035

Mayer, A. L. (2019). Family forest owners and landscape-scale interactions: A review. *Landscape and Urban Planning, 188*, 4 – 18.: https://doi.org/10.1016/j.landurbplan.2018.10.017.

Meter group. (2024). *NDVI (Normalized Difference Vegetation Index) and PRI (Photochemical Reflectance Index) - the researcher's complete guide*. https://metergroup.com/education-guides/ndvi-and-pri-the-researchers-complete-guide/

Meunier, F., Visser, M. D., Shiklomanov, A., Dietze, M.C., Guzmán Q, J.A., Sanchez-Azofeifa, G.A., De Deurwaerder, H.P.T., Krishna, S.M., Schnitzer, S.A., Marvin, D.C., Longo, M., Liu, C., Broadbent, E.N., Almeyda, Z.A.M., Muller-Landau, H.C., Detto, M, Verbeeck, H. (2021). Liana optical traits increase tropical forest albedo and reduce ecosystem productivity. *Global Change Biology*, *28*(1), 227–244. https://doi.org/10.1111/gcb.15928

MoE (2020a). *The National Red List - Conservation Status of the Flora of Sri Lanka*. Biodiversity Secretariat, Ministry of Environment and the Department of National Botanic Gardens.

MoE (2020b). *Assessment of the Threat Status of the Freshwater Fishes of Sri Lanka.* Biodiversity Secretariat, Ministry of Environment

MoE (2021). *The National Red list-conservation status of the birds of Sri Lanka,* Biodiversity Secretariat, Ministry of Environment

MoFE (1998). *Biodiversity Conservation in Sri Lanka: A Framework for Action*. Ministry of Forestry and Environment, Sri Lanka.

Neth, S., Babu, K. Dar, A., Parthasarathy, N. (2022). Increasing liana biomass and carbon stocks in tropical dry evergreen forests of Southern India. *Notulae Scientia Biologicae*, *14*(3), 11279. https://doi.org/10.55779/nsb14311279

Ng, C. K., Payne, J., Oram, F. (2021). Small habitat matrix: How does it work? *Ambio*. *50*(3), 601-614. https://10.1007/s13280-020-01384-y

Palihawadana, A. (2015). *Kodigahakanda Biodiversity New Report*

Panagopoulos, T. (2009). Linking Forestry, Sustainability and Aesthetics. *Ecological Economics, 68*, 2485-2489. https://doi.org/10.1016/j.ecolecon.2009.05.006

Pandapotan S. J., Sugianto, S., Darusman, D. (2016). Estimation of Carbon Stock stands using EVI and NDVI vegetation index in production forest of Lembah Seulawah Sub-district, Aceh Indonesia. *Aceh International Journal of Science and Technology, 5*(3), 126– 139. https://doi.org/10.13170/aijst.5.3.5836

R Core Team. (2012). *_R: A Language and Environment for Statistical Computing. R Foundation for Statistical Computing, Vienna, Austria*. https://www.R-project.org/

Rahmat, A., Hamid, M. A., Zaki, M. K. & Mutolib, A. (2018). Normalized difference vegetation index (NDVI) in the integration conservation education forest at Wan Abdul Rachman using modis data. *Indonesian* J. *Sci. Technol, 3*, 47–52. https://doi.org/10.17509/ijost.v3i1.10798

Rolston H. & Coufal J. H. (*1991*). Forest Ethic and Multivalue Forest Management *Journal* of *Forestry, 89*(4), 35-40. https://doi.org/10.1093/jof/89.4.35

Sarkar, D., & Haldar, A. (2005). *Physical and chemical methods in soil analysis: Fundamental concepts of analytical chemistry and instrumental techniques*. New Age International.

Schnitzer, S. A., & Bongers, F. (2011). Increasing liana abundance and biomass in tropical forests: emerging patterns and putative mechanisms. *Ecol. Lett., 14,* 397–406. https://doi.org/10.1111/j.1461-0248.2011.01590.x

SLTDA. (2020). *Annual Report of Sri Lanka Tourism Development Fund. Tourism Development Agency, Sri Lanka*. https://www.sltda.gov.lk/en/annual-report.

Sumanapala, D. & Wolf, I. D. (2020). Think globally, act locally: Current understanding and future directions for nature-based tourism research in Sri Lanka, *Journal of Hospitality and Tourism Management, 45*, 295-308. https://doi.org/10.1016/j.jhtm.2020.08.009

Toledo-Aceves, T. & Swaine, M. D. (2007). Above & below-ground competition between the liana *Acacia kameruensis* and tree seedlings in contrasting light environments. *Plant Ecology, 196*, 233-244. https://doi.org/10.1007/s11258-007-9347-0

Van der Heijden, G.M., Schnitzer, S.A., Powers, J.S., Phillips, O.L. (2013) Liana impacts on carbon cycling, storage and sequestration in tropical forests. *Biotropica, 45*, 682–692. https://doi.org/10.1111/btp.12060

Visser, M.D., Wright, S.J., Muller-Landau, H.C., Jongejans, E. (2018). Tree species vary widely in their tolerance for liana infestation: a case study of differential host response to generalist parasites. *J. Ecol, 106*, 781–794. https://doi.org/10.1111/1365-2745.12815

Weier & Herring (2000). Measuring vegetation (NDVI & EVI). *NASA Earth Observatory*. https://earthobservatory.nasa.gov/features/MeasuringVegetation

Wickramasinghe. K. (2013). Ecotourism as a tool for sustainable forest management in Sri Lanka. *Journal of Environmental Professionals Sri Lanka, 1*(2), 16-29. http://dx.doi.org/10.4038/jepsl.v1i2.5145

Wohl, E., Lane, S.N., Wilcox, A.C. (2015). The Science and Practice of River Restoration. *Water Resources Research, 51*(8), 5974–97. https://doi.org/10.1002/2014WR016874

Supplementary information attached seperately.

J.Natn.Sci.Foundation Sri Lanka 2025 53 (4): 403 - 420
DOI: http://dx.doi.org/10.4038/jnsfsr.v53i4.12748

RESEARCH ARTICLE

Crop Science

Changes in crop productivity and the harvested area of rice grown in Sri Lanka over the last four decades (1979-2021) as affected by the season, district, and water management system

SS Wijesooriya[1], HMKC Nawarathna[1], SS Kumari[1], A Sooriyarachchi[2], JMAK Jayaweera[3], C Perera[4] and LDB Suriyagoda[1*]

[1] *Department of Crop Science, Faculty of Agriculture, University of Peradeniya, Peradeniya, Sri Lanka.*
[2] *Socio Economic and Planning Centre, Department of Agriculture, Peradeniya, Sri Lanka.*
[3] *Mahaweli Authority of Sri Lanka, Colombo 10, Sri Lanka.*
[4] *Natural Recourses Management Centre, Department of Agriculture, University of Peradeniya, Peradeniya, Sri Lanka.*

Submitted: 21 July 2025; Revised: 05 November 2025; Accepted: 25 November 2025

Abstract: In Sri Lanka, rice (*Oryza sativa* L.) is cultivated during two seasons, known as *Yala* and *Maha*, across 25 districts either with or without access to irrigation water. However, variations in crop productivity and harvested extent in the last few decades remain unknown, particularly in relation to the district, season and water management systems (minor and major irrigation schemes, and rainfed). In this context, we conducted this study to determine the changes in rice crop productivity and harvested extent during the last forty years, and how they are affected by the season, district and water management systems. The relevant data for the period from 1979 to 2021 were obtained from the Department of Agriculture. Results revealed that rice crop productivity remained unchanged or increased with time for all the districts, seasons and water management systems, except for Galle where productivity declined under the major irrigation scheme during *Yala*. The harvested extent increased over the years for most districts, seasons and water management systems with a few exceptions. These exceptions were rainfed and minor irrigated paddy lands in the wet zone districts. Development and adoption of new improved varieties, better agronomic and management practices, use of modern technology and effective extension services have contributed to productivity improvement. In order to secure the harvested extent for the future, district, season and water management method-based recommendations are required apart from the common policies applicable at the national level.

Keywords: Districts, irrigation, seasons, water sources, rice productivity, Maha, Yala, Sri Lanka

INTRODUCTION

Rice (*Oryza sativa* L.) is the staple food for most Sri Lankans (Amarasingha et al., 2017) and with an increasing population the demand for rice is also rising. To fulfill the market demand, rice production must be increased (Kekulandara et al., 2019; Suriyagoda, 2022). Rice cultivation in Sri Lanka is dependent on the rainfall received from the two monsoons and two inter-monsoons. The two main cultivation seasons in Sri Lanka are *Yala* and *Maha* and the cultivated extents in these seasons are determined by the amount and distribution of rainfall (Amarasingha et al., 2017).

Rice is cultivated in all districts of Sri Lanka, except at elevations above 1200 m from mean sea level (Amarasingha et al., 2014). Therefore, a large diversity exists in the rice cultivation systems. Rice is grown either as a supplementary irrigated or rain-fed crop (Amarasingha et al., 2014). This is determined by the amount and distribution of rainfall during the cropping season, and the availability of reservoirs and canal systems to store and distribute excess water from rainfall for cultivation.

Although rice has been cultivated for a long period in Sri Lanka, no detailed studies have been conducted

* Corresponding author (lalith.suriyagoda@agri.pdn.ac.lk; https://orcid.org/0000-0002-5253-2717)

This article is published under the Creative Commons CC-BY-ND License (http://creativecommons.org/licenses/by-nd/4.0/). This license permits use, distribution and reproduction, commercial and non-commercial, provided that the original work is properly cited and is not changed in anyway.

to examine changes in crop productivity (kg ha^{-1}) and harvested extent (ha) over time. Due to pressure on paddy lands for alternate land uses, pest and disease incidences and reduced productivity, the extent of cultivation may have reduced in some districts. In contrast, crop productivity may also have increased over the years due to the introduction of new agricultural techniques, varieties, awareness programs and expansion of irrigation schemes. Changes in crop productivity and cultivated extent could also be affected by the cultivation season, district and irrigation water availability. This information is vital to understand and implement administrative and agronomic decisions for the sustainable management of the rice sector in Sri Lanka. Therefore, this study was conducted to determine the changes in rice crop productivity and cultivated extent over the last forty years, and the effect of the two seasons, districts and water management system used. Our hypothesis is that crop productivity and cultivation extent have not changed over the years, and were not affected by the season, district and water management system used.

MATERIALS AND METHODS

Seasonal rice crop productivity (kg ha^{-1}) and harvested extent (ha) data for all 25 districts for the *Yala* and *Maha* seasons, and for major, minor, and rainfed irrigation systems in Sri Lanka were obtained for the period 1979 to 2021 from the Socio Economic and Planning Centre of the Department of Agriculture, Sri Lanka. The number of years of rice crop productivity and harvested extent data available for this study, including different districts, seasons and water management systems are presented in Tables S1 and S2.

After compiling, the data was screened, tested for outliers, and descriptive statistics were generated. Average crop productivity in each district, season and water management system was calculated by calculating the arithmetic average over the years. Then, the effects of districts, seasons, water management systems and their interactions on average crop productivity were tested using the ANOVA (PROC GLM) procedure (Table S3). Since the higher order interactions were significant, average crop productivity among districts within each season and water management system was compared. Means were compared using the LSMEANS procedure. A similar approach was adopted to compare the differences in harvested extents among districts, seasons and water management systems. Changes in crop productivity and harvested extent over time, from 1979 to 2021, for each district, season and water management system were examined through simple linear regression analysis (PROC REG). The productivity among districts was compared using the average of the last five years (2017-2021). The last five-year average was considered to avoid any bias in average calculation as it changed over the years. The level of significance of all statistical tests was set at α=0.05.

RESULTS AND DISCUSSION

Variation in crop productivity

Statistical significance of the district, season, water management system and their interactions on the variation of average rice crop productivity as determined by the ANOVA is shown in Table S3. All the main effects and two-way interactions of the variables considered affected crop productivity (p<0.05). The overall model explained 48% of the total variability of crop productivity (Table S3).

Statistical significance of the simple linear regression analysis between rice crop productivity and time (i.e., years) for each district, season and water management system is given in Table 1. Crop productivity has increased over the years from 1979 to 2021 for most districts, seasons and water management systems (Table 1). In Kalutara, Matale, Matara, Mullaitivu, Puttalam, and Ratnapura districts, crop productivity has increased over the years, irrespective of the season and water management system. For other districts, seasons, and water management systems, rice crop productivity has either increased or remained unchanged over the years. However, crop productivity has declined in the Galle district under major irrigation schemes during the *Yala* season.

Developing new improved varieties with higher yield potential, widespread adoption of new improved varieties to replace traditional rice varieties, minimizing the gap between potential and actual yield of already released varieties through better agronomic and management practices, use of modern technology and effective extension services have contributed to the productivity improvement during this period (Dhanapala, 1999; Suresh et al., 2021).

Table 1: Statistical significance of the changes in rice crop productivity from 1979 to 2021, for different districts, water management systems and seasons in Sri Lanka. The symbols +, −, NS and NA indicate an increase, decrease, unchanged productivity over the years or data not available, respectively.

District	Major		Minor		Rainfed	
	Yala	***Maha***	***Yala***	***Maha***	***Yala***	***Maha***
Ampara	(+)***	(+)***	(+)***	(+)*	NS	NS
Anuradhapura	(+)***	(+)***	(+)***	(+)***	NS	(+)***
Badulla	(+)***	NS	(+)*	NS	NS	(+)*
Batticaloa	(+)***	(+)*	(+)**	NS	(+)*	(+)*
Colombo	NS	NS	(+)***	(+)***	(+)***	(+)***
Galle	(−)*	NS	(+)*	(+)*	(+)***	(+)***
Gampaha	(+)**	(+)*	NS	(+)*	(+)*	(+)***
Hambantota	(+)***	(+)***	(+)***	(+)***	NS	(+)***
Jaffna	NS	NS	NA	NA	NA	(+)**
Kalutara	(+)***	(+)***	(+)***	(+)***	(+)***	(+)***
Kandy	(+)***	(+)***	NS	NS	(+)*	(+)*
Kegalle	NA	NA	NS	(+)***	NS	(+)**
Kilinochchi	NS	(+)**	NS	(+)**	NS	(+)***
Kurunegala	(+)***	(+)**	(+)***	(+)***	NS	(+)***
Mannar	NS	(+)*	(+)*	(+)***	NS	NS
Matale	(+)***	(+)***	(+)***	(+)***	(+)***	(+)*
Matara	(+)***	(+)***	(+)***	(+)***	(+)***	(+)***
Moneragala	(+)***	(+)***	(+)***	(+)***	NS	(+)***
Mullativu	(+)***	(+)**	(+)**	(+)*	(+)*	(+)***
Nuwaraeliya	(+)***	NS	NS	NS	NS	(+)*
Polonnaruwa	(+)***	(+)**	(+)***	(+)***	NS	(+)*
Puttalam	(+)***	(+)***	(+)***	(+)***	(+)*	(+)***
Ratnapura	(+)***	(+)***	(+)***	(+)***	(+)***	(+)***
Trincomalee	(+)***	(+)***	(+)***	(+)***	NS	(+)***
Vavuniya	(+)***	(+)***	(+)**	(+)***	NS	(+)***
Sri Lanka	(+)***	(+)***	(+)**	(+)***	(+)***	(+)***

Note: * $p < 0.05$, ** $p < 0.01$, ***, $p < 0.001$

In Sri Lanka, rice breeding programs were aimed at developing varieties that are adapted to local field conditions while reaching higher crop productivity (Suriyagoda, 2022). As a result, over 100 new improved rice varieties have been released by the Department of Agriculture with acceptable productivity and grain quality characteristics. Additionally, with the initiation of the *Mahaweli* Development Project in 1961, the number of irrigation systems and the extent of paddy lands that could be irrigated have increased. This has ensured the availability of irrigation water to cultivate more paddy lands over the years and contributed to minimize the gap between actual and expected yield. Along with this, seasonal planning meetings and pre-season meetings were mandated by the Irrigation Act to ensure effective water management, and adopt collective decisions made

at those meetings on other agronomic practices (Salman et al., 2022). Comprehensive extension and farmer training programs conducted by the Department of Agriculture over the years have improved the knowledge and technical efficiency of farmers (Athukorala, 2017). As a result, mechanization was introduced to reduce the cost of production and improve the efficiency of field practices (Ayoob & Fowsar, 2020). Fertilizer subsidy schemes operated by the government from time to time ensured proper nutrient management of the rice crop. Additionally, location-specific fertilizer guidelines are available for improving nutrient-use efficiency (Sandika & Dushani, 2009). All these interventions have collectively contributed to substantial increases in the productivity of rice over the years.

During the *Maha* season, as indicated by the slope of the relationship between crop productivity and the year, rice crop productivity increased by 28.3, 23.1 and 23.3 kg ha^{-1} yr^{-1} from 1979-2021 for major irrigation, minor irrigation and rainfed systems, respectively (Table 2). In the *Yala* season, rice crop productivity increased by 37.4, 28.1 and 25.2 kg ha^{-1} yr^{-1} for major irrigation, minor irrigation and rainfed systems, respectively (Table 3). Moreover, this productivity increment of major irrigation systems was significantly higher than that of minor irrigation and rainfed systems during both seasons ($p < 0.05$).

Table 2: Simple linear regression models explaining the relationships between rice crop productivity (y-kg ha^{-1}) and the year of cultivation (x-1971-2021) for different districts and water management systems during the *Maha* season

District	Major irrigation	R^2	Minor irrigation	R^2	Rainfed	R^2
Ampara	y = 35.1x - 65823	0.41	y = 20.4x - 37454	0.11	NS	NS
Anuradhapura	y = 32.7x - 60859	0.37	y = 40.5x - 77227	0.48	y = 35.1x - 66975	0.35
Badulla	NS	NS	NS	NS	y = 19.7x - 36293	0.13
Batticaloa	y = 13.9x - 24800	0.09	NS	NS	y = 11.1x - 19627	0.05
Colombo	NS	NS	y = 27.8x - 52644	0.33	y = 12.8x - 22523	0.21
Galle	NS	NS	y = 29.4x - 55835	0.21	y = 34.3x - 65681	0.62
Gampaha	y = 10.2x - 17070	0.05	y = 16.5x - 29893	0.11	y = 17.7x - 32236	0.39
Hambantota	y = 47.6x - 90319	0.55	y = 51.2x - 98500	0.48	y = 36.7x - 70235	0.49
Jaffna	NS	NS	NA	NA	y = 28.6x - 55019	0.31
Kalutara	y = 36.1x - 69249	0.51	y = 25.2x - 47623	0.51	y = 27.3x - 51874	0.55
Kandy	y = 34.4x - 64464	0.36	NS	NS	y = 11.1x - 19167	0.11
Kegalle	NA	DNA	y = 13.6x - 23518	0.27	y = 16.5x - 29474	0.24
Kilinochchi	y = 23.5x - 43723	0.16	y = 49.1x - 95724	0.33	y = 47.6x - 92654	0.37
Kurunegala	y = 19.4x - 34588	0.17	y = 26.3x - 49106	0.42	y = 22.8x - 42349	0.42
Mannar	y = 27.8x - 51610	0.17	y = 46.1x - 88980	0.33	NS	NS
Matale	y = 26.7x - 49120	0.31	y = 26.3x - 48949	0.33	y = 19.5x - 35480	0.18
Matara	y = 36.9x - 70224	0.55	y = 34.7x - 66093	0.55	y = 36.9x - 70682	0.65
Monaragala	y = 39.5x - 74771	0.44	y = 33.6x - 63759	0.52	y = 27.1x - 51194	0.41
Mullaitivu	y = 33x - 62812	0.26	y = 35.1x - 67441	0.24	y = 37.5x - 72540	0.41
Nuwara Eliya	NS	NS	NS	NS	y = 24.9x - 46553	0.25
Polonnaruwa	y = 15.9x - 27253	0.11	y = 31.9x - 59848	0.27	y = 11.4x - 19140	0.05
Puttalam	y = 47.5x - 91531	0.55	y = 44.7x - 86458	0.62	y = 54.1x - 105210	0.76
Ratnapura	y = 34.1x - 63634	0.41	y = 26.5x - 49945	0.41	y = 26.9x - 51128	0.50
Trincomalee	y = 36.7x - 69525	0.44	y = 46.2x - 89380	0.45	y = 40.7x - 78532	0.48
Vavuniya	y = 50.5x - 97574	0.52	y = 56.2x - 109115	0.37	y = 54.9x - 106759	0.44
Sri Lanka	y = 28.3x - 52457	0.43	y = 23.1x - 52732	0.55	y = 23.2x - 43478	0.58

Note: NS- Not significant, NA- Data not available

Table 3: Simple linear regression models explaining the relationships between rice crop productivity (y-kg ha^{-1}) and the year of cultivation (x-1971-2021) for different districts and water management systems during the *Yala* season

District	Major irrigation	R^2	Minor irrigation	R^2	Rainfed	R^2
Ampara	y = 29.1x - 53687	0.54	y = 32.1x - 60102	0.42	NS	NS
Anuradhapura	y = 51.1x - 98175	0.71	y = 43.8x - 84100	0.65	NS	NS
Badulla	y = 65.2x - 126375	0.74	y = 22.1x - 40463	0.26	NS	NS
Batticaloa	y = 25.3x - 46952	0.37	y = 32.7x - 62011	0.33	y = 22.6x - 41602	0.15
Colombo	NS	NS	y = 35.5x - 68491	0.39	y = 18.7x - 34883	0.29
Galle	y = (-104.3)x + 213303	0.62	y = 23.8x - 44976	0.16	y = 35.3x - 68178	0.75
Gampaha	y = 20.8x - 38395	0.19	NS	NS	y = 10.5x - 18223	0.09
Hambantota	y = 48.6x - 92594	0.65	y = 51.7x - 99716	0.61	NS	NS
Jaffna	NS	NS	DNA	DNA	NA	DNA
Kalutara	y = 36.8x - 71303	0.52	y = 24.4x - 46323	0.51	y = 31.1x - 59543	0.75
Kandy	y = 26.8x - 49622	0.24	NS	NS	y = 13.4x - 24055	0.14
Kegalle	NA	DNA	NS	NS	NS	NS
Kilinochchi	NS	NS	NS	NS	NS	NS
Kurunegala	y = 37.9x - 71867	0.58	y = 25.5x - 47898	0.37	NS	NS
Mannar	NS	NS	y = 53.9x - 104927	0.33	NS	NS
Matale	y = 62.8x - 121895	0.83	y = 33.2x - 62947	0.54	y = 26.7x - 50566	0.43
Matara	y = 38.7x - 73915	0.59	y = 26.9x - 50882	0.51	y = 35.2x - 67674	0.69
Monaragala	y = 52.4x - 100910	0.64	y = 34.6x - 66103	0.44	NS	NS
Mullaitivu	y = 38.5x - 73560	0.45	y = 39.8x - 76391	0.41	y = 163.1x - 323758	0.89
Nuwara Eliya	y = 10.9x - 18028	0.02	NS	NS	NS	NS
Polonnaruwa	y = 42.7x - 80966	0.74	y = 57.4x - 110914	0.74	NS	NS
Puttalam	y = 48.1x - 92393	0.66	y = 43.5x - 84233	0.57	y = 24.2x - 45465	0.16
Ratnapura	y = 36.1x - 68139	0.34	y = 27.8x - 52484	0.52	y = 24.4x - 46286	0.61
Trincomalee	y = 43.5x - 82900	0.75	y = 44.1x - 84487	0.64	NS	NS
Vavuniya	y = 50.8x - 97644	0.53	y = 47.9x - 92141	0.42	NS	NS
Sri Lanka	y = 37.4x - 70715	0.77	y = 28.1x - 42892	0.27	y = 25.2x - 47666	0.71

Note: NS- Not significant, NA- Data not available

Productivity can be lower during the *Maha* season than in the Y*ala* season due to cloud cover (Jiang et al., 2021). Additionally, the *Yala* season benefits from longer daylight hours, which correlate with increased photosynthesis and crop growth, leading to higher productivity compared to the *Maha* season (Marikar et al., 1992; Suriyagoda et al., 2022). Occasionally, the *Maha* season is more productive due to higher rainfall, while the *Yala* season's production often suffers from irregular weather patterns and lower water availability, leading to reliance on irrigation. Therefore, it is important to identify the strategies that can be used to uplift productivity in both seasons.

Productivity improvement data showed that large-scale irrigation infrastructure played a key role in improving rice production. Under major irrigation schemes, water is issued according to a prescheduled rotation, and channel systems are better equipped than minor irrigation systems. Therefore, crop productivity is enhanced through efficient water management practices, including storing, regulating and distributing the right amount of water at the right time. The Irrigation Department ensures this by conducting pre-seasonal and seasonal planning, scheduling, and coordinating water allocations. This could be a possible reason for higher productivity and productivity increment in major irrigation schemes.

Water management in minor irrigation schemes is based on different types of delivery mechanisms and faces several limitations. Continuous delivery, only practiced in the wet zone, depends on constant rainfall. Rotational delivery ensures fair water distribution but requires full canal flow and careful scheduling. Intermittent delivery helps conserve water but relies heavily on rainfall and frequent adjustments to meet demand. Demand-based delivery is effective in water-scarce regions but is labor-intensive, requiring frequent soil moisture monitoring and precise planning (Salman et al., 2022). Due to these limitations, managing water efficiently in minor irrigation systems is challenging and can cause a reduction in productivity compared to major irrigation systems.

Rainfed systems face limitations due to their reliance on unpredictable and uneven rainfall. Seasonal dependence on monsoons makes crops vulnerable to droughts, delayed rains, and water scarcity during critical growth stages. Farmers have limited control over water availability, resulting in lower productivity compared to irrigated systems (Yoshino & Suppiah, 1984). In this context the possibilities of using rainwater harvesting systems, drought-resistant varieties, and improved soil management need to be explored.

Rainfed systems were more vulnerable during *Yala* than *Maha*. During *Yala* only 12 districts showed significant gains in productivity compared to 23 districts during *Maha*. This highlights the vulnerability of rainfed agriculture to seasonal variability and underscores the need for targeted interventions, such as improved irrigation infrastructure and rainwater harvesting systems (Amarasinghe et al., 2021). Water availability is a critical determinant of productivity, with the *Maha* season benefiting from the North-East monsoon rains. Bridging the productivity gap between the two seasons requires addressing water scarcity during *Yala*.

When comparing districts during the *Maha* season the productivity improvement ranged from 10.2 to 50.5, 13.6 to 56.2 and 11.1 to 54.9 kg ha^{-1} yr^{-1} under major irrigation, minor irrigation and rainfed systems, respectively (Table 2). When comparing districts during the *Yala* season the productivity varied from 104.3 to 65.2, 22.1 to 57.4 and 13.4 to 163.1 kg ha^{-1} yr^{-1} under major irrigation, minor irrigation, and rainfed systems, respectively (Table 3). A decrease in rice crop productivity of 104.3 kg ha^{-1} yr^{-1} was observed in the Galle district under the major irrigation system during *Yala* (Table 3).

The average rice crop productivity in the *Maha* season from 2017 to 2021 under major irrigation schemes ranged from 3,215 to 5,771 kg ha^{-1} with the highest in Hambantota, followed by Monaragala, Ratnapura, Kurunegala, Anuradhapura, Kandy, Polonnaruwa, Matale, Ampara, Badulla, Trincomalee and Mannar districts (Table S4). The average rice crop productivity under minor irrigation schemes ranged from of 3,072 to 5,058 kg ha^{-1} with the highest in Hambantota, followed by Polonnaruwa, Mullaitivu, Matale, Vavuniya, Anuradhapura, Monaragala, Badulla, Kegalle, Ratnapura, Puttalam and Kurunegala districts (Table S4). The average rice crop productivity under rainfed systems ranged from 3,030 to 4,369 kg ha^{-1} with the highest in Matale, followed by Kegalle, Vavuniya, Nuwara-Eliya, Kurunegala, Polonnaruwa, Anuradhapura, Hambantota, Puttalam, Gampaha, Matara, Kandy, Kilinochchi, Mullaitivu, Badulla, Kalutara, Ampara, Galle, Monaragala, Colombo and Ratnapura districts (Table S4).

The average rice crop productivity in the *Yala* season from 2017 to 2021 under major irrigation schemes ranged from 2,583 to 6,107 kg ha^{-1} with the highest in Hambantota, followed by Vavuniya, Polonnaruwa, Mannar and Trincomalee districts (Table S5). The average rice crop productivity under minor irrigation schemes ranged from 2,822 to 4,989 kg ha^{-1} with the highest in Polonnaruwa, followed by Hambantota, Vavuniya, Trincomalee, Ampara, Mullaitivu, Batticaloa, Badulla, Matale, Monaragala, Anuradhapura and Kilinochchi districts (Table S5). The average rice crop productivity under rainfed systems ranged from 2,700 to 4,092 kg ha^{-1} with the highest in Ampara, followed by Batticaloa, Trincomalee, Matale, Puttalam, Badulla, Anuradhapura, Kurunegala, Kandy, Matara, Hambantota, Polonnaruwa, Kalutara, Vavuniya, Kegalle and Ratnapura districts (Table S5). Despite the improved rice crop productivity over the last few decades, the variation of soil and climate among districts, and the lack of equitable distribution of resources and attention to marginalized areas have exacerbated the productivity disparity between districts.

Variation in the harvested extent

Statistical significance of the district, season, water management system and their interactions on the variation of harvested rice extent as determined by the ANOVA is shown in Table S6. All main effects and interactions of the variables considered affected the extent of harvested rice ($p < 0.05$). Overall, the model explained 94% of the total variability of the harvested rice extent (Table S6).

The statistical significance of the simple linear regression analysis between the harvested extent of the rice crop and the year of cultivation for each district,

season and water management system is given in Table 4. Most districts, seasons and water management systems have shown an increase in the harvested extent over the years from 1979 to 2021 (Table 4). However, the harvested extent has declined over the years in both seasons and under all three water management systems in the Kalutara district, both minor irrigated and rainfed systems in Kandy, Kegalle, Matara and Ratnapura districts, rainfed systems in Trincomalee and Vavuniya districts, and major irrigation systems in Gampaha and Kalutara districts.

Table 4: Statistical significance of the changes in the harvested extent of rice from 1979 to 2021, for different districts, water management systems and seasons in Sri Lanka. The symbols +, −, NS and NA indicate an increase, decrease, unchanged productivity over the years or data not available, respectively.

District	Major		Minor		Rainfed	
	Yala	*Maha*	*Yala*	*Maha*	*Yala*	*Maha*
Ampara	(+)***	(+)***	(+)***	(+)***	(+)*	(+)***
Anuradhapura	(+)***	(+)**	(+)***	(+)***	NS	(+)**
Badulla	(+)***	(+)***	(+)***	(+)***	NS	(+)***
Batticaloa	(+)***	(+)***	(+)***	(+)***	(+)*	(+)***
Colombo	(+)*	(+)*	NS	(+)**	(-)***	(+)*
Galle	NS	(+)*	(+)*	(+)***	(-)***	(+)*
Gampaha	NS	(-)*	(+)*	(+)*	(-)***	(-)*
Hambantota	(+)***	(+)***	(+)***	(+)***	(+)*	(+)***
Jaffna	NS	NS	NA	NS	NA	NS
Kalutara	(-)***	(-)***	(-)***	(-)*	(-)***	(-)***
Kandy	NS	NS	(-)***	(-)***	(-)***	NS
Kegalle	NA	NA	(-)***	(-)***	(-)***	NS
Kilinochchi	NS	NS	NS	(+)***	NA	NS
Kurunegala	NS	(+)**	(+)**	NS	NS	(+)**
Mannar	(+)***	NS	(+)*	NS	NS	NS
Matale	(+)***	(+)***	NS	NS	NS	(+)***
Matara	NS	NS	(-)*	(-)***	(-)***	NS
Moneragala	(+)***	(+)***	(+)***	(+)***	(+)**	(+)***
Mullativu	(+)**	(+)**	(+)**	(+)**	NS	(+)**
Nuwaraeliya	NS	NS	(-)***	(-)***	NS	NS
Polonnaruwa	(+)***	(+)***	(+)***	(+)***	NS	(+)***
Puttalam	(+)***	(+)***	(+)***	(+)*	(+)***	(-)***
Ratnapura	(+)***	(+)**	(-)***	(-)***	(-)***	(+)**
Trincomalee	(+)***	(+)**	(+)***	(+)***	NS	(-)**
Vavuniya	(+)*	NS	(+)*	(+)*	(-)***	NS
Sri Lanka	(+)***	(+)***	(+)***	(+)**	(-)***	(-)***

Note: *; $p < 0.05$, **; $p < 0.01$, ***; $p < 0.001$

During the *Maha* season, as indicated by the trend in the relationship between harvested extent and year of cultivation from 1979 to 2021, the harvested extent of paddy has increased by 3,269 under major irrigation and 1,464 ha yr^{-1} under minor irrigation systems, while decreasing by 166 ha yr^{-1} under rainfed systems

(Table 5). Moreover, the expansion of the harvested area under major irrigation areas was significantly higher than that in rainfed areas ($p<0.05$). In the *Yala* season, the harvested extent of paddy has increased by 3,758 under major irrigation and 1,227 ha yr^{-1} under minor irrigation systems, but decreased by 1,264 ha yr^{-1} under rainfed systems (Table 6). Additionally, the expansion of the harvested area in major irrigation areas was significantly higher than in minor irrigation and rainfed areas ($p<0.05$).

Table 5: Simple linear regression models explaining the relationships between harvested extent of rice (y-ha) and time (x-1971-2021) for different districts and water management systems during the *Maha* season

District	Major irrigation	R^2	Minor irrigation	R^2	Rainfed	R^2
Ampara	y = 700.8x - 60263	0.73	y = 70.1x - 138187	0.30	y = 165.2x - 323800	0.27
Anuradhapura	y = 426.1x - 826654	0.24	y = 606.3x - 42657	0.27	y = 227.6x - 451244	0.42
Badulla	y = 94.9x - 180492	0.43	y = 43.4x - 78128	0.28	y = 87.8x - 172747	0.45
Batticaloa	y = 269.1x - 524030	0.42	y = 64.7x - 127945	0.54	y = 369.3x - 716009	0.23
Colombo	y = 5.9x - 11833	0.29	y = 12.7x - 24738	0.17	y = (-120.4) x + 245101	0.90
Galle	y = 11.1x - 22183	0.44	y = 24.2x - 48098	0.39	y = (-285.1) x + 585892	0.79
Gampaha	y = (-10.7) x + 22938	0.08	y = 26.3x - 50582	0.14	y = (-198.2x + 405050	0.90
Hambantota	y = 276.7x - 536022	0.51	y = 51.2x - 98646	0.33	y = 0.95x - 672.22	0.12
Jaffna	NS	NS	NS	NS	NS	NS
Kalutara	y = (-10.5) x + 21406	0.75	y = (-16.2) x + 34635	0.16	y = (-192.5) x + 398183	0.89
Kandy	NS	NS	y = (-113.1) x + 23264	0.82	NS	NS
Kegalle	NA	DNA	y = -17.8x + 37868	0.31	NS	NS
Kilinochchi	NS	NS	y = 9.6x - 18965	0.50	NS	S
Kurunegala	y = 103.5x - 194974	0.27	NS	NS	y = (-76.6) x + 177510	0.02
Mannar	y = 94.2x - 180383	0.07	NS	NS	NS	NS
Matale	y = 79.1x - 152975	0.80	NS	NS	y = 37.6x - 72022	0.23
Matara	NS	NS	y = (-21.1) x + 45438	0.28	NS	NS
Monaragala	y = 141.9x - 278351	0.73	y = 182.8x - 359932	0.75	y = 286.6x - 567311	0.52
Mullaitivu	y = 64.7x - 125869	0.22	y = 39.1x - 76180	0.21	y = (-11.1) x + 25175	0.06
Nuwara Eliya	NS	NS	y = (-41.3) x + 87268	0.42	NS	NS
Polonnaruwa	y = 798.6x - 22645	0.86	y = 114.8x - 226905	0.44	y = 7.2x - 13138	0.02
Puttalam	y = 92.6x - 180805	0.39	y = 72.3x - 138292	0.15	y = (-7.4) x + 16243	0.02
Ratnapura	y = 32.1x - 62321	0.28	y = (-73.1) x + 153364	0.66	y = (-87.5) x + 179565	0.85
Trincomalee	y = 148.6x - 283201	0.27	y = 111.7x - 219921	0.45	y = 10.5x - 15121	0.002
Vavuniya	NS	NS	y = 99.2x - 192782	0.14	NS	NS
Sri Lanka	y = 3269.1x - 66236	0.78	y = 1464.5x - 32306	0.26	y = (-165.6)x + 495183	0.04

Note: NS- Not significant, NA- Data not available

Table 6: Simple linear regression models explaining the relationships between harvested extent of rice (y-ha) and time (x-1971-2021) for different districts and water management systems during the *Yala* season

District	Major irrigation	R^2	Minor irrigation	R^2	Rainfed	R^2
Ampara	y = 658.4x - 15616	0.59	y = 45.6x - 90068	0.83	y = 11.3x - 22422	0.17
Anuradhapura	y = 395.6x - 778455	0.36	y = 367.2x - 727908	0.39	NS	NS
Badulla	y = 97.6x - 188548	0.38	y = 28.4x - 53623	0.36	NS	NS
Batticaloa	y = 342x - 670746	0.64	y = 89.4x - 177503	0.72	y = 19.8x - 38816	0.13
Colombo	y = 4.7x - 9542.1	0.25	NS	NS	y = (-98.2) x + 198765	0.55
Galle	y = 7.8x - 15812	0.12	y = 11.2x - 22329	0.18	y = (-359.4) x + 729950	0.62
Gampaha	y = 6.3x - 11835	0.02	y = 22.4x - 43871	0.13	y = (-149.2) x + 302479	0.43
Hambantota	y = 340.3x - 665810	0.64	y = 73.1x - 143613	0.61	y = 8.9x - 17143	0.14
Jaffna	NS	NS	NA	NA	NA	DNA
Kalutara	y = (-7.7) x + 15769	0.54	y = (-22.8) x + 47420	0.29	y = (-223.5) x + 457063	0.72
Kandy	NS	NS	y = (-86.7) x + 17724	0.69	y = (-123.4) x + 250208	0.711
Kegalle	NA	DNA	y = (-27.8) x + 57577	0.36	y = (-150.3) x + 306226	0.70
Kilinochchi	NS	NS	NS	NS	NA	DNA
Kurunegala	NS	NS	y = 324.7x - 634127	0.23	NS	NS
Mannar	y = 30.3x - 60033	0.47	y = 12.6x - 25110	0.19	NS	NS
Matale	y = 97.8x - 192916	0.62	NS	NS	NS	NS
Matara	NS	NS	y = (-13.7) x + 30514	0.10	y = (-147.7) x + 303731	0.71
Monaragala	y = 161.9x - 320200	0.77	y = 131.3x - 260073	0.66	y = 16.5x - 32676	0.25
Mullaitivu	y = 58.7x - 115835	0.30	y = 19.8x - 39299	0.26	NS	NS
Nuwara Eliya	NS	NS	y = (-27.9) x + 58028	0.27	NS	NS
Polonnaruwa	y = 818.5x - 25646	0.72	y = 113.3x - 224715	0.59	NS	NS
Puttalam	y = 126.5x - 249702	0.52	y = 126.8x - 250837	0.43	y = 14.3x - 28356	0.34
Ratnapura	y = 30.5x - 59208	0.36	y = (-88.7) x + 18360	0.68	NS	NS
Trincomalee	y = 198.2x - 385393	0.34	y = 77.2x - 153321	0.54	y = 7.3x - 14505	0.23
Vavuniya	y = 19.5x - 38404	0.14	y = 33.3x - 66090	0.17	y = (-0.2) x + 496.76	0.15
Sri Lanka	y = 3757.9x - 74566	0.68	y = 1226.6x - 26596	0.36	y = (-1264.3) x + 34676	0.49

Note: NS- Not significant, NA- Data not available

Positive slopes in Table 5 and 6 for the extent of paddy harvested and major and minor irrigation systems, during *Yala* and *Maha* seasons indicate the expansion of cultivation under irrigation over the last forty years. However, the extent of rainfed paddy declined during both *Yala* and *Maha* seasons with a higher reduction in *Yala*. These disparities in the trends of harvested extent among irrigation systems highlight the critical role of water management in sustaining rice cultivation. Major irrigation systems were the most promising out of the three water management methods, supported by the North-East monsoon rains, initiation of the *Mahaweli* development project, renovation of large reservoirs, and irrigation schemes in drought-prone regions (Amarasingha et al., 2014). In contrast, minor irrigation systems showed moderate growth, constrained by the maintenance of infrastructure and water losses in unlined canals (Jayasiri et al., 2024). Rehabilitating underutilized rainfed rice fields and improving minor irrigation systems in the dry and intermediate zones could contribute to a more balanced and resilient agricultural landscape in those regions (Pokharel, 2024). The contrasting trends between irrigated and rainfed systems also highlight the inequities in resource access. Additionally, increasing climate variability has threatened the stability of rainfed systems more than the irrigated systems (Withanachchi et al., 2014).

During *Maha*, the rate of area expansion by districts ranged between 10.7 and 798.6 ha yr^{-1} for major irrigation, 113.1 and 606.3 ha yr^{-1} for minor irrigation, and 285.1 and 369.3 ha yr^{-1} for rainfed systems (Table 5). During *Yala*, the rate of district wise area expansion ranged between 7.7 and 818.5 ha yr^{-1} under major irrigation, 88.7 and 367.2 ha yr^{-1} under minor irrigation, and 359.4 and 19.8 ha yr^{-1} under rainfed systems (Table 6). The harvested extent of rice in 9 districts (out of 25 districts) increased significantly under the rainfed system during the *Maha* season whereas only 5 districts increased their harvested extent under the rainfed system during the *Yala* season.

Many districts in the dry zone have shown a consistent increase in the extent of paddy harvested during the last forty years, driven by land availability and government-led settlement programs (Mohamed & Naseer, 2005). These gains are largely attributed to investments in large-scale irrigation infrastructure, such as the *Mahaweli* development program, and settlement schemes in the Dry Zone. Moreover, supplementary irrigation has buffered against rainfall variability, leading to an increase in the harvested extent (Mahaweli Authority, 2018).

The decline in the harvested extent during *Yala* and *Maha* seasons under rainfed and minor irrigation schemes in most of the wet zone districts highlights the vulnerability of those systems to erratic rainfall, inadequate availability of irrigation water, and soil degradation (Chandrasiri et al., 2023). Weak or delayed monsoon rains and increased frequency of droughts or floods negatively influenced the area of paddy sown in rainfed systems (De Silva et al., 2007). Additionally, land fragmentation, urbanization and weak policy enforcement have led to a significant decline in the cultivated extents, as paddy fields are converted for industrial and residential purposes (De Silva et al., 2007; De Silva & Yamao, 2010). Moreover, some of the paddy lands are converted to cash crops such as other field crops and leafy vegetables. This transformation is particularly evident in highland regions, where economic incentives prioritize commercial crops over traditional paddy farming (Brow & Weeramunda, 1993; Sirisena & Suriyagoda, 2018). Despite these regional disparities, the overall harvested extent remained relatively stable, reflecting resilience in land-use for rice cultivation (Sandika & Dushani, 2009; DCS, 2021). Our results show that the stability of the paddy extent in the country was largely and positively contributed by the extent under major irrigation schemes in the dry zone districts, while minor irrigation schemes and rainfed systems in the wet zone districts contributed negatively.

The average harvested extent of paddy in the *Maha* season from 2017 to 2021 under major irrigation schemes ranged from 118 to 59,937 ha, with the highest in the Ampara district (Table S7). The harvested extent under minor irrigation schemes ranged from of 501 to 35,382 ha, with the highest in the Anuradhapura district (Table S7). Similarly, the harvested extent under rainfed system ranged from 14 to 33,949 ha, with the highest in the Batticaloa district (Table S7).

The average harvested extent of paddy in the *Yala* season from 2017 to 2021 under major irrigation schemes ranged from 102 to 52,154 ha, with the highest in Polonnaruwa and Ampara districts (Table S8). The harvested extent under minor irrigation schemes ranged from 89 to 18,046 ha, with the highest in the Kurunegala district (Table S8). Similarly, the harvested extent under rainfed system ranged from 2 to 13,467 ha, with the highest in the Kurunegala district (Table S8).

Policy interventions are necessary to expand the harvested extent of rice cultivation in Sri Lanka. Strict land-use regulations and investments in irrigation can enhance the harvested extent. Additionally, strengthening irrigation maintenance in irrigated systems and promoting drought-resistant varieties in rainfed areas are crucial steps. Effective water management practices, especially in minor irrigation tank systems such as alternate wetting and drying compared to continuous flooding, are essential to enhance resilience against rainfall variability and stabilize the extent of rice cultivation (Amarasingha et al., 2014, 2017; Chandrasiri et al., 2020). These approaches would contribute to securing the extent of paddy cultivated in Sri Lanka.

CONCLUSION

During the last 43 years (1979 to 2021), rice crop productivity (kg ha^{-1}) varied among districts, seasons and water management methods. On average, national rice crop productivity in major irrigation, minor irrigation and rainfed-systems increased by 28.3, 23.1, and 23.2 kg ha^{-1} yr^{-1} during the *Maha* season and by 37.4, 28.1, and 25.2 kg ha^{-1} yr^{-1} during *Yala* season , respectively. Similarly, the harvested area for major irrigation, minor irrigation and rainfed systems changed by 3,269, 1,464, and -165.6 ha yr^{-1} during the *Maha* season and, by 3,757, 1,226, and -1,264 ha yr^{-1} during the *Yala* season respectively. To ensure enhancement of rice crop productivity and secure the harvested extent in the future, district, season and water management method-based recommendations are required, in addition to common policies applicable at the national level.

REFERENCES

Amarasingha, R.P.R.K., Galagedara, L.W., Marambe, B., Silva, G.L.L.P., Punyawardena, R., Nidumolu, U., Howden, M., &Suriyagoda, L.D.B. (2014). Aligning sowing dates with the onset of rains to improve rice yields and water productivity: modelling rice (*Oryzasativa* L.) yield of the *Maha* season in the dry zone of Sri Lanka. *Tropical Agricultural Research, 25*, 277-286. https://doi.org/10.4038/tar.v25i3.8038

Amarasingha, R.P.R.K., Suriyagoda, L.D.B., Marambe, B., Rathnayake, W.M.U.K., Gaydon, D.S., Galagedara, L.W., Punyawardena, R., Silva, G.L.L.P., Nidumolu, U., & Howden, M. (2017). Improving water productivity in moisture-limited rice-based cropping systems through incorporation of maize and mungbean: a modelling approach. *Agricultural Water Management, 189*, 111-122. https://doi.org/10.1016/j.agwat.2017.05.002

Amarasinghe, U. A., Amarnath, G., Alahacoon, N., Aheeyar, M., Ghosh, S., Chandrasekharan, K., &Nakada, T. (2021). Adaptation to Climate Variability in Sri Lanka: A Case Study of the Huruluwewa Irrigation System in the Dry Zone (Vol. 200). International Water Management Institute, IWMI, Colombo, Sri Lanka. https://doi.org/10.5337/2021.229

Athukorala, W. (2017). Identifying the role of agricultural extension services in improving technical efficiency in the paddy farming sector in Sri Lanka. *Sri Lanka Journal of Economic Research, 5*, 63-77. https://doi.org/10.4038/sljer.v5i1.58

Ayoob, S.M., & Mohamed Fowsar, M.A. (2020). Invasion of paddy combine harvester (PCH) and its socioeconomic impacts: a study based on Ampara District, Sri Lanka. *Academic Journal of Interdisciplinary Studies, 9*, 138-146. https://doi.org/10.36941/ajis-2020-0092

Brow, J., &Weeramunda, J. (1993). Agrarian change in Sri Lanka, *The Journal of Asian Studies, 52*, 1049-1050. https://doi.org/10.2307/2059406

Chandrasiri, C.K., Tsusaka, T.W., Zulfiqar, F., &Datta, A. (2023). Impact of climate change on paddy crop failure under different water regimes in Sri Lanka. *Singapore Journal of Tropical Geography, 44*, 86-413. https://doi.org/10.1111/sjtg.12495

Chandrasiri, S., Galagedara, L., &Mowjood, M. (2020). Impacts of rainfall variability on paddy production: A case from Bayawa minor irrigation tank in Sri Lanka. *Paddy and Water Environment, 18*, 443-454. https://doi.org/10.1007/s10333-020-00793-9

De Silva, C. S., Weatherhead, E. K., Knox, J. W., & Rodriguez-Diaz, J. A. (2007). Predicting the impacts of climate change-A case study of paddy irrigation water requirements in Sri Lanka. *Agricultural Water Management, 93*, 19-29. https://doi.org/10.1016/j.agwat.2007.06.003

De Silva, D. A. M., &Yamao, M. (2010). Urbanization and its impact on paddy land in Sri Lanka: A case study of Colombo and Gampaha districts. *Journal of Land Use Policy, 27*, 123-130. https://doi.org/10.1016/j.landusepol.2009.07.003

DCS (2021). Paddy Statistics. Department of Census and Statistics (2021) Available at: https://www.statistics.gov.lk/Agriculture/StaticalInformation/PaddyStatistics (Accessed: 01.03.2025).

Dhanapala, M. P. (1999). *Bridging the rice yield gap in Sri Lanka*. Food and Agriculture Organization of the United Nations. FAO Home

Jayasiri, M.M.J.G.C.N., Dayawansa, N.D.K., Ingold, K., &Yadav, S. (2024). Are rice systems sustainable in Sri Lanka?-A case of DeduruOya reservoir irrigation scheme. *Environmental Impact Assessment Review, 106*, 107503. https://doi.org/10.1016/j.eiar.2024.107503

Jiang, R., Sanchez-Azofeifa, A., Laakso, K., Xu, Y., Zhou, Z., Luo, X., Huang, J., Chen, X., &Zang, Y. (2021). Cloud cover throughout all the paddy rice fields in Guangdong, China: Impacts on Sentinel 2 MSI and Landsat 8 OLI optical observations. *Remote Sensing, 13*, 2961. https://doi.org/10.3390/rs13152961

Kekulandara, D.S., Sirisena, D.N., Bandaranayake, P.C.G., Samarasinghe, G., Wissuwa, M., &Suriyagoda, L.D.B. (2019). Variation in grain yield, and nitrogen, phosphorus and potassium nutrition of irrigated rice cultivars grown at fertile and low-fertile soils. *Plant and Soil, 434*, 107-123. https://doi.org/10.1007/s11104-018-3663-0

Mahaweli Authority (2018). Annual Report 2018. Mahaweli Authority, Colombo, Sri Lanka. Available at: https://mahaweli.gov.lk/PDF/document/Annual%20Report%202018%20-%20English.pdf (Accessed: [01.03.2025]).

Marikar, F., Wilkin-Wells, J., Smolnik, S., &Sampath, R.K. (1992). Irrigation system performance and its impact on crop productivity in Sri Lanka. *International Journal of Water Resources Development, 8*, 226-234. https://doi.org/10.1080/07900629208722559

Mohamed, A.R., &Naseer, A.A. (2005). Trends in paddy production in Sri Lanka. *Journal of Management, 3*, 26-33.

Pokharel, A. (2024). Beyond collective action problems: perceived fairness and sustained cooperation in farmer managed irrigation systems in Nepal. Oxford University Press. https://doi.org/10.1093/oso/9780197755792.001.0001

Salman, M., Suzuki, H., Ahmad, W., Giusti, S., Ali, A., Rathnayake, W.M.U.K., Sirisena, D.N., et al., (2022). Efficient Agricultural Water Use and Management in Paddy Fields in Sri Lanka - National outlook. Rome: FAO.

Sandika, A. L., &Dushani, S. N. (2009). Growth performance of rice sector: The present scenario in Sri Lanka. *Tropical Agricultural Research and Extension, 12*, 71-76. https://doi.org/10.4038/tare.v12i2.2793

Sirisena, D., &Suriyagoda, L.D.B. (2018). Toward sustainable phosphorus management in Sri Lankan rice and vegetable-based cropping systems: A review. *Agriculture and Natural Resources, 52*, 9-15. https://doi.org/10.1016/j.anres.2018.03.004

Suresh, K., Wilson, C., Khanal, U., Managi, S., & Santhirakumar, S. (2021). How productive are rice farmers in Sri Lanka? The impact of resource accessibility, seed sources and varietal diversification. *Heliyon, 7*, e07398. https://doi.org/10.1016/j.heliyon.2021.e07398

Suriyagoda, L. B. D. (2022). Rice production in nutrient-limited

soils: Strategies for improving crop productivity and land sustainability. *Journal of the National Science Foundation of Sri Lanka, 50*, 521-539. https://doi.org/10.4038/jnsfsr.v50i3.10601

Suriyagoda, L., Illangakoon, T., Wijerathna, S., Devasinghe, U. (2022). Degree-day requirement for heading and maturity of three most popular rice varieties in Sri Lanka as influenced by location and season. *Ceylon Journal of Science. 51*, 229-245. https://doi.org/10.4038/cjs.v51i3.8031

Withanachchi, S.S., Köpke, S., Withanachchi, C.R., Pathiranage, R., &Ploeger, A. (2014). Water resource management in dry zonal paddy cultivation in Mahaweli River Basin, Sri Lanka: An analysis of spatial and temporal climate change impacts and traditional knowledge. *Climate, 2*, 329-354. https://doi.org/10.3390/cli2040329

Yoshino, M.M., &Suppiah, R. (1984). Rainfall and paddy production in Sri Lanka. *Journal of Agricultural Meteorology, 40*, 9-20. https://doi.org/10.2480/agrmet.40.9

Supplementary Data

Table S1: Data available (number of years) on rice crop productivity (kg ha^{-1}) under each district, season and major water source used for rice cultivation

District	Major irrigation		Minor irrigation		Rainfed	
	Yala	*Maha*	*Yala*	*Maha*	*Yala*	*Maha*
Ampara	42	43	42	43	23	43
Anuradhapura	43	43	43	43	16	41
Badulla	43	43	43	43	20	43
Batticaloa	41	42	40	41	40	42
Colombo	26	26	42	43	43	43
Galle	9	11	42	35	43	43
Gampaha	43	43	43	43	43	43
Hambantota	43	43	43	43	43	43
Jaffna	4	6	NA	NA	NA	38
Kalutara	43	43	43	43	43	43
Kandy	43	43	43	43	43	43
Kegalle	NA	NA	43	43	43	43
Kilinochchi	26	30	20	23	NA	30
Kurunegala	43	43	43	43	43	43
Mannar	30	36	22	35	2	24
Matale	43	42	43	43	43	43
Matara	43	43	43	43	43	43
Monaragala	42	43	43	43	27	43
Mullaitivu	32	34	32	34	5	33
Nuwara Eliya	42	41	43	43	24	43
Polonnaruwa	43	43	43	43	4	43
Puttalam	42	43	43	43	38	43
Ratnapura	42	43	43	43	43	43
Trincomalee	33	33	30	32	6	33
Vavuniya	31	37	28	38	6	33
Sri Lanka	43	43	43	43	43	43

NA- Data not available

Table S2: Data available (number of years) on rice crop harvested (ha) extent under each district, season and major water source used for rice cultivation

District	Major irrigation		Minor irrigation		Rainfed	
	Yala	*Maha*	*Yala*	Location	*Yala*	*Maha*
Ampara	42	43	42	43	30	43
Anuradhapura	43	43	43	43	22	42
Badulla	43	43	43	43	34	43
Batticaloa	41	42	40	42	40	42
Colombo	26	26	43	43	43	43
Galle	9	11	43	43	43	43
Gampaha	43	43	43	43	43	43
Hambantota	43	43	43	43	43	43
Jaffna	5	6	NA	6	NA	41
Kalutara	41	41	43	43	43	43
Kandy	43	43	43	43	43	43
Kegalle	NA	NA	43	43	43	43
Kilinochchi	30	30	26	29	NA	30
Kurunegala	43	43	43	43	43	43
Mannar	37	41	32	41	5	31
Matale	43	43	43	43	43	43
Matara	43	43	43	43	43	43
Monaragala	43	43	43	43	38	43
Mullaitivu	40	40	40	40	6	39
Nuwara Eliya	43	43	43	43	35	43
Polonnaruwa	43	43	42	43	9	43
Puttalam	43	43	43	43	40	43
Ratnapura	42	43	43	43	43	43
Trincomalee	41	41	37	41	11	41
Vavuniya	39	41	37	41	9	38
Sri Lanka	43	43	43	43	43	43

Note: NA- Data not available

Table S3: Statistical significance of the variables considered when determining rice crop productivity from 1979 to 2021 in Sri Lanka

Source of variability	*df*	F value	Pr > F
Overall model	153	32.49	<.0001
District	27	57.98	<.0001
Season	1	34.44	<.0001
Water mgt.	2	471.88	<.0001
District×Season	27	14.42	<.0001
District×Water mgt.	48	9.3	<.0001
Season×Water mgt.	2	0.71	0.4915
District×Season×Water mgt.	46	1.18	0.1895
Error	5472		
Corrected Total	5625		
R-Square	*Coefficient of Variation*	*Root Mean Square Error*	*Productivity Mean*
0.48	*18.7*	*654.6*	*3496.9*

Table S4: Rice crop productivity (kg ha-1) in different districts under various water management systems in the Maha season during 2017-2021

Major irrigation District	Mean ±Std Error	Minor irrigation District	Mean ± Std Error	Rainfed District	Mean ± Std Error
Hambantota	5771± 475^{a}	Hambantota	5058±510^{a}	Matale	4369±351^{a}
Monaragala	5273±496^{ab}	Polonnaruwa	4989±197^{ab}	Kegalle	4283±236^{a}
Ratnapura	5123±345^{abc}	Mullaitivu	4399±320^{abc}	Vavuniya	4071±573^{ab}
Kurunegala	5027±425^{abcd}	Matale	4337±114^{abcd}	Nuwara Eliya	4001±64^{abc}
Anuradhapura	5001±538^{abcde}	Vavuniya	4306±555^{abcd}	Kurunegala	3977±194^{abc}
Kandy	4788±456^{abcdef}	Anuradhapura	4249±448^{abcd}	Polonnaruwa	3849±387^{abc}
Polonnaruwa	4770±402^{abcdef}	Monaragala	4194±198^{abcd}	Anuradhapura	3822±385^{abc}
Matale	4649±459^{abcdefg}	Badulla	4143±198^{abcd}	Hambantota	3720±258^{abcd}
Ampara	4631±402^{abcdefg}	Kegalle	4094±193^{abcd}	Puttalam	3684±286^{abcd}
Badulla	4499±432^{abcdef}	Ratnapura	3796±331^{abcd}	Gampaha	3646±188^{abcd}
Trincomalee	4421±309^{abcdefg}	Puttalam	3787±478^{abcd}	Matara	3617±303^{abcd}
Mannar	4392±432^{abcdefg}	Kurunegala	3758±261^{abcd}	Kandy	3556±283^{abcd}
Vavuniya	4319±498^{bcdefg}	Mannar	3720±372^{bcd}	Kilinochchi	3455±408^{abcd}
Matara	4259±296^{cdefg}	Gampaha	3632±275^{bcd}	Mullaitivu	3443±410^{abcd}
Nuwara Eliya	4104±226^{cdefg}	Nuwara Eliya	3616±238^{bcd}	Badulla	3380±392^{abcd}
Mullaitivu	3994±537^{defg}	Kilinochchi	3576±300^{bcd}	Kalutara	3362±204^{abcd}
Puttalam	3977±423^{defg}	Ampara	3533±316^{bcd}	Ampara	3359±402^{abcd}
Kilinochchi	3944±305^{defg}	Trincomalee	3532±373^{bcd}	Galle	3291±256^{abcd}
Colombo	3586±98^{efg}	Kandy	3519±157^{bcd}	Monaragala	3286±304^{abcd}
Kalutara	3559±134^{fg}	Matara	3428±132^{bcd}	Colombo	3278±195^{abcd}
Galle	3499±255^{fg}	Kalutara	3277±234^{cd}	Ratnapura	3231±277^{abcd}
Batticaloa	3221±354^{g}	Colombo	3206±248^{cd}	Trincomalee	3054±332^{cd}
Gampaha	3215±460^{g}	Galle	3072± 255^{d}	Mannar	3030±81^{d}

Means followed by the same letter within each column are not significantly different at $p < 0.05$.

Table S5: Rice crop productivity (kg ha^{-1}) in different districts under various water management systems in the *Yala* season from 2017 to 2021

Major irrigation District	Mean ±Std Error	Minor irrigation District	Mean ± Std Error	Rainfed District	Mean ± Std Error
Hambantota	6107±180^{a}	Polonnaruwa	4989±197^{a}	Ampara	4092±301^{a}
Vavuniya	5340±366^{ab}	Hambantota	4859±186^{a}	Batticaloa	4066±457^{ab}
Polonnaruwa	5253±112^{abc}	Vavuniya	4749±371^{ab}	Trincomalee	3860±729^{abc}
Mannar	5219±163^{abc}	Trincomalee	4504±244^{abc}	Matale	3710±189^{abcd}
Trincomalee	5177±100^{abc}	Ampara	4441±196^{abc}	Puttalam	3703±378^{abcd}
Monaragala	5140±372^{bc}	Mullaitivu	4399±320^{abc}	Badulla	3624±543^{abcd}
Badulla	5111±121^{bcd}	Batticaloa	4378±222^{abc}	Anuradhapura	3615±213^{abcd}
Matale	5049±199^{cde}	Badulla	4346±239^{abcd}	Kurunegala	3499±166^{abcd}
Anuradhapura	5033±247^{cde}	Matale	4337±114^{abcd}	Kandy	3372±227^{abcd}
Ampara	4965±194^{cde}	Monaragala	4194±198^{abcde}	Matara	3366±71^{abcd}
Kurunegala	4899±97^{cde}	Anuradhapura	4173±306^{abcde}	Hambantota	3318±130^{abcd}
Ratnapura	4834±509^{cde}	Kilinochchi	3862±542^{abcdef}	Polonnaruwa	3316±461^{abcd}
Kilinochchi	4770±228^{cde}	Puttalam	3861±465^{bcdef}	Kalutara	3131±98^{abcd}
Puttalam	4657±305^{cde}	Ratnapura	3841±138^{bcdef}	Vavuniya	3124±85^{abcd}
Mullaitivu	4612±418^{cde}	Kurunegala	3758±261^{cdef}	Kegalle	3091±156^{abcd}
Nuwara Eliya	4338±604^{cdef}	Mannar	3720±372^{cdefg}	Ratnapura	3074±92^{abcd}
Kandy	4327±559^{cdef}	Nuwara Eliya	3616±238^{cdefg}	Gampaha	3042±256^{bcd}
Batticaloa	4062±264^{def}	Matara	3428±132^{defg}	Galle	2890±127^{cd}
Matara	3993±192^{ef}	Colombo	3333±277^{efg}	Colombo	2876±156^{cd}
Gampaha	3592±172^{fg}	Kegalle	3199±182^{fg}	Monaragala	2732±156^{d}
Kalutara	3024±272^{gh}	Kandy	3187±121^{fg}	Nuwara Eliya	2700±165^{d}
Colombo	2901±179^{gh}	Kalutara	2992±84^{fg}		
Galle	2583±121^{h}	Gampaha	2943±173^{fg}		
		Galle	2822±252^{g}		

Means followed by the same letter within each column are not significantly different at $p < 0.05$.

Table S6: Statistical significance of the variables considered when determining the harvested extent of rice crop during the period from 1979-2021 in Sri Lanka

Source of variability	*df*	F Value	Pr > F
Overall model	156	555.88	<.0001
District	27	2429.3	<.0001
Season	1	391.43	<.0001
Water mgt.	2	441.97	<.0001
District×Season	27	178.4	<.0001
District×Water mgt.	50	257.62	<.0001
Season×Water mgt.	2	5.8	0.003
District×Season×Water mgt.	47	6.29	<.0001
Error	5866		
Corrected Total	6022		
R-Square	*Coefficient of Variation*	*Root Mean Square Error*	*Productivity Mean*
0.94	*69.2*	8707.5	12578.5

Table S7: Harvested extent of rice crop (ha) in different districts under various water management systems in the Maha season from 2017 to 2021

Major irrigation		Minor irrigation		Rainfed	
District	Mean ±Std Error	District	Mean ±Std Error	District	Mean ±Std Error
Ampara	59937±619^{a}	Anuradhapura	35382±8837^{a}	Batticaloa	33949±4374^{a}
Polonnaruwa	53465±2898^{b}	Kurunegala	26303±6581^{b}	Kurunegala	19791±4483^{b}
Anuradhapura	38850±8964^{c}	Monaragala	9063±1079^{c}	Kilinochchi	12199±1861^{c}
Hambantota	25993±2105^{d}	Vavuniya	8961±1982^{c}	Ampara	11934±1453^{c}
Batticaloa	21894±1291^{d}	Badulla	8885±546^{c}	Monaragala	10327±2354^{cd}
Trincomalee	19460±1092de	Puttalam	7218±1962^{cd}	Kalutara	8728±461^{cde}
Kurunegala	14648±2003^{ef}	Polonnaruwa	6693±399^{cd}	Trincomalee	8643±2009^{cde}
Mannar	14457±844^{ef}	Trincomalee	6449±971^{cd}	Anuradhapura	8083±2645^{cde}
Kilinochchi	11352±419^{fg}	Matale	6226±954^{cd}	Jaffna	7806±1562^{cdef}
Badulla	9503±913^{fgh}	Hambantota	5161±524^{cd}	Galle	7627±526^{cdefg}
Monaragala	7884±590^{fghi}	Ratnapura	5035±273^{cd}	Matara	5670±217^{defgh}
Matale	6627±522^{ghi}	Kandy	4618±279^{cd}	Gampaha	4965±670^{defgh}
Mullaitivu	6191±808^{ghi}	Ampara	3817±582^{cd}	Mullaitivu	4357±1175^{efgh}
Puttalam	5815±1189^{ghi}	Mannar	3663±262^{cd}	Badulla	4204±740^{efgh}
Kandy	4092±139^{ghi}	Batticaloa	3484±227^{cd}	Kegalle	3510±599^{efgh}
Matara	3886±134^{ghi}	Mullaitivu	3359±577^{cd}	Matale	3379±694^{efgh}
Vavuniya	3637±458^{hi}	Nuwara Eliya	3275±508^{cd}	Ratnapura	2328±224^{fgh}
Ratnapura	3164±490^{hi}	Gampaha	2949±316^{cd}	Colombo	2169±175^{gh}
Gampaha	1359±157^{i}	Matara	2949±89^{cd}	Polonnaruwa	1996±400^{h}
Nuwara Eliya	801±99^{i}	Kegalle	1507±209^{cd}	Kandy	1971±245^{h}
Colombo	246±50^{i}	Galle	1406±313^{cd}	Vavuniya	1496±497^{h}
Galle	162±26^{i}	Kalutara	1397±4^{cd}	Puttalam	1249±294^{h}
Kalutara	118±7^{i}	Colombo	650±49^{d}	Hambantota	1150±54^{h}
		Kilinochchi	501±50^{d}	Mannar	72±8^{h}
				Nuwara Eliya	14±4^{h}

Means followed by the same letter within each column are not significantly different at $p < 0.05$.

Table S8: Harvested extent of rice crop (ha) in different districts under various water management systems in the *Yala* season from 2017 to 2021

Major irrigation District	Mean ± Std Error	Minor irrigation District	Mean ± Std Error	Rainfed District	Mean ± Std Error
Polonnaruwa	52154±3979^{a}	Kurunegala	18046±4965^{a}	Kurunegala	13467±3367^{a}
Ampara	50871±3981^{a}	Anuradhapura	10467±3259^{b}	Kalutara	6272±1125^{b}
Hambantota	24172±2574^{b}	Monaragala	5541±574^{c}	Matara	5351±446^{bc}
Anuradhapura	21648±5995^{bc}	Polonnaruwa	5058±317^{cd}	Galle	5229±1209^{bc}
Batticaloa	20319±805^{bc}	Puttalam	4696±1560^{cde}	Gampaha	3097±776^{bcd}
Trincomalee	15849±2127^{cd}	Hambantota	4160±298^{cdef}	Kegalle	2907±658^{d}
Kurunegala	10854±1915de	Ratnapura	4140±396^{cdef}	Batticaloa	1660±296^{d}
Badulla	7210±531^{efg}	Batticaloa	3983±342^{cdef}	Kandy	1418±329^{d}
Monaragala	7014±432^{efg}	Badulla	3598±179^{cdef}	Ratnapura	1274±336^{d}
Kilinochchi	6325±2128^{efg}	Trincomalee	2930±580^{cdef}	Colombo	1235±344^{d}
Puttalam	5069±1222^{efg}	Matara	2868±207^{cdef}	Hambantota	929±98^{d}
Matale	4506±698^{efg}	Matale	2646±633^{cdef}	Puttalam	630±164^{d}
Matara	3742±261^{fg}	Kandy	2438±320^{cdef}	Monaragala	531±116^{d}
Kandy	3427±308^{fg}	Ampara	2048±159^{cdef}	Matale	422±123^{d}
Mullaitivu	3366±1005^{fg}	Gampaha	1993±472^{cdef}	Ampara	372±73^{d}
Ratnapura	3080±471^{fg}	Nuwara Eliya	1951±468^{cdef}	Trincomalee	263±146^{d}
Mannar	1296±381^{fg}	Kegalle	1148±237^{cdef}	Anuradhapura	261±89^{d}
Gampaha	1116±163^{fg}	Kalutara	1104±153^{cdef}	Badulla	27±83^{d}
Vavuniya	895±392^{g}	Vavuniya	1037±487^{def}	Vavuniya	4±1.1^{d}
Nuwara Eliya	468±101^{g}	Galle	829±316^{def}	Nuwara Eliya	3±1.1^{d}
Colombo	163±53^{g}	Mullaitivu	763±240^{def}	Polonnaruwa	3±1.5^{d}
Kalutara	125±16^{g}	Colombo	289±80^{ef}		
Galle	102±66^{g}	Mannar	163±121^{f}		
		Kilinochchi	89±12^{f}		

Means followed by the same letter within each column are not significantly different at $p< 0.05$.

J.Natn.Sci.Foundation Sri Lanka 2025 53 (4): 421- 436
DOI: http://dx.doi.org/10.4038/jnsfsr.v53i4.12573

RESEARCH ARTICLE

Environmental Microbiology

Faecal indicator bacteria and microbial source tracking as tools for testing water quality and sources of contamination of Rawan-Oya tributary of the Mahaweli River, in Sri Lanka

GK Kapukotuwa[1,2], CL Abayasekara[3], KC Weerakoon[4] and RS Rajakaruna[1,5*]

[1] *Postgraduate Institute of Science, University of Peradeniya, Peradeniya, Sri Lanka.*
[2] *Faculty of Fisheries and Protection of Waters, South Bohemian Research Center of Aquaculture and Biodiversity of Hydrocenoses, University of South Bohemia in Ceské Budejovice, Vodnany, Czech Republic.*
[3] *Department of Botany, Faculty of Science, University of Peradeniya, Peradeniya, Sri Lanka.*
[4] *Department of Zoology, Faculty of Natural Sciences, The Open University of Sri Lanka, Nugegoda, Sri Lanka.*
[5] *Department of Zoology, Faculty of Science, University of Peradeniya, Peradeniya, Sri Lanka.*

Submitted: 21 February 2025; Revised: 24 November 2025; Accepted: 04 January 2026

Abstract: Faecal indicator bacteria (FIB) are used to assess water quality, indicating potential contamination from faeces, while microbial source tracking (MST) identifies the specific source of that contamination. These are essential tools for assessing the level and source of faecal contamination in water, and this study evaluated faecal contamination in the Rawan-Oya tributary of the Mahaweli River, a crucial drinking water source in Sri Lanka, using these tools. Water samples were collected from nine sites representing forested (n = 19), agricultural (n = 38), rural (n = 38), semi-urban (n = 38), and urban (n = 38) areas. These samples were analysed for FIBs including total coliforms (TC), faecal coliforms (FC), *Escherichia coli*, and faecal streptococci (FS) using membrane filtration method. DNA markers were used in order to identify human and animal faecal contaminant sources. Results showed an increase in FIB concentrations from forested to urban areas, indicating increased numbers in urban areas compared to those in forested areas. TC concentration in water ranged from 2.7 × 10^2 to 1.6 × 10^5 CFU/100 mL. FC counts increased from 16 to 3.2×10^4 CFU/100 mL, and FS counts fluctuated between 5.4×10^2 and 6.2×10^3 CFU/100 mL. All samples tested positive for the universal FIB DNA marker. Microbial source tracking analysis using human- and cattle-specific *Bacteroides* markers indicated the highest levels of human faecal contamination in urban sites, while significant cattle faeces contamination was observed in both agricultural and urban areas. The microbial quality of water did not meet the drinking water standards (FC and TC, 0 CFU/100 mL) in any of the sites tested. However, the forested area met the recreational water standards (FC ≤ 235 CFU/100 mL). This study identifies the potential of using FIB and MST as a means of confirming the specific sources and locations of faecal contamination in water bodies, which is crucial for developing targeted water management strategies and for alerting local communities and authorities about the status of drinking water quality and factors that contribute towards the deterioration of the quality of water bodies.

Keywords: Faecal indicator bacteria, microbial source tracking, PCR, water quality, *Bacteroides*

INTRODUCTION

Faecal contamination from anthropogenic and zoogenic activities is a primary source of microbial pollution in natural waters; therefore, microbiological parameters are crucial in determining the quality of surface water. Faecal indicator bacteria (FIB) are used to assess the microbial quality and faecal contamination levels of water (Devane et al., 2020; Kostyla et al., 2015). They reveal the presence of intestinal pathogens, helping to prevent the spread of water-borne diseases. It has been shown that the presence of pathogens correlates well with the presence of faecal contamination (Leclerc et al., 2001), and as a result, modern drinking water testing relies on faecal bacteria as indicators of both faecal contamination and the possible presence of disease-causing organisms.

* Corresponding author (rupika.rajakaruna@sci.pdn.ac.lk; https://orcid.org/0000-0001-7939-947X)

This article is published under the Creative Commons CC-BY-ND License (http://creativecommons.org/licenses/by-nd/4.0/). This license permits use, distribution and reproduction, commercial and non-commercial, provided that the original work is properly cited and is not changed in anyway.

Faecal indicator bacteria are consistently found in the intestines and faeces of humans and animals, and their survival characteristics are similar to those of intestinal pathogens. They are easy to isolate and enumerate, making them effective indicators of pollution levels. Typically, FIB are non-pathogenic and do not multiply significantly once they leave the body and enter the water, making them reliable for assessing microbial contamination in aquatic environments (Fujioka et al., 2015; Goshu et al., 2021).

The most commonly used FIB includes total coliforms (TC), faecal coliforms (FC), *Escherichia coli* (*E. coli*), and faecal streptococci (FS). Total coliforms are widely distributed in nature and can be found in the intestines of both homeothermic and poikilothermic animals, as well as in the soil and animal manure. Faecal coliforms, a subgroup of TC, are more specific to faecal material from homeothermic animals, with *E. coli* being the most common member (Edberg et al., 2000; Devane et al., 2020). Faecal streptococci, which include enterococci and non-enterococci species, are considered superior to coliforms as pollution indicators due to their ability to grow at elevated temperatures and in bile broth, closely mimicking many pathogens (Boehm & Sassoubre, 2014; Raji et al., 2015; Devane et al., 2020). They are considered to be better in some cases due to their ability to survive under environmental stress.

Traditional methods for monitoring FIB contamination often fail to distinguish between human and animal sources (Toledo-Hernandez et al., 2013). The ratio of FC to FS can provide some indication of the source, but novel molecular-based microbial source tracking (MST) methods are more reliable (Hagedorn et al., 2011). These methods, which often utilize PCR assays targeting bacterial genomic DNA, do not require the culture of microbes, making them time- and cost-effective (Ebentier et al., 2013; Kapoor et al., 2015; Goshu et al., 2021). They are used to identify the sources of faecal contamination, such as human, animal, and bird waste (Hagedorn et al., 2011). Host-specific markers such as *Bacteroides* spp., *Faecalibacterium* spp., *E. coli* toxin genes, or human-associated viruses can be used to detect the source of faecal contamination (Bower et al., 2005). PCR assays targeting members of the order *Bacteroidales* are the most widely used faecal source identifiers in water (Ballesté & Blanch, 2010; Ahmed et al., 2016). These bacteria are obligate anaerobes and cannot multiply in the environment outside the host (Zheng et al., 2009; Zhang et al., 2020). Microbial source tracking (MST) is crucial for controlling water pollution, especially in environments affected by both point and non-point sources of faecal pollution (Garcia-Armisen & Servais, 2007; Frick et al., 2020; Goshu et al., 2021).

Faecal contamination of surface waters can vary with time of day, rainfall patterns, and other environmental factors (Kostyla et al., 2015). Coliform bacteria are prevalent in streams, particularly following rainfall when surface runoff is significant. However, stormwater can sometimes dilute coliform counts, especially if bacteria enter the stream primarily through point sources (Augustyn et al., 2016). During dry weather, coliform counts are more likely to be related to point source pollution, such as wastewater discharges. Moreover, FIB is interrelated with the physical and chemical parameters of the water (Augustyn et al., 2016; Bisimwa et al., 2022).

In developing countries, including Sri Lanka, freshwater resources are significantly affected by faecal pollution due to inadequate sanitary conditions (Kumar et al., 2019). Water quality deterioration from faecal contamination is a significant issue, with several studies revealing high levels of FIB contamination in major rivers like the Kelani (Kumar et al., 2020), Mahaweli (Liyanage et al., 2021), and Pussalla-Oya (Rajapakshe et al., 2008). However, most studies have focused on the main rivers rather than their tributaries. This study aims to fill that gap by examining FIB levels and tracking pollution sources in the Rawan-Oya tributary of the Mahaweli River, the primary source that provides drinking and household water for the nearby community, and a freshwater source that sustains local ecosystems and agricultural fields.

The main objective of this study is to examine TC, FC, and FS contamination along the Rawan-Oya tributary. Specific objectives include identifying differences in TC, FC, and FS levels across nine sampling sites representing forested, agricultural, rural, semi-urban, and urban habitats, as well as between dry and wet seasons. Additionally, the study aims to track faecal contamination sources using both culture-dependent FC-to-FS ratio methods and culture-independent genotypic MST methods. These observations will provide valuable insights for developing water quality management strategies for the Rawan-Oya tributary (Kolawole et al., 2011).

MATERIALS AND METHODS

Study site

The Rawan-Oya is a perennial stream and one of the major water sources of the Polgolla reservoir located in the Kandy District of the Central Province of Sri Lanka. Rawan-Oya begins from the Hunnasgiriya mountain (1,400 m), located in the Campbell's Lane Forest Reserve. The upper watershed area of the stream is covered with evergreen montane and sub-montane forest

cover. Thereafter, the stream flows through secondary forests, home gardens, agricultural lands, semi-urban and urban landscapes, and joins the Mahaweli River through the Polgolla reservoir at Polgolla, Kandy (longitude 80º 39 – 42' E and latitude 7º 19 – 23'N). Rawan-Oya is a 13.5 km long stream with a stream watershed area of 31.07 km^2. The mean annual daily temperature ranges between 22 – 27 °C, and the mean annual precipitation exceeds 2,000 mm in the watershed area of the tributary. The catchment boundaries and land-use types along the stream were identified using QGIS desktop 2.18.3 software and Google Maps (2017). Sample collection was conducted at nine sites along the stream, ranging from a pristine, forested upstream area to the downstream site near the end of the tributary (S1 to S9; Table 1), indicating the presence of human activities adjacent to the waterway (Figure 1).

Table 1: Description of the nine sampling sites along the Rawan-Oya tributary of Mahaweli River

Site ID	Land use classification	Coordinates (Latitude, Longitude)	Site description and anthropogenic activities
S1	Forested (Pristine reference site)	7°22'31"N, 80°42'20"E	Headwaters originating from Hunasgiriya Mountain (1400 m) within Campbell's Lane Forest Reserve. Covered by evergreen montane and submontane forest; minimal anthropogenic impact.
S2	Agricultural	7°21'23"N, 80°41'47"E	Dominated by paddy fields in the Udugoda village area. Potential source of microbial load from agricultural runoff.
S3	Rural	7°20'53"N, 80°41'31"E	Low population density. Landscape features include steep terrain, forest gardens, dense forest, and a waterfall.
S4	Semi-Urban	7°20'35"N, 80°41'05"E	Moderately populated residential area (Pitiyegedara). Characterized by moderate human density and some agricultural practices.
S5	Urban	7°20'41"N, 80°40'39"E	Highly residential and commercial area in Wattegama Town. Expected to receive high microbial input from domestic wastewater and commercial activities.
S6	Urban	7°19'41"N 80°40'26"E	Highly residential and commercial area in Madawala Town. High population density implies significant discharge of domestic and commercial waste.
S7	Rural	7°20'01"N, 80°39'28"E	Low population density with forest gardens as the predominant land use in the Megammana-Polgolla area.
S8	Agricultural	7°19'50"N, 80°39'18"E	Agricultural practices, including paddy fields, vegetable plantations, and animal husbandry (Polgolla area). High potential for contamination from animal and agricultural waste.
S9	Semi-Urban	7°19'35"N, 80°39'08"E	Moderately populated residential and commercial area in Polgolla, located close to the Polgolla Dam. Represents the final cumulative microbial load before the reservoir/dam area.

Sample collection

Water samples were collected monthly from June 2020 to March 2022 to evaluate the FIB contamination pattern during both dry and rainy seasons and to implement molecular-based tracking. Samples were collected into pre-sterilised glass sampling bottles (1000 mL) from a depth of about 20–30 cm below the water surface, against the direction of water flow. All samples were placed in an insulated box filled with ice packs and transported to the laboratory, and kept in a refrigerator at 4 °C. The analysis commenced within 24 h of collecting the first sample.

Tests for faecal indicator bacteria: total coliforms (TC), faecal coliforms (FC), and faecal streptococci (FS)

Enumeration of TC and FC was performed using the membrane filtration (MF) method, as described by APHA (1992) and Oshiro (2002). For each sample, several dilutions of the water samples were made, and duplicate plates were inoculated with each dilution to determine the number of specific bacteria present in the sample. Water samples from the forested area were filtered without dilution, and all other samples were subjected to

10^{-1}, 10^{-2}, and 10^{-3} dilutions, appropriate for each type of FIB to obtain a countable number of 20 to 200 colonies (Nnadozie & Harcourt, 2016). Samples were diluted with sterilised distilled water to a final volume of 100 ml. Each diluted sample was filtered through a sterilised 47 mm diameter cellulose nitrate membrane filter with a pore size of 0.45 µm (Sartorius, Germany). The filtration apparatus was sterilised using UV radiation before filtering each sample to prevent cross-contamination.

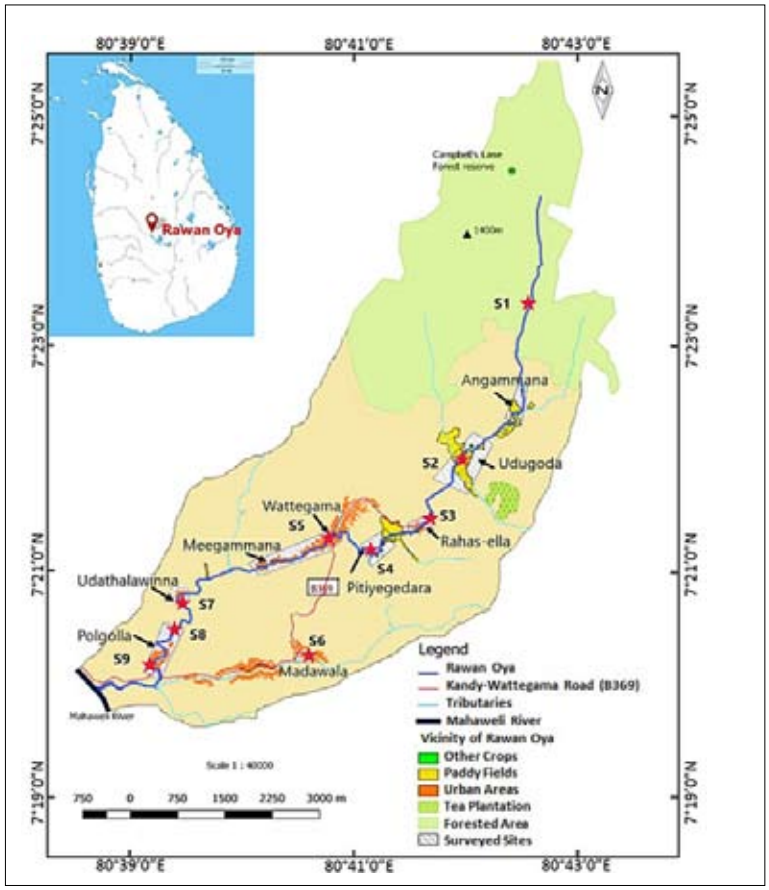

Figure 1: The location of the study site, Rawan-Oya tributary, the distribution of different land use patterns along the tributary, and the selected sampling sites (S1- Forested area, S2- Agricultural area, S3- Rural area, S4- Semi-urban area, S5 and S6- Urban area, S7- Rural area, S8- Agricultural area, and S9- Semi-urban area)

Membrane filters were aseptically placed on pre-sterilised Petri dishes with M-Endo agar LES (HiMedia, India) and M-FC agar (HiMedia, India). Plates with M-Endo agar and M-FC agar were incubated for 24 – 48 h at 35 ± 0.5 °C and at 44.5 ± 0.2 °C for the detection of TC and FC, respectively. Sterilised distilled water and standard culture of coliform (*Escherichia coli*: ATCC 25922) were used as negative and positive controls, respectively, in the detection of coliforms. Colonies with a typical red colour and a green metallic sheen on the M-Endo medium were counted as TC, while colonies with a typical blue colour on the M-FC medium were counted as FC. The concentrations of TC, FC, and FS were expressed as colony-forming units (CFU) per 100 mL. The CFU count from the membrane filter was divided by the volume of the original (undiluted) sample represented by the filtered volume to calculate the concentration. Given that the volume filtered for the diluted samples was 100 mL and the final concentration is expressed per 100 mL.

A confirmation test for coliforms was performed by inoculating colonies into brilliant green bile (BGB) (Oxoid, UK) broth tubes and incubated at 37 °C for 24 – 48 h. The formation of gas in the Durham tubes was considered a positive test for confirmed TC. Similarly, colonies isolated on M-FC medium were confirmed by inoculating into BGB broth tubes and incubated at 44.5 ºC for 24 – 48 h. The formation of gas in the Durham tubes was considered a positive FC test. Two or three drops from the positive BGB tubes were added to tryptone water tubes. Following incubation at 44.5 ºC for 24 h, 0.2 – 0.3 ml of Kovac's reagent was added to the culture. The immediate appearance of a red/pink colour ring in the upper layer was recorded as a positive indole reaction, confirming the presence of *E. coli.*

For the detection and enumeration of FS, an MF procedure similar to that used for the coliform test was followed with the filtration step. Subsequently, membrane filters were aseptically placed on pre-sterilised petri dishes with KF Streptococcus agar (Oxoid, UK). The plates were incubated for 48 h at 35 ± 0.5 °C. Sterilised distilled water and a standard culture of *Enterococcus faecalis* (ATCC 24212) were used as negative and positive controls, respectively, in the detection of FS. Pink to dark red colonies with yellow halos on the KF streptococcal medium were counted as FS. For FS confirmation, positive colonies were sub-cultured into tubes containing brain heart infusion (BHI) broth (Sinton et al., 1993). The formation of gas in the Durham tube and a cloudy broth at 37 ºC in BHI broth confirmed the presence of FS. A loop-full of inocula from the BHI broth were streaked on bile esculine agar (BEA) slants and incubated at 37 ºC for 24 h. The black colour formation of the slant confirmed the presence of FS.

Inference of faecal contamination source by the FC/FS ratio method

The ratio of FC to FS counts in water samples, from each of the sampling sites, was used to distinguish between faecal pollution of human and animal origin, as described previously.

The standard FC/FS ratios used were as follows (Table 2, Coyne & Howell, 1994):

The FC/FS ratio was calculated with the results obtained from the FC and FS tests.

Table 2: The standard FC/FS ratios for different sources of contamination

Source of contamination	FC/FS ratio
Human faeces	greater than 4.0.
Faeces of domesticated animals	between 0.1 and 4.0,
Faeces of wild animals	less than 0.1

Library independent molecular-based microbial source tracking tests

Faecal sample collection for microbial source tracking marker evaluation

To test the sensitivity and specificity of the MST markers used for the experiment, fresh faecal samples were collected from humans, cattle, and dogs from the same geographical area as the water sample collection. Faecal samples were collected in sterile containers, avoiding contact with soil and grass as much as possible. Samples were placed in an insulated box filled with ice packs, transported to the laboratory, and kept in a refrigerator at 4 °C. Each sample was processed individually by mixing 1 g of faecal material with 4.0 ml of nuclease-free water. The resulting slurry was stored at 4 °C for a minimum of 2 h and up to a maximum of 24 h prior to DNA extraction.

Water and faecal sample preparation and DNA extraction

The water samples were filtered in the laboratory using the filtration apparatus with a vacuum pump within 24 h of collecting the first sample. For the filtration, sterilised 47 mm diameter cellulose nitrate membrane filters with a 0.45 µm pore size (Sartorius, Germany) were used. Then, the membrane filters were transferred into sterile 15 mL plastic conical tubes using flame-sterilised tweezers. The tubes containing membrane filters were stored at -20 ºC until DNA extraction. In addition, DNA extracted from membrane filters and faecal slurry samples were prepared using the ReliaPrep™ g DNA Tissue Miniprep System (Promega, USA) following the manufacturer's instructions with minor modifications. For the PCR assay, 12 µL of the DNA product from each sample extraction was used. Four aliquots of 3 µL were combined with each forward and reverse primer, master mix (GO Taq Green

Master Mix, Promega, USA), and nuclease-free water to produce a final volume of 25 µL. Each sample was primed with a Bac32F, HF183F, and CF193F forward primer and a Bac708R reverse primer and an ED-1F forward, and an ED-1R reverse primer to amplify universal and human- and cattle-specific *Bacteroides* markers and a dog-specific *Faecalibacterium* marker, respectively. The specificities of the MST primers used for this study are depicted in Table 3. Thereafter, PCR amplifications were performed in an Applied Biosystems-Veriti Thermal Cycler under the following cycling conditions: one initial denaturation step at 95 °C, 1 min at the optimum annealing temperature (55 °C for Ba32F, HF183F, and CF193F and 64 °C for ED-1F), and 1 min at 72 °C. PCR products were visualised on a 1.5% agarose gel with ethidium bromide using a 50 bp DNA ladder (GeneRuler 50 bp DNA Ladder, Thermo Scientific, USA). The gel was visualised using the UV gel doc system (BioPrint, Vilber, France).

Table 3: Primers used for microbial source tracking and their respective sequences, annealing temperatures, and times

Target	Primer	Sequence (5′–3′)	Annealing temperature (°C)	Annealing time(s)
Universal	Bac32F	AAC-GCT-AGC-TAC-AGG-CTT	54	60
	Bac708R	CAA-TCG-GAG-TTC-TTC-GTG		
Human	HF183F	ATC-ATG-AGT-TCA-CAT-GTC-CG	55	60
	Bac708R	CAA-TCG-GAG-TTC-TTC-GTG		
Cattle	CF193F	TAT-GAA-AGC-TCC-GGC-C	55	30
	Bac708R	CAA-TCG-GAG-TTC-TTC-GTG		
Dog	ED-1F	CAGGCGGACTCTTAAGTC	64	60
	ED-1R	GCGATCGGAGTTCTTCAT		

(Source: Somnark et al., 2018; Zhang et al., 2020)

Faecal indicator bacteria and microbial Source tracking

The specificity and sensitivity of the MST markers were tested using faecal DNA extracts from local animals and humans. Sensitivity (r) and specificity (s) are defined as $r = a/(a + c)\times100$ and $s = d/(b + d)\times100$, where a is when a faecal DNA sample is positive for the PCR marker of its own target (true positive); b is when a faecal DNA sample is positive for a PCR marker of another target (false positive); c is when a faecal DNA sample is negative for a PCR marker of its own target (false negative); d is when a faecal DNA sample is negative for a PCR marker of another target (true negative) (Balleste et al., 2020).

Statistical analysis

A generalised linear model with a negative binomial distribution was used to determine whether the FIB counts varied by site. A post-hoc multiple comparison of this model was performed to determine whether the FIB counts differed between the dry and wet weather conditions. A standard Pearson correlation analysis was performed to check the correlation between the three FIB groups tested. The enumerated bacterial data were $\log_{10}$-transformed to attain a normal distribution. The $\log_{10}$ transformed colony counts (log CFU/100 mL) were used in the Pearson correlation analysis. The hierarchical cluster analysis (CA) was implemented by means of Ward's method, using squared Euclidean distances as a measure of similarity to emulate the underlying patterns of variation of FIB in relation to anthropogenic activities and land use patterns of the study sites (Emad & Eethar, 2012). A chi-square statistical test was performed to determine whether there were significant differences in MST markers between the sampling sites and across seasons. The statistical analyses were performed using Microsoft Excel (2013), PAST version 4.03 (Hammer et al., 2001), and R statistical software version 4.0.3 (R Core Team, 2021), using package MASS (Venables & Ripley, 2002) for negative binomial models and package multcomp (Hothorn et al., 2008) for multiple comparison tests.

RESULTS AND DISCUSSION

Distribution and concentration of faecal indicator bacteria along Rawan-Oya

The TC and FC were identified and enumerated based on colony morphology, with the concentration of the specific type of FIB expressed in CFU per 100 mL of water sample.

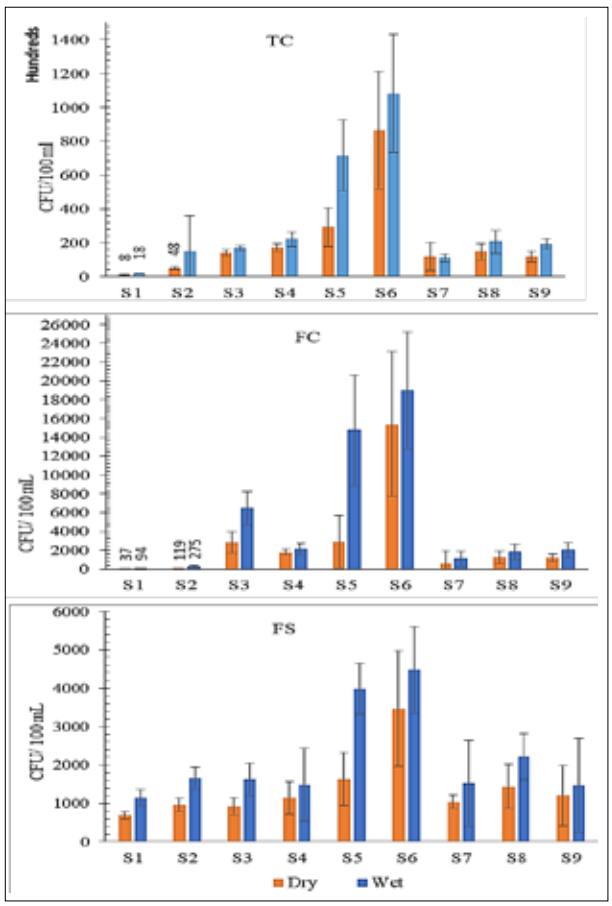

Figure 2: The geometric means of total coliform (TC), faecal coliform (FC) and faecal streptococcus (FS) concentrations (CFU/100 mL) at nine sites along the Rawan-Oya tributary of the Mahaweli River during dry and wet seasons from June 2020 to March 2022. (S1- Forested area, S2- Agricultural area, S3- Rural area, S4- Semi-urban area, S5 and S6- Urban area, S7- Rural area, S8- Agricultural area, and S9- Semi-urban area).

Results showed significant variability in TC, FC, and FS counts spatially and temporally. The TC concentration in stream water ranged from 2.7×10^2 to 1.6×10^5 CFU/100 mL, FC counts varied from 16 to 3.2×10^4 CFU/100 mL, and FS concentrations fluctuated between 5.4×10^2 to 6.2×10^3 CFU/100 mL throughout the study period between the nine sampling sites along the stream.

Figure 2 illustrates the geometric means of TC, FC, and FS concentrations (CFU/100 mL) at nine sites along the tributary during dry and wet seasons. The lowest geometric means of TC (1.2×10^3 CFU/100 mL), FC (6.1×10^1 CFU/100 mL), and FS (8.3×10^2 CFU/100 mL) were observed in the forested area (S1). Specifically, at site S1, the lowest TC (2.7×10^2 CFU/100 mL) and FC (1.6×10^1 CFU/100 mL) values were recorded during February 2021, the driest month with the least precipitation (0.1 mm), while the lowest FS concentration (5.4×10^2 CFU/100 mL) was observed in June 2020. The highest geometric mean of TC (9.7×10^4 CFU/100 mL), FC (1.7×10^4 CFU/100 mL), and FS (3.9×10^3 CFU/100 mL) counts were recorded at site S6 located in a highly urban area. The highest TC (1.6×10^5 CFU/100 mL) and FC (3.2×10^4 CFU/100 mL) concentrations were recorded in the urban area in April 2021, following a 5.6 mm rainfall event after a dry period. The peak of the FS (6.2×10^3 CFU/100 mL) concentration was observed in February 2022, also a dry period with 0.1 mm of precipitation. There was an increase in TC, FC, and FS counts during the wet season compared to the dry season. Even with less rainfall (5 – 6 mm) after a dry season, the FIB levels increased rapidly (Figure 3).

Figure 4 presents a map of the Rawan-Oya tributary illustrating the distribution patterns of TC, FC, and FS in the nine sampling sites along the stream.

The presumptive identification of isolates from the membrane filtration method was confirmed using standard biochemical assays to determine the reliability of the identification, with the following results: Total coliforms showed 100% positive results for the BGB confirmation test at 37 °C for 24 – 48 h. The FC demonstrated 98% positivity for the BGB test at 44.5 °C for 24 – 48 h. The Indole test confirmed 95% positive results for *E. coli*. Faecal Streptococci showed 100% positive results for the BEA slant test.

The generalized linear model showed no significant differences in TC, FC, and FS concentrations in water samples between wet and dry seasons. (GLM, $p > 0.05$).

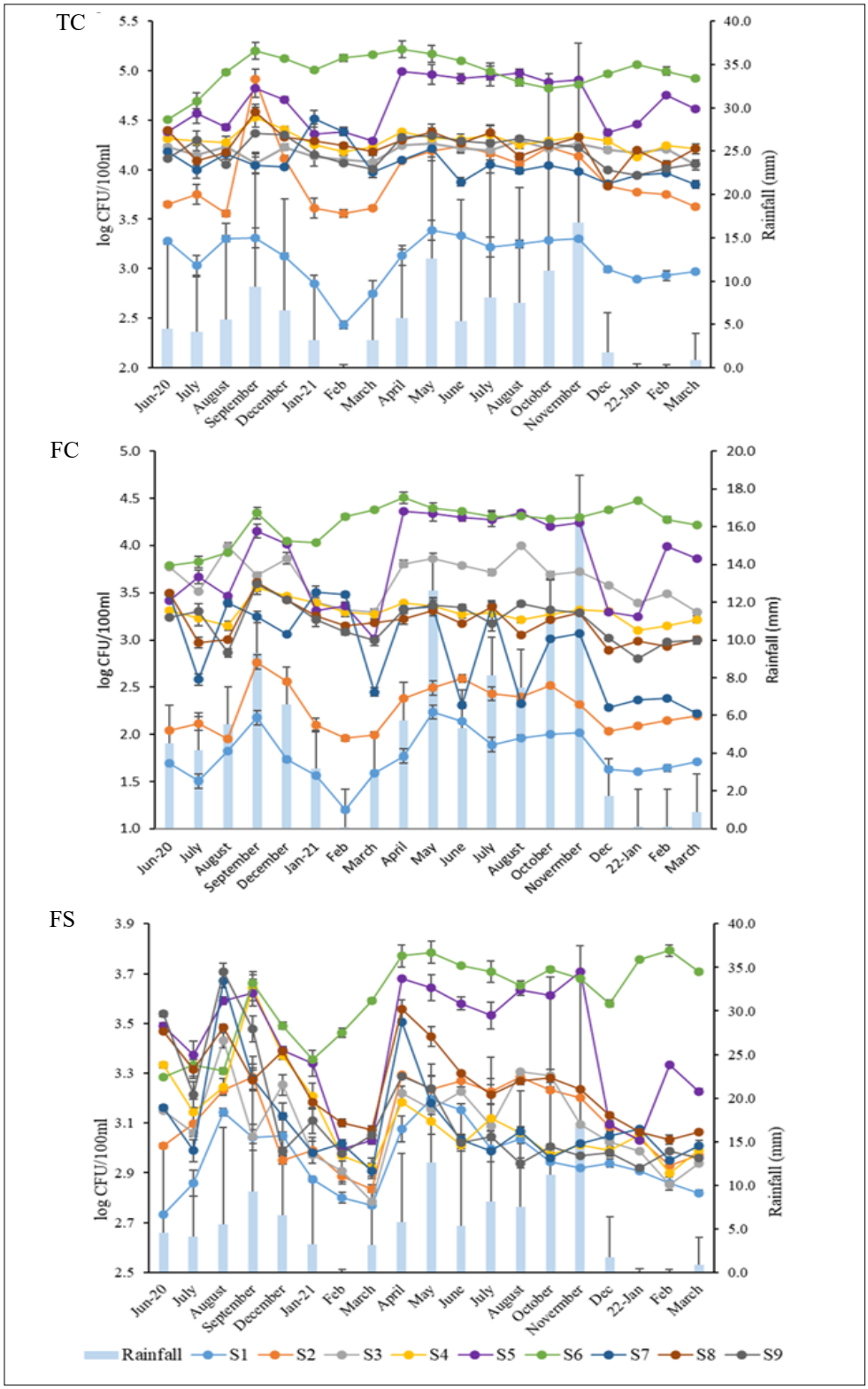

Figure 3: Total coliform (TC), Faecal coliform (FC), and Faecal Streptococcus (FS) levels measured at nine sites along the Rawan-Oya Tributary of the Mahaweli River from June 2020 to March 2022 against monthly rainfall data (Sampling sites: S1- Forested area, S2- Agricultural area, S3- Rural area, S4- Semi-urban area, S5 and S6- Urban area, S7- Rural area, S8- Agricultural area, and S9- Semi-urban area).

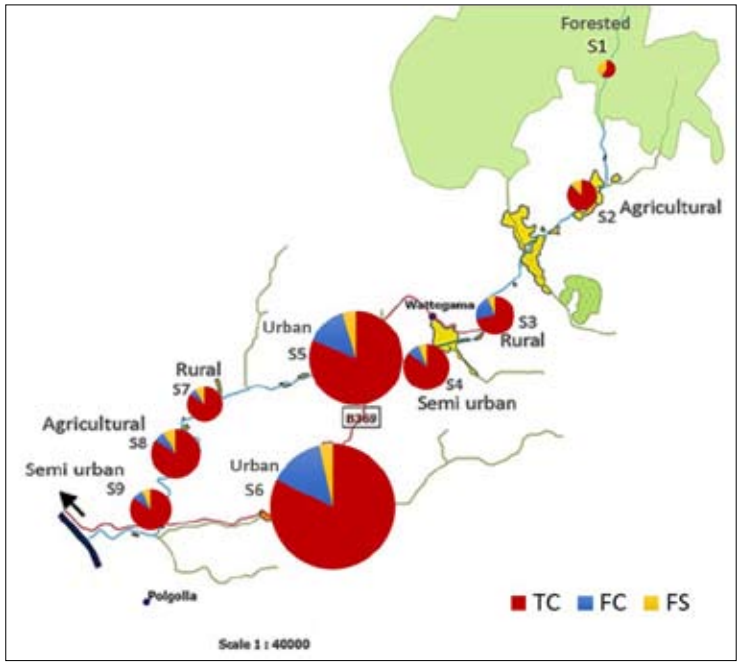

Figure 4: Map of the Rawan-Oya tributary of the Mahaweli River illustrating the distribution patterns of total coliform (TC), faecal coliform (FC) and faecal streptococci (FS) at nine sampling sites from June 2020 to March 2022 (S1- Forested area, S2- Agricultural area, S3- Rural area, S4- Semi-urban area, S5 and S6- Urban area, S7- Rural area, S8- Agricultural area, and S9- Semi-urban area).

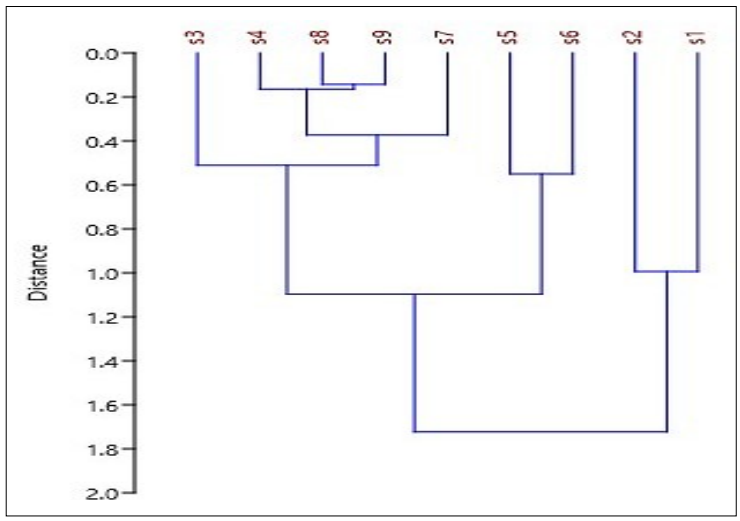

Figure 5: Hierarchical clustering of sampling sites of the Rawan-Oya tributary of the Mahaweli River based on the distribution of FIB levels. (Sampling areas: S1- Forested area, S2- Agricultural area, S3- Rural area, S4- Semi-urban area, S5 and S6- Urban area, S7- Rural area, S8- Agricultural area, and S9- Semi-urban area).

A significantly higher concentration of TC was found at site S6 (GLM, z = 2.16, p = 0.03) compared to other sites during both wet and dry seasons. Faecal coliform levels fluctuated significantly between all sites (GLM, p < 0.05), except between sites S1, S2, and S7 (GLM, z = 0.78, p = 0.4 and GLM, z = 1.69, p = 0.09). However, FS concentrations did not vary significantly between sites or during the wet and dry seasons (GLM, p > 0.05).

The hierarchical cluster analysis showed similarities in FIB distribution among the study sites with three main clusters. Cluster 1 consisted of sites S1 and S2, with S1 being the most upstream site in a forested area with minimal human activity, and S2 located approximately 1.5 km downstream of S1, characterized by predominantly agricultural land use. Cluster 2 consisted of S5 and S6 in urban habitats with high population densities. Cluster 3 comprised sites S3, S4, S7, S8 and S9, surrounded by rural, semi-urban and agricultural land-use types (Figure 5).

A Pearson correlation coefficient was computed to assess the linear relationship between FIB concentrations. There was a strong positive correlation between the TC and FC distributions (r = 0.92, df = 169, $p < 0.001$). The Pearson correlation between TC and FS was 0.71, and the p-value was less than 0.001. Moreover, a moderately positive correlation was observed between FC and FS counts along the stream (r = 0.68, df = 169, $p < 0.001$) (Figure 6).

Inference of faecal source based on FC/FS ratio method

According to the results of the FC/FS standard ratios, the primary source of faecal contamination in the forested area (S1) was primarily attributed to wild animals. Sites S2, S4, S7, S8, and S9 showed faecal pollution from domestic animals. Site S3 and S5 showed pollution from domestic animals only during the dry season; however, during the wet season, it was determined to be human-origin faecal contamination. Site S6 had the highest FIB counts, and the FC/FS ratio showed that the main source of contamination at this site during both seasons was human faecal matter (Figure 7).

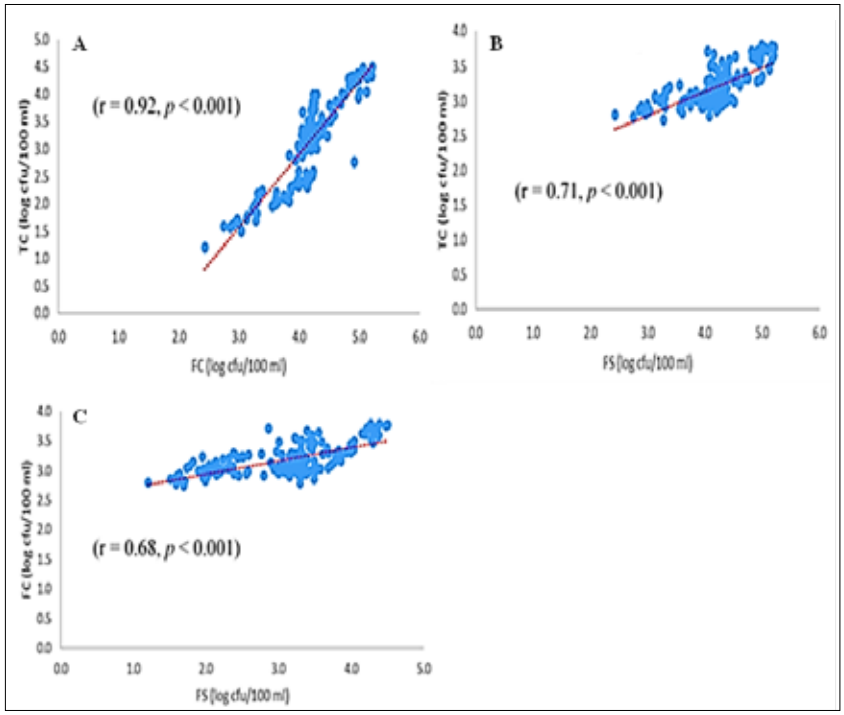

Figure 6: Correlations among faecal indicator bacteria in the Rawan-Oya tributary, showing the relationships between A. Total coliforms (TC) and faecal coliforms (FC); B. Total coliforms and faecal streptococcus (FS); and C. Faecal coliforms and faecal streptococcus, from June 2020 to March 2022.

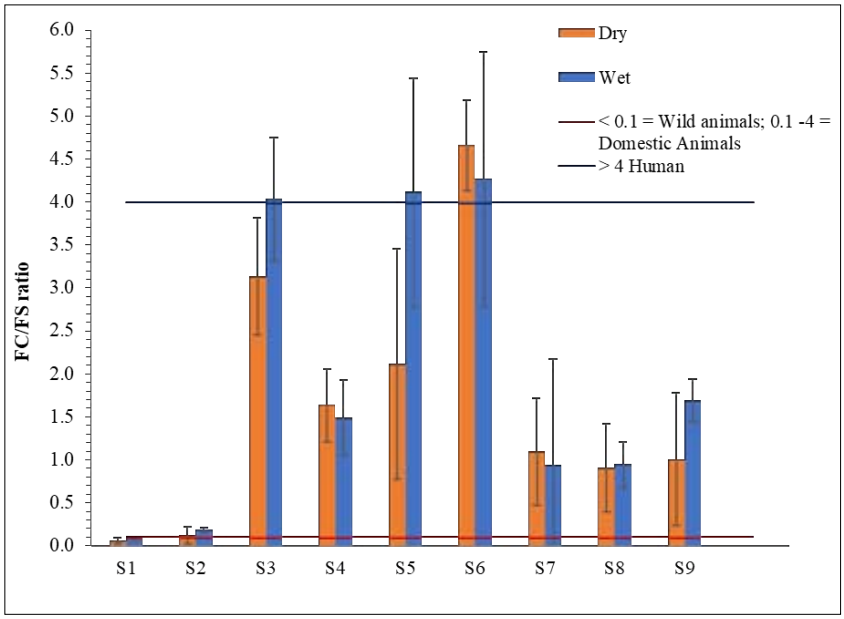

Figure 7: FC/FS ratio of nine sites along the Rawan-Oya tributary of the Mahaweli river during dry and wet seasons (Sampling sites: S1- Forested area, S2- Agricultural area, S3- Rural area, S4- Semi-urban area, S5 and S6- Urban area, S7- Rural area, S8- Agricultural area, and S9- Semi-urban area).

Site S6 is in a highly urban area where all drainage channels and wastewater outlets from houses, meat shops and other buildings directly flow into the stream. Moreover, dumping solid waste into the river and in the vicinity was common in this area. However, the most important factor for this high faecal contamination is likely the public toilets located on the riverbank at this site.

Faecal contamination source identification with microbial source tracking (molecular method)

In this study, Bac32 was used as a universal marker, while human and cattle faecal contaminations were detected through the use of human-specific (HF183) and cattle-specific (CF193) *Bacteroides* markers. Dog faecal contamination was traced using the dog-specific *Faecalibacterium* (Ed-1) marker. Results were reported as positive or negative for each host-specific marker, with DNA fragment confidence being assessed through a comparison with a DNA ladder. The accuracy of the DNA fragment was determined by its location in relation to the ladder, with an acceptable range of ± 10% of the "true" base-specific value (Universal *Bacteroides* = 676, cow 193 = 515, human 183 = 525, dog = 145) (Somnark et al., 2018; Zhang, 2020). Sensitivity analysis further revealed that the universal marker (Bac32) and the human marker exhibited 100% sensitivity, while the cattle and dog markers showed 90% and 70% sensitivity, respectively. Specificities for all markers were 90% or higher.

All samples tested positive for the universal *Bacteroides* marker, confirming faecal contamination in all samples. The distribution patterns of MST markers at the nine sites along the stream are illustrated in Figure 8.

There were significant differences in the distribution of human ($\chi^2 = 68.69$; df = 8; $p < 0.0001$), cattle ($\chi^2 = 62.47$; df = 8; $p < 0.0001$), and dog-specific ($\chi^2 = 50.12$; df = 8; $p < 0.0001$) markers between the nine sampling sites. Water samples collected from the forested area (S1) did not contain human-specific markers. The agricultural areas, sites S2 and S8, were positive for the HF183 marker at 26% and 52%, respectively. A rural site (S3) with high recreational activities showed human faecal contamination in 84% of the samples, while in the other rural site (S7), 47% of the samples were positive for human contamination. Two semi-urban sites (S4 and S9) contained human-specific markers in 58% and 63% of the samples, respectively. All the samples (100%) collected from the urban sites (S5 and S6) were positive for the HF183 assay. The presence of cattle-specific markers was

also low (21%) at the forested site. The CF193 marker was prominent in agricultural areas (S2 = 95% and S8 = 100%) and the urban site S6 (100%). Subsequent sites to the agricultural areas (S3 and S9) contained 68% and 78% of the cattle-specific marker. When considering the dog-specific marker distribution, only 10% of the samples from the forested area contained the ED-1 marker. It was noticeably high in urban areas (S6 = 89%, S5 = 84%) and in semi-urban sites (S4 = 84%). In agricultural areas, about 30% of samples were positive.

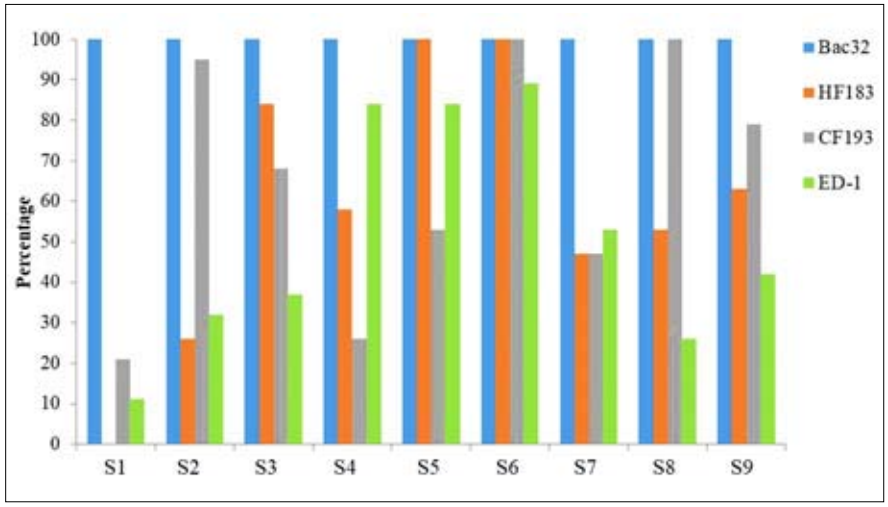

Figure 8: Percentage of positive results for the MST markers at nine sites along the Rawan-Oya tributary: Bac32- Universal *Bacteroides* marker, HF183- Human-specific *Bacteroides* marker, CF193- Cattle specific *Bacteroides* marker, Ed-1- Dog-specific *Faecalibacterium* marker (Sampling sites: S1- Forested area, S2- Agricultural area, S3- Rural area, S4- Semi-urban area, S5 and S6- Urban area, S7- Rural area, S8- Agricultural area, and S9- Semi-urban area).

Variations of human-specific (χ^2 = 29.18; df = 1; $p < 0.0001$) and dog-specific (χ^2 = 4.23; df = 1; p = 0.039) markers were significantly higher during the wet season compared to the dry season. However, there were no significant differences in the presence of cattle-specific markers between seasons (χ^2 = 2.15; df = 1; p = 0.14). Surface runoff due to rainfall is a major transporter of faeces into streams (Kostyla et al., 2015). The Rawan-Oya tributary exhibited diverse patterns of faecal contamination along the waterway. Moreover, the results obtained from the MST procedure were more specific and informative than those from the FC/FS ratio method. The type of faecal contamination at all sites, except sites S1 and S2, was significantly compatible between the MST and ratio methods (χ^2; $p < 0.05$).

DISCUSSION

The consistently high concentrations of FIB (TC, FC, and FS) observed across all sampling sites indicate widespread and significant faecal contamination of the Rawan-Oya tributary, originating from anthropogenic and/or mammalian sources. The observed variation in FIB concentrations along the tributary can be attributed to changing land use patterns (from forested to agricultural and urbanized zones), anthropogenic activities encountered along the course, as well as natural influences such as the presence of wildlife, precipitation, and surface runoff. Increasing human activity and population density along the catchment of the Rawan-Oya tributary has been reported (Kapukotuwa et al., 2023), which is consistent with similar findings reported for other Sri Lankan catchments (Rajapakshe et al., 2008), supporting the hypothesis that land use is a major contributor to the microbiological quality of the water.

According to the regulatory standards, the Rawan-Oya stream water at all locations tested was not suitable for direct consumption, as both TC and FC levels significantly exceeded the Sri Lanka Standard (SLS, 2013) limits for potable water. Furthermore, except for the upstream forested area, the water quality at all other

study sites exceeded the permissible microbial limits for recreational use (FC: 235 CFU/100 mL; FS: 70 CFU/100 mL) set by the WHO and EPA (USEPA, 2012; WHO, 2021). This is a critical public health issue, particularly considering the local context, as Kapukotuwa et al. (2023) showed a substantial portion of the population in the areas (~75%) utilizes this water for bathing, washing clothes, and other household activities. The fact that some households (28.3%) receive chlorinated water derived from this source (Kapukotuwa et al., 2023), particularly in sites S1, S2, and S5, underscores the necessity of robust treatment and source-specific contamination control. The bacteriological quality of the Mahaweli River also exhibits similarly poor microbial quality (Liyanage et al., 2021), indicating that the tributary contributes to larger systemic water quality issues.

Seasonal changes in FIB content are known to be influenced by precipitation-driven runoff, temperature fluctuations, hydrological conditions, and land-use or point-source inputs. These factors often determine whether FIB levels rise during wet seasons, due to stormwater and sewage overflows, or decline in dry seasons when dilution and bacterial die-off dominate. In the present study, sampling was conducted over 18 months (June 2020 – March 2022) to capture contamination patterns across seasons; however, no significant differences in overall FIB counts were observed between the dry and wet seasons in the Rawan-Oya tributary. The absence of seasonal variation in Rawan-Oya can be attributed to continuous contamination sources, such as urban sewage, agricultural runoff, and inadequate sanitation infrastructure, which sustain persistently high bacterial loads year-round, thereby masking the influence of rainfall or hydrological seasonality. Previous studies have shown that when FIB levels remain consistently elevated in polluted river systems, seasonal fluctuations are often absent due to chronic contamination inputs (Muñoz-Delgado et al., 2025). Furthermore, seasonal drivers such as precipitation, runoff, and point-source discharges do not always produce clear FIB patterns, with variability observed across sites and years (Wilson et al., 2022). Similar findings have been reported in other river systems globally, where no significant seasonal flux in FIB concentrations was detected (Bojarczuk et al., 2018), aligning with the present study's observation of persistent contamination from diffuse sources even after centralized point-source controls were implemented (Bhat & Danek, 2012). Nevertheless, other studies have documented increases in FIB levels during wet seasons due to precipitation and stormwater inputs, with dry-season conditions favoring dilution and bacterial die-off (Dila et al., 2018). Conversely, strong positive correlations between FIB and precipitation have been reported in certain systems (Sinclair et al., 2009), highlighting the variability in seasonal responses across different hydrological and contamination contexts.

Significant differences in human, cattle, and dog-specific markers were observed across nine sites in the Rawan-Oya tributary. Human contamination was absent in the forested site (S1) but highest in urban areas (S5, S6: 100%) and a rural recreational site (S3: 84%). The absence of human-specific markers in the forested site (S1) indicates minimal anthropogenic activity. In contrast, urban sites (S5, S6) showed 100% positivity, consistent with untreated sewage discharges, leaking septic systems, and poor sanitation infrastructure. The high prevalence at the rural recreational site (S3) suggests direct inputs from visitors and inadequate waste management. Cattle markers were most prominent in agricultural sites S2 (95%) and S8 (100%), as well as in urban site S6 (100%), reflecting the proximity of livestock and manure runoff. The presence of cattle markers in urban S6 likely results from mixed land use, including peri-urban farming and improper disposal of animal waste. The lack of seasonal variation in cattle markers suggests that continuous inputs from livestock operations occur, independent of rainfall. Dog markers peaked in urban (S5, S6: >80%) and semi-urban sites (S4: 84%), highlighting the role of domestic pets and stray dog populations. Poor waste disposal practices and high densities of companion animals contribute to persistent contamination. Seasonal increases in dog markers during wet periods are likely due to stormwater mobilizing fecal deposits from streets and open areas. Human and dog markers increased significantly during wet seasons, consistent with rainfall-driven runoff and sewage overflows transporting fecal material into streams. Conversely, cattle markers remained stable across seasons, reflecting year-round agricultural inputs that mask hydrological variability. Similar distribution patterns are reported in studies using comparable genotypic analyses, such as the Dargle River in Dublin, where human markers peaked in urban areas and ruminant markers in agricultural regions (Balleste et al., 2010).

To identify host sources of faecal pollution, both the conventional FC/FS ratio and PCR-based MST methods were applied. The FC/FS ratio offered a rapid, preliminary indication of contamination sources (wildlife in forested areas, human in urban sites, and domestic animals elsewhere) based on established human-to-animal ratios (Jagals et al., 1995). However, its reliability is limited by environmental factors such as temperature, pH, and organic matter (Bisimwa et al., 2022). In contrast, the library- and culture-independent PCR-based MST method provided definitive source attribution, revealing

diverse and spatially variable contamination patterns strongly aligned with local anthropogenic activities; MST thus offered scientifically robust evidence beyond general contamination levels.

As Bussi et al. (2017) point out, the specificity of the data derived from this study is crucial for effective resource management. The site-specific source identification provided by the MST analysis offers local authorities essential, actionable data to inform targeted source control and implement long-term water planning and management schemes. For instance, the detection of human markers in urban zones justifies focused investment in sanitation infrastructure, while the detection of ruminant markers in agricultural areas necessitates the implementation of best management practices for livestock waste. The findings are therefore important for developing effective strategies for water quality management and ensuring the safety of drinking water supplied by the Rawan-Oya tributary, as well as serving as a model for managing other vital water resources in Sri Lanka facing similar faecal pollution threats.

CONCLUSION

The study confirmed significant faecal contamination in the Rawan-Oya tributary, a critical freshwater source for nearby communities. Contamination levels, measured by FIB counts, increased progressively from the upstream forested areas to the downstream urban areas, rendering the water unsafe for both drinking (SLS, 2013) and recreational use (WHO, 2021). Only the forested area met acceptable microbial quality standards for recreational use.

This research represents a pioneering effort in Sri Lanka by successfully implementing the MST method to accurately identify and differentiate specific sources of pollution. These insights offer local authorities essential, actionable data to inform targeted water management strategies. Ultimately, the study not only quantifies the extent of pollution but also charts a clear path towards protecting public health. The findings are crucial for developing effective strategies for water quality management and the long-term protection of public health, particularly in relation to the Rawan-Oya tributary and other vital water resources in Sri Lanka.

Acknowledgment

The authors would like to acknowledge Dr. Nilmini Jayasena for her advice on data analysis. Financial assistance from the National Science Foundation of Sri Lanka (Grant No. NSF/SCH/2019/04) is also acknowledged.

REFERENCES

Ahmed, W., Hughes, B. & Harwood, V.J., (2016). Current status of marker genes of Bacteroides and related taxa for identifying sewage pollution in environmental waters. *Water*, *8*(6), p.231.

APHA (1992). Standard Methods for the Examination of Water and Wastewater. 18th Edition, American Public Health Association (APHA), American Water Works Association (AWWA) and Water Pollution Control Federation (WPCF), Washington DC.

Augustyn, Ł., Babula, A.M., Joniec, J., Stanek-Tarkowska, J., Hajduk, E. & Kaniuczak, J., (2016). Microbiological indicators of the quality of river water, used for drinking water supply. *Polish Journal of Environmental Studies*, *25*(2), pp.511-519.

Ballesté, E. & Blanch, A.R., (2010). Persistence of Bacteroides species populations in a river as measured by molecular and culture techniques. *Applied and Environmental Microbiology*, *76*(22), pp.7608-7616.

Ballesté, E., Demeter, K., Masterson, B., Timoneda, N., Sala-Comorera, L. & Meijer, W.G., (2020). Implementation and integration of microbial source tracking in a river watershed monitoring plan. *Science of The Total Environment*, *736*, p.139573.

Bhat, S., & Danek, L. J. (2012). Comparison of fecal coliform before and after wastewater treatment facility: a case study near a coastal town in the Southeastern USA. *Water, Air, & Soil Pollution*, *223*(5), 1923-1930.

Bisimwa, A.M., Kisuya, B., Kazadi, Z.M., Muhaya, B.B. & Kankonda, A.B., (2022). Monitoring faecal contamination and relationship of physicochemical variables with faecal indicator bacteria numbers in Bukavu surface waters, tributaries of Lake Kivu in Democratic Republic of Congo. *Hygiene and Environmental Health Advances*, *3*, p.100012.

Boehm, A.B. & Sassoubre, L.M., (2014). Enterococci as indicators of environmental fecal contamination. https://europepmc.org/article/nbk/nbk190421

Bojarczuk, A., Jelonkiewicz, Ł. & Lenart-Boroń, A., 2018. The effect of anthropogenic and natural factors on the prevalence of physicochemical parameters of water and bacterial water quality indicators along the river Białka, southern Poland. *Environmental Science and Pollution Research*, *25*(10), pp.10102-10114.

Bower, P.A., Scopel, C.O., Jensen, E.T., Depas, M.M. & McLellan, S.L., (2005). Detection of genetic markers of fecal indicator bacteria in Lake Michigan and determination of their relationship to Escherichia coli densities using standard microbiological methods. *Applied and Environmental Microbiology*, *71*(12), pp.8305–8313.

Bussi, G., Whitehead, P.G., Thomas, A.R., Masante, D., Jones, L., Cosby, B.J., Emmett, B.A., Malham, S.K., Prudhomme, C. & Prosser, H., (2017). Climate and land-use change impact on faecal indicator bacteria in a temperate

maritime catchment (the River Conwy, Wales). *Journal of Hydrology*, *553*, pp.248–261.

Coyne, M.S. & Howell, J.M., (1994). The fecal coliform/fecal streptococci ratio (FC/FS) and water quality in the bluegrass region of Kentucky. Available via: https://uknowledge.uky.edu/cgi/viewcontent.cgi?article=1036&context=pss_views.

Devane, M.L., Moriarty, E., Weaver, L., Cookson, A. & Gilpin, B., (2020). Fecal indicator bacteria from environmental sources; strategies for identification to improve water quality monitoring. *Water Research*, *185*, p.116204.

Dila, D. K., Corsi, S. R., Lenaker, P. L., Baldwin, A. K., Bootsma, M. J., & McLellan, S. L. (2018). Patterns of host-associated fecal indicators driven by hydrology, precipitation, and land use attributes in Great Lakes watersheds. Environmental Science & Technology, 52(14), 7847–7857. https://doi.org/10.1021/acs.est.8b01945

Ebentier, D.L., Hanley, K.T., Cao, Y., Badgley, B.D., Boehm, A.B., Ervin, J.S., Goodwin, K.D., Gourmelon, M., Griffith, J.F., Holden, P.A. and Kelty, C.A., (2013). Evaluation of the repeatability and reproducibility of a suite of qPCR-based microbial source tracking methods. *Water Research*, *47*(18), pp.6839–6848.

Edberg, S.C.L., Rice, E.W., Karlin, R.J. & Allen, M.J., (2000). Escherichia coli: the best biological drinking water indicator for public health protection. *Journal of Applied Microbiology*, *88*(S1), pp.106S-116S.

Emad AM, S. and Eethar M, A.O., 2012. Assessment of water quality of Euphrates River using cluster analysis. *Journal of Environmental Protection*, *2012*.

Frick, C., Vierheilig, J., Nadiotis-Tsaka, T., Ixenmaier, S., Linke, R., Reischer, G.H., Komma, J., Kirschner, A.K., Mach, R.L., Savio, D. and Seidl, D., 2020. Elucidating fecal pollution patterns in alluvial water resources by linking standard fecal indicator bacteria to river connectivity and genetic microbial source tracking. *Water Research*, *184*, p.116132.

Fujioka, R.S., Solo-Gabriele, H.M., Byappanahalli, M.N. and Kirs, M., 2015. US Recreational Water Quality Criteria: A Vision for the Future. *International Journal of Environmental Research and Public Health*, *12*(7), p.7752.

Garcia-Armisen, T. and Servais, P., 2007. Respective contributions of point and non-point sources of E. coli and enterococci in a large urbanized watershed (the Seine river, France). *Journal of Environmental Management*, *82*(4), pp.512-518.

Goshu, G., Koelmans, A.A. and de Klein, J.J.M., 2021. Performance of faecal indicator bacteria, microbial source tracking, and pollution risk mapping in tropical water. *Environmental Pollution*, *276*, p.116693.

Hagedorn, C., Blanch, A. R., & Harwood, V. J. (Eds.). (2011). *Microbial source tracking: methods, applications, and case studies*. Springer Science & Business Media.

Hammer, Ø., Harper, D. and Ryan, P., 2001. PAST: Palaeontological Statistics Software Package for Education and Data Analysis, Version 4.03. Palaeontol Electron 4: 9. Available via: https://palaeo-electronica.org/2001_1/past/past.pdf.

Hothorn, T., Bretz, F. and Westfall, P., 2008. Simultaneous inference in general parametric models. *Biometrical Journal: Journal of Mathematical Methods in Biosciences*, *50*(3), pp.346-363.

Jagals, P.W.O.K., Grabow, W.O.K. and De Villiers, J.C., 1995. Evaluation of indicators for assessment of human and animal faecal pollution of surface run-off. *Water Science and Technology*, *31*(5-6), pp.235-241.

Kapoor, V., Pitkänen, T., Ryu, H., Elk, M., Wendell, D. and Santo Domingo, J.W., 2015. Distribution of human-specific Bacteroides and fecal indicator bacteria in an urban watershed impacted by sewage pollution, determined using RNA-and DNA-based quantitative PCR assays. *Applied and Environmental Microbiology*, *81*(1), pp.91-99.

Kapukotuwa, G.K., Weerakoon, K.C., Abayasekara, C.L. and Rajakaruna, R.S., 2023. Community Survey on Anthropogenic Activities Affecting the Rawan-Oya Tributary of Mahaweli River in Kandy District, Sri Lanka. *ACS ES&T Water*, *3*(6), pp.1669-1677.

Kolawole, O.M., Ajayi, K.T., Olayemi, A.B. and Okoh, A.I., 2011. Assessment of water quality in Asa River (Nigeria) and its indigenous Clarias gariepinus fish. *International Journal of Environmental Research and Public Health*, *8*(11), pp.4332-4352.

Kostyla, C., Bain, R., Cronk, R. & Bartram, J., (2015). Seasonal variation of fecal contamination in drinking water sources in developing countries: a systematic review. *Science of the Total Environment*, *514*, pp.333–343.

Kumar, M., Chaminda, T., Honda, R. & Furumai, H. (2019). Vulnerability of urban waters to emerging contaminants in India and Sri Lanka: Resilience framework and strategy. *APN*, *9*(1), pp.57-66.

Kumar, M., Chaminda, T., Patel, A.K., Sewwandi, H., Mazumder, P., Joshi, M. & Honda, R., (2020). Prevalence of antibiotic resistance in the tropical rivers of Sri Lanka and India. *Environmental Research*, *188*, p.109765.

Leclerc, H.D.A.A., Mossel, D.A.A., Edberg, S.C. and Struijk, C.B., 2001. Advances in the bacteriology of the coliform group: their suitability as markers of microbial water safety. *Annual Reviews in Microbiology*, *55*(1), pp.201-234.

Liyanage, L.R.I.S., Nanayakkara, B.S., Abayasekara, C.L., Galketiyahewage, S.U. & Abeysundara, H.T.K., (2021). *Escherichia coli* in recreational water in selected sites of the river Mahaweli between Peradeniya and Katugastota. *Sri Lankan Journal of Infectious Diseases*, *11*.

Muñoz-Delgado, A., de Anda, J., Lugo-Melchor, O. Y., González-Díaz, R. L., Shear, H., Meza-Rodríguez, D., & Bravo-Madrigal, J. (2025). Microbial risk assessment of fecal indicator bacteria in a highly polluted river: Santiago-Guadalajara River Basin. Environmental Monitoring and Assessment, 197, Article 663. https://doi.org/10.1007/s10661-025-14023-4

Nnadozie, P.C. & Harcourt, P., (2016). Comparative Study of Two Conventional Methods Used for Coliform Enumeration from Port Harcourt Waters. *Open Access Library Journal*, *3*(03), p.1.

Oshiro, R., (2002). Method 1604: Total Coliforms and Escherichia coli in water by membrane filtration using a simultaneous detection technique (MI Medium). *Washington, DC: US*

Environmental Protection Agency. Available via: https://www.epa.gov/sites/default/files/2015-08/documents/method_1604_2002.pdf.

R Core Team, (2021). R: A Language and Environment for Statistical Computing. R Foundation for Statistical Computing, Vienna, Austria. https://www.R-project.org/.

Rajapakshe, I.H., Galagedara, L.W. & Najim, M.M.M., (2008). Microbial water quality variations in different water sources in the Pussalla Oya catchment and pollution contributions by communities. *Tropical Agricultural Research*, *20*, pp.313-325.

Raji, M.I.O., Ibrahim, Y.K.E., Tytler, B.A. & Ehinmidu, J.O., (2015). Faecal Coliforms (FC) and Faecal Streptococci (FS) ratio as tool for assessment of water contamination: A case study of River Sokoto, Northwestern Nigeria. *The Asia Journal of Applied Microbiology*, *2*(3), pp.27–34.

Santo Domingo, J., Edge, T., Griffith, J., Hansel, J., Harwood, V.J., Jenkins, M., Layton, A., Molina, M., Nakatsu, C., Oshiro, R. & Sadowsky, M., (2005). *Microbial source tracking guide document* (p. 135). EPA/600-R-05-064. US EPA.

Sinclair, A., Hebb, D., Jamieson, R., Gordon, R., Benedict, K., Fuller, K., Stratton, G.W. & Madani, A., (2009). Growing season surface water loading of fecal indicator organisms within a rural watershed. *Water Research*, *43*(5), pp.1199–1206.

Sinton, L.W., Donnison, A.M. & Hastie, C.M., (1993). Faecal streptococci as faecal pollution indicators: a review. Part I: Taxonomy and enumeration. *New Zealand Journal of Marine and Freshwater Research*, *27*(1), pp.101-115.

Somnark, P., Chyerochana, N., Mongkolsuk, S. & Sirikanchana, K., (2018). Performance evaluation of Bacteroidales genetic markers for human and animal microbial source tracking in tropical agricultural watersheds. *Environmental Pollution*, *236*, pp.100-110.

Sri Lanka Standards Organization (2013). Drinking water Standards- first Revision 614:2013.

Toledo-Hernandez, C., Ryu, H., Gonzalez-Nieves, J., Huertas, E., Toranzos, G.A. & Santo Domingo, J.W., (2013). Tracking the primary sources of fecal pollution in a tropical watershed in a one-year study. *Applied and Environmental Microbiology*, *79*(5), pp.1689-1696.

USEPA, (2012). Recreational Water Quality Criteria. Available via: https://www.epa.gov/sites/default/files/2015-10/documents/rec-factsheet-2012.pdf (Accessed 20 January 2022)

Venables, W.N. & Ripley, B.D., (2002). Random and mixed effects. In *Modern applied statistics with S* (pp. 271–300). Springer, New York, NY.

WHO, (2021). *Guidelines on recreational water quality. Volume 1: Coastal and fresh waters*. World Health Organization.

Wilson, A. M., Martin, S. L., Verhougstraete, M. P., Kendall, A. D., Zimmer-Faust, A. G., Rose, J. B., Bell, M. L., & Hyndman, D. W. (2022). Detangling seasonal relationships of fecal contamination sources and correlates with indicators in Michigan watersheds. *Microbiology Spectrum*, *10*(4), e00415-22. https://doi.org/10.1128/spectrum.00415-22

Zhang, K., Sun, D., Duan, C., Chen, H., Din, A.U., Kong, X., Qin, X., & Zhang, B. (2020). Application of a *Faecalibacterium* 16S rDNA genetic marker for species identification of dog fecal waste. *Environmental Science and Pollution Research*, *27*(24), pp.30615–30624.

Zheng, G., Yampara-Iquise, H., Jones, J.E. & Andrew Carson, C., (2009). Development of *Faecalibacterium* 16S rRNA gene marker for identification of human faeces. *Journal of Applied Microbiology*, *106*(2), pp.634–641.

J.Natn.Sci.Foundation Sri Lanka 2025 53 (4): 437 - 445
DOI: http://dx.doi.org/10.4038/jnsfsr.v53i4.12659

RESEARCH ARTICLE

Biomedical Instrumentation

Chest anteroposterior diameter measurement: Comparison of ultrasonic and manual methods across different BMI categories

C Muralidharan * and MC Jobin Christ
Department of Biomedical Engineering, Rajalakshmi Engineering College, Anna University, Chennai, India.

Submitted: 29 April 2025; Revised: 22 September 2025; Accepted: 14 November 2025

Abstract: Chest anteroposterior diameter (APD) measurement is a critical metric in evaluating thoracic dimensions, particularly in assessing conditions like pectus excavatum and guiding interventions such as laryngoscopy and cardiopulmonary resuscitation. The lateral distance measurement of the thoracic cavity using the computed tomography image provides APD, but they expose the subject to radiation. Though the manual method of chest APD measurement using a wooden ruler is radiation-free, it is time-consuming and prone to human errors. This study proposes a novel and radiation-free method of measuring chest APD using an ultrasonic sensor. The accuracy and reliability of the measured chest APD using the ultrasonic method were compared with the manual method across three distinct BMI categories of 150 participants. The measured chest APD using ultrasonic and manual methods for underweight, normal, and obese participants ranges from 17-18 cm, 18.5-20.5 cm, and 23.75-25 cm, respectively. The statistical analyses, including paired t-tests and intra-class correlation coefficients (ICC), were performed to assess agreement between the two methods. The paired t-test manifests no significant difference between the mean APD measured using ultrasonic and manual methods with p-values of 0.8742 (underweight), 0.7390 (normal), and 0.7998 (obese). The ICC values obtained from the intra- and inter-observers for the ultrasonic and manual methods were ICC $\geq$ 0.93, 0.80 $\leq$ ICC $\leq$ 0.82 and 0.91, and 0.78. The ICC value obtained from the intra- and inter-observers for the ultrasonic method was high, so the ultrasonic method is better than the manual method. This study concludes that the ultrasonic method provides a radiation-free alternative to the manual method, making it suitable for routine clinical use globally.

Keywords: Arduino Uno, body mass index, chest anteroposterior diameter, paired t-test, ultrasonic sensor.

INTRODUCTION

The chest anteroposterior diameter (APD) is the distance between the midpoint on the lower half of the sternum's anterior skin and the posterior skin on the spinal process of the spine (Pickard et al., 2006; Meyer et al., 2010; Lee et al., 2019; Kim et al., 2020). The chest APD is used to assess the severity of pectus excavatum, a chest wall deformity (Haller et al., 1987; Lain et al., 2017; Biovati et al., 2020; Tro et al., 2022). An observational study suggested that during laryngoscopy the pillow height be adjusted manually, according to the chest APD (El-Orbany et al., 2011; Choi et al., 2013; Apfelbaum et al., 2021). A finite element simulation study showed that during cardiopulmonary resuscitation (CPR), to achieve a fixed compression depth, the compression force must be increased or decreased according to the chest APD (Moradicheghamahi et al., 2023). According to the guidelines of the American Heart Association for performing effective cardiopulmonary resuscitation (CPR), the compression depth achieved for adults, children, and infants is equal to one-third of their chest APD (Kao et al., 2009; Marino et al., 2018; Panchal et al., 2020). Several studies also suggested that the chest APD varies due to age, body mass index, and disease conditions. (Lee et al., 2015; Yoo et al., 2018; Sarkar et al., 2019; Chavan et al., 2021; Atiksawedparit et al., 2023). computed tomography (CT) of the chest offers a precise way to measure the chest APD and evaluate the chest wall structure. This involves drawing a line from the anterior

* Corresponding author (muralidharan.c@rajalakshmi.edu.in; https://orcid.org/0009-0009-4609-1597)

This article is published under the Creative Commons CC-BY-ND License (http://creativecommons.org/licenses/by-nd/4.0/). This license permits use, distribution and reproduction, commercial and non-commercial, provided that the original work is properly cited and is not changed in anyway.

side of the lower half of the sternum to the posterior side of the spine on the CT image. The length of the line provides the APD (Zarb et al., 2010; Jin et al., 2016). The amount of radiation dose delivered to the patient during CT ranges from 4 to 7 millisieverts (ICRP, 2007; McCollough et al., 2008). However, taking multiple CT scans exposes the patients to harmful ionising radiation that changes the structures of DNA and chromosomes, which leads to a risk of cancer (Zhou et al., 2019; Devic et al., 2022). The calliper-based external measurement technique is also used to measure the chest APD (Ewert et al., 2017; Chen et al., 2022). This method is more affordable than a CT scan, but reproducibility between different persons in measurement is not established. The manual method of measuring chest APD is by using a wooden ruler. In this method the participant is allowed to rest in a supine position on a flat surface. The wooden ruler is placed perpendicular to the nipple line and spine. The distance between the nipple and spine is measured as chest APD. It is important to note that this manual method is time-consuming and also results in human error in measurement. The proposed study is a reliable, error-free alternative method of measuring the chest APD using an ultrasonic sensor. The sound waves generated from the ultrasonic sensor are non-ionising in nature. They are not harmful to humans like the electromagnetic waves from X-rays and CT. The aim is to verify the accuracy and robustness of the proposed ultrasonic method by validating its findings with those obtained through the manual method. This comparison is conducted across three distinct groups, categorised as underweight, normal, and obese, based on participants' BMI values.

MATERIALS AND METHODS

A prototype of a mechanical setup for mounting the ultrasonic sensor was designed and modelled using SolidWorks for this study. Figures 1, 2, and 3 are the front, side, and top views, of CAD design models of the mechanical setup. The mechanical setup was fabricated using mild steel material (Yan et al., 2014). All the dimensions mentioned in the three views were in inches.

The isometric view of the mechanical setup in Figure 4 consists of a metallic frame. The metallic frame was supported through rods.

The anteroposterior diameter of the human participant is measured through the HC-SR04 ultrasonic distance

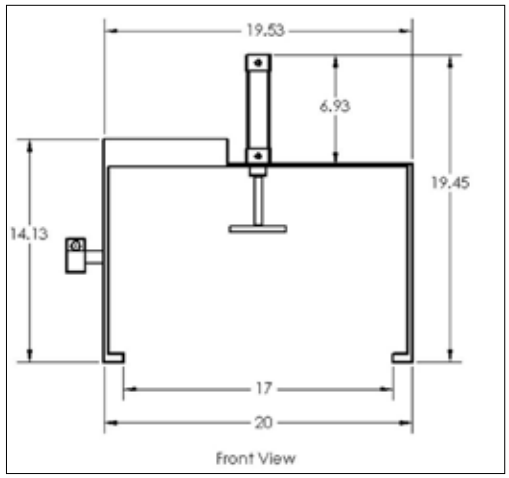

Figure 1: Front view of the mechanical setup

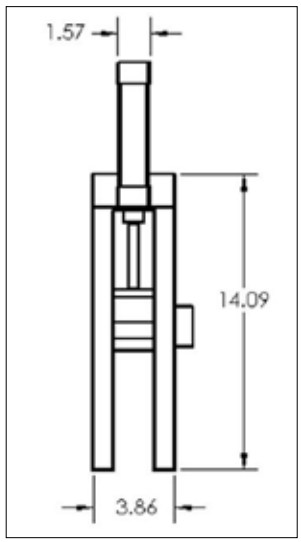

Figure 2: Side view of the mechanical setup

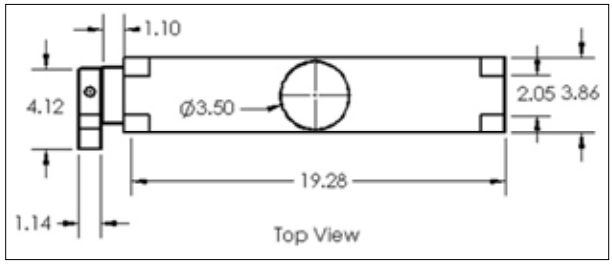

Figure 3: Top view of the mechanical setup

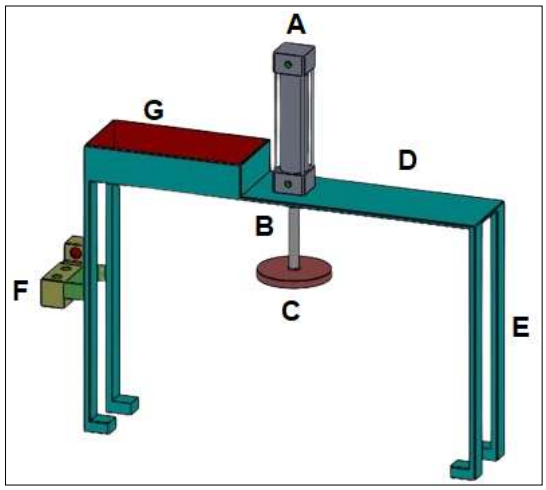

Figure 4: Isometric view of the mechanical setup (A- Pneumatic cylinder, B- Piston rod, C- Compression pad, D- Metallic frame, E- Rods, F- Solenoid valve, G- Electronic hardware setup)

sensor. Figure 5 shows the HC-SR04 ultrasonic distance sensor (Lumbanbatu et al., 2024). This is a widely used ultrasonic distance sensor capable of measuring non-contact distances ranging from 2 to 400 cm, with an accuracy of up to 3 mm. It operates using sonar technology to calculate the distance to an object. The HC-SR04 is compact, simple to set up, and features four pins for power, trigger, echo, and ground. Additionally, it includes control circuitry to ensure reliable and consistent data.

Figure 5: HC-SR04 ultrasonic sensor

The Arduino Uno microcontroller board in Figure 6 is used to interface the HC-SR04 ultrasonic distance sensor. This board features both digital and analogue input/output (I/O) pins, allowing it to connect with various expansion boards and other circuits. It includes 14 digital I/O pins and 6 analogue I/O pins. The board can be programmed using the Arduino IDE (integrated development environment) via a type B USB cable and can be powered either through a USB connection or a barrel connector that accepts voltages between 7 and 20 volts, such as a 9 volt battery.

Figure 6: Arduino Uno Board

Participant selection criteria

The 200 participants of varying age groups—young (20–35), middle (35–55), and old (56 or above), participated in the study. Out of 200 participants, 150 males were selected for the study, based on the inclusion criteria. The inclusion criteria are healthy individuals with BMI < 18.5 kg/m², 18.5 kg/m² < BMI < 25 kg/m², and 25 kg/m² < BMI < 30 kg/m². The remaining 50 participants were not selected for the study, based on the exclusion criteria. The exclusion criteria are unhealthy individuals having cardiac illness, chest injury, or spinal scoliosis, and females, including pregnant women. The selected 150 participants were grouped into underweight (BMI < 18.5 kg/m²), normal (18.5 kg/m² < BMI < 25 kg/m²), and obese (25 kg/m² < BMI < 30 kg/m²) based on the World Health Organization (WHO) guidelines (Lad et al.,

2012). There were 50 participants in the underweight group, with a mean age of 26.32 ± 5.78, a mean height of 152.77 cm ± 2.06 cm, and a mean weight of 41.52 kg ± 1.27 kg. Similarly, in the normal group, there were 50 participants with a mean age of 25.2 ± 6.50, a mean height of 172.86 cm ± 6.88 cm, and a mean weight of 67.50 kg ± 6.68 kg. Meanwhile, there were 50 participants in the obese group, with a mean age of 28.9 ± 9.28, a mean height of 167.24 cm ± 5.73 cm, and a mean weight of 86.53 kg ± 6.60 kg.

Ethical clearance

The study involving human participants was reviewed and approved by the Rajalakshmi Engineering College ethical committee (REC/IEC/005/2024). The participants also gave written informed consent to take part in this study.

Measurement protocol

The observer A and observer B performed chest anterior-posterior diameter (APD) measurements using two methods: the ultrasonic and the manual method. Observer A was the anthropometrist, and observer B was the researcher (author 1). The measurements were carried out based on the guidelines provided by the ethical committee members. In the inter-observer protocol, both observers measured chest APD on each participant only once (for each method) in the same session, under identical conditions. In the intra-observer protocol, each observer repeated the chest APD measurements on all participants one week later. The same protocol and equipment were used; observers were blind to their first measurements when re-measuring.

Ultrasonic sensor method

Figure 7 demonstrates the method of measuring the chest anteroposterior diameter of human participants using an HC-SR04 ultrasonic sensor. When the microcontroller in the Arduino Uno board sends a signal on pin number 5 to the HC-SR04 ultrasonic sensor, it triggers the ultrasonic sensor. The triggering action causes the transmitter module of the HC-SR04 to generate an ultrasonic wave. This wave travels to the participant's anterior chest, reflects off the surface, and returns back to the HC-SR04 sensor's receiver module, changing the echo pin from low to high. The time taken (t) for the ultrasonic wave to travel to the chest and reflect back is the time duration of the echo pin to change from low to high. The time duration (t) is determined using the precision timer available in the microcontroller of an Arduino Uno board. The distance (B) between the sensor and the anterior side of the chest is then computed using the time duration (t) and velocity of the ultrasonic wave (v) using equation 1.

$$B = v \times t \quad ...(1)$$

where
v = Velocity of ultrasonic waves in air (0.034 cm/μs)
t = Time taken to transmit and receive the ultrasonic waves (μs)

The distance from the ultrasonic sensor to the posterior side of the thoracic cavity of the human participant is fixed as A. The anteroposterior diameter (APD) is then computed using the A and B values from equation 2.

$$APD = A - B \quad ...(2)$$

Where APD, A and B are measured in centimetres (cm)

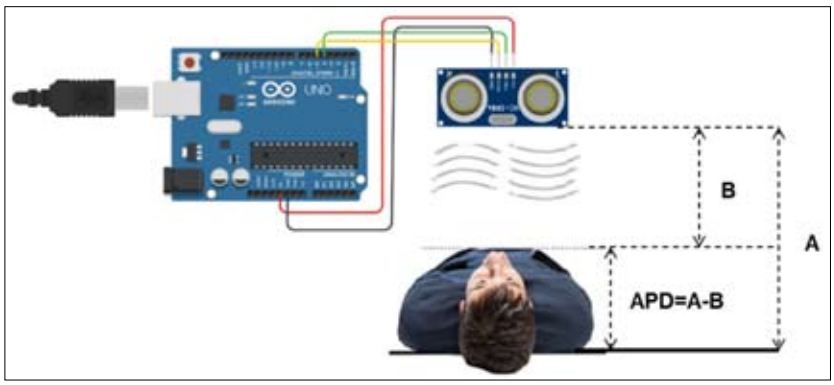

Figure 7: Anteroposterior diameter (APD) measurement using the ultrasonic method (A - the distance from the ultrasonic sensor to the posterior side of the thoracic cavity of the human, B - the distance between the sensor and the anterior side of the chest)

Figure 8 shows the placement of the ultrasonic sensor in the mechanical setup for chest APD measurement. The participant is allowed to lie in a supine position on the table. The mechanical setup was fixed on the table such that the patient's safety is ensured. The HC-SR04 ultrasonic sensor was affixed to the bottom side of its frame, ensuring it was directed towards the central region between the xiphoid and manubrium of the participant. The chest APD value of the individual participant measured using the ultrasonic method is by measuring the A and B value. The B value is measured through 10 trials for each participant and calculated their corresponding average and available as average B in cm. The A value is fixed as 28 cm. The APD is then measured using the formula APD = A-B. The same procedure is repeated to measure the APD values for 50 participants in each group to a total of 150 participants in 3 groups. Technical expertise is required to position the ultrasonic sensor to the lower half of the participant's sternum for measuring the chest APD.

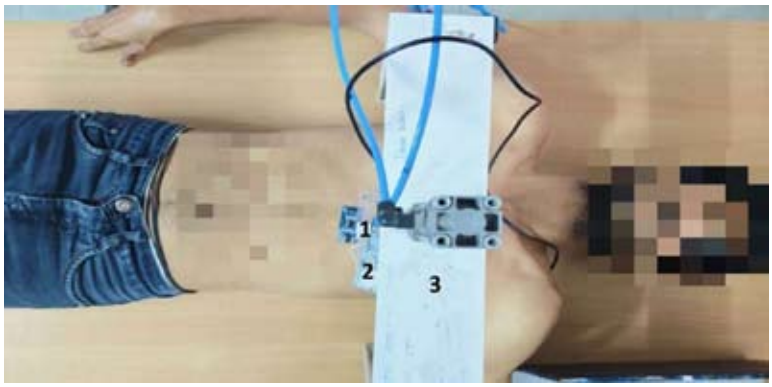

Figure 8: Ultrasonic sensor placements for anteroposterior diameter (APD) measurement- 1. Ultrasonic sensor 2. Arduino Uno board 3. Metallic frame

Validation

The measured APD values of all the 150 participants available in three groups were validated using the manual method. In this method a piece of cardboard is placed over the participant's chest. The lateral distance from the posterior side of the spine to the midpoint between the xiphoid and manubrium of the sternum is measured using a wooden ruler as shown in Figure 9. This method provides a direct means of quantifying the chest anteroposterior diameter (APD). The accuracy of the manual method is improved by using a calibrated digital ruler instead of an analogue wooden ruler.

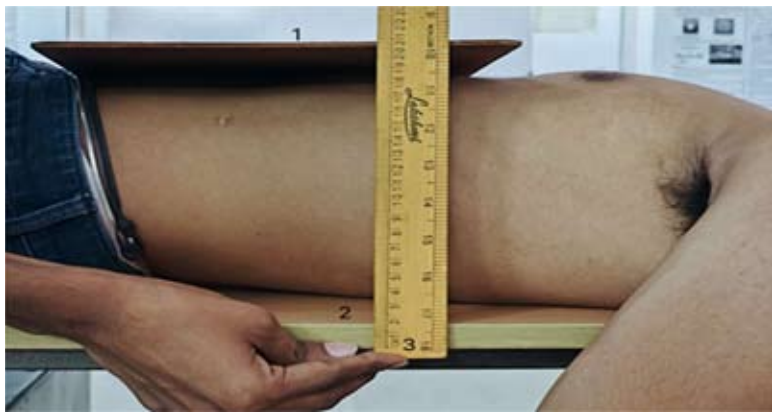

Figure 9: APD measurement using the manual method

Statistical tests and plots

The Statistical Package for Social Sciences (SPSS) statistical tool was used for testing the measured chest APD using the ultrasonic method and the manual method. The paired t-test was used to compare the mean APD measured using the ultrasonic and manual methods. The null hypothesis (H_0): no significant difference between the mean values of the APD measured by ultrasonic and manual methods. The alternative hypothesis (H_1): significant difference between the mean values of APD measurement between the two measurement methods. The significance level was set at $p > 0.05$. The scatter plot was plotted to visualise the correlation and overall relationship between the two methods for underweight, normal, and obese group participants. The intra-class correlation coefficient was also computed to assess the consistency or agreement of APD measurements made by both the inter-observer and the intra-observer.

RESULTS AND DISCUSSION

The measured chest APD using ultrasonic and manual methods for underweight, normal, and obese group participants were in the ranges 17 - 18 cm, 18.5 - 20.5 cm, and 23.75 - 25 cm, respectively. The scatter plots were plotted for underweight, normal and obese group participants, using the chest APD measured from ultrasonic and manual methods, in Figures 10(a), 10(b), and 10(c), respectively. A few data points in the scatter plot of the underweight group participants fall along the trend line, and others fall away from the trend line. But for normal and obese group participants, most of the data points fall along the trend line. The correlation coefficients for the scatter plots plotted for underweight, normal, and obese participants in Figures 10(a), 10(b), and 10(c) were 0.6234, 0.9788, and 0.8057 respectively.

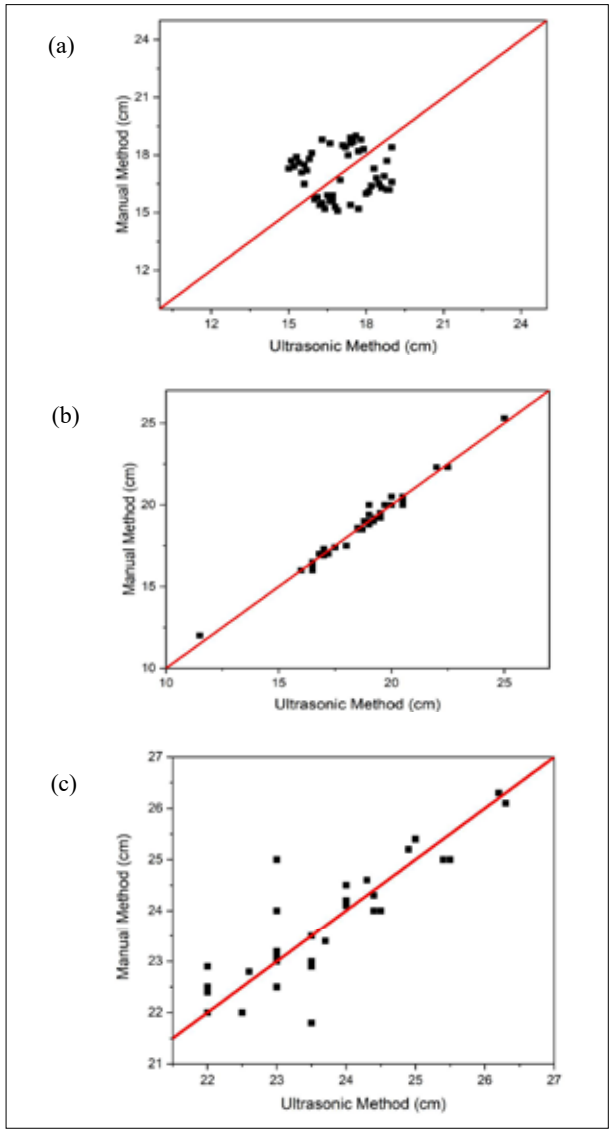

Figure 10: Comparison between chest APD measurements of Ultrasonic and Manual methods a. Underweight participant's b. Normal participant's c. Obese participant's

Table 1: Paired t-test results for underweight, normal and obese groups

Parameters and Values	MM-UWG	UM-UWG	MM-NG	UM-NG	MM-OG	UM-OG
Age	26.32 ± 5.78	26.32 ± 5.78	25.2 ± 6.5	25.2 ± 6.5	28.9 ± 9.3	28.9 ± 9.3
Height (cm)	152.77 ± 2.06	152.77 ± 2.06	172.86 ± 6.88	172.86 ± 6.88	167.24 ± 5.73	167.24 ± 5.73
Weight (kg)	41.52 ± 1.27	41.52 ± 1.27	67.5 ± 6.7	67.5 ± 6.7	86.53 ± 6.60	86.53 ± 6.60
APD (cm)	17.05 ± 1.17	17.01 ± 1.21	18.57 ± 2.03	18.55 ± 2.02	23.75 ± 1.22	23.73 ± 1.24
P-value	0.8742		0.7391		0.7998	
t-statistic	0.1590		0.3349		0.2549	

According to Table 1, the mean APD values obtained from the paired t-test for the underweight, normal, and obese group participants using the manual and ultrasonic sensor methods were 17.05 ± 1.17 cm and 17.01 ± 1.21 cm, 18.57 ± 2.03 cm and 18.55 ± 2.02 cm, 23.75 ± 1.22 cm, and 23.73 ± 1.24 cm, respectively. In the underweight group, the paired t-test results yielded a t-statistic value and high p-value (t-statistic = 0.1590 and $p = 0.8743$, $p > 0.05$). Meanwhile, in the normal group, the test results yielded a t-statistic value that is much less than the p value (t-statistic = 0.3349 and $p = 0.7391$, $p > 0.05$). Similarly, for the obese group, the test results also yielded a t-statistic value that is less than the p-value (t-statistic =0.2549 and $p = 0.7998$, $p > 0.05$). The intra-observer ICC values obtained from observers A and B for the ultrasonic method were 0.93 and 0.95. Similarly, the intra-observer ICC values obtained from observers A and B for the manual method were 0.80 and 0.82. Meanwhile, the inter-observer ICC values obtained from observers A and B for the ultrasonic and manual methods were 0.91 and 0.78, respectively. The measured chest APD using both the methods was normally distributed.

The paired t-test results in Table 2 indicated that there is no significant difference ($p > 0.05$) in APD measurements between the two measurement methods for the underweight, normal, and obese groups. The high P-value ($p > 0.05$) reinforces the null hypothesis, which posits no significant difference between the APD measured using ultrasonic and manual methods. The correlation coefficients obtained from the scatter plots of the underweight, normal, and obese group show a good correlation between the two methods. Similarly, it is especially evident that the majority of data points align along the trend lines for the underweight, normal, and obese groups. This alignment with the trend lines indicates that the measurements from the two methods are very similar, with minimal systematic bias. The ultrasonic method showed excellent intra-observer reliability for observer A (anthropometrist) and observer B (researcher) (ICCs ≥ 0.93), while the manual method showed only adequate reliability ($0.80 \leq ICC \leq 0.82$), with higher variability. The inter-observer agreement was similarly better in the ultrasonic method (ICC=0.91) compared to the manual method (ICC=0.78). Thus, for precise chest APD measurements, particularly in populations with different body types (underweight, normal, and obese), the ultrasonic method is preferred. The manual method can be used for the screening process.

CONCLUSION

The experimental study concludes that the ultrasonic sensor method measures the chest anteroposterior diameter for underweight, normal, and obese participants effectively. The ultrasonic waves generated from the ultrasonic sensor produce non-ionising radiation. Meanwhile, measuring the chest APD using the manual method results in human error. Similarly, the X-rays generated in the CT methods produce ionising radiation. Measuring the chest APD provides insight into the anatomy of the thorax and respiratory health. The changes in APD due to chronic obstructive pulmonary diseases like asthma, pulmonary fibrosis, and emphysema can be easily detected. Congenital chest wall deformation, like pectus excavatum or pectus carinatum, can also be detected using the chest APD. The early measurement of chest APD avoids the surgical procedure to overcome the severe deformation of the chest wall.

The limitations of our study are that, whenever the human participant is not positioned in the line of sight of the ultrasonic sensor, the ultrasonic signal deflected away rather than reflected back to the ultrasonic sensor. In this scenario, the calculated chest APD is incorrect. While measuring the chest APD, the participant should not wear any fabrics, because fabrics absorb the ultrasonic signal. The room used for measuring chest APD should be free from air conditioners and ceiling fans, because the ultrasonic sensor absorbs the acoustic signals and pulse signals generated by air conditioners and ceiling fans.

Future work

The future work of our research will be deputising a female observer and supervisor for measuring the chest APD of female participants using the same setup and protocol. This concept of measuring the chest APD will be incorporated in a simple chest compression device. And then, based on the measured the chest APD modelling and designing will be done to produce different types of CPR manikins. These CPR manikins will mimic the underweight, normal and obese participants. This simple chest compression device will be programmed to perform CPR on the manikins to achieve a compression depth of $1/3^{rd}$ of chest APD of the manikins resulting in effective CPR. This simple mechanical chest compression device will replace the existing mechanical CPR devices and perform effective CPR across different BMI categories.

REFERENCES

Apfelbaum, J. L., Hagberg, C. A., Connis, R. T., Abdelmalak, B. B., Agarkar, M., Dutton, R. P., *et al.* (2021). 2022 American Society of Anesthesiologists practice guidelines for management of the difficult airway. *Anesthesiology*, *136*(1), 31-81. https://doi.org/10.1097/aln.0000000000004002

Atiksawedparit, P., Sathapornthanasin, T., Chalermdamrichai, P., Sanguanwit, P., Saksobhavivat, N., Saelee, R., & Phattharapornjaroen, P. (2023). Using computed tomography to evaluate proper chest compression depth for cardiopulmonary resuscitation in Thai population: A retrospective cross-sectional study. *Plos One*, *18*(2), e0279056. https://doi.org/10.1371/journal.pone.0279056

Biavati, M., Kozlitina, J., Alder, A. C., Foglia, R., McColl, R. W., Peshock, R. M., Kelly Jr, R. E., Kim Garcia, C. (2020). Prevalence of pectus excavatum in an adult population-based cohort estimated from radiographic indices of chest wall shape. *Plos One*, *15*(5), e0232575. https://doi.org/10.1371/journal.pone.0232575

Chavan, S. D., Patil, V. S., & Patil, B. K. (2021). Comparison of thoracic dimensions of chronic obstructive pulmonary disease patients and healthy controls: A cross-sectional study. *International Journal of Advanced Research in Medicine*, *3*, 75-77. https://doi.org/10.22271/27069567.2021.v3.i1b.105

Chen, T., Chen, C., Zeng, Q., Zhang, Y., Jiao, J., Zhang, X., *et al.* (2022). Use of caliper-based external measurement of body surface in assessing the severity of pectus excavatum. *Frontiers in Pediatrics*, *10*, 1015026. https://doi.org/10.3389/fped.2022.1015026

Choi, J. W., Kim, J. A., Kim, H. K., Oh, M. S., & Kim, D. K. (2013). Chest anteroposterior diameter affects difficulty of laryngoscopy for non-morbidly obese patients. *Journal of Anesthesia*, *27*, 563-568. https://doi.org/10.1007/s00540-013-1572-1

Devic, C., Bodgi, L., Sonzogni, L., Pilleul, F., Ribot, H., Charry, C., Le Moigne, F., Paul, D., Carbillet, F., Munier, M., & Foray, N. (2022). Influence of cellular models and individual factor in the biological response to chest CT scan exams. *European radiology experimental*, *6*(1), 14. https://doi.org/10.1186/s41747-022-00266-0

El-Orbany, M., Woehlck, H., & Salem, M. R. (2011). Head and neck position for direct laryngoscopy. *Anesthesia & Analgesia*, *113*(1), 103-109. https://doi.org/10.1213/ANE.0b013e31821c7e9c

Ewert, F., Syed, J., Wagner, S., Besendoerfer, M., Carbon, R. T., & Schulz-Drost, S. (2017). Does an external chest wall measurement correlate with a CT-based measurement in patients with chest wall deformities. *Journal of Pediatric Surgery*, *52*(10), 1583-1590. https://doi.org/10.1016/j.jpedsurg.2017.04.011

Haller, J. A., Kramer, S. S., & Lietman, S. A. (1987). Use of CT scans in selection of patients for pectus excavatum surgery: a preliminary report. *Journal of Pediatric Surgery*, *22*(10), 904-906. https://doi.org/10.1016/s0022-3468(87)80585-7

Jin, S. Y., Oh, S. B., & Kim, Y. O. (2016). Estimation of optimal pediatric chest compression depth by using computed tomography. *Clinical and Experimental Emergency Medicine*, *3*(1), 27. https://doi.org/10.15441/ceem.16.119

Kao, P. C., Chiang, W. C., Yang, C. W., Chen, S. J., Liu, Y. P., Lee, C. C., *et al.* (2009). What is the correct depth of chest compression for infants and children? A radiological study. *Pediatrics*, *124*(1), 49-55. https://doi.org/10.1542/peds.2008-2536

Kim, Y. H., Lee, J. H., Lee, D. W., Song, Y. G., Lee, K. Y., Lee, Y. H., *et al.* (2020). Applicability of anatomical landmarks for chest compression depth in cardiopulmonary resuscitation for children. *Scientific Reports*, *10*(1), 1921. https://doi.org/10.1038/s41598-020-58649-5

Lad, U. P., Satyanarayana, P., Shisode-Lad, S., Siri, C. C., & Kumari, N. R. (2012). A study on the correlation between the body mass index (BMI), the body fat percentage, the handgrip strength and the handgrip endurance in underweight, normal weight and overweight adolescents. *Journal of Clinical and Diagnostic Research: JCDR*, *7*(1), 51. https://doi.org/10.7860/JCDR/2012/5026.2668

Lain, A., Garcia, L., Gine, C., Tiffet, O., & Lopez, M. (2017). New methods for imaging evaluation of chest wall deformities. *Frontiers in Pediatrics*, *5*, 257. https://doi.org/10.3389/fped.2017.00257

Lee, H., Oh, J., Lee, J., Kang, H., Lim, T. H., Ko, B. S., *et al.* (2019). Retrospective study using computed tomography to compare sufficient chest compression depth for cardiopulmonary resuscitation in obese patients. *Journal of the American Heart Association*, *8*(23), e013948. https://doi.org/10.1161/jaha.119.013948

Lee, S. H., Kim, D. H., Kang, T. S., Kang, C., Jeong, J. H., Kim, S. C., & Kim, D. S. (2015). The uniform chest compression depth of 50 mm or greater recommended by current guidelines is not appropriate for all adults. *The American Journal of Emergency Medicine*, *33*(8), 1037-1041. https://doi.org/10.1016/j.ajem.2015.04.034

Lumbanbatu, E. M., Hamdani, D., & Setiawan, I. (2024). Development of Arduino Uno-Based Doppler Effect Trainer with FC-04 Sensor and HCSR-04 Sensor in Senior High School. *Asian Journal of Science Education*, *6*(1), 34-45. https://doi.org/10.24815/ajse.v6i1.35884

Marino, B. S., Tabbutt, S., MacLaren, G., Hazinski, M. F., Adatia, I., Atkins, D. L., *et al.* (2018). Cardiopulmonary resuscitation in infants and children with cardiac disease: a scientific statement from the American Heart Association. *Circulation*, *137*(22), e691-e782. https://doi.org/10.1161/CIR.0000000000000524

McCollough, C., Cody, D., Edyvean, S., Geise, R., Gould, B., Keat, N., Huda, W., Judy, P., Kalender, W., McNitt-Gray, M., *et al.* (2008). The Measurement, Reporting, and Management of Radiation Dose in CT; Report of AAPM Task Group; *American Association of Physicists in Medicine*: Alexandria, VA, USA; Volume 23, pp. 1–28. https://doi.org/10.37206/97

Meyer, A., Nadkarni, V., Pollock, A., Babbs, C., Nishisaki, A., Braga, M., *et al.* (2010). Evaluation of the Neonatal Resuscitation Program's recommended chest compression depth using computerized tomography imaging. *Resuscitation*, *81*(5), 544-548. https://doi.org/10.1016/j.resuscitation.2010.01.032

Moradicheghamahi, J., Fortuny, G., López, J. M., Puigjaner, D., Herrero, J., & Azeli, Y. (2023). The effect of thoracic dimensions on compression depth during cardiopulmonary resuscitation. *International Journal for Numerical Methods in Biomedical Engineering*, *39*(7), e3718. https://doi.org/10.1002/cnm.3718

Panchal, A. R., Bartos, J. A., Cabañas, J. G., Donnino, M. W., Drennan, I. R., Hirsch, K. G., *et al.* (2020). Part 3: adult basic and advanced life support: 2020 American Heart Association guidelines for cardiopulmonary resuscitation and emergency cardiovascular care. *Circulation*, *142*(16_Suppl_2), S366-S468. DOI: https://doi.org/10.1161/cir.0000000000000901

Pickard, A., Darby, M., & Soar, J. (2006). Radiological assessment of the adult chest: implications for chest compressions. *Resuscitation*, *71*(3), 387-390. https://doi.org/10.1016/j.resuscitation.2006.04.012

Sarkar, M., Bhardwaz, R., Madabhavi, I., & Modi, M. (2019). Physical signs in patients with chronic obstructive pulmonary disease. *Lung India*, *36*(1), 38-47. https://doi.org/10.4103/lungindia.lungindia_145_18

The 2007 Recommendations of the International Commission on Radiological Protection. *ICRP publication* 103. Ann. ICRP 2007, *37*, 1–332. https://doi.org/10.1016/j.icrp.2007.10.003

Trò, R., Martini, S., Stagnaro, N., Sambuceti, V., Torre, M., & Fato, M. M. (2022). A new tool for assessing Pectus Excavatum by a semi-automatic image processing pipeline calculating the classical severity indexes and a new marker: the Volumetric Correction Index. *BMC Medical Imaging*, *22*(1), 30. https://doi.org/10.1186/s12880-022-00754-0

Yan, J. B., Liew, J. R., Zhang, M. H., & Wang, J. Y. (2014). Mechanical properties of normal strength mild steel and high strength steel S690 in low temperature relevant to Arctic environment. *Materials & Design*, *61*, 150-159. https://doi.org/10.1016/j.matdes.2014.04.057

Yoo, K. H., Oh, J., Lee, H., Lee, J., Kang, H., Lim, T. H., et al. (2018). Comparison of heart proportions compressed by chest compressions between geriatric and non-geriatric patients using mathematical methods and chest computed tomography: a retrospective study. *Annals of Geriatric Medicine and Research*, *22*(3), 130. https://doi.org/10.4235/agmr.2018.22.3.130

Zarb, F., Rainford, L., & McEntee, M. F. (2010). AP diameter shows the strongest correlation with CTDI and DLP in abdominal and chest CT. *Radiation Protection Dosimetry*, *140*(3), 266-273. https://doi.org/10.1093/rpd/ncq115

Zhou, Y., Zheng, Y., Wen, Y., Dai, X., Liu, W., Gong, Q., Huang, C., Lv, F., & Wu, J. (2021). Radiation dose levels in chest computed tomography scans of coronavirus disease 2019 pneumonia: A survey of 2119 patients in Chongqing, southwest China. Medicine 2021, 100, e26692. https://doi.org/10.1097/md.0000000000026692

J.Natn.Sci.Foundation Sri Lanka 2025 53 (4): 447 - 457
DOI: http://dx.doi.org/10.4038/jnsfsr.v53i4.12519

RESEARCH ARTICLE

Fisheries Ecology

A multidimensional study on Spotted Sardinella: Biometric, ecological, and heavy metal perspectives from Negombo, Sri Lanka

WMNS Wijesooriya, HACC Perera*, AMPM Abeysinghe and KABP Perera
Department of Zoology and Environmental Management, Faculty of Science, University of Kelaniya, Sri Lanka.

Submitted: 10 March 2025; Revised: 11 October 2025; Accepted: 26 November 2025

Abstract: Biometric parameters, feeding habits, heavy metal content, and fisheries aspects of *Amblygaster sirm* (Spotted sardinella) in the coastal waters off Negombo, Sri Lanka were studied from August 2022 to March 2023. Length-weight relationships for males, females, and the pooled data were $W=0.0029\ TL^{3.3546}$, $W=0.0035\ TL^{3.2819}$ and $W=0.0030\ TL^{3.3459}$, respectively showing positive allometric growth. Fulton's condition factors for males, females and pooled data were 0.9047 ± 0.1074, 0.94392 ± 0.08699, and 0.92331 ± 0.09995 respectively. Food mainly consisted of animal parts (77.56%) with crustacean larvae being the most abundant food item (25.51%). The gastro-somatic index showed the highest and lowest feeding intensities in the size classes of 17.5-18.5 cm and 12.5-13.5 cm respectively. Outboard fiberglass reinforced plastic boats and gillnets of mesh sizes 1¼ and 1½ inches are widely used for fishing. The results of the principal component analysis showed that variables such as total length, standard length, head length, body weight, gut length, and gut weight were positively associated with each other. The mean concentrations of Cr, Zn, Cu and Cd in the edible muscles of *A. sirm* were 10.067 ± 3.658 mg/kg, 7.878 ± 1.856 mg/kg, 5.3857 ± 0.0818 mg/kg and 0.5209 ± 0.0447 mg/kg respectively. These values did not exceed the permissible limits declared by FAO and WHO. Overall, the study found that the fishes were in good physical condition with safe levels of heavy metal content for human consumption.

Keywords: *Amblygaster sirm,* food, heavy metal content, length-weight relationship, stomach fullness.

INTRODUCTION

Sri Lanka is one of the major fishing countries situated to the south of the Indian subcontinent with a coastline spanning approximately 1739 km (Thivviyan & Jayakody, 2017). Sri Lanka, as a coastal nation, relies on fisheries resources for sustenance and economic prosperity, making them a crucial source of food and a significant contributor of protein to local communities (Suseno et al., 2014; Thivviyan & Jayakody, 2017; Bandaranayake et al., 2024). Fish are important for a balanced and healthy diet because they provide protein, long-chain omega-3 polyunsaturated fatty acids, micronutrients such as iodine and selenium, potassium, vitamins such as D and B. (Medeiros et al., 2012; Weichselbaum et al., 2013; Ali et al., 2020). Approximately 40% of the fish caught in Sri Lanka consist of small pelagics (Jayasuriya, 2007). Among the small pelagics, spotted sardinella (*Amblygaster sirm),* which belongs to the family Clupeidae of the order Clupeiformes, is characterized by a slender body with a series of 10 to 20 gold spots down the flank (Devi et al., 2018). It is a schooling fish and is also associated with reefs. It is recorded in depths ranging from 10-70 m (Devi et al., 2018; Osman et al., 2021). In Sri Lanka, coastal fishery is operated year-round using gillnets and 17-feet fiberglass reinforced plastic boats equipped with 30 HP

* Corresponding author (chinthap@kln.ac.lk; https://orcid.org/0000-0001-8681-9663)

This article is published under the Creative Commons CC-BY-ND License (http://creativecommons.org/licenses/by-nd/4.0/). This license permits use, distribution and reproduction, commercial and non-commercial, provided that the original work is properly cited and is not changed in anyway.

outboard motors. Earlier studies have shown that *A. sirm* contributes for >40% of the small pelagic fish production of Sri Lanka (Karunasinghe & Wijeyaratne, 1995). Nets with mesh sizes of 20 mm and 38 mm are commonly used in this fishery (Karunasinghe &Wijeyaratne, 1991a; Jayasuriya, 2007).

The fisheries sector in Sri Lanka is facing multiple challenges, including overfishing, diminishing fish stocks, and ecosystem degradation due to habitat destruction, pollution and climate change. To ensure food security and meet the domestic demand for fish, it is crucial to implement sustainable fisheries management practices (World Bank, 2021; Bandaranayake et al., 2024). *A. sirm* fishery in the coastal waters off Negombo, Sri Lanka appears to be heavily overexploited and in order to exploit this fishery at the optimum level, it is recommended that gillnets with a mesh sizes of >25 mm should be used (Karunasinghe & Wijeyaratne (1995). It has also been shown that the best fishing season for this species in the coastal waters off Negombo is from April to November and the full moon period (Karunasinghe and Wijeyaratne, 1996).

The length-weight relationship (LWR) of fish is significant in the field of fisheries science as it serves multiple purposes including the extrapolation of total catch from length-frequency samples, estimation of biomass based on underwater length observations, and assessment of fish condition (Ceyhan et al., 2009). The LWR also helps to determine whether somatic growth follows an isometric or allometric pattern.

Fulton's condition factor (K) is an important measure used to assess the "condition" or physical health of a fish stock (Lizama & Ambrosio, 2002). It evaluates the plumpness or relative weight of individuals within a population (Osman et al., 2021). It provides insights into variation in the physiological status among fish and allows for comparison between populations living in different feeding, climatic, and environmental conditions (Devi et al., 2018). By assessing K, one can determine the feeding activity of a species and evaluate whether it is effectively utilizing the food sources (Lizama & Ambrosio, 2002). Fisheries scientists use this information to make management recommendations for fish stocks to ensure their well-being and sustainability (Osman et al., 2021).

The intensity of feeding of fish, which is based on the fullness of their stomach varies with the season, availability of preferred food items, maturity stage, and spawning season. It can be quantified using the gastro-somatic index (GaSI) (Khongngain et al., 2017).

Feeding habits of fish can be determined based on the predominant food items found in their stomachs (Hynes, 1950). Qualitative and quantitative analyses of gut contents are used to determine the composition of the diet of fish (Mahesh et al., 2018). The diet of *A. sirm* predominantly consists of copepods, nauplii and zoea larvae, bivalve larvae, gastropods, as well as dinoflagellates such as *Peridinium* and *Ceratium* (Whitehead, 1985).

Due to the ecological position of fish as prominent members of the aquatic food chain, they have the inherent ability to accumulate heavy metals derived from their diet, water, and sediment (El-Moselhy et al., 2014). The presence of toxic heavy metals in fish can cause adverse effects on human health (Castro-González & Méndez-Armenta, 2008), resulting in renal failure, liver damage, cardiovascular diseases, and even fatality (El-Moselhy et al., 2014). Therefore, it is important to analyze the heavy metal content in fish muscles also.

The objective of this study is to quantify the length-weight relationship, condition factor, relative gut length, gastro-somatic index, stomach contents, and heavy metal contents in the muscles of *A. sirm*. It is hypothesized that there is a significant difference between the length-weight relationship of males and females of *A. sirm* and the heavy metal content in their muscles is within the safe levels for human consumption.

MATERIALS AND METHODS

Monthly sampling of *A. sirm* specimens was conducted the at Sea Street landing site in Negombo, located on the west coast of Sri Lanka (7.2040°N and 79.8277°E) from August 2022 to March 2023. In each month, 25 specimens were randomly collected from five boats operating the gillnets of mesh sizes 1¼ and 1½ inches, and another 30 specimens were randomly collected for heavy metal analysis from October 2022 to March 2023. Samples were packed in ice and transported to the laboratory and stored at -20^{0}C for further analysis. Standard length (SL), total length (TL), fork length (FL), and head length (HL) were measured to the nearest 0.1 cm and the total body weight was measured to the nearest 0.1g.

Length-weight relationship and condition factor

The length-weight relationship of the fish, was calculated using the following equation proposed by Gulland (1969).

$W = aL^b$

W = Body weight of fish in g
L = Standard length of fish in cm
a = Antilogarithmic value of the intercept of the plot of log W against log L
b = Slope of the plot of log W against log L

Regression analysis was conducted on log weight (g) against log standard length (cm) to determine the length–weight relationship. To verify whether the slope 'b' significantly deviated from the expected value for isometric growth (b=3), a one-sample t-test was performed.

Fulton's Condition factor (K) was calculated using the following relationship proposed by Gulland (1969).

$K = 100W / L^3$

W = Body weight of fish in g
L = Standard length of fish in cm

Food and feeding

Each fish was dissected, the digestive tract was separated from the body and its length was measured. The relative gut length of the fish was calculated using the following formula proposed by Al-Hussaini (1949).

RGL = LG / TL

LG = Length of gut in cm
TL = Total length of fish in cm

Stomach fullness was visually assessed as full, three-fourths (3/4) full, half (1/2) full, one-fourth (1/4) full, and empty. Stomach contents of each fish were scooped out, weighed and gastro-somatic index (GaSI) was calculated using the following formula proposed by Hynes (1950).

GaSI = (Weight of stomach contents / Weight of fish) x 100

Stomach contents were identified to the lowest possible taxonomic level using a microscope and the frequency of occurrence of different food items was determined using the method proposed by Hynes (1950).

% Oi = (Ni/ N) x 100

% Oi = Frequency of occurrence of food item i
Ni = Number of stomachs containing the food item i
N = Total number of stomachs with food

Heavy metal analysis

The body weight and length of fish were measured and the edible portions of the fish muscle were separated and labeled for further analyses. These muscles were homogenized using a mortar and pestle. From each fish, 1.00 g of homogenized muscle tissue was digested using 10 mL of 70% nitric acid and 1 mL of hydrogen peroxide in closed Teflon tubes using a microwave digester at a temperature of 45^0C for 3 hours. Blanks containing the digestion medium were also digested concurrently. At the end of the digestion process, the samples were cooled to room temperature, filtered using filter papers and diluted to 20 mL using deionized water (Milli-Q ultrapure water). Samples were then transferred to acid-washed labeled polypropylene bottles. All reagents used were of analytical grade The glassware was pre-soaked in 10% nitric acid and later rinsed with distilled water to avoid metal contamination as described by El-Moselhy et al. (2014). The concentrations of Cr, Zn, Cu, and Cd in the digested solutions were determined in triplicate using an atomic absorption spectrophotometer (Analytik Jena Model Nova 400 P). Standard solutions of each metal were prepared from commercial standard calibration solutions. The limit of quantification values were obtained for each heavy metal and the results were expressed as mg/kg of wet weight.

RESULTS AND DISCUSSION

Length frequency distribution

Length frequency distribution of *A. sirm* caught in gill nets operated in the coastal waters off Negombo is shown in Table 1. The mid-length (cm) of the group that showed the highest and the lowest frequencies were 18 cm and 23 cm.

Length-weight relationship, condition factor (K), and sex ratio

The length–weight relationship plots of log W against vs log SL are shown in Figure 1.

The length-weight relationships of males, females and for pooled data are given in Table 2.

The b value of the length weight relationship was significantly different from 3 ($P < 0.05$) indicating positive allometric growth. Devi et al. (2018) observed positive allometric growths for *A. sirm* in the Andaman coast. Abdussamad et al. (2010) have observed that the

Table 1: Lenth frequency distribution of *A. sirm* in the gillnet catches operated in the coastal waters off Negombo

Standard length size class (cm)	Frequency
12.5-13.4	6
13.5-14.4	18
14.5-15.4	16
15.5-16.4	31
16.5-17.4	29
17.5-18.4	39
18.5-19.4	36
19.5-20.4	18
20.5-21.4	4
21.5-22.4	2
22.5-23.4	1
Grand total	200

Table 2: Length-weight relationships (LWR) of *A. sirm*

	N	LWR	r^2
Pooled	200	$W= 0.0030\ TL^{3.3459}$	0.9376
Male	105	$W=0.0029TL^{3.3546}$	0.9230
Female	95	$W=0.0035\ TL^{3.2819}$	0.9497

b = 3.207 for the pooled *A. sirm* in the Gulf of Mannar, which is similar to the b value obtained in the current study (3.345). However, in a study conducted in the the Bay of Bengal off Bangladesh, *A. sirm* showed an overall negative allometric growth (Rahman et al., 2025).

The mean values for total length, weight, and condition factor (K) for *A. sirm* (pooled, male, and female values) are shown in Table 3.

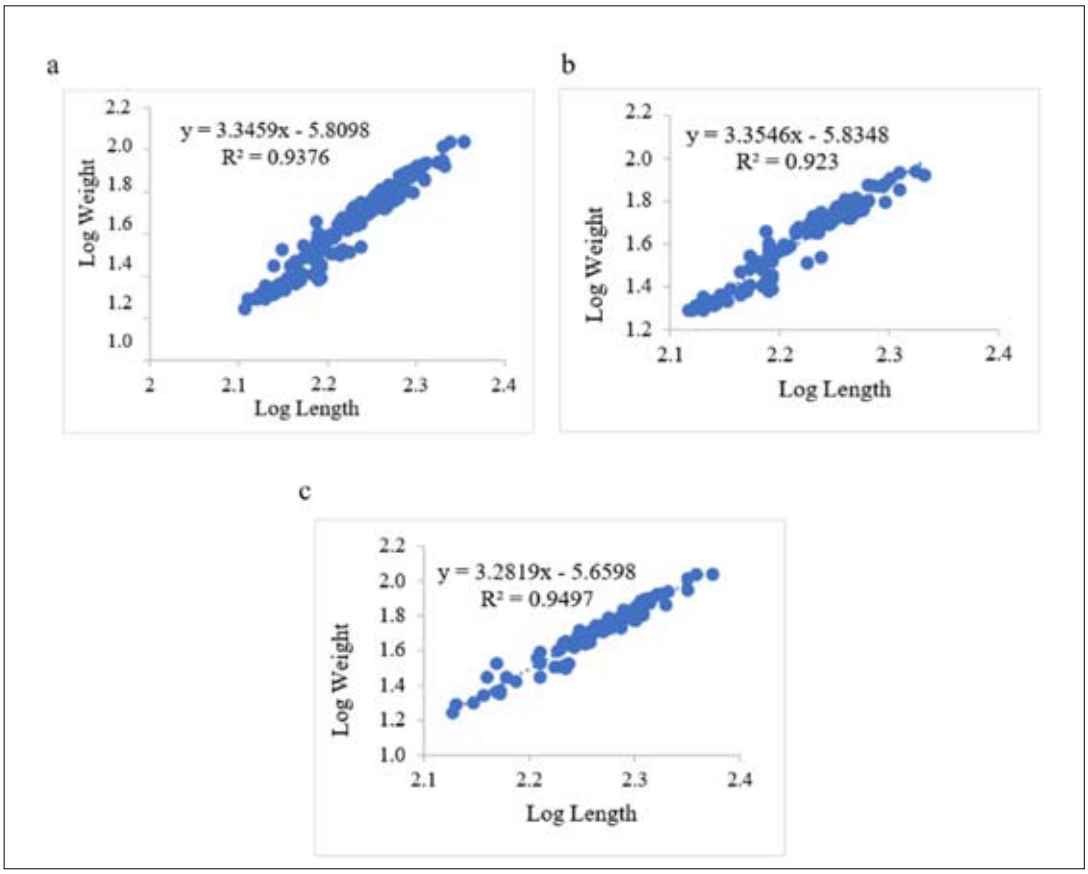

Figure 1: The plots of log weight (g) vs standard length (mm) of *A. sirm*: (a) pooled data, (b) males, and (c) females

Table 3: The mean values for total length, weight and condition factor (K) for *A. sirm*

	TL (cm)		Weight (g)		K
	Min - Max	Mean ± SD	Min - Max	Mean ± SD	Mean ± SD
Pooled	12.8 - 22.6	17.231 ± 2.037	17.5 -09.0	49.81±19.12	0.92331±0.09995
Male	13.1 - 21.5	16.809 ± 1.976	19.5-87.0	45.27±17.48	0.9047±0.1074
Female	12.8 - 22.6	17.697 ± 2.011	17.5-109.0	54.83±19.68	0.94392±0.08699

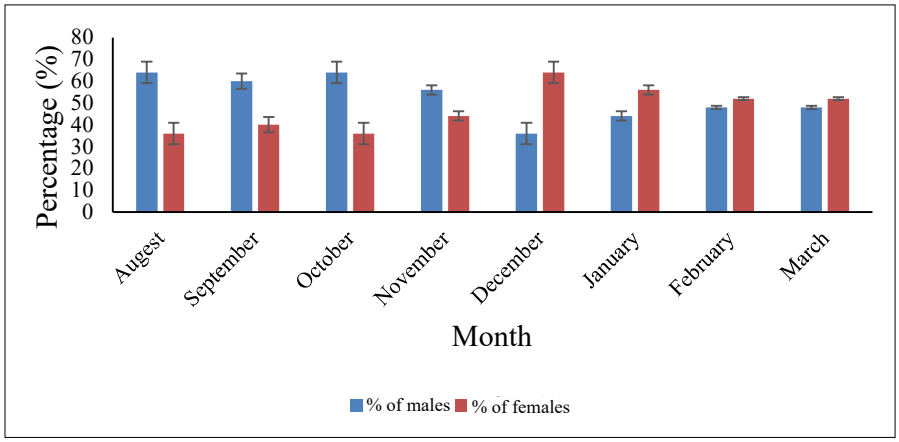

Figure 2: The percentage of males and females of *A. sirm* during August 2022 - March 2023

The Maximum length and the maximum weight of *A.sirm* recorded by Rahman et al. (2025) in the coastal waters of Bay of Bengal off Bangladesh were 30.5 cm and 142.56 g respectively. The asymptotic length of *A sirm* in the western coastal waters of Sri Lanka has been estimated to be 25.23 cm (Karunasinghe & Wijeyaratne, 1991b). Hence, the maximum length of *A. sirm* caught in the coastal waters of Bay of Bengal off Bangladesh is higher than the asymptotic length of this species in the western coastal waters of Sri Lanka. Different factors, such as sex, habitat, stomach fullness, gonadal maturity stage and ontogenetic development stage can make differences in the length weight relationship parameters of fishes.

The variation of the percentages of males and females of the *A. sirm* during the study period is shown in Figure 2. From August to November, the males were more abundant while the vice-versa was observed from December to March.

Earlier studies have shown that from January to April in 1984, May 1985 and in April, May and October in 1986, females were more abundant in the gillnet catches of the coastal fishery off Negombo, Sri Lanka (Karunasinghe & Wijeyaratne (1998). Nevertheless, statistical analysis has shown that it is not significantly different from 1:1 (Karunasinghe & Wijeyaratne (1998). Dayaratne (1984) reported that *A. sirm* in the western coastal waters off Sri Lanka breeds twice a year.

The condition factor can be used to get an idea about the physical and biological environment conditions, health, food reserves, feeding intensity, growth, and reproductive cycle of fish. Condition factor is affected by several factors, inclusing feeding intensity and gonad development (Jayakumar et al., 2022). In the present study, the mean condition factor ± SD for the males, females and for the pooled data were 0.9047±0.1074, 0.94392±0.08699 and 0.92331±0.09995 respectively. The mean condition factor of females was significantly higher than that of the males ($p<0.05$). Similar results have been recorded for *A. sirm* in the Andaman coastal waters in India (Devi et al., 2018). Results of the present study indicate that *A. sirm* stock in the coastal waters off Negombo is in good physical condition.

Stomach content analysis

Feeding is a major concern in the daily life of fish, and they use a large portion of their energy searching for food (Purusothaman et al., 2014). The number of fish and percentages for each category of stomach fullness are given in Table 4. Out of the 200 fish examined, 5% had a full stomach, 27.5% had three-quarter fullness, 12.5% had half fullness and 15% had quarter fullness while 40% had empty stomachs.

Table 4: The distribution of stomach fullness of *A. sirm* from the coastal waters off Negombo during the study period

Stomach fullness	Number of fish
Full	10
Three-fourth (3/4) full	55
Half (1/2) full	25
One-fourth (1/4) full	30
Empty	80
Total	200

Feeding intensity refers to the degree of feeding as indicated by the relative fullness of the stomach. It varies with seasonal changes, availability of preferred food items, maturity stage of the fish, and spawning season of the species (Khongngain et al., 2017). Stomach fullness indices and empty stomachs are important in assessing feeding intensity, which is negatively related to empty stomachs (Purusothaman et al., 2014).

The frequency of occurrence (%) for each food item is given in Table 5. The major food was crustaceans and their larvae (copepods, zoea larvae, nauplii) accounting for 25.51% followed by plankton accounting for 14.29%.

Synthetic fibers and unknown particles were also present in 2.6% and 4.1% of the stomachs analyzed respectively, which is evident for contamination of marine ecosystems by human-made materials. This can have detrimental effects on their physiology, growth, reproduction, and overall survival. Furthermore, synthetic materials can act as carriers of toxic substances, potentially magnifying the harmful effects on fish and other organisms in the food chain. The ingestion of these synthetic materials by fish poses a threat not only to their health but also to the overall ecological balance of marine habitats.

Table 5: Frequency of occurrence (%) of different food items consumed by *A. sirm*.

Prey item	Frequency of occurrence(%)
Plankton	14.29
Algae	1.53
Mollusk larvae	11.22
Crustacean larvae	25.51
Gastropod larvae	12.76
Fish eggs	15.31
Appendages	12.76
Synthetic fibers	2.55
Unknown particles	4.08

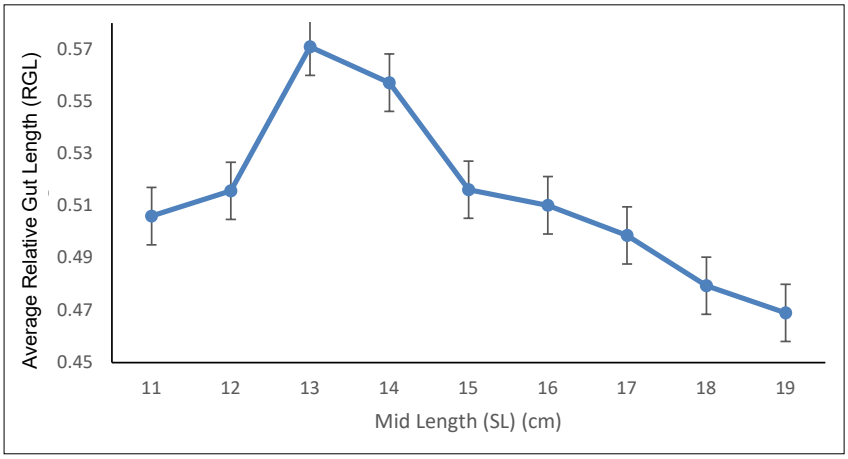

Figure 3: Variation of mean relative gut Length of different size classes (SL) (cm) of *A. sirm*

Relative gut length (RGL) and gastro somatic index (GaSI)

Variations of RGL and mean GaSI of different size classes are shown in Figures 3 and 4 respectively. The ranges of RGL and GaSI were 0.469-0.571 and 1.898-2.571 while their mean±SD values were 0.5137 ± 0.0110 and 2.2103 ± 0.0587 respectively.

RGL is used for classifying fish as carnivores, herbivores, and omnivores. These values are closely related to the presence of vegetable matter and animal matter in the diet. It increases with more vegetable matter and decrease with more animal matter in the diet (Dasgupta, 2004). In this study, the range of RGL was 0.469-0.571, with a mean ± SD of 0.5137 ± 0.0110. According to Karachle & Stergiou (2010), the RGL values are <1 when the fish are carnivorous, 1-3 when they are omnivorous and >3 when they are vegetarian. According to this criterion, *A. sirm* is a carnivore.

The GaSI is used to examine the feeding intensity of fish (Hynes 1950). The range of GaSI in this study was 1.898-2.571 with a mean ± SD value of 2.2103 ± 0.0587. The highest and the lowest feeding intensities were recorded the size classes of 17.5-18.5 cm and 12.5-13.5 cm respectively.

Heavy metal analysis of fish muscles of *A. sirm*

Mean concentrations (mg/Kg wet weight) of Cr, Zn, Cu, and Cd in the edible muscles of *A sirm* collected from Negombo coastal water are given in Table 6.

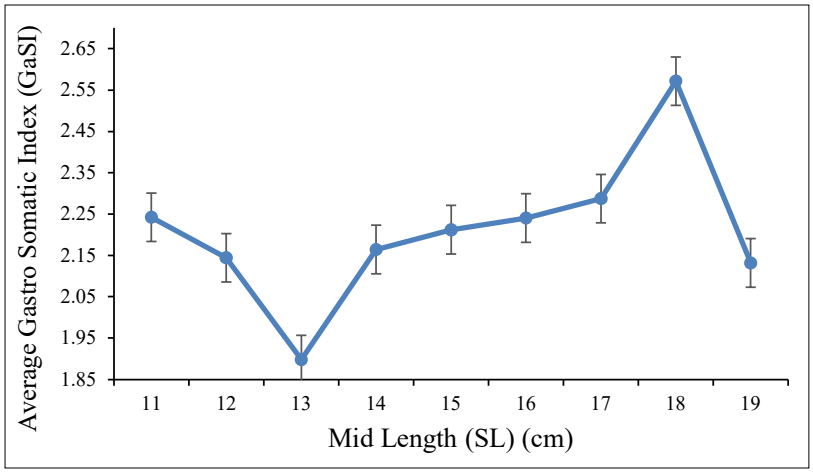

Figure 4: Variation of the mean gastro somatic index (GaSI) in different size classes (SL) (cm) of *A. sirm*

Table 6: Concentrations of heavy metals (mg/Kg wet weight) in *A. sirm*

Heavy metal	Mean ±SD (mg/Kg wetweight)	Minimum (mg/ Kg wet weight)	Maximum (mg/ Kg wetweight)	Maximum permissible level
Cr	10.07 ± 3.66	2.73	14.56	50
Zn	7.88 ±1.86	4.61	10.59	40
Cu	5.39 ± 0.08	5.29	5.57	30
Cd	0.52 ± 0.04	0.40	0.55	0.5

Table 7: Eigen analysis of the correlation matrix

Component	PC_1	PC_2	PC_3	PC_4	PC_5	PC_6	PC_7	PC_8
Eigenvalue	5.003	1.4141	0.9914	0.4895	0.0788	0.0122	0.0100	0.0016
Proportion	0.625	0.177	0.124	0.061	0.010	0.002	0.001	0.000
Cumulative	0.625	0.802	0.926	0.987	0.997	0.999	1.000	1.000

Table 8: Eigen vectors (coefficient in the linear combinations of variables making up PCs)

Variable	PC_1	PC_2	PC_3	PC_4	PC_5	PC_6	PC_7	PC_8
Total Length	0.440	0.043	0.031	-0.176	0.348	-0.329	0.262	0.689
Standard Length	0.438	0.050	0.041	-0.177	0.366	0.711	-0.362	-0.037
Head Length	0.318	0.065	0.320	0.890	-0.004	0.003	-0.003	0.011
Body Weight	0.433	0.043	0.119	-0.203	-0.514	-0.367	-0.597	-0.026
Gut Length	0.348	0.463	-0.285	-0.045	0.265	-0.296	0.225	-0.610
Weight of stomach contents	0.414	-0.209	-0.223	-0.054	-0.569	0.329	0.548	-0.019
RGL	-0.153	0.661	-0.497	0.178	-0.232	0.183	-0.153	0.388
Ga. SI	0.098	-0.543	-0.709	0.259	0.183	-0.146	-0.266	0.009

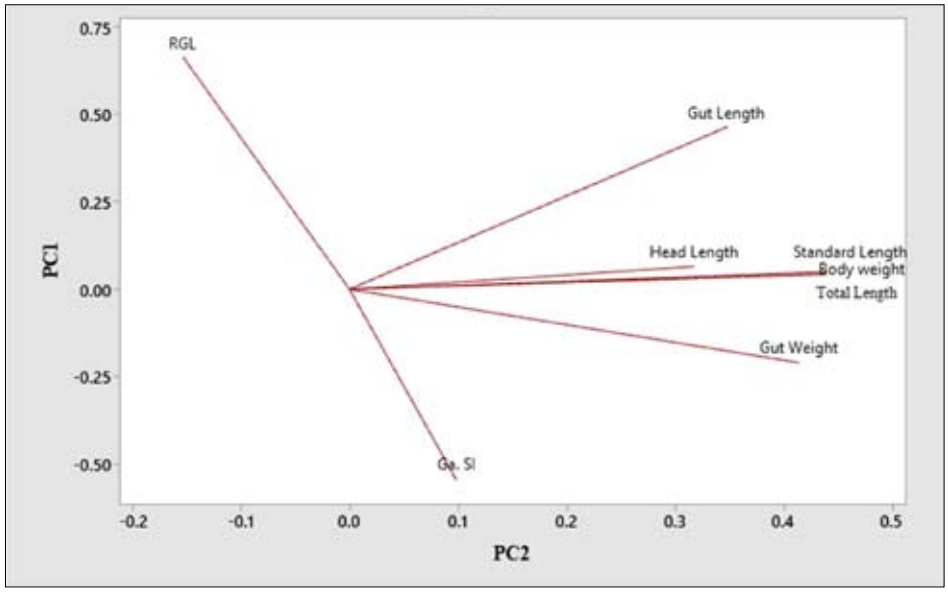

Figure 5: Loading plot of gut length, standard length, head length, total length, body weight, weight of stomach contents, gastro-somatic Index (GaSI), and relative gut length (RGL).

Principal component analysis (PCA) of various biometric traits

In the eigen analysis of the correlation matrix, only two eigen values were >1 (Table 7), which is a Kaiser criterion. Therefore, since most of the variables are captured in these two components, they are considered to be sufficient for further analysis.

The loadings of various variables on principal components (PCs), which provide insights into how each variable contributes to the underlying structure captured by these components, are given in Table 8. Loadings represent the correlation between variables and PCs, with higher absolute values indicating a stronger association. In this analysis, the total length, standard length, head length, body weight, gut length, and weight of stomach contents showed high positive loadings on PC1. This suggests that they are closely aligned with the structure represented by PC1 and are positively correlated with each other. Conversely, RGL is negatively loaded on PC1.

A loading plot of the 1st and 2nd PCs illustrates the relationship between the original variables and these two components. In this plot, each variable is represented as a vector, and the direction and length of the vector indicate the variable's contribution and direction of influence on the PCs. Figure 5 gives the coordinates and the intensity of each component based on the standardized PC scores and the first two components. As Figure 5 suggests, the variables of standard length, total length, gut length, head length, body weight, and weight of stomach contents are closer to each other than RGL and GaSI.

The biplot given in Figure 6 provides coordinates of each observation and variable based on the rotation (loading) of the first two components. The shorter distance between the two observations of standard length, total length, gut length, head length, body weight, and weight of stomach contents indicates higher similarities between them.

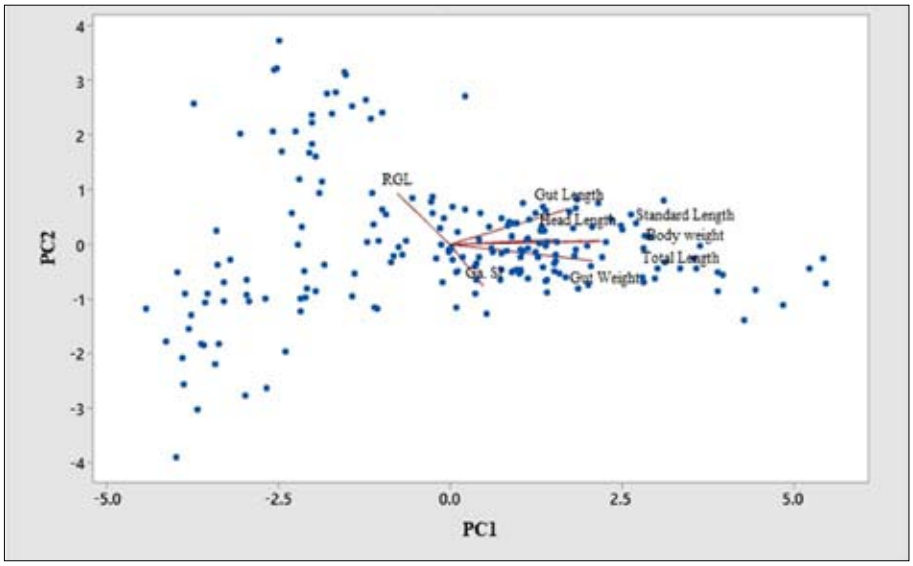

Figure 6: Biplot of gut length, standard length, head length, total length, body weight, weight of stomach contents, gastro-somatic index (GaSI) and relative gut length (RGL).

According to the PCA, variables such as total length, standard length, head length, body weight, gut length, and weight of the stoch contents were positively associated with each other.

The presence of toxic heavy metals in fish muscles can diminish the advantageous properties with adverse effects on human health (Castro-Gonzales & Mendez-Armenta, 2008). Heavy metals include both biologically essential (e.g. Cu and Zn) and not essential metals (e.g. Cd) (Kennish, 1998). According to this study, the mean concentrations of Cr, Zn, Cu and Cd (mg/kg wet weight) in edible muscles of *A. sirm,* are 10.07 ± 3.66, 7.88 ± 1.86, 5.39 ± 0.08 and 0.52 ± 0.04 respectively. These values did not exceed the maximum permissible limits recommended by the FAO and WHO (FAO, 1983;

FAO/WHO 2009). Therefore, these fish are suitable for human consumption.

CONCLUSION

The *A. sirm* stock in the western coastal waters of Sri Lanka has been found to be overharvested and it has been suggested to use the gillnets of >25 mm mesh size (Karunasinghe and Wijeyaratne (1995). During the present study, it was found that the mesh size of the gillnets used in this fishery is 1¼ inches (31.8 mm) and 1½ inches (38.1 mm), which are >25 mm of mesh size. This shows that the recommendations made through scientific studies are very important to maintain the sustainable utilization of the resources.

A. sirm stock in the coastal waters off Negombo showed a positive allometric growth, with fish being in good physical condition. The mean condition factor of females (0.9439 ± 0.8699) was higher than that of males (0.9047 ± 0.1074).

The most preferred food item was crustacean larvae. The frequency of occurrence of synthetic material in stomach contents was 2.55%. This can affect their physiology, growth, reproduction, and overall survival. The RGL of the fish was <1, indicating that this species is carnivorous. The GaSI showed the different feeding intensities in different length classes.

The Cr concentration was observed to range from 2.73 mg/Kg to 14.56 mg/Kg with a mean value of 10.07 ± 3.66 mg/Kg. According to WHO (1989), the maximum permissible limit (MPL) for Cr is 50.0 mg/Kg. The mean Zn concentration was observed to be 7.88±1.86 mg/Kg, with a range of 4.61-10.59 mg/Kg. According to FAO/WHO (2009), MPL of Zn is 40 mg/Kg. The mean Cu concentration was observed to be 5.39 ± 0.08 mg/Kg with a range of 5.29-5.57 mg/Kg. According to the FAO/WHO (2009), MPL of Cu is 30 mg/Kg. The mean Cd concentration was observed to be 0.52 ± 0.04 mg/Kg, with a range of 0.40-0.55 mg/Kg. According to FAO/WHO (2009), the MPL of Cd is 0.5 mg/Kg Therefore the present study indicates that the concentration of Cr, Zn, Cu and Cd in the edible parts of the fish indicated safe levels for human consumption (WHO, 1989; FAO/WHO, 2009).

Acknowledgement

The authors gratefully acknowledge the Department of Zoology and Environmental Management, University of Kelaniya for providing research facilities and the fishermen in the Negombo Sea Street landing site for providing fish samples.

REFERENCES

Abdussamad, E. M., Pillai, N. G. K., Habeeb Mohammed, O. M. M. J. & Jayabalan, K. (2010). Sardines of the Gulf of Mannar ecosystem-fishery and resource characteristics of major species. *Indian Journal of Fisheries 57*(4), 7-11.

Al-Hussaini, A. H. (1949). On the functional morphology of the alimentary tract of some fish in relation to differences in their feeding habits: anatomy and histology. *Journal of Cell Science 90*(10), 109–139.

Ali, S.S.R., Abdhakir, E.S. & Muthukkaruppan, R. (2020). Proximate and mineral composition of commercially important marine fin fishes from the Kasimedu fish landing centre, Chennai. *Journal of Fisheries and Life sciences 5*(1), pp.20-25.

Bandaranayake, K.H.K., Gunasekara, S.S., Haputhantri, S.S.K. & Jayasinghe, R.P.P.K., (2024). Some warning signs detected in coastal pelagic fisheries of the west coast of Sri Lanka: Declining trend of Amblygaster sirm suggesting the need for immediate management initiatives. *Sri Lanka Journal of Aquatic Sciences 29*(1), pp.31-41. https://doi.org/10.4038/sljas.v29i1.7613

Ceyhan, T., Akyol, O. & Erdem, M. (2009). Length-Weight Relationships of Fishes from Gökova Bay, Turkey (Aegean Sea). *Turkish Journal of Zoology 33*(1), 69-72 https://doi.org/10.3906/zoo-0802-9

Dasgupta, M. (2004) Relative length of the gut of some freshwater fishes of West Bengal in relation to food and feeding habit. *Indian Journal of Fisheries 51*(3), 381-384

Dayaratne, P. (1984). *Fisheries Biology of some small pelagic fish species (Clupeoids) from the west coast of Sri Lanka*, PhD Tesis, University of Bergen, Norway.

Devi, S. M., Jaiswar, A. K., Kumar, R., Ali, M., Velakkandy, S., Shirke, S. S., Jahageerdar, S. & Chakraborty, S. K. (2018). Biometric Studies on Spotted Sardinella *Amblygaster sirm* (Walbaum, 1792) (Pisces: Clupeidae) Occurring along Andaman Coast, India. *Indian Journal of Geo-Marine Sciences 47*(1), 135–140.

El-Moselhy, K. M., El-Sherbiny, I. M., El-Azem, H. A. & El-Metwally, M. E. A. (2014). Bioaccumulation of heavy metals in some tissues of fish in the Red Sea, Egypt. *Egyptian Journal of Basic and Applied Sciences 1*(2), 97–105. https://doi.org/10.1016/j.ejbas.2014.06.001

FAO. (1983) Compilation of legal limits for hazardous substances in fish and fishery products. FAO Fishery Circular No. 464. Food and Agriculture Organization, pp. 5e100.

FAO/WHO (2009) Evaluation of Certain Food Additives and Contaminants: Sixty-Ninth Report of the Joint FAO/WHO Expert Committee on Food Additives; World Health Organization: Geneva, Switzerland, 2009.

Gulland, J.A. (1969). Manual of Methods for Fish Stock Assessment Part I – Fish Population Analysis. FAO Manuals in Fisheries Science *4*. 154 p.

Hynes, H.B.N. (1950) The food of freshwater sticklebacks (*Gasterosteus aculeatus* and *Pygosteus pungitius*) with a review of methods used in studies of the Food of Fishes. *Journal of Animal Ecology 19*, 36-58. https://doi.org/10.2307/1570

Jayakumar, T. T., Lal, K. K., Murali, S., Mary, A. A., Kumar, T. A., Mishra, A. & Singh, M. (2022). The biology of a newly discovered sardine: Length-weight relationship and condition factor of Amblygaster indiana Mary, Balasubramanian, Selvaraju & Shiny, 2017 from the South-west coast of India. *Indian Journal of Geo-Marine Sciences (IJMS) 51*(01), 104-107.

Jayasuriya, P. (2007). Some aspects of the biology and population dynamics of *Amblygaster sirm* (Walbaum) from the west coast of Sri Lanka. *National Science Foundation of Sri Lanka 17*(1), 53. https://doi.org/10.4038/jnsfsr.v17i1.8241

Karachle, P. K. & Stergiou, K. I. (2010). Intestine Morphometrics of Fishes: A Compilation and Analysis of bibliographic data. *Acta Ichthyologica Et Piscatoria 40*(1), 45–54. https://doi.org/10.3750/aip2010.40.1.06

Karunasinghe, W.P.N. & Wijeyaratne, M.J.S. (1991a). Selectivity estimates for *Amblygaster sirm* (Clupeidae) in the small-meshed gill net fishery on the west coast of Sri Lanka. *Fisheries Research 10*, 199-205.

Karunasinghe, W.P.N. & Wijeyaratne, M.J.S. (1991b). Population dynamics of the trenched sardine *Amblygaster sirm* (Clupeidae) in the western coastal waters of Sri Lanka, *Asian Fisheries Science 4*, 329-334.

Karunasinghe, W.P.N. & Wijeyaratne, M.J.S. (1995). Studies on the exploitation of trenched sardine Amblygaster sirm (Walbaum) off Negombo coast, *Journal of the National Science Council, Sri Lanka 23*(1), 1-7.

Karunasinghe, W.P.N. & Wijeyaratne, M.J.S. (1996). Effects of monsoonal currents, rainfall and lunar phase on the abundance of *Amblygaster sirm* in the coastal waters off Negombo, Sri Lanka, *Sri Lanka Journal of Aquatic Sciences 1*, 53-58.

Karunasinghe, W.P.N. & Wijeyaratne, M.J.S. (1998). Reproductive Biology of the Trenched sardine *Amblygaster sirm* (Walbaum) from the western coastal waters of Sri Lanka, *Ceylon Journal of Science (Bio Science) 25*, 35-49.

Khongngain, O., Das, S. K. & Bhakta, D. (2017). Study on food and feeding biology of *Trichogaster fasciata* Bloch & Schneider, 1801 from a wetland of Nadia district of West Bengal. *Journal of the Inland Fisheries Society of India 49*(2), 03-09.

Lizama, M. A. P. & Ambrósio, A. M. (2002). Condition factor in nine species of fish of the Characidae family in the upper Paraná River floodplain, Brazil. *Brazilian Journal of Biology 62*(1), 113–124. https://doi.org/10.1590/s1519-69842002000100014

Mahesh, V., Gop, A. & Nair, R.J. (2018) Stomach content analysis techniques in fishes. In: Nair, R. J., Gop, A. P. & Mahesh, V. (Eds.) Recent advancesin fishery biology techniques for biodiversity evaluation and conservation. Kochi, India: *Central Marine Fisheries Research Institute*, pp. 104–115.

Medeiros, R. F., Santos, L. M. G. D., Freire, A. S., Santelli, R. E., Braga, A. C., Krauss, T. F. & Jacob, S. D. C. (2012). Determination of inorganic trace elements in edible marine fish from Rio de Janeiro State, Brazil. *Food Control 23*(2), 535–541. https://doi.org/10.1016/j.foodcont.2011.08.027

Mookerjee H. K, Gupta S. N. S. & Choudhury P. K. R (1946) Food and its percentage composition of the adult food fishes of Bengal. *Science and Culture 12*, 247-249

Osman, Y. a. A., Mansour, E., El-Mahdy, S. & Mohammad, A. S. (2021). Age, growth and management of *Amblygaster sirm* (Walbaus, 1792) from the Red Sea, Egypt. *Egyptian Journal of Aquatic Biology and Fisheries 25*, 819–835

Purusothaman, S., Silambarasan, A., Jayaprabha, N. & Murugesan, P. (2014). Feeding strategies and diet composition of oil sardine Sardinella longiceps Valenciennes 1847 in the trawl bycatches off Parangipettai, southeast Coast of India. *Asian Fisheries Science*, *27*, 137-148.

Thivviyan, S. & Jayakody, D. (2017). Assessment on the present status of coastal fisheries at Gurunagar, Jaffna. *Vingnanam Journal of Science 12*(1-2), 18-31, https://doi.org/10.4038/vingnanam.v12i1-2.4121

WHO (1989). Health Criteria Other Supporting Information, Guidelines for Drinking Water Quality, 2nd ed.; WHO: Geneva, Switzerland, 1989.

J.Natn.Sci.Foundation Sri Lanka 2025 53 (4): 459 - 464
DOI: http://dx.doi.org/10.4038/jnsfsr.v53i4.12583

RESEARCH COMMUNICATION

Plant Pathology

First report of rubber circular leaf spot disease pathogen *Colletotrichum siamense* Prihastuti, L. Cai & K.D. Hyde in *Cinnamomum zeylanicum* blume in Sri Lanka

AHMNR Aberathne, THPS Fernando* and EADD Siriwardena
Department of Plant Pathology and Microbiology, Rubber Research Institute of Sri Lanka, Agalawatta, Sri Lanka.

Submitted: 03 March 2025; Revised: 12 December 2025; Accepted: 29 December 2025

Abstract: *Cinnamomum zeylanicum,* a member of the family Lauraceae, is commonly grown as an intercrop in Sri Lankan rubber plantations to provide additional income for growers. However, diseases affecting intercrops pose a potential threat to rubber, as pathogens may spread between host species and increase economic losses. This study aimed to identify potential pathogens associated with diseased cinnamon leaves. Leaf samples collected from lesion margins were surface sterilized and cultured on potato dextrose agar (PDA). Distinct fungal colonies were sub-cultured, and ten morphologically different isolates were purified through single-spore isolation. Pathogenicity tests were conducted according to standard procedures to establish Koch's postulates. The most virulent isolate was selected for morphological characterization and molecular identification using bi-directional sequencing of the ITS gene region. The pathogen was identified as *Colletotrichum siamense* (WDCM accession number RRISL87), which showed high pathogenicity on both cinnamon and rubber leaves. This study represents the first report of *C. siamense* infecting cinnamon and highlights the importance of further pathogen identification to strengthen quarantine measures and improve disease management strategies.

Keywords: *Cinnamomum zeylanicum*, circular leaf spot disease, *Colletotrichum siamense, Hevea brasiliensis.*

INTRODUCTION

The genus *Colletotrichum* comprises some of the most successful plant pathogenic species, causing significant economic damage to crops in tropical, subtropical, and temperate regions (Batureine, 2009). They can cause a wide range of disease symptoms including die-back, leaf spots, seedling blight, and leaf blight in almost all parts of a variety of economically important crops, which include vegetables, cereals, legumes, fruits, and even ornamental plants (Cai *et al.*, 2009). *Cinnamomum zeylanicum*, a member of the Lauraceae family is the hardiest spice tree. The inner bark of plants is used as a spice. It has been used for cooking, where it improves the flavour of foods. They are evergreen trees, which are mainly cultivated for their dried inner bark (Ravindran, 2003).

Because of its significant economic returns and proven health-promoting properties, cinnamon has become a strategically important intercrop that is rapidly expanding within Sri Lankan rubber plantations. The leaf spots/blight caused by a fungus, *Colletotrichum* spp., is found in almost all cinnamon growing areas in Sri Lanka mainly affecting the foliage (Rajapakse *et al*., 2007). The pathogens that infect cinnamon plants may similarly affect rubber plantations and vice versa. Hence, the pathogens in the alternative hosts can cause cross-infections in rubber plantations, leading to economic drawbacks.

Natural rubber plays a significant role in the Sri Lankan economy. Due to the numerous uses natural

* Corresponding author (sarojinifernando787@gmail.com; https://orcid.org/0000-0002-4524-5445)

This article is published under the Creative Commons CC-BY-ND License (http://creativecommons.org/licenses/by-nd/4.0/). This license permits use, distribution and reproduction, commercial and non-commercial, provided that the original work is properly cited and is not changed in anyway.

rubber products, humans have enhanced their mobility and daily activities through the utilization of these products in automotive and aircraft tires, water transportation, medical equipment, footwear, adhesives, and toys.

Latex production in rubber plantations can be reduced due to biotic and abiotic stresses. Among them, pathogenic diseases play a significant role and more than 60 pathogens have been recorded, which are capable of causing rubber plant diseases in Sri Lanka (Jayasinghe, 2010). Some pathogens can attack more than one host plant. When the pathogens attack the inter-crops of rubber plantations, the severity of the disease increases. Hence, identification of alternative hosts is important in order to safeguard the inter-crop as well as the main crop. The current study mainly focuses on the isolation and identification of the pathogens from cinnamon plants grown in rubber plantations as an inter-crop. This study aimed to identify *Cinnamomum zeylanicum* as an alternative host for *Colletrotrichum siamense* the main cause of circular leaf spot disease of rubber in Sri Lanka.

MATERIALS AND METHODS

Collection of leaf samples

Symptomatic leaves with brown colour lesions from cinnamon plants grown within the rubber plantations were identified. They were collected following a completely randomized design (CRD), and brought to the Plant Pathology and Microbiology laboratory in the Rubber Research Institute of Sri Lanka (RRISL) for pathogen isolation.

Isolation of pathogen

Under the cleaned laminar flow cabinet diseased leaf samples were cut into small pieces of 2 x 2 mm, from the advancing margin of lesions. Leaf pieces were surface sterilized with 70% alcohol for 2 minutes and rinsed three times with a sterile distilled water series. Finally, they were dried out using a sterilized filter paper. Surface sterilized leaf pieces were placed on the solidified PDA and incubated at 27 ^{0}C for 3 days (Hunupolagama *et al*., 2017). The different mycelia arising from the diseased tissues were sub-cultured into a new series using PDA and 10 morphologically different cultures were selected.

Single spore isolation

Single spore isolation was performed to obtain pure cultures from the sub-cultures. One sporulated mycelial plug from a 7 day old culture was cut by a 5 mm cork-borer and added to 10 mL of sterilized distilled water in a sterilized McCartney bottle. It was mixed well and 50 µL of each culture was added to a separate PDA plate. The suspension was spread throughout the PDA surface using a glass spreader. The plates were incubated for 3 days at 27 ^{0}C in the culture room. Germinating spores were transferred to new PDA plates and incubated for 3 days at 27 ^{0}C (Choi *et al*., 1999) to obtain pure cultures.

Proving Koch's postulates

The cinnamon plants were artificially inoculated with a 1x10^5 conidia/mL spore suspension of 7-day old *C. siamense* cultures. The plants were kept in a moist chamber lined with moistened papers and the spraying of the spore suspension was undertaken every other day. The pathogen was successfully re-isolated from the symptomatic inoculated plants and subsequently identified, confirming the fulfillment of Koch's postulates.

Comparison of pathogenicity

Each conidial (1x10^5 conidia/mL) suspension was prepared from ten-day-old isolate cultures by re-suspending the conidia with 10 mL of sterilized distilled water per culture and conidial concentration was adjusted using a haemocytometer. Then, six rubber leaves belonging to the RRIC 121 clone, at the maturity stage between copper brown colour and apple green colour, were inoculated by placing 06 drops of the conidial suspension per leaf (20 µL per drop) of each culture. They were applied to the upper surface of the detached rubber leaves without wounding. Another six leaves were maintained as the control by placing drops of sterilized distilled water. The same experiment was repeated three times. The inoculated leaves were incubated in a moist chamber at 28 °C and the symptoms were observed after 2 days from the spore inoculation (Lin *et al*., 2017). Disease severity was assessed using a 0–4 scale, based on a modified version of the method described by Ma & Michailides (2002).

0 - No visible infection
1 - Light lesion around inoculation point lacking spores
2 - Large dark lesion without sporulation
3 - Large lesion and weak sporulation
4 - Very strong sporulation on the upper and lower surfaces of the leaf

The results were expressed as the disease index (DI) for each leaf which was calculated using the following formula (Ma & Michialides, 2002).

$$DI = \left(\sum_{i=0}^{4} N \times i\right) / \sum_{i=0}^{4} N$$

Where,
i is the severity (0–4), and
N is the number of leaves with the severity of i.

The *DI* for each leaf in each isolate was calculated using a modified method described in Ngobisa et al., (2013). The most pathogenic culture was selected for further studies.

Morphological analysis

Observation of reproductive characteristics

Reproductive characteristics such as conidia size, shape, and mycelial characters were observed under an Olympus light microscope with the addition of lacto phenol-cotton blue as the stain.

Observation of cultural characteristics

A mycelial plug was cut from the growing edge of each 7 day old colony using a 5 mm cork-borer and transferred on to the middle of a pure PDA plate. Cultural characters such as shape, elevation, nature, margin and pigmentation were recorded after 10 days of incubation under normal light and dark conditions at room temperature (27±2 °C).

Molecular level identification

Pure cultures of the selected isolate were prepared and submitted to Macrogen (Korea) via Genetech (Sri Lanka) for bi-directional Sanger sequencing of the internal transcribed spacer (ITS) gene region. Genomic DNA was extracted using the cetyltrimethylammonium bromide (CTAB) method, and PCR amplification of the ITS region was carried out using the primers ITS1 and ITS4.

RESULTS AND DISCUSSION

Brown circular lesions were observed on the cinnamon leaves. The lesion enlarges with time making a silvery area in the middle (Figure 1). Out of the 10 isolates, only *Colletrotrichum* sp. showed the pathogenicity for cinnamon (Koch's postulates proven) and on rubber leaves under the detached leaf assay (Figure 2). All the resulting *Colletotrichum* sp. isolated were morphologically determined as the same species. Based on the sequencing results, the isolate was identified as *Colletrotrichum siamense* (WDCM accession number RRISL87). The colony had a circular shape, flat elevation, smooth and cloudy nature, entire margin, and opaque nature. However, both upper and lower surfaces were pale white in colour with orange colour conidiomata arranged in rings. Conidia were aseptate with a single cell, green colour, smooth-walled, cylindrical, with both ends rounded, and granular. The conidia size was (13-16) x (4-6) µm. Conidiophores were directly formed from hyphae which were septate and branched. The mycelium of the culture was septate and branched with a width of 4-6 µm (Figure 1).

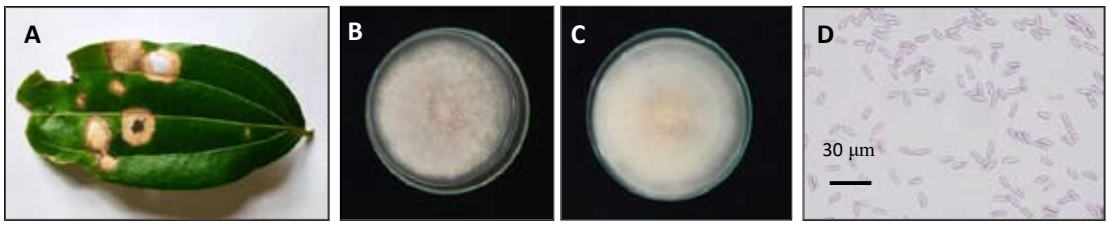

Figure 1: A: Symptomatic Cinnamon leaf; B: Upper surface of 7-day old culture grown on PDA medium; C: Lower surface of 7-day old pathogenic culture grown on PDA medium; D: Cylindrical conidia with rounded ends

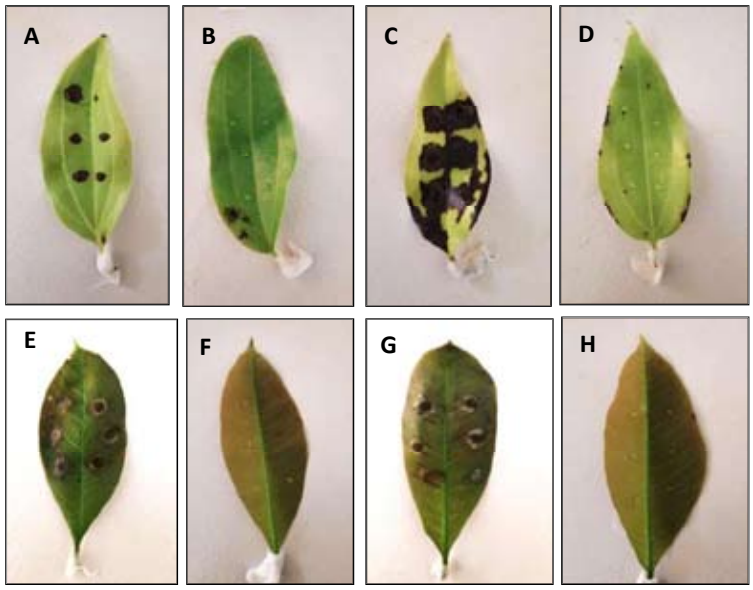

Figure 2: A: Non-wounded cinnamon leaf inoculated with *Colletotrichum siamense*; B: Non wounded cinnamon leaf inoculated with sterilized distilled water (non-wounded control); C: wounded cinnamon leaves inoculated with *C. siamense* D: wounded cinnamon leaves inoculated with sterilized distilled water (wounded control); E: Non-wounded rubber leaves inoculated with *C. siamense*; F: Non wounded rubber leaves inoculated with sterilized distilled water (non-wounded control); G: wounded rubber leaves inoculated with *C. siamense*; H: wounded rubber leaves inoculated with sterilized distilled water (wounded control).

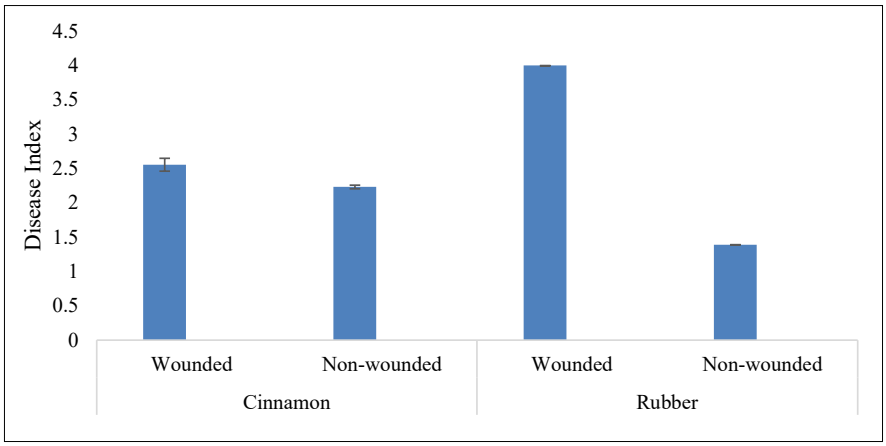

Figure 3: Disease index on the assessment of cross-infection possibility (Error bars indicate variability among replicates)

In rubber, *Colletotrichum gloeosporioides* was identified as the main causative agent of CLD (Petch, 1906) as well as in cinnamon. Later, *C. acutatum* was identified as the main cause of Colletotrichum leaf disease of rubber (Jayasinghe *et al*., 1997). Recently, *C. simmondsii, C. laticiphilum, C. nymphaeae,* and *C. citri* were identified as

the pathogens of rubber (Hunupolagama *et al.*, 2017). The leaf spots/blight caused by the fungus *C. gloeosporioides* (Anandaraj & Devashayam, 2004) is found in almost all cinnamon growing areas in Sri Lanka mainly affecting the foliage. Moreover, *C. horii* has been previously identified as a pathogen of *Cinnamomum zeylanicum* (Madhurangi *et al*., 2022). Hence, the identification of *C. siamense* as a pathogen in cinnamon with 93.14% identity in NCBI BLAST results, becomes the first report in Sri Lanka. The confirmation of *C. siamense* pathogenicity on cinnamon highlights a potential phyto pathological risk within cinnamon–rubber intercropping systems (Figure 3). Since rubber (*Hevea brasiliensis*) and cinnamon (*Cinnamomum zeylanicum*) are grown in close proximity, there is a plausible risk that pathogens affecting cinnamon could serve as alternate hosts or reservoirs, potentially facilitating cross-infection or increasing the inoculum load in the plantation. While *C. siamense* is primarily a cinnamon pathogen, its presence in intercrops may create conditions conducive to disease spread under favorable environmental conditions, such as high humidity (Hyde *et al*., 2009). Consequently, careful monitoring and integrated disease management strategies are recommended to minimize potential transmission and safeguard the health of both cinnamon and rubber crops. It is understood that a detailed study is much needed for accurate characterization of the current causative agents of this disease as the information is important for the establishment of causative pathogens, screening chemicals, and resistance breeding and also to formulate effective management practices.

CONCLUSION

According to the results of this study, *Colletotrichum siamense* was identified as a new pathogen of *Cinnamomum zeylanicum*, one of the most valuable spice crops that can be cultivated as an intercrop with rubber. However, further detailed characterization and identification are essential for the development and implementation of effective management strategies. For future studies, it is recommended to employ a multilocus molecular approach, as ITS sequencing alone may not provide sufficient resolution for accurate species-level identification within the *Colletotrichum* genus. Additionally, comprehensive assessments of disease severity across different seasons and geographical regions are necessary to evaluate the epidemiological risk and to design location-specific management practices. Such studies will provide a robust basis for minimizing potential yield losses and ensuring the sustainability of cinnamon–rubber intercropping systems.

Acknowledgement

Financial assistance by the Ministry of Plantation and Community Infrastructure is gratefully acknowledged.

REFERENCES

Anandaraj, M., & Devasahayam, S. (2004). Pests and diseases of Cinnamon and Cassia. In: Cinamon and cassia. (Eds. P. N. Ravindran, K. N. Babu and M. Shylajah), *CRC Press, New York,* 239-258.

Batureine, M. (2009). Diversity of *Colletotrichum lindemuthianum* and Reduction of common bean germplasm to anthracnose disease. *MSc thesis submitted to the school of post graduate studies, Makerere University, Uganda.*

Cai, L., Hyde, K., Taylor, P., Weir, B., Waller, J., Abang, M., Zang, J., Yang, Y., Phoulvong, S., Liu, Z., Prihastuti, H., Shivas, R., McKenzie, E., & Johnston, P. (2009). A polyphasic approach for studying *Colletotrichum*. *Fungal Diversity*, *39*, 183–204.

Choi, Y., Hyde, K., & Ho, W. (1999). Single spore isolation of fungi. *Fungal Diversity, 3*, 29-38.

Hunupolagama, D., Chandrasekaran, N., Wijesundera, W., & Kathriarachchi, H. (2017). Unveiling members of *Colletotrichum acutatum* species complex causing Colletotrichum leaf disease of *Hevea brasiliensis. Current Microbiology*. *74*, 747-756. DOI: 10.1007/s00284-017-1238-6

Hyde, K. D., Cai, L., Cannon, P. F., Crouch, J.L. *et al.* (2009). *Colletotrichum* – names in current use. *Fungal Diversity 39*, 147-182.

Jayasinghe, C.K., Fernando, T.H.P.S., & Priyanka, U.M.S. (1997).. *Colletotrichum acutatum* is the main cause of *Colletotrichum* leaf disease of rubber in Sri Lanka. *Mycopathologia 137*, 53–56. DOI: 10.1023/A:1006850119146

Jayasinghe, C. (2010). White root disease of the rubber tree: an overview. *Paper presented at the proceedings of the International workshop on White root disease of* Hevea *rubber*, 1-8. https://doi.org/10.1111/efp.12794

Lin, C., Liu, X., Shi, T., Li, C., & Huang, G. (2017). The *Colletotrichum gloeosporioides* perilipin homologue CAP 20 regulates functional appressorial formation and fungal Virulence. *Journal of Phytopathology*, *166*, 216-225. https://doi.org/10.1111/jph.12678

Ma, Z., & Michialides, T. (2002). Characterization of *Botryosphaeria dothidea* isolates collected from pistachio and other plant host in California. *Phytopathology*, *92*, 519−526. DOI: 10.1094/PHYTO.2002.92.5.519

Madhurangi, H. M. T. T., Wanigatunge, R.P., Jayasinghe, G.G., & Attanayake, R.N. (2022). Identification of the fungal pathogen causing leaf blight of *Cinnamomum zeylanicum* Blume and *in vitro* screening of Tebuconazole sensitivity. *Plant Health- The Second National Symposium of Sri Lanka Association for Mycology and Plant Pathology (SLAMPP),* 18.

Ngobisa, A., Abidin, M., Wong, M., & Noordin, M. (2013). *Neofusicoccum ribis* Associated with Leaf Blight on Rubber (*Hevea brasiliensis*) in Peninsular Malaysia. *Plant Pathology Journal*, *29*(1), 10-16. DOI: 10.5423/PPJ.OA.07.2012.0110

Petch, T. (1906). Description of new Ceylon fungi. *Annual Report of Botanical Gardens*, *Peradeniya*, *3*, 1-10.

Rajapakse, R. H. S., & Wasantha Kumara, K. L. (2007) A Review of Identification and Management of Pests and Diseases of Cinnamon (*Cinnamomum zeylanicum* Blume). *Tropical Agricultural Research & Extension, 10*, 2007. DOI: 10.4038/tare.v10i0.1864

Ravindran, P. N., Shylaja, M., Babu, K. N., & Krishnamoorthy, B. (2003). Botany and crop improvement of cinnamon and cassia. In *Cinnamon and cassia,* CRC Press. 30-95.

List of Referees- Volume 53 (2025)

Prof. A. Abeysekera
Dept. of Chemistry
University of Sri Jayewardenepura

Dr Waranatha Abeygunasekara
Dept. Electrical and Electronic Engineering
Univ. of Peradeniya

Prof. Sunil Abeyrathne
Dept. Electrical and Electronic Engineering
Univ. of Peradeniya

Dr Sachith P. Abeysundara
Dept. of Statistics and Computer Science
Univ. of Peradeniya

Dr Supunmali Ahangama
Dept. of Information Technology
Univ. of Moratuwa

Dr Ruwanga Amarasinghe
Faculty of Technology
Sri Lanka Technology Campus

Prof. Mala Amarasingha
Dept of Botany
Univ. of Kelaniya

Prof. Deepika Amarasingha
Dept. of Zoology and Environmental Management
Univ. of Kelaniya

Dr Melanie Amarasooriya
Dept. of Medical Technology
Univ. of Moratuwa

Prof. A.D. Ampitiyawatta
Dept. of Export Agriculture
Sabaragamuwa University of Sri Lanka

Dr Udara Arachchige
Dept. of Mechatronic and Industrial Engineering
National School of Business Management (NSBM)

Prof. Ludula Vidanagama Arachchige
Dept. of Electrical Engineering
Univ. of Moratuwa

Prof. Vasanthy Arasaratnam
Dept. of Biochemistry
Univ. of Jaffna

Dr. Malima Atapattu
Dept. of Statistics & Computer Science
Univ. of Peradeniya

Prof. Renuka Aththanayaka
Dept. of Plant & Molecular Biology
Univ. of Kelaniya

Prof. H.H. Asanthi
Dept. of Limnology and Water Technology
Univ. of Ruhuna

Prof. Abhaya Balasooriya
Dept. of Plant Science
Rajarata University of Sri Lanka

Prof. Chathuranga Bamunuarachchige
Dept. of Bioprocess Technology
Rajarata University of Sri Lanka

Dr Janaka Bamunawala
Tohoku University
Japan

Prof. R.M.A.S. Bandara
Dept. of Livestock Production
Sabaragamuwa University of Sri Lanka

Prof. B.F.A. Basnayake
Dept. of Agricultural Engineering
Univ. of Peradeniya

Dr J.A.P. Bodhika
Dept. of Physics
Univ. of Ruhuna

Dr S. B. Barbuddhe
ICAR - National Meat Research Institute
India

Dr A.W.S. Chandana
Dept. of Sports Sciences and Physical Education
Sabaragamuwa University of Sri Lanka

Dr A. W. S. Chandana
Faculty of Applied Science
Sabaragamuwa University of Sri Lanka

Prof. S. Chakrewarthy
Dept. of Biochemistry and Clinical Chemistry
Univ. of Kelaniya

Dr Nadeeka Chandraratne
Dept. of Community Medicine
Univ. of Colombo

Prof. C. Christopher Columbus
School of Computer Science Engineering (SCOPE) Vellore Institute of Technology
India

Dr Asitha T. Cooray
Dept. of Chemistry
Univ. of Jayewardenepura

Dr J.M. Dahanayake
Dept. of Ayurveda Pharmacology, Pharmaceutics and Community Medicine
Univ. of Colombo

Prof. Warshi Dandeniya
Dept of Soil Science
Univ. of Peradeniya

Dr Isuru Dassanayake
Dept. Electrical and Electronic Engineering
Univ. of Peradeniya

Prof. R. Saman Dharmakeerthi
Dept. of Soil Science
Univ. of Peradeniya

Dr Randima Dinalankara
Dept. of Computer Engineering
Univ. of Sri Jayewardenepura

Dr. Kasun de Silva
Dept of Civil Engineering
Univ. of Moratuwa

Dr Senuri de Silva
Dept. of Computer Science
Univ. of Moratuwa

Dr S.N.T. De Silva
Dept. of Nano Science Technology
Wayamba University of Sri Lanka

Prof. Nelum Deshappriya
Dept. of Botany
Univ. of Sri Jayewardenepura

Prof. Chamari Dissanayake
Dept. of Zoology
Univ. of Sri Jayewardenepura

Dr Surani Ediriweera
Dept. of Plant Sciences
Univ. of Colombo

Prof. Sisira Ediriweera
Dept. of Science & Technology
Uwa Wellassa University of
Sri Lanka

Prof. Janaka Ekanayake
Dept. of Electrical & Electronic
Engineering
Univ. of Peradeniya

Dr S. Fernando
Dept. of Zoology
The Open University of Sri Lanka

Prof. Naleen Ganegoda
Dept. of Mathematics
Univ. of Sri Jayawardenapura

Prof. Mangalika Hettiarachchi
Dept. of Zoology and
Environmental Management
Univ. of Kelaniya

Dr Chamod Hettiarachchi
Dept. of Civil Engineering
Univ of Moratuwa

Dr Sandamali Sakunthala Herath
Dept. of Fisheries and Aquaculture
Univ. of Ruhuna

Prof G.B.B. Herath
Dept. of Civil Engineering
Univ.of Peradeniya

Prof. Indika Herath
Dept. of Plantation Management
Wayamba University of Sri Lanka

Dr Samudu Herath
Dept. of Civil Engineering
Univ.of Moratuwa

Prof. H.M. K. Herath
Dept. of Export Agriculture
Uva Wellassa University of
Sri Lanka

Dr Damayanthi Herath
Dept. of Computer Engineering
Univ. of Peradeniya

Prof. Isuru Hewapathirana
Software Engineering Teaching
Unit
Univ. of Kelaniya

Prof. Sanath Hettiarachchi
Dept. of Biological Sciences
Rajarata University of Sri Lanka

Dr Budditha Hettige
Dept. of Knowledge Engineering
and Communication
Univ. of Sri Jayewardenepura

Prof. H.M.G.S.B. Hitinayake
Dept. of Crop science
Univ. of Peradeniya

Prof. Udeni Jayalal
Dept. of Natural Resources
Sabaragamuwa University of
Sri Lanka

Prof. L.P. Jayatissa
Dept of Botany
Univ. of Ruhuna

Prof. Sharmila Jayasena
Dept. Biochemistry and Molecular
Biology
Univ. of Colombo

Prof. K.G.L.R. Jayathunga
Dept. of Biosystems Technology
Univ. of Sri Jayewardenepura

Prof. T. Jayasingham
Dept. of Botany
Eastern University of Sri Lanka

Dr Nadika Jayasooriya
Department of Interdisciplinary
Studies
Faculty of Engineering
Univ. of Sri Jayewardenepura

Prof. Gehan Jayasuriya
Dept. of Botany
Univ. Peradeniya

Yasith Jayawardana
Old Dominion University
USA

Dr Chamnida Jayawardana
American National Business
University
USA

Prof. Hiran H.E. Jayaweera
Dept. Physics
Univ. of Colombo

Prof. Inoka Karunaratne
Dept. of Zoology
Univ. of Peradeniya

Dr Namalika Karunaratne
Dept. of Farm Animal Production
and Health
Univ. of Peradeniya

Dr Hasani S. Karunarathna
Dept. of Statistics
Univ. of Colombo

Dr Anuruddha Karunaratne
Dept. of Agricultural Engineering
Univ. of Peradeniya

Prof. Nadira Karunaweera
Dept. of Parasitology
Univ. of Colombo

Prof. Sunanda Kodikara
Dept. of Botany
Univ. of Ruhuna

Dr Heshan Kodithuwakku
Dept. of Livestock and Avian
Sciences
Wayamba University of Sri Lanka

Dr Renuka Kolandasamy
KLEF,
Vaddeswaram, Guntur

Prof. Nisha Kottearachchi
Faculty of Agriculture & Plantation Management
Wayamba University of Sri Lanka

Dr Anoop Kumar
Dept. of Statistics
Central University of Haryana
India

Dr. W.G.C.W. Kumara
Dept. of Computer Science and Engineering
South Eastern University of Sri Lanka

Dr K.D.N. Kumari
Dept. of Mathematics and Philosophy of Engineering
The Open University of Sri Lanka

Dr B.M.T. Kumarika
Dept. of Statistics and Computer Science
Univ. of Kelaniya

Dr M. Kayanana
Dept. of Physical Sciences
Univ. of Vavuniya

Prof. G.J. Lanel
Dept. of Mathematics
University of Sri Jayewardenepura

Dr Gayan Lankeshwara
Univ. of Queensland
Australia

Dr Dilani Lokuhetty
Dept. of Pathology
Univ. of Colombo

Dr Thanuja Liyanage
Dept. of Animal Science
Univ. of Ruhuna

Dr J.R. Gamage
Dept. of Mechanical Engineering
Univ. of Moratuwa

Prof. Mangala Ganehiarachchi
Dept. of Zoology and Environmental Management
Univ. of Kelaniya

Prof. Naleen Ganegoda
Department of Mathematics
Univ. of Sri Jayewardenepura

Prof. Sudarshanee Geekiyanage
Dept. of Agricultural Biology
Univ. of Ruhuna

Dr D. R. Gimhani
Dept. of Biotechnology
Wayamba University of Sri Lanka

Prof. Mangala Gunatilake
Dept. of Physiology
Univ. of Colombo

Dr Gayan Lakeshwara
Univ. of Queensland
Australia

Dr Chiranthi Liyanage
Dept. of Pharmacology
Univ. of Colombo

Prof. G.D. K. Mahanama
Dept. of Physics
Univ. of Ruhuna

Prof. A.C. Mahasinghe
Dept of Mathematics
Univ. of Colombo

Prof. B. A. G. G. Mahendra
Dept. of Pathology
Univ. of Kelaniya

Prof. Mahen Mahendran
Queensland University of Technology (QUT)
Australia

Prof. H.M.Y.C Mallikarachchi.
Dept. of Civil Engineering
Univ. of Moratuwa

Dr Dimuthu Manamgoda
Dept. of Botany
Univ. of Sri Jayewardenepura

Prof. Dulani Meedeniya
Dept. of Computer Science & Engineering
Univ. of Moratuwa

Prof. G. Mikunthan
Dept. of Agricultural Biology
Univ. of Jaffna

Prof. D.H.N. Munasinghe
Dept. of Zoology
Univ. of Ruhuna

Dr I. Munaweera
Dept. of Chemistry
Univ. of Sri Jayewardenepura

Prof. C. M. Nanayakkara
Dept. of Plant Science
Univ. of Colombo

Dr Sudheera Navarathna
Dept. of Electrical and Electronic Engineering Univ. of Peradeniya

Dr Panduka Neluwala
Dept. of Civil Engineering
Univ. of Peradeniya

Dr Ledya Novamizanti
Telkom University
Indonesia

Prof. P. Paranagama
Dept. of Chemistry
Univ. of Kelaniya

Dr Hasanthi Pathberiya
Dept. of Statistics
Univ. of Sri Jayewardenepura

Prof. Ranjith Pathirana
Dept. of Chemistry
Univ. of Ruhuna

Dr T. Pathmathas
Dept. of Physics
Univ. of Jaffna

Dr M.T.M. Perera
Dept. of Mathematics
Univ. of Sri Jayewardenepura

Dr Oshadee Peiris
Dept. of Mathematics
The Open University of Sri Lanka

Prof. P.K.D.D.P. Pitigala
Dept. of Physics
Univ. of Sri Jayewardenepura

Prof. S. Priyadhasini
Dept. of Mathematics
SK Arts and Science College
India

Dr Thilini Piyathilake
Dept. of Computational Mathematics
Univ. of Moratuwa

Dr G.A.S. Premakumara
Dept. of Basic Science and Social Sciences for Nursing
Univ. of Colombo

Dr Nadeeka Premarathna
Dept. of Mathematics
Univ. of Kelaniya

Prof. S. S. N. Perera
Dept. of Mathematics
Univ. of Colombo

Dr K.K.K.R. Perera
Dept. of Mathematics
Univ. of Kelaniya

Dr. P. Rajarajeswari
Dept. of Mathematics
Chikkanna Govt. Arts College
Tiruppur, India

Prof. Roshan Ragel
Dept. of Computer Engineering
Univ. of Peradeniya

Prof. Gamini Rajapakse
Dept. of Chemistry
Univ. of Peradeniya

Prof. A. Ramanan
Dept. of Computer Science
Univ. of Jaffna

Dr Kokila Ramanayaka
Dept. of Information Technology
Univ. of Ruhuna

Dr Bandula Ranaweera
Dept. of Horticulture and Landscape Gardening
Wayaba University of Sri Lanka

Prof. K. K. D. S. Ranaweera
Dept. of Food Science and Technology
Univ. of Sri Jayewardenepura

Prof. Nalika Ranatunga
Dept. of Agricultural Biology
Univ. of Ruhuna

Dr. Udari Rathnathunga
Dept. of Urban Bioresources
Univ. of Sri Jayewardenepura

Dr K.R.M.N. Ratnayake
Dept. of Electrical and Electronic Engineering
Univ. of Peradeniya

Mrs Y. Raviraj
Dept. of Mathematics
South Eastern University of Sri Lanka

Ashish Routray
National Centre for Medium Range Weather Forecasting
Noida, India

Prof. Sumudu Rubasingha
Dept. of Botany
Univ. of Peradeniya

Prof. U. Samarajeewa
Dept. of Food Science & Technology
Univ. of Peradeniya

Dr Nalin Samarasinha
Planetary Science Institute
USA

Prof. Gamini Senanayake
Dept. of Agricultural Biology
Univ. of Ruhuna

Prof. S. P. Senanayake
Dept. of Plant and Molecular Biology
Univ. of Kelaniya

Dr D.M.J.B. Senanayake
Rice Research and Development Institute Batalagoda

Dr. Jagath Senarathne
Dept. of Statistics and Computer Science
Univ. of Peradeniya

Dr M.D.S. Seneviratne
Faculty of Computing
Univ. of Sri Jayewardenepura

Dr Prayas Sharma
Dept. of Statistics
Babasaheb Bhimrao Ambedkar University,
India

Prof. Housila P. Singh
School of Studies in Statistics
Vikram University
India

Prof. Nirmala Sirisena
Dept. of Anatomy
Univ. of Colombo

Prof. M. Siyamalan
Dept. of Computer Science
Univ. of Jaffna

Nishal Silva
University of Trento Trento
Italy

Prof. S.C. Somasiri
Dept. of Animal and Food Sciences
Rajarata University

Prof. S. Subasingha
Dept. of Crop Science
Univ. of Ruhuna

Prof. WL Sumathipala
Faculty of Natural Science
The Open University of Sri Lanka

Prof. Samantha Thelijjagoda
Sri Lanka Information and Technology Institute

Prof. K. Tennakone
National Institute of Fundamental Studies
Hantana Road, Kandy

Dr T. M. S. G. Tennekone
Link Natural Products (Pvt.) LTD

Dr. Ramajeyam Tharshan
Dept. of Mathematics and Statistics
Univ. of Jaffna

Mr. Navod Neranjan Thilakarathne
Dept. of Information and Communication Technology
Univ. of Colombo

Prof. Preethi Udagama
Dept. of Zoology & Environment Sciences
Univ. of Colombo

Prof. R.J.M. Uduporuwa
Dept. of Geography & Environmental Management
Sabaragamuwa University of Sri Lanka

Dr K.D.B. Ukuwela
Department of Biological Sciences
Rajarata University of Sri Lanka

Prof. K.S. Wanniarachchi
Dept. of Civil & Environmental Engineering
Univ. of Ruhuna

Prof. W. K. I. L. Wanniarachchi
Dep. of Physics
Univ. of Sri Jayewardenepura

Prof. DL. Wathugala
Dept. of Crop Science
Univ. of Ruhuna

Dr D.R. Welikanna
Dept. of Surveying and Geodesy
Sabaragamuwa University of Sri Lanka

Dr. Nimal Wijayaratna
Dept. of Civil Engineering
Univ. of Moratuwa

Prof. W. L. I. Wijesekara
Dept of Food Science and Technology
Univ. of Sri Jayawardenepura

Dr Eranga Wijesinghe
Dept. of Electrical & Electronic Engineering
Sri Lanka Institute of Information Technology (SLIIT)

Prof. W. A. J. P. Wijesinghe
Dept. of Food Science and Technology
Uva Wellassa University of Sri Lanka

Prof. Eranga Wijewickrama
Dept. of Clinical Medicine
Univ. of Colombo

Dr Maheshwari Wikrama
Dept. of Earth Resources Engineering
Univ. of Moratuwa

Dr Eranga M. Wimalasiri
Dept. of Export Agriculture
Sabaragamuwa University of Sri Lanka

Dr N.U.S. Yapa
Dept. of Physics
The Open University of Sri Lanka
Kandy Regional Center
Polgolla

Prof. Surangi Yasawardene
Dept. of Anatomy
Univ. of Sri Jayewardenepura

AUTHOR INDEX - VOL. 53 All – Issue 2025

Abayasekara C *see* Weerakoon S *et al*. (2025)

Abayasekara CL *see* Kapukotuwa GK *et al*. (2025)

Aberathne AHMNR, Fernando THPS & Siriwardena EADD - First report of rubber circular leaf spot disease pathogen Colletotrichum siamense Prihastuti, L. Cai & K.D. Hyde in Cinnamomum zeylanicum blume in Sri Lanka **53**: 459-464 (2025)

Abeysinghe AMPM *see* Wijesooriya WMNS *et al*. (2025)

Abeysundara H *see* Weerakoon S *et al*. (2025)

Afzal MZ and Siddiqi SS - A comparison of optimizers in a PyTorch based artificial neural network to predict normal boiling points of alkanes **53**: 165-172 (2025)

Amarasinghe KP *see* Murugananthan A *et al*. (2025)

Amaratunga KSP *see* Fernando AJ *et al*. (2025)

Ampitiyawatta AD *see* Kaushalya KC *et al*. (2025)

Anandappa JM s*ee* Ediriweera MK & Anandappa JM (2025)

Ashraf M *see* Muhammad A *et al*. (2024)

Athapattu AMCUM s*ee* Fernando CLR & Athapattu AMCUM (2025)

Ayodya NAI *see* Kumara AGYM *et al*. (2025)

Bandara CS *see* Kumara AGYM *et al*. (2025)

Basri NRH, Mohktar MS & Mahadi WNLW - Machine learning methods to classify engineering students' ability to perform recreational archery activities using biomechanical data **53**: 73-83 (2025)

BM Jinendra s*ee* Yasintha KW & BM Jinendra (2025)

Chinthaka SDM s*ee* Thathsara KAH & Chinthaka SDM (2025)

De Silva PHGAD *see* Iroshani HPDU *et al*. (2025)

De Silva THKR *see* Fernando AJ *et al*. (2025)

Dharmasena DNA *see* Fernando AJ *et al*. (2025)

Dissanayake DMKI *see* Silva CS *et al*. (2025)

Ediriweera MK & Anandappa JM - The first report on the in-vitro HDAC inhibitory potential of Sri Lankan traditional rice varieties **53**: 201-204 (2025)

Ekanayaka N, Rathnayake S, Ratnayake P, Perera K & Udagama P - BRAF (V600E) gene mutation in patients with thyroid cancer in Sri Lanka: A pilot study **53**: 3-12 (2025)

Farhan MSM & Samarasekara P - Magnetic properties of body-centred cubic ferromagnetic thin films described by the fourth order perturbed Heisenberg Hamiltonian **53**: 363-373 (2025)

Fari MJM *see* Jayawardhana JMJM *et al*. (2025)

Fernando AJ, Amaratunga KSP, Dharmasena DNA & De Silva THKR - effect of temperature on drying kinetics and quality attributes of coffee beans during hot air drying **53**: 293-306 (2025)

Fernando CLR & Athapattu AMCUM - An upper bound for star chromatic index of simple connected sub cubic graphs and applications **53**: 317-331 (2025)

Fernando MCS *see* Madhushika TDT *et al*. (2025)

Fernando MMPM *see* Tantrigoda DA *et al*. (2025)

Fernando THPS *see* Aberathne AHMNR *et al*. (2025)

Geekiyanage S *see* Pushpakumari WHDU *et al*. (2025)

Gnanathasan A *see* Murugananthan A *et al*. (2025)

Ileperuma IASR *see* Ruwanmalie WAPU *et al*. (2025)

Iroshani HPDU, Rathnasiri PG, Wasala MKRTW Bandara & De Silva PHGAD - Performance evaluation of a lab-scale upflow anaerobic sludge blanket (UASB) reactor for landfill leachate treatment under ambient temperature conditions **53**: 283-292 (2025)

Jayaprada NVT *see* Pushpakumari WHDU *et al*. (2025)

Jayasekara LALW *see* Pushpakumari WHDU *et al*. (2025)

Jayasinghe JASC *see* Kumara AGYM *et al*. (2025)

Jayawardhana JMJM, Fari MJM & Liyanage R - development of pasta using composite flour of sweet potato (Ipomoea batatas), soy (Glycine max) & rice (Oryza sativa) flours **53**: 233-244 (2025)

Jayaweera JMAK *see* Wijesooriya SS *et al*. (2025)

Jegatheesan N *see* Rengarasu TM *et al*. (2025)

Jinendra BM s*ee* Suneetha C & Jinendra BM (2025)

Jinendra BM s*ee* Suneetha C & Jinendra BM (2025)

Jobin Christ MC s*ee* Muralidharan C & Jobin Christ MC (2025)

Kadono H *see* Srimal LKT *et al*. (2025)

Kapukotuwa GK, Abayasekara CL, Weerakoon KC & Rajakaruna RS - Faecal indicator bacteria and microbial source tracking as tools for testing water quality and sources of contamination of Rawan Oya tributary of the Mahaweli River, in Sri Lanka **53**: 421-436 (2025)

Kaushalya KC, Kumara JBDAP, Ampitiyawatta AD & Wimalasiri EM - Annual and seasonal trends in extreme precipitation events in the dry zone of Sri Lanka **53**: 187-199 (2025)

Kaushalya SDN *see* Maduwage CSDS *et al*. (2025)

Khan WA *see* Muhammad A *et al*. (2024)

Kumanan T *see* Murugananthan A *et al*. (2025)

Kumara AGYM, Pigera ACD, Ayodya NAI, Jayasinghe JASC & Bandara CS - effect of initial imperfections on the seismic performance of thin- walled steel hollow piers: a numerical approach **53**: 259-272 (2025)

Kumara JBDAP *see* Kaushalya KC *et al*. (2025)

Kumari SS *see* Wijesooriya SS *et al*. (2025)

Lakshitha NVD, Samarasekara RSM & Siriwardana HPAM - Optimizing beach nourishment composition for coastal protection in Sri Lanka: Insights from flume experiments **53**: 125-38 (2025)

Liyanage I *see* Weerakoon S *et al*. (2025)

Liyanage R *see* Jayawardhana JMJM *et al*. (2025)

Madhushika TDT, Somathilake LW & Fernando MCS - optimal control strategies for diabetes population management using mathematical models **53**: 219-232 (2025)

Maduwage CSDS, Kaushalya SDN & Wijesinghe WAJP - Utilization of jackfruit seed flour (Artocarpus heterophyllus L.) as a thickening agent in tomato sauce production **53**: 173-185 (2025)

Mahadi WNLW *see* Basri NRH *et al*. (2025)

Manage PM *see* Meddage AKMMK *et al*. (2025)

Meddage AKMMK, Manage PM & Withanage PM - Impact of probiotics mixture as a water additive on water quality, growth performance and survival of Catla catla fry **53**: 151-164 (2025)

Mohktar MS *see* Basri NRH *et al*. (2025)

Muhammad A, Taouti A, Khan WA & Ashraf M -Networking model based on fuzzy graphs of almost primary fuzzy ideals of near-rings **53**: 13-20 (2025)

Muralidharan C & Jobin Christ MC - Chest anteroposterior diameter measurement: Comparison of ultrasonic and manual methods across different BMI categories **53**: 437-445 (2025)

Murugananthan A, Gnanathasan A, Kumanan T, Amarasinghe KP & Pirasath S - Molecular phylogeography of Echis carinatus revisited: Insights from the Sri Lankan population of saw-scaled viper (Serpentes: Viperidae: Echis) **53**: 85-105 (2025)

Nanayakkara B *see* Weerakoon S *et al*. (2025)

Nawarathna HMKC *see* Wijesooriya SS *et al*. (2025)

Nissanka S *see* Weerakoon B *et al*. (2025)

Perera HACC *see* Wijesooriya WMNS *et al*. (2025)

Perera HACC *see* Wijesooriya WMNS *et al*. (2025)

Perera C *see* Wijesooriya SS *et al*. (2025)

Perera K *see* Ekanayaka N *et al*. (2025)

Pigera ACD *see* Kumara AGYM *et al*. (2025)

Pirasath S *see* Murugananthan A *et al*. (2025)

Pradeepika NGJ & Ranawake AL - Assessing the impact of salinity stress on Na+, K+, and Ca2+ contents of 125 rice genotypes **53**: 109-24 (2025)

Pushpakumari WHDU, Jayaprada NVT, Jayasekara LALW, Senanayake G, Senanayake DMJB & Geekiyanage S - Coincidence of inductive photoperiod and early vegetative phase leads to early flowering and increased yield in selected Sri Lankan traditional rice varieties **53**: 33-43 (2025)

Rajagopalan UM *see* Srimal LKT *et al*. (2025)

Rajakaruna RS *see* Kapukotuwa GK *et al*. (2025)

Ranawake AL s*ee* Pradeepika NGJ & Ranawake AL (2025)

Ranawake AL *see* Safwa MFZ *et al*. (2025)

Ranwala SMW *see* Ruwanmalie WAPU *et al*. (2025)

Rathnasiri PG *see* Iroshani HPDU *et al*. (2025)

Rathnayake RSMPW *see* Silva CS *et al*. (2025)

Rathnayake S *see* Ekanayaka N *et al*. (2025)

Ratnayake P *see* Ekanayaka N *et al*. (2025)

Rengarasu TM, Jegatheesan N & Wasala MKRTW Bandara - Use of carbonised wood particles as filler replacement in hot mix asphalt **53**: 375-389 (2025)

Ruwanmalie WAPU, Ileperuma IASR & Ranwala SMW - Ecological characterization of the 40-year-old regenerated rainforest patch in Olaboduwa-Kodigahakanda adds value in promoting forest-based nature tourism **53**: 391-402 (2025)

Safwa MFZ, Samarasinghe TN, Wijevardhana AN, Shyamalee HAPA & Ranawake AL - Evaluation of genotypic variability and yield performance of selected indigenous and improved Ipomoea batatas L. genotypes under poly sack cultivation **53**: 57-72 (2025)

Samaranayake SA *see* Tantrigoda DA *et al*. (2025)

Samarasekara RSM *see* Lakshitha NVD *et al*. (2025)

Samarasinghe TN *see* Safwa MFZ *et al*. (2025)

Sathsara NTA *see* Silva CS *et al*. (2025)

Senanayake DMJB *see* Pushpakumari WHDU *et al*. (2025)

Senanayake G *see* Pushpakumari WHDU *et al*. (2025)

Shahbaz MQ s*ee* Shahbaz SH & Shahbaz MQ (2025)

Shahbaz SH & Shahbaz MQ - On recursive computation for the moments of generalized order statistics for the Kumaraswamy family of distributions with characterizations **53**: 139-150 (2025)

Shyamalee HAPA *see* Safwa MFZ *et al*. (2025)

Siddiqi SS s*ee* Afzal MZ & Siddiqi SS (2025)

Silva CS, Dissanayake DMKI, Rathnayake RSMPW & Sathsara NTA - aerial crack detection in building structures using convolutional neural networks **53**: 273-282 (2025)

Siriwardana HPAM *see* Lakshitha NVD *et al*. (2025)

Siriwardena EADD *see* Aberathne AHMNR *et al*. (2025)

Somathilake LW *see* Madhushika TDT *et al*. (2025)

Sooriyarachchi A *see* Wijesooriya SS *et al*. (2025)

Srimal LKT, Rajagopalan UM, Kadono H & Yonekura T - Visualizing changes in internal layers of chinese chives leaf under short-term ozone exposure with biospeckle optical coherence tomography **53**: 245-258 (2025)

Suneetha C & Sukumar M- Seasonal variation in crop yield and reduction of phytic acid content through soaking and germination of kodo millet (Paspalum scrobiculatum L.) germplasm **53**: 345-362 (2025)

Suriyagoda LDB *see* Wijesooriya SS *et al*. (2025)

Tantrigoda DA, Fernando MMPM & Samaranayake SA - A technique for extracting gravity anomalies originating from sediments deposited on folded oceanic crust **53**: 311-315 (2025)

Taouti A *see* Muhammad A *et al*. (2024)

Thathsara KAH & Chinthaka SDM - Physiochemical characterization of critically endangered Coscinium fenestratum (gaertn.) Colebr. seed fat for potential niche applications in cosmetics and nutritional supplements **53**: 21-32 (2025)

Udagama P *see* Ekanayaka N *et al*. (2025)

Wasala MKRTW Bandara *see* Iroshani HPDU *et al*. (2025)

Wasala MKRTW Bandara *see* Rengarasu TM *et al*. (2025)

Weerakoon B, Wolseley P, Wijesundara S, Nissanka S & Weerakoon G - Lichens of Sri Lanka: Past discoveries, present knowledge, and future directions **53**: 207-217 (2025)

Weerakoon G *see* Weerakoon B *et al*. (2025)

Weerakoon KC *see* Kapukotuwa GK *et al*. (2025)

Weerakoon S, Nanayakkara B, Abayasekara C, Abeysundara H & Liyanage I - Recreational water quality in the river Mahaweli, Sri Lanka: Enumeration and antibiotic sensitivity of Escherichia coli and sociological aspects **53**: 45-55 (2025)

Wijesinghe WAJP *see* Maduwage CSDS *et al*. (2025)

Wijesooriya SS, Nawarathna HMKC, Kumari SS, Sooriyarachchi A, Jayaweera JMAK, Perera C & Suriyagoda LDB - Changes in crop productivity and the harvested area of rice grown in Sri Lanka over the last four decades (1979-2021) as affected by the season, district, and water management system **53**: 403-420 (2025)

Wijesooriya WMNS, Perera HACC, Abeysinghe AMPM & Perera KABP - A multidimensional study on Spotted Sardinella: Biometric, ecological, and heavy metal perspectives from Negombo, Sri Lanka **53**: 447-457 (2025)

Wijesundara S *see* Weerakoon B *et al*. (2025)

Wijevardhana AN *see* Safwa MFZ *et al*. (2025)

Wimalasiri EM *see* Kaushalya KC *et al*. (2025)

Withanage PM *see* Meddage AKMMK *et al*. (2025)

Wolseley P *see* Weerakoon B *et al*. (2025)

Yasintha KW & BM Jinendra - Use of near infrared spectroscopy for rapid and non-destructive identification of morphologically similar seeds of different paddy varieties [Oryza sativa L.] **53**: 333-343 (2025)

Yonekura T *see* Srimal LKT *et al*. (2025)

SUBJECT INDEX 2025

2-connected graphs
An upper bound for star chromatic index of simple connected sub cubic graphs and applications (Fernando CLR & Athapattu AMCUM) **53:** 317-331 (2025)

Activity performance
Machine learning methods to classify engineering students' ability to perform recreational archery activities using biomechanical data (Basri NRH, Mohktar MS & Mahadi WNLW) **53:** 73-83 (2025)

Agro-morphological characteristics
Evaluation of genotypic variability and yield performance of selected indigenous and improved Ipomoea batatas L. genotypes under poly sack cultivation (Safwa MFZ, Samarasinghe TN, Wijevardhana AN, Shyamalee HAPA, Ranawake AL) **53:** 57-72 (2025)

Alkanes
A comparison of optimizers in a PyTorch based artificial neural network to predict normal boiling points of alkanes (Afzal MZ and Siddiqi SS) **53:** 165-172 (2025)

Almost primary fuzzy ideal in near-rings
Networking model based on fuzzy graphs of almost primary fuzzy ideals of near-rings (Muhammad A, Taouti A, Khan WA & Ashraf M) **53:** 13-20 (2025)

Ambient temperature treatment
Performance evaluation of a lab-scale upflow anaerobic sludge blanket (uaSB) reactor for landfill leachate treatment under ambient temperature conditions (Iroshani HPDU, Rathnasiri PG, Wasala MKRTW Bandara & De Silva PHGAD) **53:** 283-292 (2025)

Amblygaster sirm
A multidimensional study on Spotted Sardinella: Biometric, ecological, and heavy metal perspectives from Negombo, Sri Lanka (Wijesooriya WMNS, Perera HACC, Abeysinghe AMPM & Perera KABP) **53:** 447-457 (2025)

Anaerobic digestion
Performance evaluation of a lab-scale upflow anaerobic sludge blanket (uaSB) reactor for landfill leachate treatment under ambient temperature conditions (Iroshani HPDU, Rathnasiri PG, Wasala MKRTW Bandara & De Silva PHGAD) **53:** 283-292 (2025)

Antibiotic resistance
Recreational water quality in the river Mahaweli, Sri Lanka: Enumeration and antibiotic sensitivity of Escherichia coli and sociological aspects (Weerakoon S, Nanayakkara B, Abayasekara C, Abeysundara H & Liyanage I) **53:** 45-55 (2025)

Aquaculture
Impact of probiotics mixture as a water additive on water quality, growth performance and survival of Catla catla fry (Meddage AKMMK, Manage PM & Withanage PM) **53:** 151-164 (2025)

Arduino Uno
Chest anteroposterior diameter measurement: Comparison of ultrasonic and manual methods across different BMI categories (Muralidharan C & Jobin Christ MC) **53:** 437-445 (2025)

Bacteroides
Faecal indicator bacteria and microbial source tracking as tools for testing water quality and sources of contamination of Rawan Oya tributary of the Mahaweli River, in Sri Lanka (Kapukotuwa GK, Abayasekara CL, Weerakoon KC & Rajakaruna RS) **53:** 421-436 (2025)

Bathing water
Recreational water quality in the river Mahaweli, Sri Lanka: Enumeration and antibiotic sensitivity of Escherichia coli and sociological aspects (Weerakoon S, Nanayakkara B, Abayasekara C, Abeysundara H & Liyanage I) **53:** 45-55 (2025)

Beach nourishment
Optimizing beach nourishment composition for coastal protection in Sri Lanka: Insights from flume experiments (Lakshitha NVD, Samarasekara RSM & Siriwardana HPAM) **53:** 125-138 (2025)

Biodiversity
Ecological characterization of the 40-year-old regenerated rainforest patch in Olaboduwa-Kodigahakanda adds value in promoting forest-based nature tourism (Ruwanmalie WAPU, Ileperuma IASR & Ranwala SMW) **53:** 391-402 (2025)

Biogeography
Molecular phylogeography of Echis carinatus revisited: Insights from the Sri Lankan population of saw-scaled viper (Serpentes: Viperidae: Echis) (Murugananthan A, Gnanathasan A, Kumanan T, KP Amarasinghe KP & Pirasath S) **53:** 85-105 (2025)

Bio-indicators
Lichens of Sri Lanka: Past discoveries, present knowledge, and future directions (Weerakoon B, Wolseley P, Wijesundara S, Nissanka S & Weerakoon G) **53:** 207-217 (2025)

Biological activities
Visualizing changes in internal layers of chinese chives leaf under short-term ozone exposure with biospeckle optical coherence tomography (Srimal LKT, Rajagopalan UM, Kadono H & Yonekura T) **53:** 245-258 (2025)

Biomechanical analysis
Machine learning methods to classify engineering students' ability to perform recreational archery activities using biomechanical data (Basri NRH, Mohktar MS & Mahadi WNLW) **53:** 73-83 (2025)

Biospeckle optical coherence tomography (bOCT)
Visualizing changes in internal layers of chinese chives leaf under short-term ozone exposure with biospeckle optical coherence tomography (Srimal LKT, Rajagopalan UM, Kadono H & Yonekura T) **53:** 245-258 (2025)

Biospeckles
Visualizing changes in internal layers of chinese chives leaf under short-term ozone exposure with biospeckle optical coherence tomography (Srimal LKT, Rajagopalan UM, Kadono H & Yonekura T) **53:** 245-258 (2025)

Body mass index
Chest anteroposterior diameter measurement: Comparison of ultrasonic and manual methods across different BMI categories (Muralidharan C & Jobin Christ MC) **53:** 437-445 (2025)

Boiling points of alkanes
A comparison of optimizers in a PyTorch based artificial neural network to predict normal boiling points of alkanes (Afzal MZ and Siddiqi SS) **53:** 165-172 (2025)

BRAF(V600E) gene mutation
BRAF (V600E) gene mutation in patients with thyroid cancer in Sri Lanka: A pilot study (Ekanayaka N, Rathnayake S, Ratnayake P, Perera K & Udagama P) **53:** 3-12 (2025)

Ca^{2+} content
Assessing the impact of salinity stress on Na+, K+, and Ca^{2+} contents of 125 rice genotypes (Pradeepika NGJ & Ranawake AL) **53:** 109-124 (2025)

Carbonised wood particles
Use of carbonised wood particles as filler replacement in hot mix asphalt (Rengarasu TM, Jegatheesan N & Wasala MKRTW Bandara) **53:** 375-389 (2025)

Catla catla
Impact of probiotics mixture as a water additive on water quality, growth performance and survival of Catla catla fry (Meddage AKMMK, Manage PM & Withanage PM) **53:** 151-164 (2025)

Characterizations
On recursive computation for the moments of generalized order statistics for the Kumaraswamy family of distributions with characterizations (Shahbaz SH & Shahbaz MQ) **53:** 139-150 (2025)

Chest anteroposterior diameter
Chest anteroposterior diameter measurement: Comparison of ultrasonic and manual methods across different BMI categories (Muralidharan C & Jobin Christ MC) **53:** 437-445 (2025)

Cinnamomum zeylanicum
First report of rubber circular leaf spot disease pathogen Colletotrichum siamense Prihastuti, L. Cai & K.D. Hyde in Cinnamomum zeylanicum blume in Sri Lanka (Aberathne AHMNR, Fernando THPS & Siriwardena EADD).**53:** 459-464 (2025)

Circular leaf spot disease
First report of rubber circular leaf spot disease pathogen Colletotrichum siamense Prihastuti, L. Cai & K.D. Hyde in Cinnamomum zeylanicum blume in Sri Lanka (Aberathne AHMNR, Fernando THPS & Siriwardena EADD) **53:** 459-464 (2025)

Coastal protection
Optimizing beach nourishment composition for coastal protection in Sri Lanka: Insights from flume experiments (Lakshitha NVD, Samarasekara RSM & Siriwardana HPAM) **53:** 125-138 (2025)

Coffee
Effect of temperature on drying kinetics and quality attributes of coffee beans during hot air drying (Fernando AJ, Amaratunga KSP, Dharmasena DAN & De Silva THKR) **53:** 293-306 (2025)

Colletotrichum siamense
First report of rubber circular leaf spot disease pathogen Colletotrichum siamense Prihastuti, L. Cai & K.D. Hyde in Cinnamomum zeylanicum blume in Sri Lanka (Aberathne AHMNR, Fernando THPS & Siriwardena EADD) **53:** 459-464 (2025)

Composite flour
development of pasta using composite flour of sweet potato (Ipomoea batatas), soy (Glycine max) & rice (Oryza sativa) flours (Jayawardhana JMJM, Fari MJM & Liyanage R) **53:** 233-244 (2025)

Convolutional neural network
Aerial crack detection in building structures using convolutional neural networks (Silva CS, Dissanayake DMKI, Rathnayake RSMPW & Sathsara NTA) **53:** 273-282 (2025)

Correlation length
Visualizing changes in internal layers of chinese chives leaf under short-term ozone exposure with biospeckle optical coherence tomography (Srimal LKT, Rajagopalan UM, Kadono H & Yonekura T) **53:** 245-258 (2025)

Coscinium fenestratum
Physiochemical characterization of critically endangered *Coscinium fenestratum* (gaertn.) Colebr. seed fat for potential niche applications in cosmetics and nutritional supplements (Thathsara KAH & Chinthaka SDM) **53:** 21-32 (2025)

Cosmetics and nutritional supplements
Physiochemical characterization of critically endangered *Coscinium fenestratum* (gaertn.) Colebr. seed fat for potential niche applications in cosmetics and nutritional supplements (Thathsara KAH & Chinthaka SDM) **53:** 21-32 (2025)

Crack detection and identification
Aerial crack detection in building structures using convolutional neural networks (Silva CS, Dissanayake DMKI, Rathnayake RSMPW & Sathsara NTA) **53:** 273-282 (2025)

Crushed-glass
Optimizing beach nourishment composition for coastal protection in Sri Lanka: Insights from flume experiments (Lakshitha NVD, Samarasekara RSM & Siriwardana HPAM) **53:** 125-138 (2025)

Cyclic loading
Effect of initial imperfections on the seismic performance of thin-walled steel hollow piers: a numerical approach (Kumara AGYM, Pigera ACD, Ayodya NAI, Jayasinghe JASC & Bandara CS) **53:** 259-272 (2025)

Days to flowering
Coincidence of inductive photoperiod and early vegetative phase leads to early flowering and increased yield in selected Sri Lankan traditional rice varieties (Pushpakumari WHDU, Jayaprada NVT, Jayasekara LALW, Senanayake G, Senanayake DMJB & Geekiyanage S) **53:** 33-43 (2025)

Deep learning
Aerial crack detection in building structures using convolutional neural networks (Silva CS, Dissanayake DMKI, Rathnayake RSMPW & Sathsara NTA) **53:** 273-282 (2025)

Diabetes population dynamics
Optimal control strategies for diabetes population management using mathematical models (Madhushika TDT, Somathilake LW & Fernando MCS) **53:** 219-232 (2025)

Districts
Changes in crop productivity and the harvested area of rice grown in Sri Lanka over the last four decades (1979-2021) as affected by the season, district, and water management system (Wijesooriya SS, Nawarathna HMKC, Kumari SS, Sooriyarachchi A, Jayaweera JMAK, Perera C & Suriyagoda LDB) **53:** 403-420 (2025)

Dry zone of Sri Lanka
Annual and seasonal trends in extreme precipitation events in the dry zone of Sri Lanka (Kaushalya KC, Kumara JBDAP, Ampitiyawatta AD & Wimalasiri EM) **53:** 187-199 (2025)

Drying
Effect of temperature on drying kinetics and quality attributes of coffee beans during hot air drying (Fernando AJ, Amaratunga KSP, Dharmasena DAN & De Silva THKR) **53:** 293-306 (2025)

Ecological value
Ecological characterization of the 40-year-old regenerated rainforest patch in Olaboduwa-Kodigahakanda adds value in promoting forest-based nature tourism (Ruwanmalie WAPU, Ileperuma IASR & Ranwala SMW) **53:** 391-402 (2025)

Eco-tourism
Ecological characterization of the 40-year-old regenerated rainforest patch in Olaboduwa-Kodigahakanda adds value in promoting forest-based nature tourism (Ruwanmalie WAPU, Ileperuma IASR & Ranwala SMW) **53:** 391-402 (2025)

Enzyme
assays The first report on the in-vitro HDAC inhibitory potential of Sri Lankan traditional rice varieties (Ediriweera MK & Anandappa JM) **53:** 201-204 (2025)

Epigenetics
The first report on the in-vitro HDAC inhibitory potential of Sri Lankan traditional rice varieties (Ediriweera MK & Anandappa JM) **53:** 201-204 (2025)

Extreme precipitation
Annual and seasonal trends in extreme precipitation events in the dry zone of Sri Lanka (Kaushalya KC, Kumara JBDAP, Ampitiyawatta AD & Wimalasiri EM) **53:** 187-199 (2025)

Faecal contamination
Recreational water quality in the river Mahaweli, Sri Lanka: Enumeration and antibiotic sensitivity of Escherichia coli and sociological aspects (Weerakoon S, Nanayakkara B, Abayasekara C, Abeysundara H & Liyanage I) **53:** 45-55 (2025)

Faecal indicator bacteria
Faecal indicator bacteria and microbial source tracking as tools for testing water quality and sources of contamination of Rawan Oya tributary of the Mahaweli River, in Sri Lanka (Kapukotuwa GK, Abayasekara CL, Weerakoon KC & Rajakaruna RS) **53:** 421-436 (2025)

Faecal indicator organisms
Recreational water quality in the river Mahaweli, Sri Lanka: Enumeration and antibiotic sensitivity of Escherichia coli and sociological aspects (Weerakoon S, Nanayakkara B, Abayasekara C, Abeysundara H & Liyanage I) **53:** 45-55 (2025)

Fatty acids
Physiochemical characterization of critically endangered *Coscinium fenestratum* (gaertn.) Colebr. seed fat for potential niche applications in cosmetics and nutritional supplements (Thathsara KAH & Chinthaka SDM) **53:** 21-32 (2025)

FE modelling
Effect of initial imperfections on the seismic performance of thin-walled steel hollow piers: a numerical approach (Kumara AGYM, Pigera ACD, Ayodya NAI, Jayasinghe JASC & Bandara CS) **53:** 259-272 (2025)

Field and poly sack cultivation
Evaluation of genotypic variability and yield performance of selected indigenous and improved Ipomoea batatas L. genotypes under poly sack cultivation (Safwa MFZ, Samarasinghe TN, Wijevardhana AN, Shyamalee HAPA, Ranawake AL) **53:** 57-72 (2025)

Flume experiment
Optimizing beach nourishment composition for coastal protection in Sri Lanka: Insights from flume experiments (Lakshitha NVD, Samarasekara RSM & Siriwardana HPAM) **53:** 125-138 (2025)

Food
A multidimensional study on Spotted Sardinella: Biometric, ecological, and heavy metal perspectives from Negombo, Sri Lanka (Wijesooriya WMNS, Perera HACC, Abeysinghe AMPM & Perera KABP) **53:** 447-457 (2025)

Fourier transforms
A technique for extracting gravity anomalies originating from sediments deposited on folded oceanic crust (Tantrigoda DA, Fernando MMPM & Samaranayake SA) **53:** 311-315 (2025)

Fourth order perturbed Heisenberg Hamiltonian
Magnetic properties of body-centred cubic ferromagnetic thin films described by the fourth order perturbed Heisenberg Hamiltonian (Farhan MSM & Samarasekara P) **53:** 363-373 (2025)

Functional properties
Utilization of jackfruit seed flour (Artocarpus heterophyllus L.) as a thickening agent in tomato sauce production (Maduwage CSDS, Kaushalya SDN & Wijesinghe WAJP) **53:** 173-185 (2025)

Fuzzy graphs
Networking model based on fuzzy graphs of almost primary fuzzy ideals of near-rings (Muhammad A, Taouti A, Khan WA & Ashraf M) **52:** 13-20 (2025)

Fuzzy ideals of near-rings
Networking model based on fuzzy graphs of almost primary fuzzy ideals of near-rings (Muhammad A, Taouti A, Khan WA & Ashraf M) **53:** 13-20 (2025)

Fuzzy prime ideal of near-rings
Networking model based on fuzzy graphs of almost primary fuzzy ideals of near-rings (Muhammad A, Taouti A, Khan WA & Ashraf M) **53:** 13-20 (2025)

Gene network model
Coincidence of inductive photoperiod and early vegetative phase leads to early flowering and increased yield in selected Sri Lankan traditional rice varieties (Pushpakumari WHDU, Jayaprada NVT, Jayasekara LALW, Senanayake G, Senanayake DMJB & Geekiyanage S) **53:** 33-43 (2025)

Generalized order statistics
On recursive computation for the moments of generalized order statistics for the Kumaraswamy family of distributions with characterizations (Shahbaz SH & Shahbaz MQ) **53:** 139-150 (2025)

Geometric imperfections
Effect of initial imperfections on the seismic performance of thin-walled steel hollow piers: a numerical approach (Kumara AGYM, Pigera ACD, Ayodya NAI, Jayasinghe JASC & Bandara CS) **53:** 259-272 (2025)

Gravity anomaly
A technique for extracting gravity anomalies originating from sediments deposited on folded oceanic crust (Tantrigoda DA, Fernando MMPM & Samaranayake SA) **53:** 311-315 (2025)

HDAC
The first report on the in-vitro HDAC inhibitory potential of Sri Lankan traditional rice varieties (Ediriweera MK & Anandappa JM) **53:** 201-204 (2025)

Heavy metal content
A multidimensional study on Spotted Sardinella: Biometric, ecological, and heavy metal perspectives from Negombo, Sri Lanka (Wijesooriya WMNS, Perera HACC, Abeysinghe AMPM & Perera KABP) **53:** 447-457 (2025)

Hevea brasiliensis
First report of rubber circular leaf spot disease pathogen Colletotrichum siamense Prihastuti, L. Cai & K.D. Hyde in Cinnamomum zeylanicum blume in Sri Lanka (Aberathne AHMNR, Fernando THPS & Siriwardena EADD) **53:** 459-464 (2025)

Histone modifying enzymes
The first report on the in-vitro HDAC inhibitory potential of Sri Lankan traditional rice varieties (Ediriweera MK & Anandappa JM) **53:** 201-204 (2025)

Hot mix asphalt
Use of carbonised wood particles as filler replacement in hot mix asphalt (Rengarasu TM, Jegatheesan N & Wasala MKRTW Bandara) **53:** 375-389 (2025)

Increased yield
Coincidence of inductive photoperiod and early vegetative phase leads to early flowering and increased yield in selected Sri Lankan traditional rice varieties (Pushpakumari WHDU, Jayaprada NVT, Jayasekara LALW, Senanayake G, Senanayake DMJB & Geekiyanage S) **53:** 33-43 (2025)

Indirect tensile strength
Use of carbonised wood particles as filler replacement in hot mix asphalt (Rengarasu TM, Jegatheesan N & Wasala MKRTW Bandara) **53:** 375-389 (2025)

Inverse method
A technique for extracting gravity anomalies originating from sediments deposited on folded oceanic crust (Tantrigoda DA, Fernando MMPM & Samaranayake SA) **53:** 311-315 (2025)

Ipomea batatas
Evaluation of genotypic variability and yield performance of selected indigenous and improved Ipomoea batatas L. genotypes under poly sack cultivation (Safwa MFZ, Samarasinghe TN, Wijevardhana AN, Shyamalee HAPA, Ranawake AL) **53:** 57-72 (2025)

Irrigation
Changes in crop productivity and the harvested area of rice grown in Sri Lanka over the last four decades (1979-2021) as affected by the season, district, and water management system (Wijesooriya SS, Nawarathna HMKC, Kumari SS, Sooriyarachchi A, Jayaweera JMAK, Perera C & Suriyagoda LDB) **53:** 403-420 (2025)

Jackfruit seed flour
Utilization of jackfruit seed flour (Artocarpus heterophyllus L.) as a thickening agent in tomato sauce production (Maduwage CSDS, Kaushalya SDN & Wijesinghe WAJP) **53:** 173-185 (2025)

K^+
Assessing the impact of salinity stress on Na+, K+, and Ca2+ contents of 125 rice genotypes (Pradeepika NGJ & Ranawake AL) **53:** 109-124 (2025)

Kodo millet flour
Seasonal variation in crop yield and reduction of phytic acid content through soaking and germination of kodo millet (*Paspalum scrobiculatum* L.) germplasm (Suneetha C and M Sukumar) **53:** 345-362 (2025)

Kumaraswamy family of distributions
On recursive computation for the moments of generalized order statistics for the Kumaraswamy family of distributions with characterizations (Shahbaz SH & Shahbaz MQ) **53:** 139-150 (2025)

Landfill leachate
Performance evaluation of a lab-scale upflow anaerobic sludge blanket (uaSB) reactor for landfill leachate treatment under ambient temperature conditions (Iroshani HPDU, Rathnasiri PG, Wasala MKRTW Bandara & De Silva PHGAD) **53:** 283-292 (2025)

Length-weight relationship
A multidimensional study on Spotted Sardinella: Biometric, ecological, and heavy metal perspectives from Negombo, Sri Lanka (Wijesooriya WMNS, Perera HACC, Abeysinghe AMPM & Perera KABP) **53:** 447-457 (2025)

Lichen diversity
Lichens of Sri Lanka: Past discoveries, present knowledge, and future directions (Weerakoon B, Wolseley P, Wijesundara S, Nissanka S & Weerakoon G) **53:** 207-217 (2025)

Machine learning
Machine learning methods to classify engineering students' ability to perform recreational archery activities using biomechanical data (Basri NRH, Mohktar MS & Mahadi WNLW) **53:** 73-83 (2025)

Magnetic anisotropy constant
Magnetic properties of body-centred cubic ferromagnetic thin films described by the fourth order perturbed Heisenberg Hamiltonian (Farhan MSM & Samarasekara P) **53:** 363-373 (2025)

Magnetic thin films
Magnetic properties of body-centred cubic ferromagnetic thin films described by the fourth order perturbed Heisenberg Hamiltonian (Farhan MSM & Samarasekara P) **53:** 363-373 (2025)

Maha
Changes in crop productivity and the harvested area of rice grown in Sri Lanka over the last four decades (1979-2021) as affected by the season, district, and water management system (Wijesooriya SS, Nawarathna HMKC, Kumari SS, Sooriyarachchi A, Jayaweera JMAK, Perera C & Suriyagoda LDB) **53:** 403-420 (2025)

Maha season
Annual and seasonal trends in extreme precipitation events in the dry zone of Sri Lanka (Kaushalya KC, Kumara JBDAP, Ampitiyawatta AD & Wimalasiri EM) **53:** 187-199 (2025)

Malignant types
BRAF (V600E) gene mutation in patients with thyroid cancer in Sri Lanka: A pilot study (Ekanayaka N, Rathnayake S, Ratnayake P, Perera K & Udagama P) **53:** 3-12 (2025)

Mann Kendal
Annual and seasonal trends in extreme precipitation events in the dry zone of Sri Lanka (Kaushalya KC, Kumara JBDAP, Ampitiyawatta AD & Wimalasiri EM) **53:** 187-199 (2025)

Marshall properties
Use of carbonised wood particles as filler replacement in hot mix asphalt (Rengarasu TM, Jegatheesan N & Wasala MKRTW Bandara) **53:** 375-389 (2025)

Micro nutrient bioavailability
Seasonal variation in crop yield and reduction of phytic acid content through soaking and germination of kodo millet (*Paspalum scrobiculatum* L.) germplasm (Suneetha C and M Sukumar) **53:** 345-362 (2025)

Microbial source tracking
Faecal indicator bacteria and microbial source tracking as tools for testing water quality and sources of contamination of Rawan Oya tributary of the Mahaweli River, in Sri Lanka (Kapukotuwa GK, Abayasekara CL, Weerakoon KC & Rajakaruna RS) **53:** 421-436 (2025)

Midilli model
Effect of temperature on drying kinetics and quality attributes of coffee beans during hot air drying (Fernando AJ, Amaratunga KSP, Dharmasena DAN & De Silva THKR) **53:** 293-306 (2025)

Millet germplasms
Seasonal variation in crop yield and reduction of phytic acid content through soaking and germination of kodo millet (*Paspalum scrobiculatum* L.) germplasm (Suneetha C and M Sukumar) **53:** 345-362 (2025)

Mineral filler
Use of carbonised wood particles as filler replacement in hot mix asphalt (Rengarasu TM, Jegatheesan N & Wasala MKRTW Bandara) **53:** 375-389 (2025)

Mitochondrial markers
Molecular phylogeography of Echis carinatus revisited: Insights from the Sri Lankan population of saw-scaled viper (Serpentes: Viperidae: Echis) (Murugananthan A, Gnanathasan A, Kumanan T, KP Amarasinghe KP & Pirasath S) **53:** 85-105 (2025)

Moisture diffusivity
Effect of temperature on drying kinetics and quality attributes of coffee beans during hot air drying (Fernando AJ, Amaratunga KSP, Dharmasena DAN & De Silva THKR) **53:** 293-306 (2025)

Molecular marker
BRAF (V600E) gene mutation in patients with thyroid cancer in Sri Lanka: A pilot study (Ekanayaka N, Rathnayake S, Ratnayake P, Perera K & Udagama P) **53:** 3-12 (2025)

Molecular phylogeny
Molecular phylogeography of Echis carinatus revisited: Insights from the Sri Lankan population of saw-scaled viper (Serpentes: Viperidae: Echis) (Murugananthan A, Gnanathasan A, Kumanan T, KP Amarasinghe KP & Pirasath S) **53:** 85-105 (2025)

Morphologically similar paddy varieties
Use of near infrared spectroscopy for rapid and non-destructive identification of morphologically similar seeds of different paddy varieties [*Oryza sativa* L.] (Yasintha KW & Jinendra BM) **53:** 333-343 (2025)

Na^+
Assessing the impact of salinity stress on Na+, K+, and Ca2+ contents of 125 rice genotypes (Pradeepika NGJ & Ranawake AL) **53:** 109-124 (2025)

Nature
Ecological characterization of the 40-year-old regenerated rainforest patch in Olaboduwa-Kodigahakanda adds value in promoting forest-based nature tourism (Ruwanmalie WAPU, Ileperuma IASR & Ranwala SMW) **53:** 391-402 (2025)

Nderutilized source of flour
Utilization of jackfruit seed flour (Artocarpus heterophyllus L.) as a thickening agent in tomato sauce production (Maduwage CSDS, Kaushalya SDN & Wijesinghe WAJP) **53:** 173-185 (2025)

Neural network
A comparison of optimizers in a PyTorch based artificial neural network to predict normal boiling points of alkanes (Afzal MZ and Siddiqi SS) **53:** 165-172 (2025)

NIR spectroscopy
Use of near infrared spectroscopy for rapid and non-destructive identification of morphologically similar seeds of different paddy varieties [*Oryza sativa* L.] (Yasintha KW & Jinendra BM) **53:** 333-343 (2025)

Oceanic crust
A technique for extracting gravity anomalies originating from sediments deposited on folded oceanic crust (Tantrigoda DA, Fernando MMPM & Samaranayake SA) **53:** 311-315 (2025)

Offshore-sand
Optimizing beach nourishment composition for coastal protection in Sri Lanka: Insights from flume experiments (Lakshitha NVD, Samarasekara RSM & Siriwardana HPAM) **53:** 125-138 (2025)

Optimal control
Optimal control strategies for diabetes population management using mathematical models (Madhushika TDT, Somathilake LW & Fernando MCS) **53:** 219-232 (2025)

Optimizers
A comparison of optimizers in a PyTorch based artificial neural network to predict normal boiling points of alkanes (Afzal MZ and Siddiqi SS) **53:** 165-172 (2025)

Oryza sativa L.
Use of near infrared spectroscopy for rapid and non-destructive identification of morphologically similar seeds of different paddy varieties [*Oryza sativa* L.] (Yasintha KW & Jinendra BM) **53:** 333-343 (2025)

Ozone
Visualizing changes in internal layers of chinese chives leaf under short-term ozone exposure with biospeckle optical coherence tomography (Srimal LKT, Rajagopalan UM, Kadono H & Yonekura T) **53:** 245-258 (2025)

Paired T-test
Chest anteroposterior diameter measurement: Comparison of ultrasonic and manual methods across different BMI categories (Muralidharan C & Jobin Christ MC) **53:** 437-445 (2025)

Paspalum scrobiculatum L., phytic acid
Seasonal variation in crop yield and reduction of phytic acid content through soaking and germination of kodo millet (*Paspalum scrobiculatum* L.) germplasm (Suneetha C and M Sukumar) **53:** 345-362 (2025)

Pasta
development of pasta using composite flour of sweet potato (Ipomoea batatas), soy (Glycine max) & rice (Oryza sativa) flours (Jayawardhana JMJM, Fari MJM & Liyanage R) **53:** 233-244 (2025)

PCA
Evaluation of genotypic variability and yield performance of selected indigenous and improved Ipomoea batatas L. genotypes under poly sack cultivation (Safwa MFZ, Samarasinghe TN, Wijevardhana AN, Shyamalee HAPA, Ranawake AL) **53:** 57-72 (2025)

PCR
Faecal indicator bacteria and microbial source tracking as tools for testing water quality and sources of contamination of Rawan Oya tributary of the Mahaweli River, in Sri Lanka (Kapukotuwa GK, Abayasekara CL, Weerakoon KC & Rajakaruna RS) **53:** 421-436 (2025)

Photoperiod
Coincidence of inductive photoperiod and early vegetative phase leads to early flowering and increased yield in selected Sri Lankan traditional rice varieties (Pushpakumari WHDU, Jayaprada NVT, Jayasekara LALW, Senanayake G, Senanayake DMJB & Geekiyanage S) **53:** 33-43 (2025)

Pollution
Lichens of Sri Lanka: Past discoveries, present knowledge, and future directions (Weerakoon B, Wolseley P, Wijesundara S, Nissanka S & Weerakoon G) **53:** 207-217 (2025)

Pontryagin's maximum principle
Optimal control strategies for diabetes population management using mathematical models (Madhushika TDT, Somathilake LW & Fernando MCS) **53:** 219-232 (2025)

Principal component analysis
Use of near infrared spectroscopy for rapid and non-destructive identification of morphologically similar seeds of different paddy varieties [*Oryza sativa* L.] (Yasintha KW & Jinendra BM) **53:** 333-343 (2025)

Probiotics as a water additive
Impact of probiotics mixture as a water additive on water quality, growth performance and survival of Catla catla fry (Meddage AKMMK, Manage PM & Withanage PM) **53:** 151-164 (2025)

PyTorch
A comparison of optimizers in a PyTorch based artificial neural network to predict normal boiling points of alkanes (Afzal MZ and Siddiqi SS) **53:** 165-172 (2025)

RClimDex
Annual and seasonal trends in extreme precipitation events in the dry zone of Sri Lanka (Kaushalya KC, Kumara JBDAP, Ampitiyawatta AD & Wimalasiri EM) **53:** 187-199 (2025)

Recerational archery
Machine learning methods to classify engineering students' ability to perform recreational archery activities using biomechanical data (Basri NRH, Mohktar MS & Mahadi WNLW) **53:** 73-83 (2025)

Recurrence relations
On recursive computation for the moments of generalized order statistics for the Kumaraswamy family of distributions with characterizations (Shahbaz SH & Shahbaz MQ) **53:** 139-150 (2025)

Residual stresses
Effect of initial imperfections on the seismic performance of thin-walled steel hollow piers: a numerical approach (Kumara AGYM, Pigera ACD, Ayodya NAI, Jayasinghe JASC & Bandara CS) **53:** 259-272 (2025)

Rice
development of pasta using composite flour of sweet potato (Ipomoea batatas), soy (Glycine max) & rice (Oryza sativa) flours (Jayawardhana JMJM, Fari MJM & Liyanage R) **53:** 233-244 (2025)

Rice productivity
Changes in crop productivity and the harvested area of rice grown in Sri Lanka over the last four decades (1979-2021) as affected by the season, district, and water management system (Wijesooriya SS, Nawarathna HMKC, Kumari SS, Sooriyarachchi A, Jayaweera JMAK, Perera C & Suriyagoda LDB) **53:** 403-420 (2025)

Rice
The first report on the in-vitro HDAC inhibitory potential of Sri Lankan traditional rice varieties (Ediriweera MK & Anandappa JM) **53:** 201-204 (2025)

River water
Recreational water quality in the river Mahaweli, Sri Lanka: Enumeration and antibiotic sensitivity of Escherichia coli and sociological aspects (Weerakoon S, Nanayakkara B, Abayasekara C, Abeysundara H & Liyanage I) **53:** 45-55 (2025)

Salinity tolerance
Assessing the impact of salinity stress on Na^+, K^+, and Ca^{2+} contents of 125 rice genotypes (Pradeepika NGJ & Ranawake AL) **53:** 109-124 (2025)

Seasons
Changes in crop productivity and the harvested area of rice grown in Sri Lanka over the last four decades (1979-2021) as affected by the season, district, and water management system (Wijesooriya SS, Nawarathna HMKC, Kumari SS, Sooriyarachchi A, Jayaweera JMAK, Perera C & Suriyagoda LDB) **53:** 403-420 (2025)

Secondary forests
Ecological characterization of the 40-year-old regenerated rainforest patch in Olaboduwa-Kodigahakanda adds value in promoting forest-based nature tourism (Ruwanmalie WAPU, Ileperuma IASR & Ranwala SMW) **53:** 391-402 (2025)

Sediments
A technique for extracting gravity anomalies originating from sediments deposited on folded oceanic crust (Tantrigoda DA, Fernando MMPM & Samaranayake SA) **53:** 311-315 (2025)

Seed fat
Physiochemical characterization of critically endangered *Coscinium fenestratum* (gaertn.) Colebr. seed fat for potential niche applications in cosmetics and nutritional supplements (Thathsara KAH & Chinthaka SDM) **53:** 21-32 (2025)

Seedling stage
Assessing the impact of salinity stress on Na^+, K^+, and Ca^{2+} contents of 125 rice genotypes Pradeepika NGJ & Ranawake AL) **53:** 109-124 (2025)

Simple graphs
An upper bound for star chromatic index of simple connected sub cubic graphs and applications (Fernando CLR & Athapattu AMCUM) **53:** 317-331 (2025)

Snakes
Molecular phylogeography of Echis carinatus revisited: Insights from the Sri Lankan population of saw-scaled viper (Serpentes: Viperidae: Echis) (Murugananthan A, Gnanathasan A, Kumanan T, KP Amarasinghe KP & Pirasath S) **53:** 85-105 (2025)

Soft independent modeling of class analogy
Use of near infrared spectroscopy for rapid and non-destructive identification of morphologically similar seeds of different paddy varieties [*Oryza sativa* L.] (Yasintha KW & Jinendra BM) **53:** 333-343 (2025)

Sonar sensors
Aerial crack detection in building structures using convolutional neural networks (Silva CS, Dissanayake DMKI, Rathnayake RSMPW & Sathsara NTA) **53:** 273-282 (2025)

Soy
development of pasta using composite flour of sweet potato (Ipomoea batatas), soy (Glycine max) & rice (Oryza sativa) flours (Jayawardhana JMJM, Fari MJM & Liyanage R) **53:** 233-244 (2025)

Spin exchange interaction
Magnetic properties of body-centred cubic ferromagnetic thin films described by the fourth order perturbed Heisenberg Hamiltonian (Farhan MSM & Samarasekara P) **53:** 363-373 (2025)

Spin layers
Magnetic properties of body-centred cubic ferromagnetic thin films described by the fourth order perturbed Heisenberg Hamiltonian (Farhan MSM & Samarasekara P) **53:** 363-373 (2025)

Sri Lanka
Changes in crop productivity and the harvested area of rice grown in Sri Lanka over the last four decades (1979-2021) as affected by the season, district, and water management system (Wijesooriya SS, Nawarathna HMKC, Kumari SS, Sooriyarachchi A, Jayaweera JMAK, Perera C & Suriyagoda LDB) **53:** 403-420 (2025)

Sri Lankan traditional rice
Coincidence of inductive photoperiod and early vegetative phase leads to early flowering and increased yield in selected Sri Lankan traditional rice varieties (Pushpakumari WHDU, Jayaprada NVT, Jayasekara LALW, Senanayake G, Senanayake DMJB & Geekiyanage S) **53:** 33-43 (2025)

Star chromatic index
An upper bound for star chromatic index of simple connected sub cubic graphs and applications (Fernando CLR & Athapattu AMCUM) **53:** 317-331 (2025)

Star edge coloring
An upper bound for star chromatic index of simple connected sub cubic graphs and applications (Fernando CLR & Athapattu AMCUM) **53:** 317-331 (2025)

Steel hollow piers
Effect of initial imperfections on the seismic performance of thin-walled steel hollow piers: a numerical approach (Kumara AGYM, Pigera ACD, Ayodya NAI, Jayasinghe JASC & Bandara CS) **53:** 259-272 (2025)

Stomach fullness
A multidimensional study on Spotted Sardinella: Biometric, ecological, and heavy metal perspectives from Negombo, Sri Lanka (Wijesooriya WMNS, Perera HACC, Abeysinghe AMPM & Perera KABP) **53:** 447-457 (2025)

Sub-cubic graphs
An upper bound for star chromatic index of simple connected sub cubic graphs and applications (Fernando CLR & Athapattu AMCUM) **53:** 317-331 (2025)

Sub-urban forests
Ecological characterization of the 40-year-old regenerated rainforest patch in Olaboduwa-Kodigahakanda adds value in promoting forest-based nature tourism (Ruwanmalie WAPU, Ileperuma IASR & Ranwala SMW) **53:** 391-402 (2025)

Survival
Impact of probiotics mixture as a water additive on water quality, growth performance and survival of Catla catla fry (Meddage AKMMK, Manage PM & Withanage PM) **53:** 151-164 (2025)

Sweet potato
development of pasta using composite flour of sweet potato (Ipomoea batatas), soy (Glycine max) & rice (Oryza sativa) flours (Jayawardhana JMJM, Fari MJM & Liyanage R) **53:** 233-244 (2025)

Targeted therapy
BRAF (V600E) gene mutation in patients with thyroid cancer in Sri Lanka: A pilot study (Ekanayaka N, Rathnayake S, Ratnayake P, Perera K & Udagama P) **53:** 3-12 (2025)

Taxonomy
Lichens of Sri Lanka: Past discoveries, present knowledge, and future directions (Weerakoon B, Wolseley P, Wijesundara S, Nissanka S & Weerakoon G) **53:** 207-217 (2025)

Temporal characteristics
Visualizing changes in internal layers of chinese chives leaf under short-term ozone exposure with biospeckle optical coherence tomography (Srimal LKT, Rajagopalan UM, Kadono H & Yonekura T) **53:** 245-258 (2025)

Thickening agent
Utilization of jackfruit seed flour (Artocarpus heterophyllus L.) as a thickening agent in tomato sauce production (Maduwage CSDS, Kaushalya SDN & Wijesinghe WAJP) **53:** 173-185 (2025)

Thin layer drying
Effect of temperature on drying kinetics and quality attributes of coffee beans during hot air drying (Fernando AJ, Amaratunga KSP, Dharmasena DAN & De Silva THKR) **53:** 293-306 (2025)

Thyroid cancer
BRAF (V600E) gene mutation in patients with thyroid cancer in Sri Lanka: A pilot study (Ekanayaka N, Rathnayake S, Ratnayake P, Perera K & Udagama P) **53:** 3-12 (2025)

Traditional rice accessions
Assessing the impact of salinity stress on Na+, K+, and Ca2+ contents of 125 rice genotypes (Pradeepika NGJ & Ranawake AL) **53:** 109-124 (2025)

Tropical climate
Performance evaluation of a lab-scale upflow anaerobic sludge blanket (uaSB) reactor for landfill leachate treatment under ambient temperature conditions (Iroshani HPDU, Rathnasiri PG, Wasala MKRTW Bandara & De Silva PHGAD) **53:** 283-292 (2025)

Tropical forests
Lichens of Sri Lanka: Past discoveries, present knowledge, and future directions (Weerakoon B, Wolseley P, Wijesundara S, Nissanka S & Weerakoon G) **53:** 207-217 (2025)

UASB reactor
Performance evaluation of a lab-scale upflow anaerobic sludge blanket (uaSB) reactor for landfill leachate treatment under ambient temperature conditions (Iroshani HPDU, Rathnasiri PG, Wasala MKRTW Bandara & De Silva PHGAD) **53:** 283-292 (2025)

Ultrasonic sensor
Chest anteroposterior diameter measurement: Comparison of ultrasonic and manual methods across different BMI categories (Muralidharan C & Jobin Christ MC) **53:** 437-445 (2025)

Unmanned aerial vehicle
Aerial crack detection in building structures using convolutional neural networks (Silva CS, Dissanayake DMKI, Rathnayake RSMPW & Sathsara NTA) **53:** 273-282 (2025)

Unsaponifiable matter
Physiochemical characterization of critically endangered *Coscinium fenestratum* (gaertn.) Colebr. seed fat for potential niche applications in cosmetics and nutritional supplements (Thathsara KAH & Chinthaka SDM) **53:** 21-32 (2025)

Upper mantle
A technique for extracting gravity anomalies originating from sediments deposited on folded oceanic crust (Tantrigoda DA, Fernando MMPM & Samaranayake SA) **53:** 311-315 (2025)

Vipers
Molecular phylogeography of Echis carinatus revisited: Insights from the Sri Lankan population of saw-scaled viper (Serpentes: Viperidae: Echis) (Murugananthan A, Gnanathasan A, Kumanan T, Amarasinghe KP & Pirasath S) **53:** 85-105 (2025)

Vision sensors
Aerial crack detection in building structures using convolutional neural networks (Silva CS, Dissanayake DMKI, Rathnayake RSMPW & Sathsara NTA) **53:** 273-282 (2025)

Wastewater treatment
Performance evaluation of a lab-scale upflow anaerobic sludge blanket (uaSB) reactor for landfill leachate treatment under ambient temperature conditions (Iroshani HPDU, Rathnasiri PG, Wasala MKRTW Bandara & De Silva PHGAD) **53:** 283-292 (2025)

Water quality
Faecal indicator bacteria and microbial source tracking as tools for testing water quality and sources of contamination of Rawan Oya tributary of the Mahaweli River, in Sri Lanka (Kapukotuwa GK, Abayasekara CL, Weerakoon KC & Rajakaruna RS) **53:** 421-436 (2025)

Water quality improvement
Impact of probiotics mixture as a water additive on water quality, growth performance and survival of Catla catla fry (Meddage AKMMK, Manage PM & Withanage PM) **53:** 151-164 (2025)

Water sources
Changes in crop productivity and the harvested area of rice grown in Sri Lanka over the last four decades (1979-2021) as affected by the season, district, and water management system (Wijesooriya SS, Nawarathna HMKC, Kumari SS, Sooriyarachchi A, Jayaweera JMAK, Perera C & Suriyagoda LDB) **53:** 403-420 (2025)

Yala
Changes in crop productivity and the harvested area of rice grown in Sri Lanka over the last four decades (1979-2021) as affected by the season, district, and water management system (Wijesooriya SS, Nawarathna HMKC, Kumari SS, Sooriyarachchi A, Jayaweera JMAK, Perera C & Suriyagoda LDB) **53:** 403-420 (2025)

***Yala* season**
Annual and seasonal trends in extreme precipitation events in the dry zone of Sri Lanka (Kaushalya KC, Kumara JBDAP, Ampitiyawatta AD & Wimalasiri EM) **53:** 187-199 (2025)

Yield determinants of Ipomea batatas
Evaluation of genotypic variability and yield performance of selected indigenous and improved Ipomoea batatas L. genotypes under poly sack cultivation (Safwa MFZ, Samarasinghe TN, Wijevardhana AN, Shyamalee HAPA, Ranawake AL) **53:** 57-72 (2025)

JOURNAL OF THE
NATIONAL SCIENCE FOUNDATION
OF SRI LANKA

GUIDANCE TO CONTRIBUTORS

GENERAL INFORMATION

Scope

The Journal of the National Science Foundation of Sri Lanka publishes the results of research in all aspects of Science and Technology. It is open for publication of Research Articles, Reviews, Research Communications and Correspondence.

Use of AI Tools in Manuscript Preparation

To ensure transparency and uphold scholarly standards, authors must disclose any use of Artificial Intelligence (AI) tools during the research and manuscript preparation process.
The use of AI tools (e.g., for language editing, summarization, data analysis, or figure generation) **must be declared in the manuscript, typically before the Acknowledgements**.
AI tools must not be credited as authors. Human authors remain fully responsible for the integrity, accuracy, and originality of the submitted work.
AI-generated content must be critically reviewed by the authors to ensure quality and ethical compliance, including data privacy and bias mitigation.
AI must not be used to fabricate or manipulate original research data, unless it is part of the approved research methodology and explicitly described.
Non-compliance with these guidelines may lead to rejection of the manuscript or post-publication corrective actions.

IT related and other non-empirical articles

The JNSF is a journal primarily devoted to natural sciences. It also considers for publication significant and novel contributions from formal sciences. Authors of emerging sub-disciplines of Computing and related areas such as Machine Learning, Artificial Intelligence and Data Sciences are requested to carefully adhere to the following guidelines when submitting manuscripts for this journal.

- Clear formulation of outcome-oriented **Research Objective/s** for targeted knowledge (sub)domain/s or (sub)discipline/s.
- Selection and comprehensive summarization of **appropriate Research Method/s** adopted to achieve the stated Research Objective/s.
- Reporting a sound **(Empirical) Evaluation** of the research finding/s thereby arguing reliability, validity, and generalizability of research claim/s.

Categories of manuscripts

Research Articles: Research Articles are papers that present complete descriptions of original research. Research Articles should include an Abstract, Keywords, Introduction, Methodology, Results and Discussion, Conclusion and Recommendations where relevant. References should be prepared according to the "Guidelines for the preparation of manuscripts". Maximum length of the article should be limited to 30 pages (Times New Roman, font size 12 , line space 1.5) with a word count less than 10,000 including references, figures and tables. Any articles above this limit will be returned. Please refer author guidelines for further details (https://jnsfsl.sljol.info/about/submissions#author-guidelines)

Reviews: Reviews are critical presentations on selected topics of Science or Technology. They should be well focused and organized and avoid general "textbook" style. As reviews are intended to be critical presentations on selected topics, the author (or the principal author in a multi-author review) need to have had substantial leadership in research supported by a publication track record in the areas covered by the review. A person/s wishing to submit a Review Article should obtain prior approval from the Editorial Board by submitting a concise summary of the intended article, along with a list of the author's publications in the related area (jnsf@nsf.gov.lk). Maximum length of the article should be limited to 40 pages (Times New Roman, font size 12 , line space 1.5) with a word count of 12,000 including references, figures and tables. Any articles beyond this limit will be returned.

Research Communications: Research Communications are intended to communicate important new findings in a specific area of limited scope that are worthy of rapid dissemination among the scientific community. Authors are required to provide a statement justifying the suitability of the submission for a Research Communication. The article should include an Abstract, Keywords, Introduction, Methodology, Results & Discussion, Conclusion and References. Maximum length of the article should be limited to 10 pages (Times New Roman, font size 12 , line space 1.5) with a word count of 2,500 including references, figures and tables. Any articles beyond this limit will be returned.

Correspondence: Correspondence will be accepted regarding one or more articles in the preceding four issues of the Journal, as well as Letters to the Editor. Articles covering important scientific events or any other news of interest to scientists, reviews of books of scientific nature, articles presenting views on issues related to science and scientific activity will also be considered. Publication will be made at the discretion of the Editor-in Chief. Maximum length of the article should be limited to 05 pages (Times New Roman, font size 12 , line space 1.5) with a word count of 1,500 including references, figures and tables. Any articles beyond this limit will be returned.

SUBMISSION OF MANUSCRIPT

Authors submitting articles to the JNSF should first create an account in the Sri Lanka Journals Online System (https://jnsfsl.sljol.info/). All manuscripts should be in MS Word format and must be submitted to the journal's online platform at https://jnsfsl.sljol.info/submit/start/. Submissions *via* emails are not encouraged. Please make sure that **no** author information is mentioned in the article submitted other than in the title page. Complete names and details of affiliations of all authors must be fed into the system during the online submission process. Authors are required to provide their personal, validated ORCID ID (by obtaining an ORCID ID from https:// orcid.org/) when submitting the manuscript. No change to the

authors or order of authors will be accepted after the submission. All those who have made significant contributions should be listed as co-authors. The corresponding author should ensure that all contributing co-authors are included in the author list and have approved the final version of the paper and have agreed to its submission for publication.

All submissions should be in English. If the manuscript conforms to the guidelines specified, the date received will be the date that the manuscript was submitted to the online system.

Submissions are accepted for processing on the understanding that they will be reviewed and that they have not been submitted for publication elsewhere (including publication as a full paper or extended abstract as a part of Conference Proceedings).

Suggesting potential reviewers by authors
The authors are requested to suggest three names of referees when submitting their manuscript, in the Cover Letter space provided at the bottom of the page in the first stage of online submission. Referees should not be from the institution where the work was carried out and should not have been co-authors in previous publications. The address, institutional affiliation and e-mail of the suggested referees should be provided. Please note that the JNSF is not bound to select all or any of the suggested referees for sending the manuscript for reviewing

Authorship
All authors designated as authors should be eligible for authorship. Those who have made a substantial contribution to the concept or design of the work; or acquisition, analysis or interpretation of data are recognized as Authors.
The corresponding author should be prompt and ensure adherence to timelines when responding to requests, queries and recommendation of reviewers conveyed by or on behalf of the Editor-in Chief and Editorial Board.

Avoiding predatory references in manuscripts

Authors of the manuscripts should identify and not include predatory journal articles in the reference list.
If any paper that is cited is published in an Open Access journal, the authors are advised to ensure that the journal is listed in the DOAJ (Directory of Open Access Journals) or by the COPE (Committee on Publication Ethics). Please note that authors should check with DOAJ and COPE by themselves, and not assume that the statements given in the journal websites are accurate.
If the journal is included either in DOAJ or COPE, it can be presumed as legitimate. If not, authors need to review the journal website and published articles for characteristics of predatory journals. At the same time, authors can check whether the journal or relevant publisher is included in the directory of predatory journals and publishers.
If it is revealed that the manuscript is supported by articles published in predatory journals, it could be rejected by the JNSF at any stage of the publication process.

Supplementary materials
Any experimental data necessary to evaluate the claims made in the paper but not included in the paper should be provided as supplementary materials. Supplementary materials will be sent to the reviewers and published online with the manuscript if accepted. The supplementary materials should conform to Journal guidelines and should be uploaded as separate files. Authors should number Supplementary Tables and Figures as, for example, 'Supplementary Table S1'. Refer to each piece of supplementary material at the appropriate point(s) in the main article. Supplementary Materials may include description of the materials and methods, controls, or tabulated data presented in Tables or Figures, and programming codes.

Peer review
The manuscripts submitted to the JNSF will initially be screened by the Editorial Board and, if suitable, will be referred to at least two subject experts in the relevant field. The peer-review process of the JNSF is double-blind.
When revision of a manuscript has been requested, the revised manuscript should be submitted on or before the stated deadline. The authors' response to the comments of referees should be tabulated with the comment and response. The decision of the Editorial Board shall be final.
Accepted papers are subject to editing. The date of acceptance will be the date the Editorial Board accept the paper for publication.

Article processing fee
Article processing fee of US$ 250 will be levied for each manuscript in two stages, except when the corresponding author is affiliated with a Sri Lankan institution,

- An initial processing fee of US$ 20 will be levied for each manuscript at the peer-review stage.
- The remaining US$ 230 will be charged for accepted articles at the time of publication.

Payments can be made online via NSF Payment Portal (http://pg.nsf.gov.lk/)

Authors' declaration
The authors are required to accept the conditions indicated in the online author declaration statement.

Copyright
Articles in JNSF are published under the Creative Commons License CC-BY-ND. This license permits use, distribution and reproduction of articles for commercial and non-commercial purposes, provided that the original work is properly cited and is not changed in anyway. The copyright of the article is with the National Science Foundation of Sri Lanka. Therefore, authors are requested to check with institution's copyright and publication policy before submitting an article to the JNSF. Authors secure the right to reproduce any material that has already been published or copyrighted elsewhere. When an article is accepted for publication, the authors are required to submit the Transfer of Copyright document signed by all the authors.

Post-publication corrections
The Editorial Board reserves the right to take action on publishing an erratum or corrigendum. If serious errors are identified in a published article, the Journal may consider a retraction or publishing a correction.

STRUCTURE OF MANUSCRIPT

Manuscript
The manuscript should be free of errors and prepared in single column, using 1.5 line spaced text of Times New Roman 12 font leaving 1 inch margins. Pages should be numbered consecutively.

a. Style
The paper should be written clearly and concisely. The style of writing should conform to scholarly writing. Slang, jargon, unauthorized abbreviations, abbreviated phrasings should not be used. In general, the impersonal form should be used. Poor usage of language will result in rejection of the manuscript during initial screening.

b. Layout
Manuscripts other than review articles should be generally organized as follows: Title, Abstract, Keywords, Introduction, Methodology, Results and Discussion, Conclusions and Recommendations (where relevant), Acknowledgements and References. Pages should be arranged in the following order:

First page should include the title of the manuscript and **complete names and affiliations** of all authors. **Author information should not be mentioned in other places of the manuscripts.** Any statement (including acknowledgment) which can reveal author identity should be removed. If a major part of the research has been published as an abstract in conference proceedings, it should be mentioned with citation in the space provided for "Comments for Editor". Authors must also indicate the **general and specific research area** of the manuscript in the title page.

***Title*:** Should accurately and concisely reflect the contents of the article.

***Running title*:** Should be a shortened title (limited to a maximum of 50 characters) that could be printed at the top of every other page of the Journal article.

***Abstract*:** Should be between 200 - 250 for research articles and 200 - 300 for reviews. It should not contain any references and should be able to stand on its own. It should outline objectives and methodology together with important results and conclusions.

***Keywords*:** Include a maximum of six keywords, which may include the names of organisms (common or scientific), methods or other important words or phrases specific to the study.

***Introduction*:** This should state the reasons for performing the work with a brief review of related research studies in the context of the work described in the paper. Objectives of the study should be clearly stated.

***Materials and Methods*:** This section should give the details of how you conducted your study. New methods may be described in detail with an indication of their limitations. Established methods can be mentioned with appropriate references. Sufficient details should be included to allow direct repetition of the work by others. Where human subjects are involved, they should be referred to by numbers or fictitious names. A paper reporting the results of investigations on human subjects or on animals must include a statement to the effect that the relevant national or other administrative and ethical guidelines have been adhered to, and a copy of the ethical clearance certificate should be submitted. Methods of statistical analyses used should be mentioned where relevant.

Results and Discussion
Results: the results should be concisely and logically presented. Repetition of the same results in figures, tables or text should be avoided.
Discussion: data essential for the conclusions emerging from the study should be discussed. Long, rambling discussions should be avoided. The discussion should deal with the interpretation of results. It should logically relate new findings to earlier ones. Unqualified statements and conclusions not completely supported by data should be avoided.
Molecular sequence data, such as gene or rDNA sequences, genome sequences, metagenomic sequences etc. must be deposited in a public molecular sequence repository, such as GenBank, that is part of the International Nucleotide Sequence Database Collaboration (INSDC). The accession numbers obtained must be cited in the text, Table or on Figures of phylogenetic trees of the manuscript.

***Conclusion*:** The conclusion should be brief, highlight the outcomes of the study and should be aligned with the objectives of the study. It should not contain references.

Competing Interest statement: The authors should include a statement on conflict of interest disclosing any financial or other substantive conflicts of interest that may influence the results or interpretation of the research in the space provided in the online article submission form. All sources of financial support for the project should also be disclosed.

***Acknowledgement*:** Should be brief and made for specific scientific, financial and technical assistance only. If a significant part of the research was performed in an institution other than the authors' affiliations should be acknowledged. All those who have made substantial contribution to the research but do not qualify to be authors should be acknowledged.

***References* :**
The JNSF uses APA (7th Edition) reference style
All research work of other authors, when used or referred to or cited, should be correctly acknowledged in the text and in the References.
All the references in the text should be in the list and vice versa

Citing references in the text:
- References to the literature must be indicated in the text and tables as per the Author-Year System, by the author's last name and year, in parenthesis (i.e. Able, 1997) or (Able & Thompson, 1998).
- Citation to work by more than two authors should be abbreviated with the use of et al. (i.e. Able *et al*., 1997).
- Multiple publications by the same first author in the same year should be coded by letters, (i.e. Thompson, 1991a, 1991b,1992,1993).
- Multiple citations of different authors should be made in chronological order and separated by a semicolon, (i.e. Zimmerman *et al*., 1986; Able *et al*., 1997).

Citing references in the List of references:
- The list of References should be arranged in alphabetical order based on the last name of the first author.
- In APA 7th ed., **up to 20 authors** should be included in a reference list entry. Write out the last name and first initial(s) for each contributor.

Example for 2–20 authors:

Wright, A., Komal, G., Siddharth, D., Boyd, G., Cayson, N., Beverley, K., Travers, K., Begum, A., Redmond, M., Mills, M., Cherry, D., Finley, B., Fox, M., Ferry, F., Almond, B., Howell, E., Gould, T., Berger, B., Bostock, T., & Fountain, A. (2020). Styling royalty. London Bridge Press.

- For references with more than 20 authors, after listing the 19th author replace any additional author names with an ellipsis (…) followed by the final listed author's last name and first initial(s).

Example for 21+ authors:

Kalnay, E., Kanamitsu, M., Kistler, R., Collins, W., Deaven, D., Gandin, L., Iredell, M., Saha, S., White, G., Woolen, J., Zhu, Y., Chelliah, M., Ebisuzaki, W., Higgins, W., Janowiak, J., Mo, K.C., Ropelewski, C., Wang, J., Leetmaa, A., … Joseph, D. (1996). The NCEP/NCAR 40-year reanalysis project. Bulletin of the American Meteorological Society, 77(3), 437-471. http://doi.org/fg6rf9

- All the initials of the author must be given after the last name and the year of publication should follow in parentheses.
- This should be followed by the full title of the referred publication.
- When journal articles are listed, the journal name should be given in full and in italics and followed by the volume number, issue number in parentheses and then the inclusive pages.
- Where there are several publications by the same author(s) and published in the same year they should be differentiated by adding a lower-case letter after the year.

Example

Clarke, P. N., & Fawcett, J. (2014a). Life as a mentor. *Nursing Science Quarterly*, 27(3), 213-215. https://doi.org/10.1177/0894318414534492

Clarke, P. N., & Fawcett, J. (2014b). Life as a nurse researcher. *Nursing Science Quarterly*, 27(1), 37-41. https://doi.org/10.1177/0894318413509708

- Digital object identifiers (DOIs) should be included for all references where available.

Details about this reference style can be obtained from below links

- https://apastyle.apa.org/style-grammar-guidelines/references
- https://apastyle.apa.org/style-grammar-guidelines/references/examples
- https://libguides.jcu.edu.au/apa

Abbreviations and Symbols: Unless common, these should be defined when first used, and not included in the abstract. The SI System of units should be used wherever possible. lf measurements were made in units other than SI, the data should be reported in the same units followed by SI units in brackets, e.g. 5290 ft (1610 m).

Formulae and Equations: Equations should be typewritten and quadruple spaced. They should be started on the left margin and the number placed in parentheses to the right of the equation.

Nomenclature: Scientific names of plants and animals should be printed in italics. In the first citation, genus, species and authority must be given. e.g. *Borassus flabellifer* Linn. In latter citations, the generic name may be abbreviated, for example, *B. flabellifer* L.

Tables and figures: Tables and Figures should be clear and intelligible and kept to a minimum, and should not repeat data available elsewhere in the paper. Any reproduction of illustrations, tabulations, pictures etc. in the manuscript should be acknowledged.

Tables: Tables should be numbered consecutively with Arabic numerals and placed at the appropriate position in the manuscript. If a Table must be continued, a second sheet should be used and all the headings repeated. The number of columns or rows in each Table should be minimized. Each Table should have a title, which makes its general meaning clear, without reference to the text. All Table columns should have explanatory headings. Units of measurement, if any, should be indicated in parentheses in the heading of each column. Vertical lines should not be used and horizontal lines should be used only in the heading and at the bottom of the table. Footnotes to Tables should be placed directly below the Table and should be indicated by superscript lower case italic letters (^{a}, ^{b}, ^{c}, etc.).

Figures: All illustrations are considered as figures, and each graph, drawing or photograph should be numbered consecutively with Arabic numerals and placed at the appropriate position in the manuscript. Any lettering to appear on the illustrations should be of a suitable size for reproduction and uniform lettering should be used in all the Figures of the manuscript. Scanned figures or photographs should be of high quality (**300 dpi**), to fit the proportions of the printed page (12 × 17 cm). Each figure should carry a legend so that the general meaning of the figure can be understood without reference to the text. Where magnifications are used, they should be stated.

Units of measurement

Length: km, m, mm, µm, nm
Area: ha, km^2, m^2
Capacity: kL, L, mL, µL
Volume: km^3, m^3, cm^3
Mass: t, kg, g, mg, µg
Time: year(s), month(s), week(s), day(s), hour(s), minute(s), second(s)
Concentration: M, mM, N, %, g/L, mg/L, ppm
Temperature: °C, K
Gravity: x g
Molecular weight: mol wt
Others: Radio-isotopes: 32P
Radiation dose: Bq
Oxidation-reduction potential: rH
Hydrogen ion concentration: pH